Soil-Structure Interaction Effect of Embedded Foundation and Adjacent Buildings on Response Characteristics of Superstructures

（埋込み基礎や隣接建物による地盤と建物の動的相互作用が
建物応答特性に与える影響）

OGUT, Oguz Can

Doctor of Environmental Studies,
Graduate School of Environmental Studies,
Nagoya University

2017

Table of Contents

Chapter 1

Introduction

1.1 Background of the research

In the conventional earthquake design of buildings, the effect of the soil on the structural response, which is known as soil-structure interaction (SSI), is generally neglected because it usually benefits the earthquake response. However, according to Mylonakis and Gazetas (2000), the soil effect is not always beneficial. Moreover, Tezcan and Ipek (1973) assert that a reason for the partial collapse of a factory that was 135km from the epicenter of the 1970 Gediz Earthquake in Turkey was SSI because of the combined effect of site amplification of soil and period-elongation effect of SSI as shown in Figure 1-1. Aviles and Perez-Rocha (1998) claim that effect of soil not only detrimental for low-rise buildings but also for medium and high-rise buildings in the Valley of Mexico. In the research of Mylonakis *et al.* (2006), effect of soil structure interaction is investigated on the collapse of the 18 piers of Hanshin Expressway in Japan during the 1995 Kobe Earthquake by conducting simplified and nonlinear dynamic analyses on a one pier model. They claim that SSI is the main cause of the damage if Fukiai and Takatori records are taken representative records as shown in Figure 1-2 where C_y represents the actual yield strength ($C_{y,fix}$ = 0.53 corresponds to $C_{y,SSI}$ = 0.71 according to the study). However, it is worth noting that, according to Moghaddasi *et al*. (2011), determining the effect of SSI on a survey after an earthquake is not an easy issue since it is hard to separate the period elongation effect of SSI and nonlinear behavior of the superstructure. Therefore, more analytical research is needed on this topic for reliable design of such structures.

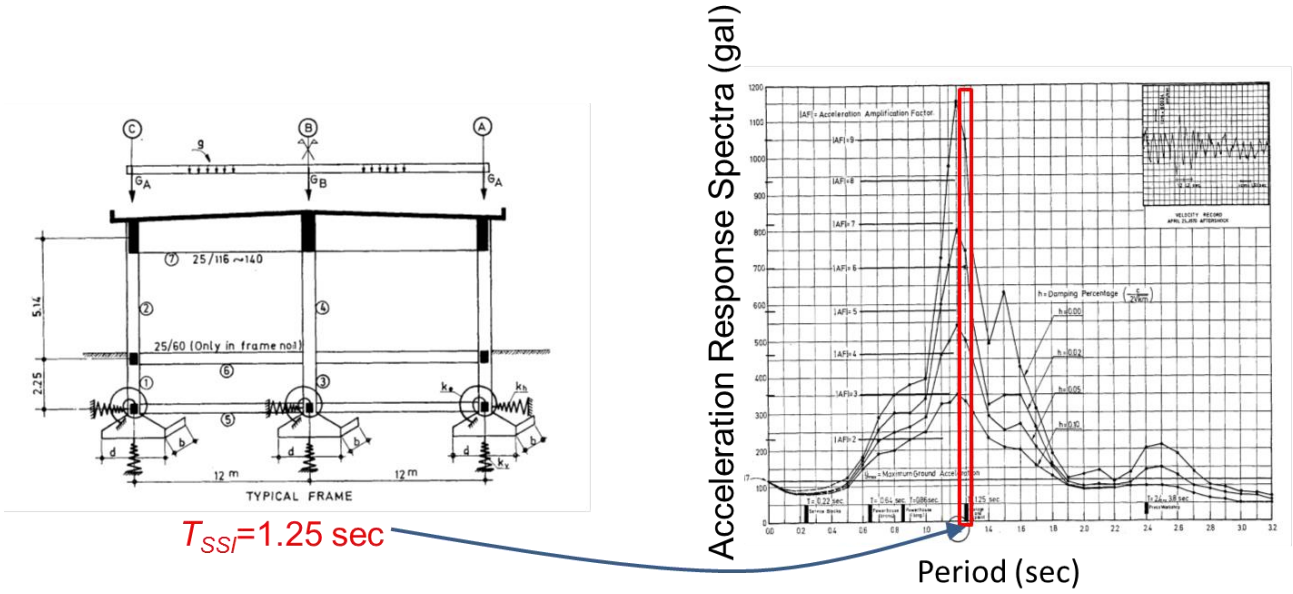

Figure 1-1: Soil-structure model of the garage building of the factory and acceleration response spectra of the earthquake record (Tezcan and Ipek, 1973)

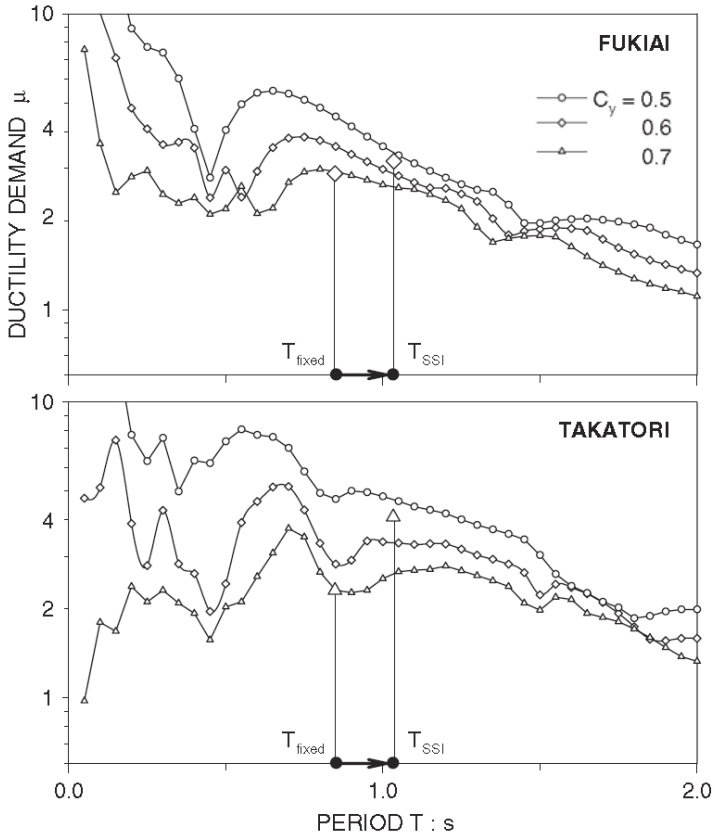

Figure 1-2: Ductility demands of one pier models for fault-normal components of Fukiai and Takatori records (Mylonakis *et al*., 2006)

In addition, there is a tendency in earthquake design to equate foundation input motion (FIM) with the free field motion (FFM) of the ground away from buildings during earthquake. This is despite the fact that other SSI effects, such as period elongation and radiation damping (which occur due to the inertial interaction) are considered. The reason for this tendency is again same: the belief of that either the difference between FFM and FIM (which occurs due to the kinematic interaction (KI)) is negligible or that FFM is more detrimental than FIM. Some American design codes also neglect KI (i.e., ATC-3-06 (1978), FEMA 369 (2001), FEMA 450 (2004)). Moreover, in FEMA 440 (2005), FEMA P-1050 (2015) and Japanese design codes KI is modeled as a low-pass filter to exploit the beneficial effect of KI. Modeling KI as a low-pass filter is reasonable for determining horizontal foundation input motion (HFIM); however KI also induces rocking foundation input motion (RFIM) to some degree depending on the embedment depth of the foundations and the mechanical properties of the soil. Additionally, according to Roesset (1980), filtering HFIM and neglecting RFIM leads to design forces being underestimated. Moreover, Mojtaba and Ghannad (2009) assert that RFIM has a significant effect on the nonlinear response of structures with deep foundations.

The effect of adjacent buildings on the response of a structure during an earthquake is known as structure-soil-structure interaction (SSSI) or dynamic cross interaction (DCI) and can be considered as a branch of SSI. According to Mason (2011) and Trombetta (2013), this phenomenon is not well understood and no design recommendations consider SSSI (or DCI) effect. However, with the growth of large cities situated on soft soils and exposed to seismic risks (e.g. Tokyo, Kobe, Nagoya, Istanbul), the effect of SSSI (or DCI) on seismic hazards is steadily increasing. Therefore, it should be determined whether this effect is beneficial or detrimental to the response of superstructures. Moreover, to the best of the author's knowledge,

there has been no parametric analysis of adjacent buildings that have different foundation embedment depths in order to determine the key parameters for such buildings.

1.2 Objective of the research

This research aims at determining the effects of SSI and SSSI (or DCI) on the responses of superstructures by conducting various parametric analyses. For the SSI branch of the study, a new lumped parameter model (LPM) that depends on the impedances of foundations with different embedment depths is constructed. These are placed on an elastic half-space with a Poisson ratio of 0.42 and shear wave velocities of 100 or 200 m/s to represent soft soil conditions. Nonlinear earthquake response analyses using the proposed LPM are then carried out using active-fault and subduction-zone earthquake records. This is done both with and without RFIM to assess the effects of RFIM on the ductility demands of structures, assuming ductility capacities of 2, 4, or 6 under fixed based conditions.

For the SSSI (or DCI) branch of the study, a wide analytical parametric study is conducted for different foundation types, embedment situations and fixed based natural frequencies of two or three closely spaced buildings. As soil model, elastic half-space and layered soil for different kinds of shear wave velocity and soil material damping are selected. Moreover, the effects of the mass and height of the superstructures on the DCI phenomenon is investigated. The mean power ratio (MPR) of the superstructures for adjacent case to single foundation case is selected as a measure parameter in this research, same as Alexander *et al*. (2013). The reasoning is that if the key parameters of the DCI phenomenon are understood, the importance of DCI effects on the design of structures can be determined more easily.

1.3 Organization of the text

This dissertation comprises six sections. In Section 1, an introduction of the research is given. In Section 2, the phenomenon of SSI is introduced and some literature on this topic is reviewed. In Section 3, the phenomenon of SSSI (or DCI) is introduced and some literature on this topic is reviewed. In Section 4, a study entitled “Effect of rocking foundation input motion on the nonlinear response characteristics of superstructures” is presented which considers only the SSI phenomenon. In Section 5, a study entitled “Dynamic behavior of adjacent buildings with different foundation embedment depths” is presented which considers both the SSI and SSSI (or DCI) phenomena. Finally, the conclusions of each section are given in Section 6.

References for Chapter1

Alexander, N. A., Ibraim, E., & Aldaikh, H. (2013). A simple discrete model for interaction of adjacent buildings during earthquakes. Computers & Structures, 124, pp.1-10.

Applied Technology Council, & Structural Engineers Association of California. (1978). Tentative provisions for the development of seismic regulations for buildings: a cooperative effort with the design professions, building code interests, and the research community (Vol. 510). Department of Commerce, National Bureau of Standards.

Aviles, J., & Perez-Rocha, L. E. (1998). Site effects and soil-structure interaction in the Valley of Mexico. Soil Dynamics and Earthquake Engineering, 17(1), pp.29-39.

Council, B. S. S. (2001). FEMA 369: NEHRP Recommended Provisions for Seismic Regulations for New Buildings and Other Structures, Commentary. Washington, DC.

FEMA, A. (2005). 440, Improvement of nonlinear static seismic analysis procedures. FEMA-440, Redwood City.

Mahsuli, M., & Ghannad, M. A. (2009). The effect of foundation embedment on inelastic response of structures. Earthquake Engineering & Structural Dynamics, 38(4), pp.423-437.

Mason, H. B. (2011). Seismic performance assessment in dense urban environments. University of California, Berkeley.

Mylonakis, G., & Gazetas, G. (2000). Seismic soil-structure interaction: beneficial or detrimental?. Journal of Earthquake Engineering, 4(03), pp.277-301.

Mylonakis, G., Syngros, C., Gazetas, G., & Tazoh, T. (2006). The role of soil in the collapse of 18 piers of Hanshin Expressway in the Kobe earthquake. Earthquake engineering & structural dynamics, 35(5), pp.547-575.

Moghaddasi, M., Cubrinovski, M., Chase, J. G., Pampanin, S., & Carr, A. (2011). Probabilistic evaluation of soil–foundation–structure interaction effects on seismic structural response. Earthquake Engineering & Structural Dynamics, 40(2), pp.135-154.

NEHRP Recommended Provisions for Seismic Regulations for New Buildings and Other Structures (FEMA 450): Provisions. Building Seismic Safety Council, National Institute of Building Sciences, 2004.

NEHRP Recommended Provisions for Seismic Regulations for New Buildings and Other Structures (FEMA P-1050): Provisions. Building Seismic Safety Council, National Institute of Building Sciences, 2015.

Roesset, J. M. (1980). A review of soil-structure interaction. Lawrence Livermore Laboratory.

Tezcan, S. S., & Ipek, M. (1972). Long distance effects of the 28 March 1970 Gediz Turkey earthquake. Earthquake Engineering & Structural Dynamics, 1(3), pp.203-215.

Trombetta, N. W. (2013). Seismic Soil-Foundation-Structure Interaction in Urban Environments. University of California, San Diego.

Chapter 2

Previous Research on Soil-structure Interaction

In conventional seismic structural design, the soil is considered to be a perfectly rigid and the free field motion (FFM), which is an earthquake record that is taken from the surface of the soil for the absence of building, is taken as foundation input motion (FIM). Although this approximation is appropriate for flexible buildings and stiff soil conditions, the effect of the soil on the dynamic response of a superstructure should be considered in analyses with other types of structure and soil in order to facilitate realistic earthquake design. This effect is known as soil-structure interaction (SSI). In this section the literature on SSI research is reviewed.

2.1 Early history of SSI

The pioneering work on this topic can be traced back to the 19th century, to research on determining the static stiffness of a half-space, which is very important for reliable SSI analysis (Kausel, 2010). The first researcher who analyzed the dynamic response of a circular disk on an elastic half-space is Erich Reissner (1936), who is known as the father of the dynamic SSI. It is interesting to note that the first analysis of soil and structure together is performed in Japan by Mononabe and Matsuo (1929) and Okabe (1926), which led to further interest about such analyses (Roesset, 2013). Merrit and Housner (1954) and Housner (1957) analyze soil/multistory building system that is referred to as an “analog computer”. That model neglects the horizontal compliance of the foundations, because from records on the foundation of a building and parking lot of the building, Merrit and Housner consider horizontal compliance to be ineffective. Instead,

they focus their attention on the effect of foundation rocking on the response of the superstructure. However, Meek and Veletsos (1972) assert that those results are unreliable because the soil response is not understood sufficiently until the work of Bycroft (1956). The research of Parmelee (1967) can be considered as a milestone for understanding the key aspect of the SSI problem (Meek and Veletsos, 1972). In that research, Parmelee asserts that the shear wave velocity is the key parameter for SSI and that the natural frequency of the soil-structure system is elongated by SSI. However, the main problem regarding the research of Parmelee (1967, 1968a, 1968b) is that, the fast Fourier transform (FFT) technique is not used for transforming the results from the frequency domain to the time domain. The first paper in which an FFT is used for this problem is that of Lui and Fagel (1971). Sarrazin (1970) and Sarrazin *et al.* (1972) also perform analyses based on Parmelee's model by using frequency independent springs and dashpots for the soil around buildings. They assert that the rocking effect of SSI is more important than the corresponding swaying effect. Meek and Veletsos (1972) and Veletsos and Meek (1974) improve a replacement oscillator, which has modified period and damping values to reflect SSI in a single degree of freedom system (SDOF) for the case of surface foundations. This model can be seen in Figure 2-1. They also emphasize the rocking effect of SSI especially for tall buildings for which the effective damping of the system diminishes at low frequency values. Jennings and Bielak (1973) and Bielak (1976) modeled an n story building coupled with elastic soil as a system of n+2 SDOF replacement oscillators. This requires a certain amount of mathematical manipulation because of the complex nature of the modal analysis of soil-structure systems. Thanks to the developments in computer technologies and the necessity for reliable designs of new nuclear power plants during the 1970s, more complex SSI

analyses are applied for research purposes and the modern era of SSI phenomenon has started (Kausel, 2010).

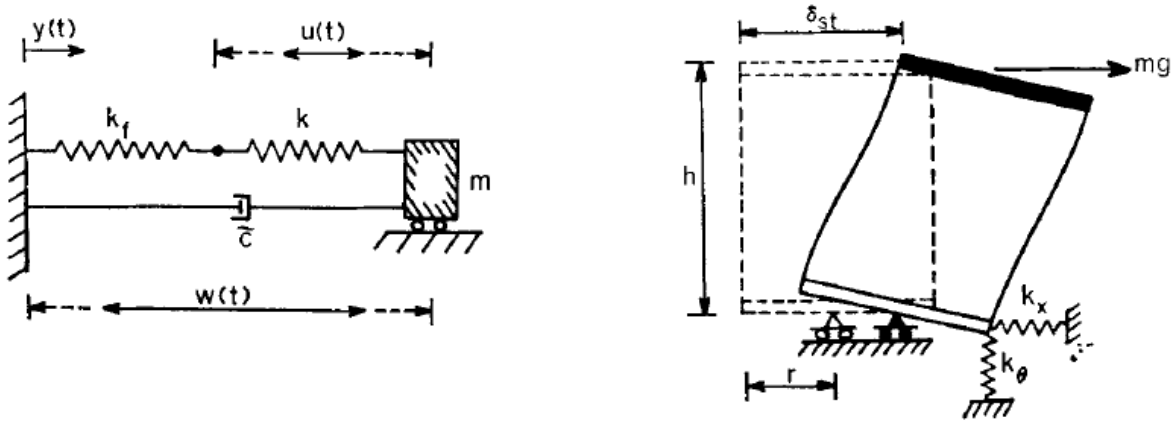

Figure 2-1: Replacement oscillator model (Veletsos and Meek, 1974)

2.2 Analysis methods of soil-structure systems

As mentioned in Section 2.1, the diversity of SSI research increases during the 1970s. Academic interest is focused on two methods in particular: the direct method and the substructure method. Furthermore, the interest on simple physical models of soil rises during the 1990s.

2.2.1 Direct method

In the direct method, soil and structures are modeled together, mainly by finite elements, and the analysis is performed in a single step. Since it is impossible to model unbounded soil by finite elements, an artificial boundary should be modeled on appropriate distance from the structure-foundation interface to represent the dynamical characteristics of the missing soil beyond the boundary.

2.2.2 Substructure method

Substructure method is introduced by Kausel (1974) because of the need to check the results of complex direct method analyses (Kausel, 2010). In this method, a three step solution is applied. In the first step, free field response of the soil without buildings and excavations is calculated. In the second step, the dynamic impedances of the soil are determined according to the excitation frequency. In the final step, the response of the superstructure is obtained by using the data from the first two steps. In the substructure method, it is convenient to subdivide the SSI problem into two subtopics: the kinematic interaction (KI) and the inertial interaction (II) as defined first by Whitman (1970). In KI, a superstructure and its foundation are considered as massless and because of difference in rigidity between the soil and the structure, the foundation input motion (FIM) occurs at the foundation level. This motion is then used for the next analysis, II, by considering only the mass properties of the superstructure. It is worth noting that this method is applicable to elastic or equivalent elastic systems, because KI+II analysis includes superposition principle. The substructure method of analysis can also be subdivided according to the method used for the scattering problem as shown in Figure 2-2 where coming wave is shown by arrows and the horizontal lines show the soil boundary. In the present study, exact impedances and FIM are calculated using the substructure method of analysis, and the flexible volume method is used.

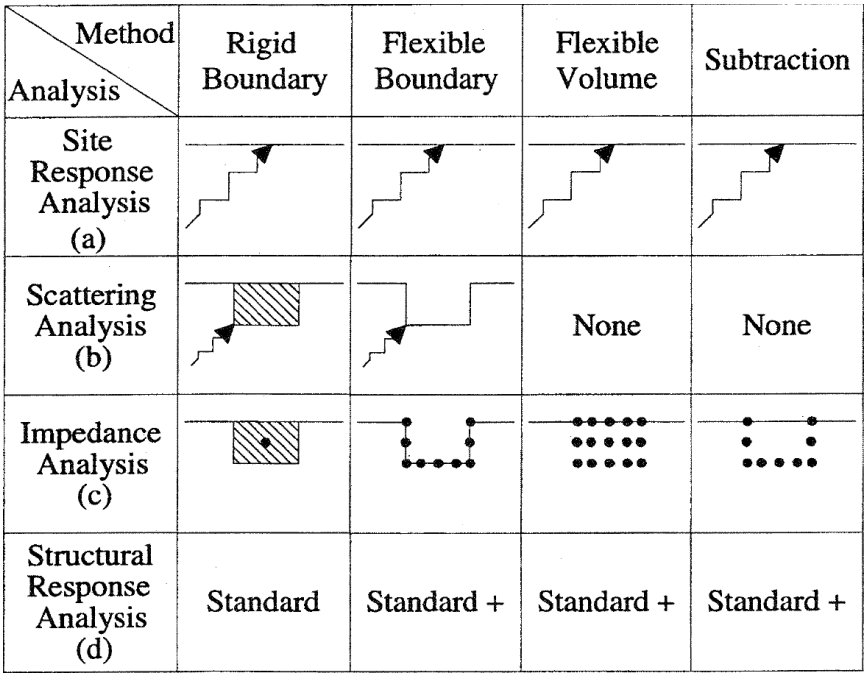

Figure 2-2: Substructure methods of SSI analysis (Ostadan, 2000)

2.2.3 Simple physical models

The substructure method for a rigid foundation and uniform-elastic soil conditions can be applied more simply by modeling the soil using springs, dashpots and masses. Because of the frequency dependence of the soil impedances, some accuracy is lost according to the selected soil model. However, if the uncertainties in the soil are considered, the loss of accuracy can become very low for engineering design purposes (Wolf, 1994). Research on the using simple soil models for SSI analyses can be subdivided into two subtopics: cone model and lumped parameter models.

(a) Cone models

The first attempt to create a simple physical model of soil can be traced back to Ehlers (1942), who models the soil by using a truncated semi-infinite cone for the vertical and horizontal motion of a foundation placed on an elastic half-space (Wolf and Deeks, 2004). Samples of cones for vertical, horizontal, rocking and torsional degree of freedoms are given in Figure 2-3. A spring, dashpot and mass model that depends on the aforementioned cone model of soil for the horizontal and rocking motion of the foundation placed on an elastic half-space is generated by Meek and Veletsos (1974). Moreover, there are further endeavors to model layered and incompressible soil conditions and embedded foundations by Meek and Wolf (1991, 1992a, 1992b, 1993). The textbooks written by Wolf (1994) and Wolf and Deeks (2004) give comprehensive insights into this topic. In the present research, foundation input motion (FIM) for embedded circular foundations is calculated using the MATLAB programs proposed by Wolf and Deeks (2004).

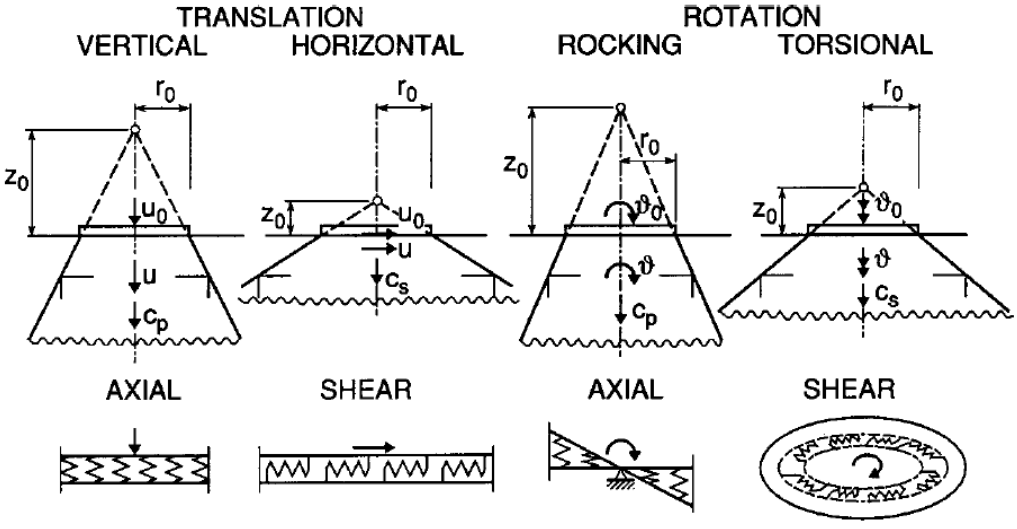

Figure 2-3: Cones for different degree of freedoms (Wolf and Deeks, 2004)

(b) Lumped parameter models

Models of soil based on simple frequency independent springs, dashpots and masses are known in general as lumped parameter models (LPMs). The difference between cone models and LPMs is that LPMs require exact values of soil impedances which are calculated by rigorous methods. The reliability of an LPM can be determined by the difference between its impedances and the aforementioned exact impedances. Because of its frequency independence, an LPM is convenient for the SSI analysis in time domain, which is inevitable for the nonlinear analysis of superstructures. Moreover, LPMs are easier to apply in SSI analysis than the method of transforming the impedances functions into an impulse response in time domains (Wolf and Obennhuber (1985), Wolf and Motosaka (1989a, 1989b), Meek (1990), Motosaka and Nagano (1992), Hayashi and Katsukura (1990) and Nakamura (2006a, 2006b, 2008a, 2008b)). This is because simple time stepping methods (such as the Newmark method used in the present study) can be applied to LPM models (Saitoh, 2012a). Moreover, there are also discrete-time filter methods for time domain analyses of SSI (Safak, 2006; Gash, 2015), but these are beyond the scope of the present study.

The simplest LPM is a sway-rocking model in which the soil impedances are represented by one constant spring and one constant dashpot. Although a sway-rocking model is suitable for the horizontal degree of freedom of a foundation placed on an elastic half-space, it is not suitable for the rocking degree of freedom of the same foundation because of the frequency dependence of the soil impedances for that degree of freedom. Moreover, according to Gash (2015), a sway-rocking model is not suitable for the nonlinear analysis of a superstructure even for the spring and dashpots calculated for fundamental frequency of soil-structure system. This is because the

fundamental frequency changes with time because of the nonlinearity of the superstructure, and hence a sway-rocking model may lead to inaccurate results for such analyses.

The many LPM models in the literature can be subdivided mainly as empirical LPMs and systematic LPMs (Saitoh, 2012a). There are also modal LPMs as created by Saitoh (2010, 2011, 2012b, 2012c), but these are beyond the scope of the present study.

(1) Empirical lumped parameter models

For such LPMs, the fitting of the impedances of the model to the exact values is done manually. The aforementioned sway-rocking model and the LPM created from a cone model by Meek and Veletsos (1974) can be classed in this group of LPMs. The LPM of Meek and Veletsos (1974) is improved by Wolf and Somaini (1986). There are also complex empirical LPMs of Nogami and Konagai (1986, 1988), De Barros and Luco (1990), Jean *et al.* (1990), and Saitoh (2007), but these are mainly for impedance functions that are strong dependent on the excitation frequency such as is the case for pile foundations. They are given in Figure 2-4.

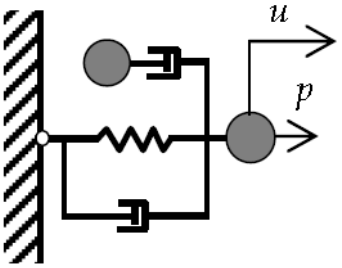

(a) Veletsos (1974); Wolf and Somaini (1986)

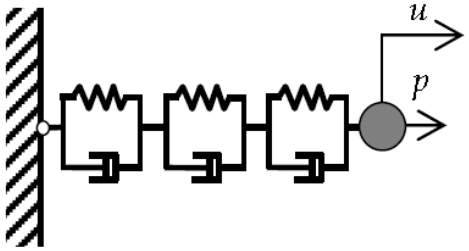

(b) Nogami and Konagai (1986, 1988)

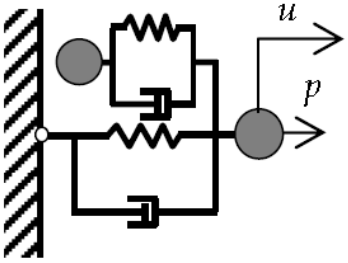

(c) De Barros and Luco (1990)

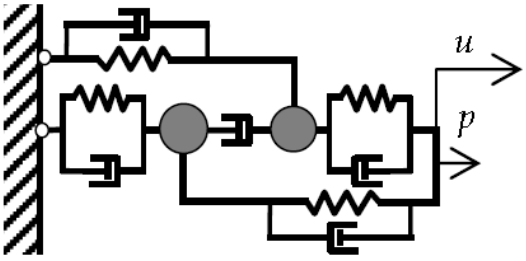

(d) Jean *et al*. (1990)

Figure 2-4: Some empirical lumped parameter models (Saitoh, 2012a)

(2) Systematic lumped parameter models

For such LPMs, the fitting of the impedances of the model to the exact values is done by systematically. Wolf (1994) is the first to propose the use of a partial-fraction expansion to create a mass–spring–damper LPM, and this now-common procedure is used in the present study to calculate the parameters of LPM. Paronesso and Wolf (1995) present a more advanced systematic procedure that also incorporates the adjacent foundations into the LPM. Wu and Cheng (2001) also present a systematic mass–spring–damper LPM by using a partial fraction expansion of the absolute values and phases of the impedances instead of their real and imaginary parts. However, Wu and Cheng assert that impedances of this LPM approximate to the exact values better for the translational degree of freedom than for the rocking degree of freedom. Nevertheless, the main problem with a LPM that includes masses is that input motion cannot be applied directly to the soil-structure system. Therefore, an intermediate calculation is necessary to determine driving forces (Wolf, 1994). Because of that, Wu and Lee (2002) propose a new LPM that includes no mass, but that model is only for surface foundations. Wu and Lee (2004) and Zhao and Du (2008) also improve the systematic procedure for LPMs by using continued fraction expansion instead of partial fraction expansion. For impedances that depended more strongly on frequency, Wang *et al.* (2013) create a systematic procedure for LPMs based on Chebyshev polynomial fractions.

2.3 SSI studies related to the study

As mentioned previously, the SSI effect can be analyzed under the subtopics of kinematic interaction (KI) which occurs because of a difference in rigidity between the foundations and the surrounding soil, and inertial interaction (II) which relates to the mass properties of the structure. Bielak (1974) analyze the response of embedded foundations under FFM neglecting the effect of

KI by using the frequency independent models of Novak (1973) and Novak and Sachs (1973). Aviles and Perez-Rocha (1996) also analyze the response of embedded foundations under FFM neglecting the effect of KI, whereas Aviles and Perez-Rocha (1998) use a replacement oscillator that incorporates KI effect. Moreover Aviles and Perez-Rocha (1999) suggest design concepts for linear structures considering SSI and KI. Takewaki *et al.* (2003) also analyze linear superstructures with embedded foundations by considering SSI and KI. They claim that the transfer function amplitudes diminish with increasing embedment depth but, for huge embedment ratio values, the phenomenon cannot be understood. According to Luco (1975), use of horizontal foundation input motion (HFIM) and RFIM instead of FFM is important for reasonable designs, especially for large foundations. Moreover, according to Morray (1975), the peak values of the acceleration response spectra are underestimated if the effect of the RFIM is neglected. For reliable design, Elsabee and Morray (1977) assert that RFIM should be considered in the analyses. Additionally, Pais and Kausel (1990) stress the importance of the effect of RFIM noting that effect of RFIM is stronger for steeply propagating SH waves than it is for shallowly propagating SH waves.

All the aforementioned studies include only elastic soil-structure systems. However, structures can respond beyond the elastic regions of their materials during a strong earthquake. The earliest studies of the response of elasto-plastic soil and a structure considering SSI is done by Minami (1973), Kobori *et al*. (1966), and Inoue *et al*. (1974). However, according to Bielak (1978), those studies are unreliable because they only consider the sway motion of the foundation. Vebric (1973) and Veletsos and Vebric (1974) assert that the effect of structural inelasticity diminishes the stiffness of the structure relative to that of the soil, and therefore the effect of SSI decreases the response. In contrast, according to Bielak (1978), at the resonant

frequency, structural deformations become large for an inelastic structure with a surface foundation if SSI is considered. Muller and Keintzel (1982) assert that SSI is beneficial for squat inelastic structures but negligible for slender inelastic structures with surface foundation. Ciampoli and Pinto (1995) say that SSI is not important for the inelastic demand of piers with surface foundations. Rodriguez and Montes (2000) claim that SSI has a negligible effect on the inelastic response of superstructures with surface foundations. Stewart *et al*. (2004) treated the KI effect as a low-pass filter and claim that KI reduces the inelastic response. Lin and Miranda (2008) research the effect of SSI on the maximum inelastic deformation of single degree of freedom (SDOF) systems by treating the KI effect as a low-pass filter also and came to the same conclusion as that of Stewart *et al*. (2004). However, according to Roesset (1980), filtering HFIM and neglecting RFIM gives unreliable results. Jarernprasert *et al*. (2013) analyze a SDOF elasto-plastic structure embedded in elastic soil without the KI effect. According to Mylonakis and Gazetas (2000), ductility demands of bridge piers increase for some earthquake motions and structural characteristics. Aviles and Perez-Rocha (2003) analyze the SDOF elastic and elasto-plastic structures embedded in elastic soil by considering the KI and RFIM effects using the approximate method proposed by Iguchi (1982) and they cannot determine that SSI is detrimental on elastic or elasto-plastic situation of superstructure. Pitilakis and Makris (2010) conduct dimensionless analysis to determine the seismic demand of yielding structures interacting with soil. They assert that seismic demand increases with increasing foundation soil mass and yielding displacement and that SSI is not always beneficial for the inelastic response of a superstructure. Karatzetzou and Pitilakis (2013) criticize the reliability of the FEMA 440 design code for determining performance-based seismic demand and claim that the FEMA 440 gives unreliable results for such analyses. There have been some attempts to determine the

strength reduction factor by considering SSI (Aviles and Perez-Rocha, 2005; Ghannad and Jahankhah, 2007) but these are beyond the scope of the present study. Mahsuli and Ghannad (2009) and Khanmohammadi *et al*. (2014) assert that the ductility demands for embedded foundations increase with increasing embedment ratio, especially for embedment ratios bigger than one because of the effect of RFIM.

References for Chapter2

Ahmadi, E., & Khoshnoudian, F. (2015). Near-fault effects on strength reduction factors of soil-MDOF structure systems. Soils and Foundations, 55(4), pp.841-856.

Avilés, J., & Pérez-Rocha, L. E. (1996). Evaluation of interaction effects on the system period and the system damping due to foundation embedment and layer depth. Soil Dynamics and Earthquake Engineering, 15(1), pp.11-27.

Aviles, J., & Perez-Rocha, L. E. (1998). Effects of foundation embedment during building-soil interaction. Earthquake Engineering and Structural Dynamics, 27(12), pp.1523-1540.

Avilés, J., & Pérez-Rocha, L. E. (1999). Diagrams of effective periods and dampings of soil-structure systems. Journal of geotechnical and geoenvironmental engineering, 125(8), pp.711-715.

Avilés, J., & Pérez‐Rocha, L. E. (2003). Soil‐structure interaction in yielding systems. Earthquake engineering & structural dynamics, 32(11), pp.1749-1771.

Avilés, J., & Pérez-Rocha, L. E. (2005). Influence of foundation flexibility on R μ and C μ factors. Journal of structural engineering, 131(2), pp.221-230.

Bielak, J. (1974). Dynamic behaviour of structures with embedded foundations. Earthquake Engineering & Structural Dynamics, 3(3), pp.259-274.

Bielak, J. (1976). Modal analysis for building-soil interaction. Journal of the Engineering Mechanics Division, 102(5), pp.771-786.

Bielak, J. (1978). Dynamic response of non‐linear building‐foundation systems. Earthquake Engineering & Structural Dynamics, 6(1), pp.17-30.

Ciampoli, M., & Pinto, P. E. (1995). Effects of soil-structure interaction on inelastic seismic response of bridge piers. Journal of structural engineering, 121(5), pp.806-814.

De Barros, F. C., & Luco, J. E. (1990). Discrete models for vertical vibrations of surface and embedded foundations. Earthquake engineering & structural dynamics, 19(2), pp.289-303.

Ehlers, G. (1942). The effect of soil flexibility on vibrating systems. Beton und Eisen, 41(21/22), pp.197-203.

Elsabee, F., & Morray, J. P. (1977). Dynamic behavior of embedded foundations. Massachusetts Institute of Technology, Department of Civil Engineering, Constructed Facilities Division.

Gash, R. J. H. (2015). On the Implementation and Applications of Discrete-Time Filters for Soil-Structure Interaction Substructure Analyses (Doctoral dissertation, UNIVERSITY OF CALIFORNIA, LOS ANGELES).

Ghannad, M. A., & Jahankhah, H. (2007). Site-dependent strength reduction factors for soil-structure systems. Soil Dynamics and Earthquake Engineering, 27(2), pp.99-110.

Hayashi, Y., & Katukura, H. (1990). Effective time-domain soil-structure interaction analysis based on FFT algorithm with causality condition. Earthquake Engineering and Structural Dynamics, 19(5), pp.693-708.

Housner, G. W. (1957). Interaction of building and ground during an earthquake. Bulletin of the Seismological Society of America, 47(3), pp.179-186.

Iguchi, M. (1982). An approximate analysis of input motions for rigid embedded foundations. Transactions of the Architectural Institute of Japan, 315, pp.61-75.

Inoue, Y., Kawano, M., & Maeda, Y. (1974). Dynamic response of nonlinear soil-structure systems. Technology Reports of the Osaka University, 24, pp.803-825.

Jarernprasert, S., Bazan-Zurita, E., & Bielak, J. (2013). Seismic soil-structure interaction response of inelastic structures. Soil Dynamics and Earthquake Engineering, 47, pp.132-143.

Jean, W. Y., Lin, T. W., & Penzien, J. (1990). System parameters of soil foundations for time domain dynamic analysis. Earthquake Engineering & Structural Dynamics, 19(4), pp.541-553.

Jennings, P. C., & Bielak, J. (1973). Dynamics of building-soil interaction. Bulletin of the Seismological Society of America, 63(1), pp.9-48.

Karatzetzou, A., Pitilakis, D. (2013). Performance-based seismic demand soil-foundation-structure systems. 4th ECCOMAS Thematic Conference on Computational Methods in Structural Dynamics and Earthquake Engineering.

Kausel, E. (1981). An explicit solution for the Green functions for dynamic loads in layered media. NASA STI/Recon Technical Report N, 82, 29505.

Kausel, E. (2010). Early history of soil–structure interaction. Soil Dynamics and Earthquake Engineering, 30(9), pp.822-832.

Kausel, E., Roesset, J., & Waas, G. (1974). Forced vibrations of circular foundations on layered media. Department of Civil Engineering, School of Engineering, Massachusetts Institute of Technology.

Khanmohammadi, L., Amiri, J. V., Davoodi, M. R., & Ghannad, M. A. (2014) Mathematical Analysis of Soil-Structure Interaction Including Kinematic and Inertial Interaction Effects. Jounal of mathematics and computer science, 12, pp.320-336.

Kobori, T., Minai, R., & Inoue, Y. (1966). On earthquake response of elasto-plastic structure considering ground characteristics. In Proc. Fourth World Conference Earthquake Engineering, Vol. 3, pp.117-132.

Lin, Y. Y., & Miranda, E. (2008). Kinematic soil-structure interaction effects on maximum inelastic displacement demands of SDOF systems. Bulletin of Earthquake Engineering, 6(2), pp.241-259.

Liu, S. C., & Fagel, L. W. (1971). Earthquake interaction by fast Fourier transform. Journal of the Engineering Mechanics Division, 97(4), pp.1223-1237.

Luco, J. E., Wong, H. L., & Trifunac, M. D. (1975). A note on the dynamic response of rigid embedded foundations. Earthquake Engineering & Structural Dynamics, 4(2), pp.119-127.

Lysmer, J., Ostadan, F., & Chin, C. C. (1999). A system for analysis of soil-structure interaction, SASSI 2000 theoretical manual. UC Berkeley.

Mahsuli, M., & Ghannad, M. A. (2009). The effect of foundation embedment on inelastic response of structures. Earthquake Engineering & Structural Dynamics, 38(4), pp.423-437.

Meek, J. W. (1990). Recursive analysis of dynamic phenomena in civil engineering. Bautechnik, 67, pp.205-210.

Meek, J. W., & Wolf, J. P. (1991). Insights on cutoff frequency for foundation on soil layer. Earthquake Engineering & Structural Dynamics, 20(7), pp.651-665.

Meek, J. W., & Wolf, J. P. (1992a). Cone models for homogeneous soil. I. Journal of geotechnical engineering, 118(5), pp.667-685.

Meek, J. W., & Wolf, J. P. (1992b). Cone models for soil layer on rigid rock. II. Journal of geotechnical engineering, 118(5), pp.686-703.

Meek, J. W., & Wolf, J. P. (1993). Cone models for nearly incompressible soil. Earthquake engineering & structural dynamics, 22(8), pp.649-663.

Meek, J. W., & Wolf, J. P. (1994). Cone models for embedded foundation. Journal of geotechnical engineering, 120(1), pp.60-80.

Meek, J., & Veletsos, A. S. (1972). Dynamic analysis and behavior of structure-foundation systems. Department of Civil Engineering, Rice University.

Meek, J., & Veletsos, A. S. (1974). Simple models for foundations in lateral and rocking motion. In Proceedings of the 5th World Conference on Earthquake Engineering, Vol. 2, pp.2610-2613.

Merritt, R. G., & Housner, G. W. (1954). Effect of foundation compliance on earthquake stresses in multistory buildings. Bulletin of the Seismological Society of America, 44(4), pp.551-569.

Minami, T. (1973). Elastic-plastic earthquake response of soil-building systems. NTIS.

Mononobe, N., & Matsuo, H. (1929, October). On the determination of earth pressures during earthquakes. In Proceedings, World Engineering Congress, Vol. 9, pp. 179-187.

Morray, J. P. (1975). The kinematic interaction problem of embedded circular foundations (Doctoral dissertation, Massachusetts Institute of Technology).

Motosaka, M., & Nagano, M. (1992). Recursive evaluation of convolution integral in nonlinear soil–structure interaction analysis and its applications. Journal of Structural and Construction Engineering (AIJ), 436, pp.71-80.

Muller, F. P., & Keintzel, E. (1982, September). Ductility requirements for flexibly supported antiseismic structures. In Proceedings of the 7th European conference on earthquake engineering, Vol. 3, pp. 27-34.

Mylonakis, G., & Gazetas, G. (2000). Seismic soil-structure interaction: beneficial or detrimental?. Journal of Earthquake Engineering, 4(03), pp.277-301.

Nakamura, N. (2006a). A practical method to transform frequency dependent impedance to time domain. Earthquake engineering & structural dynamics, 35(2), pp.217-231.

Nakamura, N. (2006b). Improved methods to transform frequency‐dependent complex stiffness to time domain. Earthquake engineering & structural dynamics, 35(8), pp.1037-1050.

Nakamura, N. (2008a). Transform methods for frequency‐dependent complex stiffness to time domain using real or imaginary data only. Earthquake Engineering & Structural Dynamics, 37(4), pp.495-515.

Nakamura, N. (2008b). Nonlinear response analysis considering dynamic stiffness with both frequency and strain dependencies. Journal of engineering mechanics, 134(7), pp.530-541.

Nogami, T., & Konagai, K. (1986). Time domain axial response of dynamically loaded single piles. Journal of Engineering Mechanics, 112(11), pp.1241-1252.

Nogami, T., & Konagai, K. (1988). Time domain flexural response of dynamically loaded single piles. Journal of Engineering Mechanics, 114(9), pp.1512-1525.

Novák, M. (1973). Vibrations of embedded footings and structures. American Society of Civil Engineers.

Novak, M., & Sachs, K. (1973). Torsional and coupled vibrations of embedded footings. Earthquake Engineering & Structural Dynamics, 2(1), pp.11-33.

Okabe, S. (1926). General theory of earth pressure. Journal of the Japanese Society of Civil Engineers, 12(1), P.311.

Pais, A. L., & Kausel, E. (1990). Stochastic response of rigid foundations. Earthquake Engineering & Structural Dynamics, 19(4), pp.611-622.

Parmelee, R. A. (1967). Building-foundation interaction effects. Journal of the Engineering Mechanics Division, 93(2), pp.131-152.

Parmelee, R. A., Perelman, D. S., Lee, S. L., & Keer, L. M. (1968a). Seismic response of structure-foundation systems. Journal of the Engineering Mechanics Division, 94(6), pp.1295-1316.

Paronesso, A., & Wolf, J. P. (1995). Global lumped‐parameter model with physical representation for unbounded medium. Earthquake engineering & structural dynamics, 24(5), pp.637-654.

Perelman, D. S., Parmelee, R. A., & Lee, S. L. (1968b). Seismic response of single-story interaction systems. Journal of the Structural Division.

Pitilakis, D., & Makris, N. (2010). A study on the effects of the foundation compliance on the response of yielding structures using dimensional analysis. Bulletin of Earthquake Engineering, 8(6), pp.1497-1514.

Reissner, E. (1936). Stationäre, axialsymmetrische, durch eine schüttelnde Masse erregte Schwingungen eines homogenen elastischen Halbraumes. Archive of Applied Mechanics, 7(6), pp.381-396.

Rodriguez, M. E., & Montes, R. (2000). Seismic response and damage analysis of buildings supported on flexible soils. Earthquake engineering & structural dynamics, 29(5), pp.647-665.

Roesset, J. M. (1980). A review of soil-structure interaction. Lawrence Livermore Laboratory.

Roesset, J. M. (2013). Soil Structure Interaction The Early Stages. Journal of Applied Science and Engineering, 16(1), 1r8.

Şafak, E. (2006). Time-domain representation of frequency-dependent foundation impedance functions. Soil Dynamics and Earthquake Engineering, 26(1), pp.65-70.

Saitoh, M. (2007). Simple model of frequency-dependent impedance functions in soil-structure interaction using frequency-independent elements. Journal of Engineering Mechanics, 133(10), pp.1101-1114.

Saitoh, M. (2010). Equivalent One-Dimensional Spring-Dashpot System Representing Impedance Functions of Structural Systems with Non-Classical Damping. Computer Modeling in Engineering and Sciences (CMES), 67(3), P.211.

Saitoh, M. (2011). Lumped parameter models representing impedance functions at the interface of a rod on a viscoelastic medium. Journal of Sound and Vibration, 330(9), pp.2062-2072.

Saitoh, M. (2012a). Application of a Highly Reduced One-Dimensional Spring-Dashpot System to Inelastic SSI Systems Subjected to Earthquake Ground Motions. INTECH Open Access Publisher.

Saitoh, M. (2012b). On the performance of lumped parameter models with gyro‐mass elements for the impedance function of a pile‐group supporting a single‐degree‐of‐freedom system. Earthquake Engineering & Structural Dynamics, 41(4), pp.623-641.

Saitoh, M. (2012c). A one‐dimensional lumped parameter model representing impedance functions in general structural systems with proportional damping. International Journal for Numerical Methods in Engineering, 90(3), pp.353-368.

Sarrazin, M. A. (1970). Soil-structure interaction in earthquake resistant design. School of Engineering, Massachusetts Inst. of Technology.

Sarrazin, M. A., Roesset, J. M., & Whitman, R. V. (1972). Dynamic soil-structure interaction. Journal of the Structural Division, 98(st 7).

Stewart, J. P., Comartin, C., & Moehle, J. P. (2004). Implementation of soil–structure interaction models in performance based design procedures. Proc. 13th WCEE, Vancouver, BS, Canada, P.1546.

Takewaki, I., Takeda, N., & Uetani, K. (2003). Fast practical evaluation of soil–structure interaction of embedded structures. Soil Dynamics and Earthquake Engineering, 23(3), pp.13-20.

Vebric, B. (1973). Analysis of certain structure-foundation interaction systems (Doctoral dissertation, Rice University).

Veletsos, A. S., & Meek, J. W. (1974). Dynamic behaviour of building‐foundation systems. Earthquake Engineering & Structural Dynamics, 3(2), pp.121-138.

Veletsos, A. S., & Verbic, B. (1974). Dynamics of elastic and yielding structure-foundation systems. In Memorias, 5th World Conference on Earthquake Engineering, Roma.

Wang, H., Liu, W., Zhou, D., Wang, S., & Du, D. (2013). Lumped-parameter model of foundations based on complex Chebyshev polynomial fraction. Soil Dynamics and Earthquake Engineering, 50, pp.192-203.

Whitman, R. V. (1970). SOIL-STRUCTURE INTERACTION. Massachusetts Inst. of Tech., Cambridge.

Wolf, J. P. (1994). Foundation vibration analysis using simple physical models. Pearson Education.

Wolf, J. P., & Deeks, A. J. (2004). Foundation vibration analysis: A strength of materials approach. Butterworth-Heinemann.

Wolf, J. P., & Motosaka, M. (1989a). Recursive evaluation of interaction forces of unbounded soil in the time domain. Earthquake engineering & structural dynamics, 18(3), pp.345-363.

Wolf, J. P., & Motosaka, M. (1989b). Recursive evaluation of interaction forces of unbounded soil in the time domain from dynamic‐stiffness coefficients in the frequency domain. Earthquake engineering & structural dynamics, 18(3), pp.365-376.

Wolf, J. P., & Obernhuber, P. (1985). Non‐linear soil‐structure‐interaction analysis using dynamic stiffness or flexibility of soil in the time domain. Earthquake engineering & structural dynamics, 13(2), pp.195-212.

Wu, W. H., & Chen, C. Y. (2001). Simple lumped‐parameter models of foundation using mass‐spring‐dashpot oscillators. Journal of the Chinese Institute of Engineers, 24(6), pp.681-697.

Wu, W. H., & Lee, W. H. (2002). Systematic lumped‐parameter models for foundations based on polynomial‐fraction approximation. Earthquake engineering & structural dynamics, 31(7), pp.1383-1412.

Wu, W. H., & Lee, W. H. (2004). Nested lumped‐parameter models for foundation vibrations. Earthquake engineering & structural dynamics, 33(9), pp.1051-1058.

Zhao, M., & Du, X. (2008). High-order lumped-parameter model for foundation based on continued fraction. Beijing, The 14th WCEE.

Chapter 3

Previous Research on Structure-soil-structure Interaction or Dynamic Cross Interaction

In large cities built on soft soil, adjacent buildings affect each other in some manner during an earthquake. This effect is termed structure-soil-structure interaction (SSSI) by Luco and Contesse (1973), dynamic cross interaction (DCI) by Kobori *et al*. (1973), and through soil coupling (TSC) by Lee and Wesley (1973) (Aldaikh *et al*., 2015). In the present study, as tends to be the case in research done in Japan about this topic, this phenomenon is referred to mainly as DCI. In this section, the literature on DCI research is reviewed.

3.1 Review of analytical DCI research

3.1.1 Research neglecting the effect of superstructures

Studies of DCI begin by analyzing the interaction between two or more adjacent foundations while neglecting any effects from the superstructures. Such research can be termed foundation–soil–foundation interaction (FSFI), and can be considered as a branch of DCI. Richardson (1969) and Warburton *et al*. (1971, 1972) analyze adjacent bodies for vertical harmonic motions (Lou *et al*., 2011). MacCalden and Matthiesen (1973) study the vertical, horizontal and rocking harmonic responses of two adjacent foundations analytically and experimentally, but the results of these two analyses do not agree. Bielak and Coronato (1981) apply the boundary element method (BEM) to determine the responses of two adjacent foundations and emphasizing the phase differences between them, and according to the results it

is asserted that non-vertically incident seismic waves have an important effect on the cross interaction between foundations. Yoshida *et al*. (1984) also apply BEM to determine the responses of two adjacent foundations and obtain similar findings to those of as Bielak and Coronato (1981). Lin *et al*. (1987) model adjacent embedded foundations and soil using a three-dimensional (3D) finite element method (FEM). From their results, they claim that FSFI increases the coupling between horizontal and vertical motion and between rocking and torsional motion. They also claim that because of the FSFI, the embedment of foundations increases the effect of inertia on the responses of the foundations. Chouw and Schmid (1990) apply 3D BEM to determine the responses of adjacent foundations placed on layered soil, and conclude that FSFI depends on the direction of the excitation and that bedrock has no particular effect on FSFI.

Qian and Beskos (1995) analyze more than two surface foundations by 3D BEM, and claim that neglecting the FSFI in the design codes is not always convenient. FSFI increases the rigidity for vertical and horizontal motions at low excitation frequency and for rocking and torsional motion at high frequency. Finally, the number of adjacent foundations is important for horizontal and vertical motions but not so important for rocking and torsional motion of foundations. Qian and Beskos (1996) also analyze two surface foundations for different incidences of excitation by using 3D BEM, and assert that FSFI causes a phase difference between the motions of adjacent foundations. The effect of FSFI on the rocking responses is more severe than on the horizontal responses of foundations. Romanini *et al*. (1996) develop a new analysis method for adjacent foundations known as the "substructure deletion method". From the results of analyzing adjacent embedded foundation they claim that the effect of soil material damping is important for the FSFI phenomenon. Betti (1997) also uses the substructure deletion method to determine the FSFI effect on more than two adjacent embedded foundations,

giving importance to the embedment of the foundations. It is asserted that FSFI has more effect on the low frequency range of the horizontal, rocking and torsional impedances. Karabalis and Mohammadi (1998) use 3D BEM analysis to determine the FSFI effect on adjacent foundations placed on layered soil and note that FSFI is important for shallow soft layers placed on rigid bedrock. Tham *et al*. (1998) investigate the effect of foundation flexibility on the FSFI phenomenon, and note that the vertical responses of foundations increase with foundation flexibility under incident excitation.

3.1.2 Research considering the effect of superstructures

Research on DCI that also considers the effect of superstructures is needed for the reliable design of nuclear power plants (NPPs) which comprise reactor buildings, turbine buildings, and control buildings built closely to each other (Lou *et al*., 2011). To this end, Lee and Wesley (1973) use 3D analysis to determine the effect of DCI on NPPs mainly giving importance to the structural mass of adjacent buildings. From their results, Lee and Wesley assert that the layout of NPP buildings is important for the DCI effect. The layout of the NPP buildings selected for this study can be seen in Figure 3-1.

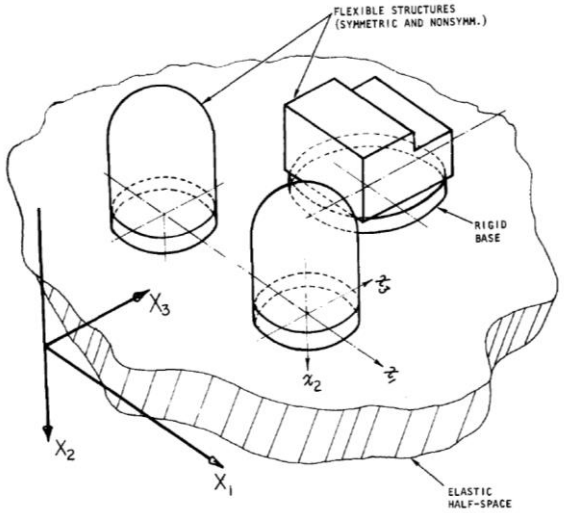

Figure 3-1: Layout of NPP buildings analyzed for DCI (Lee and Wesley, 1973)

Luco and Contesse (1973) investigate the anti-plane DCI (for excitation perpendicular to the direction of adjacent buildings) of two-dimensional (2D) adjacent shear walls for a vertically incident SH wave. They note that small buildings are strongly affected by large adjacent buildings.

Kobori *et al*. (1973) analyze the case of adjacent structures with surface foundations and examine the effect of soil layering on the DCI phenomenon. From their results Kobori *et al*. note that the effect of DCI should be considered for buildings in large cities built on soft soil. Kobori and Kusakabe (1980) use the thin layer method (TLM) to determine the DCI effect between two embedded structures. They note that the effect of DCI diminishes the responses of identical adjacent buildings. However, for adjacent structures of different natural periods and masses, the DCI effect can increase the response. Ratios of maximum responses of the structures considering to neglecting the DCI effect are given in Figure 3-2, schematically. Black circles shows where the detrimental effect of DCI is observed. In this figure ω, V_s, R_0, and x are fixed based circular frequency of superstructures, shear wave velocity of soil, radius of foundation and clearance between buildings, respectively.

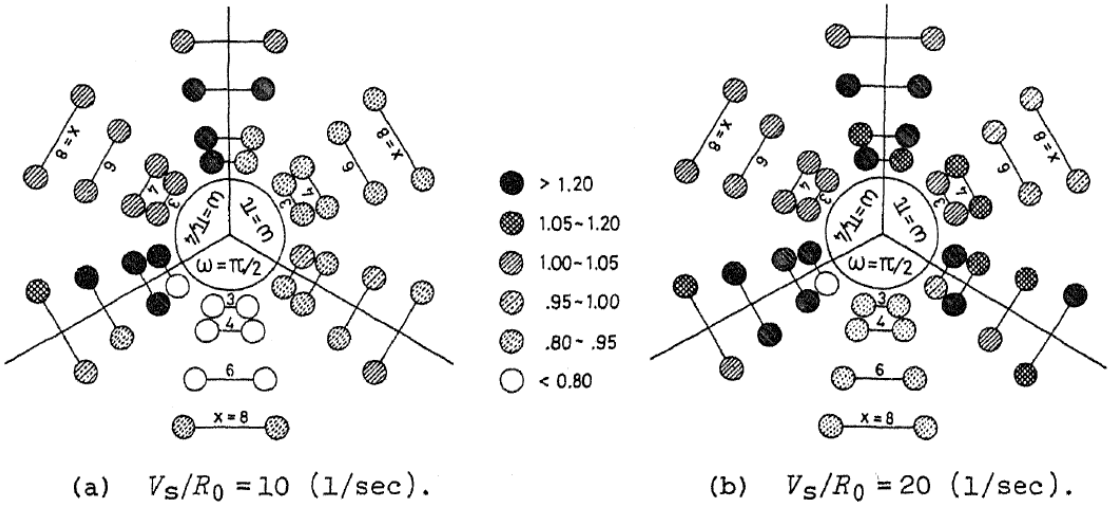

Figure 3-2: Ratios of maximum responses for adjacent situation to single situation (Kobori and Kusakabe, 1980)

Wong and Trifunac (1975) analyze two or more adjacent buildings to determine the anti-plane DCI effect for different incidence angles of excitation. They note that the clearance between foundations is a key parameter of the DCI, and small and light buildings are more affected by DCI than large and heavy buildings, and that, for non-vertical incident excitation, the layout of buildings is important for determining the DCI effect accurately. Aydinoglu and Cakiroglu (1977) use 2D FEM analysis based on a discrete soil stiffness matrix procedure to determine the DCI effect. They note that DCI affects rigid and short buildings more severely, however radiation damping of soil is not considered in their study. Matthees and Magiera (1982) conduct a large parametric study by using 2D FEM to determine the DCI effect between adjacent buildings while also considering the inelastic behavior of the soil and the superstructures. They use the excitation taken from the TAFT earthquake, and note that shallower soil is more critical than deeper soil for the DCI phenomenon. Imamura *et al*. (1992) use mixed BEM–FEM to analyze the interactions between an embedded and closely built turbine, reactor and control building of a NPP. They note that the masses of the adjacent superstructures and the soil between the buildings are important for determining the DCI effect. Wang and Schmid (1992) also use mixed BEM-FEM for adjacent structures with distributed and lumped masses, but conclude that more research is needed for the case of three adjacent buildings.

To determine the effect of DCI on regular buildings, Behnamfar and Sugimura (1998, 1999) analyze two adjacent structures for body and surface waves by considering the spatial variation of earthquake motions. They note that the DCI effect increases the maximum response of low and medium-rise buildings, whereas it decreases the maximum response of high-rise buildings. Lehman and Antes (2001) develop a new method for soil for use in DCI research known as the “symmetric Galerkin boundary element method”. They model superstructures

using FEM, and from their results, they note that such soil-structure modelling gives reasonable results. Wen (2006) determines the impedances and input motions of massless mat foundations adjacent to 3, 6 and 10 story buildings. Moreover, Wen and Fukuwa (2006) conduct similar research for pile foundations, and adjacent building model in that study is given in Figure 3-3.

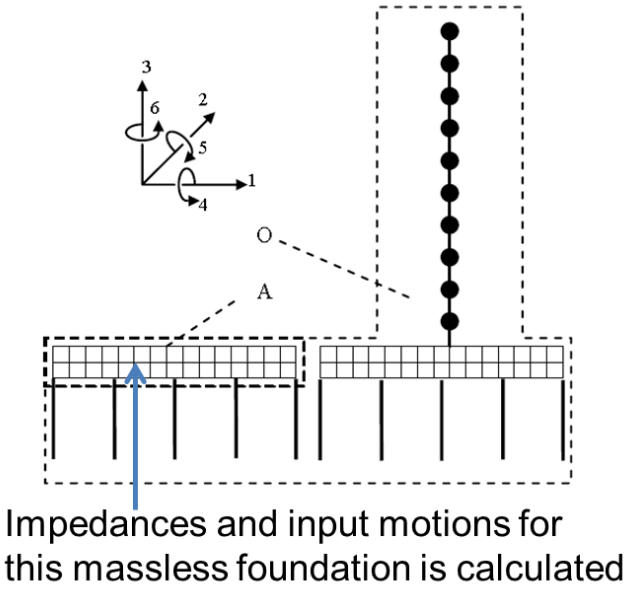

Figure 3-3: Adjacent building model (Wen and Fukuwa, 2006)

Yahyai *et al*. (2008) analyze 32 story adjacent buildings for different clearance values. From their results they note that DCI has a detrimental effect on base shear and lateral displacement, and that the period elongation effect of DCI is seen mainly in the first mode of the superstructures.

Padron *et al*. (2009) analyze adjacent pile-supported buildings by using mixed BEM-FEM analysis to determine the effect of in-plane and anti-plane DCI on the response of superstructures. They note that the worst effect of DCI is seen for buildings that are separated by half the shear wavelength of the soil as calculated by the natural period of one soil-structure system; the highest responses are seen on buildings that are placed between two buildings.

Alamo *et al*. (2015) conduct similar research for obliquely incident seismic waves and note that the DCI effect is important for short identical structures with pile foundations. Rahgozar and Ghandil (2011) and Rahgozar (2015) analyze 3D models of buildings with pile foundations by using the direct method of analysis for linear superstructures and equivalent-linear soil. From their results they note that the effect of DCI is detrimental for shorter buildings adjacent to taller buildings.

Bolisetti and Whittaker (2011) use frequency-domain methods to analyze NPP structures and note that the effect of DCI mainly on the rocking frequencies of structures and mass ratio of two adjacent buildings is an important parameter for the DCI phenomenon. Nakamura *et al*. (2011) conduct 3D FEM analysis to determine the DCI effect on NPPs and note that ground irregularity is important for the responses of NPP because of the DCI effect. However, Yue *et al*. (2013) assert that the effect of DCI is not important for NPPs. Roy *et al*. (2015) study on the DCI effect for light structures adjacent to heavy structures and heavy structures adjacent to heavy structures for NPPs, and conclude that the DCI effect is too complex to be generalized by a set of key parameters.

Knappett *et al.* (2015a, 2015b) examine the effect of soil nonlinearity on the DCI phenomenon in analytical and experimental analyses. They note that the DCI effect increases the permanent rotation of foundations which is important for determining seismic performances of adjacent buildings accurately. Madani *et al.* (2015) and Ghandil and Aldaikh (2016) determine the pounding effect between inelastic adjacent buildings considering also the DCI effect and claim that the DCI effect should be considered when determining pounding forces. Ghandil *et al.* (2016) consider soil inelasticity by using the near-field method developed by Ghandil and

Behnamfar (2015) and claim that the responses of superstructures are dominated more by the masses of adjacent structures than by their heights or periods if in-plane DCI is considered.

It is asserted in the present dissertation that it is necessary first to address the DCI effect for elastic soil-structure conditions by detailed parametric analyses before considering nonlinear soil-structure behavior. This is because there are still points of uncertainty in DCI research under elastic conditions, such as the difference between the DCI effects for mat and pile foundations, and the effect of DCI on adjacent buildings with different foundation embedment depths.

3.1.3 Analytical DCI research by using simple models

There have also been endeavors to create simple models to determine the DCI effect on structures. Mulliken and Karabalis (1998), develop a frequency independent simple model that also includes a time lag effect of wave radiation between foundations. Naserkhaki and Pourmohammad (2012) analyze adjacent twin buildings and Naserkhaki et al. (2014) use the aforementioned simple model to investigate pounding effect between adjacent buildings. Alexander et al. (2013) also suggest a frequency independent simple model by only considering the rocking motion interaction between foundations and neglecting the time lag effect of wave radiation between foundations. They analyze adjacent buildings and single buildings to obtain the ratio of these two situations which is known as the mean power ratio (MPR) of superstructures. MPR is selected as an index for determining the DCI effect. Aldaikh *et al.* (2015) analyze three adjacent buildings by using the same simple model and also take the MPR of superstructures as an index value. However, only surface foundations are treated in the research mentioned in this section.

3.2 Review of the experimental DCI research

To assess the validity of the results of the analytical studies, experimental studies are inevitable. Although a history of experimental research on DCI is given in this section, it is important to stress that only analytical analysis is conducted in the present study.

Kobori *et al*. (1977) conduct experimental and analytical studies to determine the DCI effect and note that the DCI effect should be considered in the design of structures built in large cities. Mizuno (1980) applies micro-tremor, forced vibration and earthquake observation for full-scale and model adjacent buildings, and main effect of the DCI is seen for earthquake observations. Celebi (1993a, 1993b) observes wave transfer between adjacent buildings in the data obtained from two closely adjacent buildings in the 1987 Whittier-Narrows Earthquake. To determine the effect of DCI on regular buildings, Matsuyama *et al*. (2001) conduct micro-tremor and forced vibration tests on 3 and 6 story buildings built close together. They note that the effect of DCI is more important on the 3 story building than on the 6 story building and that the DCI effect is conveyed by rocking and torsion of the building. Moreover, Hirono *et al*. (2009) conduct experiments on the same buildings by increasing the number of the measurement points and improving the animation program used to show the responses of these structures. Nuclear Power Engineering Corporation (NUPEC) conducts a long-term project (1994-2001) to determine the DCI effect on NPPs, comprising field tests, laboratory tests, and computer analyses for embedded and surface foundation cases (Kitada *et al*., 1999; Yano *et al*., 2000; Kitada *et al*., 2001; Hirotani *et al*., 2001; Kusama *et al*., 2003; Yano *et al*., 2003; Kitada *et al*., 2004). As a general result of this project, it is declared that the effect of DCI on NPPs is negligible. However, according to the results of laboratory and analytical studies, DCI increases the responses of certain superstructures even though this effect in not seen in field tests.

Therefore further research is needed to clarify this situation. Moreover, Xu *et al*. (2004), Broc (2006) and Clouteau *et al*. (2012) use analytical analyses to compare the results of NUPEC project.

Behnamfar and Sugimura (2000) verify 2D BEM analysis results by means of data recorded from twin buildings in Tohoku University, and good agreement between the results is obtained. Ikeda *et al*. (2004) excite adjacent pile foundations (without superstructures), and note that the experimental results are in reasonable agreement with those from the flexible volume method of analysis, which is also used in the present dissertation to determine the DCI effect. Li *et al*. (2012) excite adjacent 12 story reinforced concrete structures on a shaking table. From their results they assert that DCI increases the damage level of such structures, especially for strong ground motion. Trombetta *et al*. (2013a, 2013b, 2014) conduct a series of centrifuge tests to determine the in-plane, anti-plane and combined DCI effects on the nonlinear behavior of adjacent structures. They note that the restraining effect is more dominant than the wave based effect of DCI for an inelastic frame structure with a highly nonlinear foundation response. They also note that the restraining effect of DCI should be considered for low and medium intensity earthquakes, in which the soil and superstructure exhibit low-inelastic behavior. Bolisetti and Whittaker (2015) create a computer model of this centrifuge test. Barrios and Chouw (2015) conduct shaking table experiments by using a laminar box filled with soft sand to investigate the effect of DCI on the natural period difference of adjacent buildings. They note that buildings with higher natural frequency are more vulnerable to DCI than are buildings with lower natural frequency. Larkin *et al*. (2016) apply shaking table tests with a laminar box for 4 adjacent buildings, and claim that the DCI effect is more visible for adjacent buildings with different natural periods because of the energy transfer among them. Aldaikh *et al*. (2015, 2016) conduct

shaking table experiments on three adjacent buildings by using foam to represent soft soil conditions. They conclude that their experimental results are in good agreement with results obtained from a simple model created by the same authors.

3.3 Review of site-city interaction research

Although site-city interaction (SCI) is considered as a branch of DCI, it is not true in some sense. According to Mason (2011), DCI and SCI differ in two aspects. Firstly, DCI studies consider only the interaction of a limited number of structures, whereas SCI studies can include all the buildings in a city. Secondly, the SCI is a subject that is more suited to engineering seismologists who have a deep knowledge about complex wave propagation in complex media, whereas DCI studies are conducted mainly by structural and geotechnical engineers. Although SCI and DCI are separate topics in earthquake engineering, the results of an SCI study should be followed by the DCI research to establish the reliability of the former analysis. The main contributions to SCI have been made by Chávez-Garcıa and Cárdenas (2002), Guegen *et al*. (2002), Tsogka and Wirgin (2003), Boutin and Roussilon (2004), Semblat *et al*. (2004), Groby *et al*. (2005), Kham *et al*. (2006), Semblat *et al*. (2008), Ghergu and Ionescu (2009), Isbiliroglu *et al*. (2014), Ghiocel *et al*. (2014), Chen and Li (2015), and Schwan *et al*. (2016). However, the SCI effect is beyond the scope of the present dissertation.

References for Chapter3

Álamo Meneses, G. M., Padrón Hernández, L. A., Aznárez González, J. J., & Maeso Fortuny, O. (2015). Structure-soil-structure interaction effects on the dynamic response of piled structures under obliquely-incident seismic shear waves.

Aldaikh, H., Alexander, N. A., Ibraim, E., & Knappett, J. (2016). Shake table testing of the dynamic interaction between two and three adjacent buildings (SSSI). Soil Dynamics and Earthquake Engineering, 89, pp.219-232.

Aldaikh, H., Alexander, N. A., Ibraim, E., & Oddbjornsson, O. (2015). Two dimensional numerical and experimental models for the study of structure–soil–structure interaction involving three buildings. Computers & Structures, 150, pp.79-91.

Alexander, N. A., Ibraim, E., & Aldaikh, H. (2013). A simple discrete model for interaction of adjacent buildings during earthquakes. Computers & Structures, 124, pp.1-10.

Aydinoglu, M. N., & Cakiroglu, A. (1977). Dynamic interaction between soil and a group of buildings. In Proc. 6th World Conference on Earthquake Engineering, Vol. 4, pp.133-138.

Barrios, G., Chouw, N. (2015). Experimental investigations of interaction between structure, soil and adjacent structures. In NZSEE Conference, New Zealand.

Behnamfar, F., & Sugimura, Y. (1999). Dynamic response of adjacent structures under spatially variable seismic waves. Probabilistic Engineering Mechanics, 14(1), pp.33-44.

Behnamfar, F., Sugimura, Y. (1998) Cross-interaction of surface and embedded structures subject to spatial variation of ground motion. J. Struct. Constr. Eng., AIJ, No.507, pp.69-77.

Behnamfar, F., Sugimura, Y. (2000). Response analysis of adjacent structures and comparison with recorded data. In 12th world conference on earthquake engineering, New Zealand.

Betti, R. (1997). Effects of the dynamic cross‐interaction in the seismic analysis of multiple embedded foundations. Earthquake engineering & structural dynamics, 26(10), pp.1005-1019.

Bielak, J., & Coronate, J. A. (1981). Response of multiple-mass systems to nonvertically incident seismic waves. Proceedings of the international conference recent advance geotech earthquake engineering soil dynamic, St. Louis, pp.801-804.

Bolisetti, C. (2014). Site Response, Soil-Structure Interaction and Structure-Soil-Structure Interaction for Performance Assessment of Buildings and Nuclear Structures (Doctoral dissertation, Faculty of the Graduate School of the University at Buffalo, State University of New York).

Bolisetti, C., & Whittaker, A. S. (2011). Seismic structure–soil–structure interaction in nuclear power plant structures. Transactions, SMiRT, 21, pp.6-11.

Bolisetti, C., Whittaker, A.S. (2015) Structure–soil–structure interaction. Transactions, SMiRT 23.

Boutin, C., & Roussillon, P. (2004). Assessment of the urbanization effect on seismic response. Bulletin of the Seismological Society of America, 94(1), pp.251-268.

Broc, D. (2006, January). Soil-Structure Interaction: Theoretical and Experimental Results. In ASME 2006 Pressure Vessels and Piping/ICPVT-11 Conference, American Society of Mechanical Engineers, pp.81-86.

Çelebi, M. (1993a). Seismic responses of two adjacent buildings. I: data and analyses. Journal of Structural Engineering, 119(8), pp.2461-2476.

Çelebi, M. (1993b). Seismic responses of two adjacent buildings. II: Interaction. Journal of Structural Engineering, 119(8), pp.2477-2492.

Chávez-Garcıa, F. J., & Cárdenas, M. (2002). The contribution of the built environment to the 'free-field'ground motion in Mexico City. Soil Dynamics and Earthquake Engineering, 22(9), pp.773-780.

Chen, Q. J., & Li, W. T. (2015). Effects of a Group of High-Rise Structures on Ground Motions under Seismic Excitation. Shock and Vibration, 2015.

Chouw, N., & Schmid, G. (1990). Influence of the geometrical effects of the soil on structure-soil-structure interaction. WB Kratzig *et al*, pp.795-802.

Clouteau, D., Broc, D., Devésa, G., Guyonvarh, V., & Massin, P. (2012). Calculation methods of Structure–Soil–Structure Interaction (3SI) for embedded buildings: Application to NUPEC tests. Soil Dynamics and Earthquake Engineering, 32(1), pp.129-142.

Ghandil, M., & Aldaikh, H. (2016). Damage‐based seismic planar pounding analysis of adjacent symmetric buildings considering inelastic structure‐soil‐structure interaction. Earthquake Engineering & Structural Dynamics.

Ghandil, M., & Behnamfar, F. (2015). The near-field method for dynamic analysis of structures on soft soils including inelastic soil–structure interaction. Soil Dynamics and Earthquake Engineering, 75, pp.1-17.

Ghandil, M., Behnamfar, F., & Vafaeian, M. (2016). Dynamic responses of structure–soil–structure systems with an extension of the equivalent linear soil modeling. Soil Dynamics and Earthquake Engineering, 80, pp.149-162.

Ghergu, M., & Ionescu, I. R. (2009). Structure–soil–structure coupling in seismic excitation and "city effect". International Journal of Engineering Science, 47(3), pp.342-354.

Ghiocel, D.M., Bogdan, O., Cretu, D. (2014, August) Seismic structure soil-structure interaction (SSSI) effects for dense urban areas. Second European Conference on Earthquake Engineering and Seismology, Istanbul.

Groby, J. P., Tsogka, C., & Wirgin, A. (2005). Simulation of seismic response in a city-like environment. Soil Dynamics and Earthquake Engineering, 25(7), pp.487-504.

Guéguen, P., Bard, P. Y., & Chávez-García, F. J. (2002). Site-City Seismic Interaction in Mexico City–Like Environments: An Analytical Study. Bulletin of the Seismological Society of America, 92(2), pp.794-811.

Hirono, E., Tobita, J., Fukuwa, N., Mori, M., Kojima, H. (2009) Examination of complex response characteristics of two buildings using the proposed 3-D animation tool for evaluation of spatial vibration. Summaries of Technical Papers of Annual Meeting Architectural Institute of Japan. B-2, Structures II, Structural Dynamics Nuclear Power Plants, pp.577-578. (In Japanese)

Hirotani, T., Yoshida, K., Tamori, S., Yoshida, N., & Suzuki, A. (2001). Model Test on Dynamic Cross Interaction of Adjacent Buildings in Nuclear Power Plants-Laboratory Test. Transactions of SMiRT-16, Washington DC.

Ikeda, Y., Shimomura, Y., Nakamura, M., Haneda, O., & Arai, T. (2004). Dynamic influence of adjacent structures on pile foundation based on forced vibration tests and earthquake observation. EXS, 4, P.5.

Imamura, A., Watanabe, T., Ishizaki, M., & Motosaka, M. (1992). Seismic response characteristics of embedded structures considering cross interaction. In Proceeding of the tenth world conference on earthquake engineering. Rotterdam: Balkema, pp. 1719-1724.

Isbiliroglu, Y., Taborda, R., Bielak, J. (2014, July) Multiple structure-soil-structure interaction and coupling effects in building clusters. Tenth U.S. National Conference on Earthquake Engineering, Alaska.

Karabalis, D. L., & Mohammadi, M. (1998). 3-D dynamic foundation-soil-foundation interaction on layered soil. Soil Dynamics and Earthquake Engineering, 17(3), pp.139-152.

Kham, M., Semblat, J. F., Bard, P. Y., & Dangla, P. (2006). Seismic site–city interaction: main governing phenomena through simplified numerical models. Bulletin of the Seismological Society of America, 96(5), pp.1934-1951.

Kitada, Y., & Iguchi, M. (2004, August). Model test on dynamic cross interaction of adjacent buildings in nuclear power plants-an outline and outcomes of the project. In 13th world conference on earthquake engineering, Vancouver, BC, Canada.

Kitada, Y., Hirotani, T., & Iguchi, M. (1999). Models test on dynamic structure–structure interaction of nuclear power plant buildings. Nuclear Engineering and Design, 192(2), pp.205-216.

Kitada, Y., Iguchi, M., Fukuwa, N., Kusakabe, K., Nishikawa, T., & Shinozaki, Y. (2001). Model Test on Dynamic Cross Interaction of Adjacent Buildings in Nuclear Power Plants-Overview and Outline of Earthquake Observation in the Field Test. Trans. The 16th SMiRT, Session K, 10.

Knappett, J. A., Madden, P., & Caucis, K. (2015a). Seismic structure–soil–structure interaction between pairs of adjacent building structures. Géotechnique, 65(5), pp.429-441.

Knappett, J. A., Madden, P., Caucis, K., & Gu, Y. (2015b). Seismic Interaction between Pairs of Adjacent Structures and Implications for Performance-Based Earthquake Engineering.

Kobori ,T., Kusakabe, K.(1980) Cross-interaction between two embedded structures in earthquakes. Proceedings of the seventh world conference on earthquake engineering, Istanbul, Turkey, pp.65-72.

Kobori, T., Minai, R., & Kusakabe, K. (1973). Dynamical characteristics of soil-structure cross-interaction system, I. Bull Disaster Prevent Res Inst, 22, Kyoto University.

Kobori, T., Minai, R., & Kusakabe, K. (1977). Dynamical cross-interaction between two foundations. In Proceedings of the sixth world conference on earthquake engineering. New Delhi, India, pp. 1484-1489.

Kusama, K., Kitada, Y., IGUCHI, M., FUKUWA, N., & NISHIKAWA, T. (2003, August). Model test on dynamic cross interaction of adjacent building in nuclear power plants. Overview and outcomes of the project. In Proceedings of the 17th International Conference on Structural Mechanics in Reactor Technology.

Larkin, T., Qin, X., Chouw, N. (2016). Effect of local site on sfsi of clustered structures. NatHaz 16 - Soil characterization and site effects, At S. Miguel, Portugal

Lee, T. H., & Wesley, D. A. (1973). Soil-structure interaction of nuclear reactor structures considering through-soil coupling between adjacent structures. Nuclear Engineering and Design, 24(3), pp.374-387.

Lehmann, L., & Antes, H. (2001). Dynamic structure—soil—structure interaction applying the Symmetric Galerkin Boundary Element Method (SGBEM). Mechanics Research Communications, 28(3), pp.297-304.

Li, P. Z., Hou, X. Y., Liu, Y. M., & Lu, X. L. (2012). Shaking table model tests on dynamic structure–soil–structure interaction during various excitations. In 15th world conference on earthquake engineering, Lisbon, Portugal.

Lin, H. T., Roesset, J. M., & Tassoulas, J. L. (1987). Dynamic interaction between adjacent foundations. Earthquake engineering & structural dynamics, 15(3), pp.323-343.

Lou, M., Wang, H., Chen, X., & Zhai, Y. (2011). Structure–soil–structure interaction: literature review. Soil Dynamics and Earthquake Engineering, 31(12), pp.1724-1731.

Luco, J. E., & Contesse, L. (1973). Dynamic structure-soil-structure interaction. Bulletin of the Seismological Society of America, 63(4), pp.1289-1303.

MacCalden, P. B., & Matthiesen, R. B. (1973). Coupled response of two foundations. In Proceedings of the fifth world conference on earthquake engineering. Rome, Italy, pp.1913-1922.

Madani, B., Behnamfar, F., & Riahi, H. T. (2015). Dynamic response of structures subjected to pounding and structure–soil–structure interaction. Soil Dynamics and Earthquake Engineering, 78, pp.46-60.

Mason, H. B. (2011). Seismic performance assessment in dense urban environments. University of California, Berkeley.

Matsuyama, M., Fukuwa, N., Tobita, J. (2001) Dynamic characteristics of adjacent low and medium-rise buildings based on earthquake observation, forced vibration experiment and microtremor observation. J. Struct. Constr. Eng., AIJ, No.545, pp.87-94. (In Japanese)

Matthees, W., & Magiera, G. (1982). A sensitivity study of seismic structure-soil-structure interaction problems for nuclear power plants. Nuclear Engineering and Design, 73(3), pp.343-363.

Mizuno, H. (1980). Effects of structure–soil–structure interaction during various excitations. In Proc. 7th World Conf. on Earthquake Eng., Vol. 5, pp.149-156.

Mulliken, J. S., & Karabalis, D. L. (1998). Discrete model for dynamic through-the-soil coupling of 3-D foundations and structures. Earthquake Engineering and Structural Dynamics, 27(7), pp.687-710.

Nakamura, S., Nakamura, N., Suzuki, T., Inoda, K., & Kosaka, K. (2011). Study on the Influence of Irregular Ground and Adjacent Building on the Seismic Response of Nuclear Power Plant Building. Journal of Structural Engineering, pp.115-126.

Naserkhaki, S., & Pourmohammad, H. (2012). SSI and SSSI effects in seismic analysis of twin buildings: discrete model concept. Journal of Civil Engineering and Management, 18(6), pp.890-898.

Naserkhaki, S., El-Rich, M., Aziz, A., Aznieta, F. N., & Pourmohammad, H. (2014). Pounding between adjacent buildings of varying height coupled through soil. Structural Engineering and Mechanics, 52(3), pp.573-593.

Padrón, L. A., Aznárez, J. J., & Maeso, O. (2009). Dynamic structure–soil–structure interaction between nearby piled buildings under seismic excitation by BEM–FEM model. Soil dynamics and earthquake engineering, 29(6), pp.1084-1096.

Qian, J., & Beskos, D. E. (1995). Dynamic interaction between 3-D rigid surface foundations and comparison with the ATC-3 provisions. Earthquake Engineering and Structural Dynamics, 24(3), pp.419-438.

Qian, J., & Beskos, D. E. (1996). Harmonic wave response of two 3-D rigid surface foundations. Soil Dynamics and Earthquake Engineering, 15(2), pp.95-110.

Rahgozar, M. A., & Ghandil, M. (2011). Dynamic interaction of adjacent tall building structures on deep foundations. Earthquake Resistant Engineering Structures VIII, (8), P.173.

Rahgozar, M. A. (2015). Accounting for soil nonlinearity in three-dimensional seismic structure-soil structure-Interaction analyses of adjacent tall buildings structures. Int J Civil Eng, 13(3), 213-225.

Richardson, J. D. (1969). Forced vibrations of rigid bodies on a semi-infinite elastic medium (Doctoral dissertation), University of Nottingham.

Romanini, E., Carvalho, E. R., Mesquita, E., & Betti, R. (1996). Dynamic structure–soil–structure interaction by the substructure deletion method. In Proceedings of the eighteenth world conference on the boundary element method. Braga, Portugal, pp.465-470.

Roy, C., Bolourchi, S., & Eggers, D. (2015). Significance of structure–soil–structure interaction for closely spaced structures. Nuclear Engineering and Design, 295, pp.680-687.

Schwan, L., Boutin, C., Padrón, L. A., Dietz, M. S., Bard, P. Y., & Taylor, C. (2016). Site-city interaction: theoretical, numerical and experimental crossed-analysis. Geophysical Journal International, 205(2), pp.1006-1031.

Semblat, J. F., Kham, M., & Bard, P. Y. (2008). Seismic-wave propagation in alluvial basins and influence of site-city interaction. Bulletin of the Seismological Society of America, 98(6), pp.2665-2678.

Semblat, J.F., Kham, M., Bard, P., Guéguen, P. (2004, August) Could “site-city interaction” modify site effects in urban areas? In 13th world conference on earthquake engineering, Vancouver, BC, Canada.

Tham, L. G., Qian, J., & Cheung, Y. K. (1998). Dynamic response of a group of flexible foundations to incident seismic waves. Soil Dynamics and Earthquake Engineering, 17(2), pp.127-137.

Trombetta, N. W., Benjamin Mason, H., Hutchinson, T. C., Zupan, J. D., Bray, J. D., & Kutter, B. L. (2014). Nonlinear soil–foundation–structure and structure–soil–structure interaction: engineering demands. Journal of Structural Engineering, 141(7), 04014177.

Trombetta, N. W., Mason, H. B., Chen, Z., Hutchinson, T. C., Bray, J. D., & Kutter, B. L. (2013a). Nonlinear dynamic foundation and frame structure response observed in geotechnical centrifuge experiments. Soil Dynamics and Earthquake Engineering, 50, pp.117-133.

Trombetta, N. W., Mason, H. B., Hutchinson, T. C., Zupan, J. D., Bray, J. D., & Kutter, B. L. (2013b). Nonlinear soil–foundation–structure and structure–soil–structure interaction: centrifuge test observations. Journal of Geotechnical and Geoenvironmental Engineering, 140(5), 04013057.

Tsogka, C., & Wirgin, A. (2003). Simulation of seismic response in an idealized city. Soil Dynamics and Earthquake Engineering, 23(5), pp.391-402.

Wang, S., & Schmid, G. (1992). Dynamic structure-soil-structure interaction by FEM and BEM. Computational mechanics, 9(5), pp.347-357.

Warburton, G. B., Richardson, J. D., & Webster, J. J. (1971). Forced vibrations of two masses on an elastic half space. Journal of Applied Mechanics, 38(1), pp.148-156.

Warburton, G. B., Richardson, J. D., & Webster, J. J. (1972). Harmonic Response of Masses on an Elastic Half Space. Journal of Engineering for Industry, 94(1), pp.193-200.

Wen H. (2006) An Analytical Study on Effects of Foundation Type, Foundation Shape and Adjacent Building on Dynamic Soil Structure Interaction. Diss. Nagoya University. (In Japanese)

Wen, H., Fukuwa, N. (2006) Analytical study on the effects of adjacent building on dynamic soil structure interaction of pile foundation and piled raft foundation. Journal of Structural and Construction Engineering 606, pp.147-154.

Wong, H. L., & Trifunac, M. D. (1975). Two-dimensional, antiplane, building-soil-building interaction for two or more buildings and for incident planet SH waves. Bulletin of the Seismological Society of America, 65(6), pp.1863-1885.

Xu, J., Costantino, C., Hofmayer, C., & Ali, S. (2004, January). Seismic response prediction of NUPEC's field model tests of NPP structures with adjacent building effect. In ASME/JSME 2004 Pressure Vessels and Piping Conference, American Society of Mechanical Engineers, pp. 1-11.

Yahyai, M., Mirtaheri, M., Mahoutian, M., Daryan, A. S., & Assareh, M. A. (2008). Soil structure interaction between two adjacent buildings under earthquake load. American Journal of Engineering and Applied Sciences, 1(2), pp.121-125.

Yano, T., Kitada, Y., Iguchi, M., Hirotani, T., & Yoshida, K. (2000). Model test on dynamic cross interaction of adjacent buildings in nuclear power plants. In 12th world conference on earthquake engineering, New Zealand.

Yano, T., Naito, Y., Iwamoto, K., Kitada, Y., & Iguchi, M. (2003, August). Model test on dynamic cross interaction of adjacent building in nuclear power plants. Overall evaluation on field test. In Proceedings of the 17th International Conference on Structural Mechanics in Reactor Technology.

Yoshida, K., Sato, T., & Kawase, H. (1984). Dynamic response of rigid foundations subjected to various types of seismic waves. In Proceeding of the eighth World conference on earthquake engineering. San Francisco, California, USA, pp.745-752.

Yue, D., Ghiocel, D. M., Fuyama, H., Ogata, T., & Stark, G. (2013). Structure-soil-structure interaction effects for two heavy npp buildings with large-size embedded foundations. SMiRT22 Proceedings, pp.18-23.

Chapter 4

Effect of Rocking Foundation Input Motion on the Nonlinear Response Characteristics of Superstructures

4.1 Introduction

Soil–structure interaction (SSI) is important for determining the damage to structures during a strong earthquake in some situations. Therefore, research on this topic is necessary for reliable earthquake-resistant design in order to understand the key parameters of SSI that influence the inelastic behavior of superstructures.

As stated in Section 2, Ghannad (2009) and Khanmohammadi *et al*. (2014) assert that the ductility demands for embedded foundations increase with embedment ratio because of the effect of RFIM, especially for the embedment ratios greater than one. In their studies, the lumped parameter model (LPM) given by Wolf (1994) for embedded foundations is used as the soil model for the analyses. Although this model is very useful for considering the nonlinearity of superstructures because of its frequency independent elements, it is developed for soil with a Poisson ratio (v) of 0.25 because of a lack of reliable data for other values of v. However, in soft soil conditions, for which SSI effects are more pronounced, Poisson ratios as high as 0.5 are encountered. Moreover, in the aforementioned study, the fixed-base natural frequency is assumed to be independent of the height of the SDOF structure which may represent unrealistic structural characteristics. Also, only records of earthquakes associated with active faults are considered, so the results cannot be generalized to earthquakes associated with subduction zones.

In the present study a new LPM is constructed that depends on the impedances of embedded foundations with different embedment depths placed on an elastic half-space for v = 0.42 and shear wave velocities V_s = 100 or 200 m/s to represent soft soil conditions. The value v = 0.42 is selected as a specific soft soil condition and is fixed for the analyses in the present study. However, it should be noted that this method is applicable for other values of v. Nonlinear earthquake response analyses using the proposed LPM then conducted with active fault and subduction zone earthquake records both with and without RFIM to assess the effects of RFIM on the ductility demands of structures. Additionally, the method of analysis is more reliable than those of Mahsuli and Ghannad (2009) and Khanmohammadi *et al*. (2014). This is because the created LPM is more reliable for soft soil conditions (v = 0.42 instead of 0.25) in which SSI effect is more prominent. Also the parameters selected for the superstructure make it easier to understand which types of structure SSI affects more. This is done by relating the fundamental period of the superstructure (0.2–3 s) to its aspect ratio, and by assuming ductility capacities of 2, 4, or 6 under a fixed-based condition (μ_{fix}).

4.2 Analysis model and method

Determining the exact impedances and input motions for foundations requires rigorous mathematical techniques, such as the finite element method. To manage this, as stated in Section 4.1, the systematic LPM procedure of Wolf (1994) is used to create a new LPM, and horizontal and rocking FIMs are calculated by using the double cone analysis suggested by Wolf and Deeks (2004).

4.2.1 Double cone analysis for determining FIM

Double cone analysis is a very efficient tool for determining the dynamic stiffness and input motion of embedded rigid disks, and proposed first by Meek and Wolf (1994). In this

method, the embedded part of the foundation is divided into a stack of disks on an interval that is no greater than one tenth of the smallest wavelength of the excitation. This is shown in Figure 4-1, where P_i (i = 1, 2, …, m) are horizontal forces, u_j (j = 1, 2, …, m) are horizontal displacements, r_o is the foundation radius, e is the embedment depth and Δe is the interval of the stacked disks (Wolf and Deeks, 2004). This method is easy to apply thanks to the MATLAB functions created by Wolf and Deeks (2004) and detailed information about this method can be found therein.

4.2.2 Analysis flow

The flowchart of the method is shown in Figure 4-2. The analysis is applied in two stages: the driving horizontal and rocking motions are calculated, and then these forces are used to obtain the total motion of the structure because LPMs containing masses cannot be analyzed in one step.

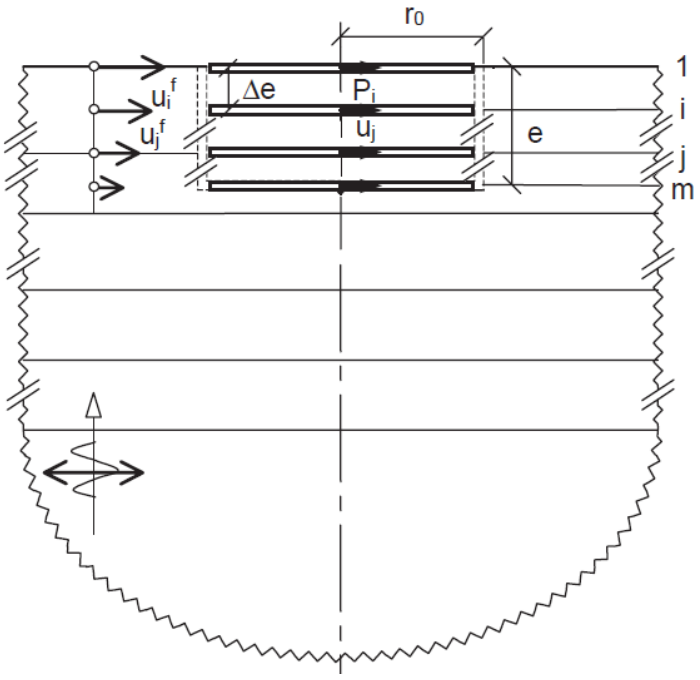

Figure 4-1: Stack of disks to represent an embedded disk foundation (Wolf and Deeks, 2004)

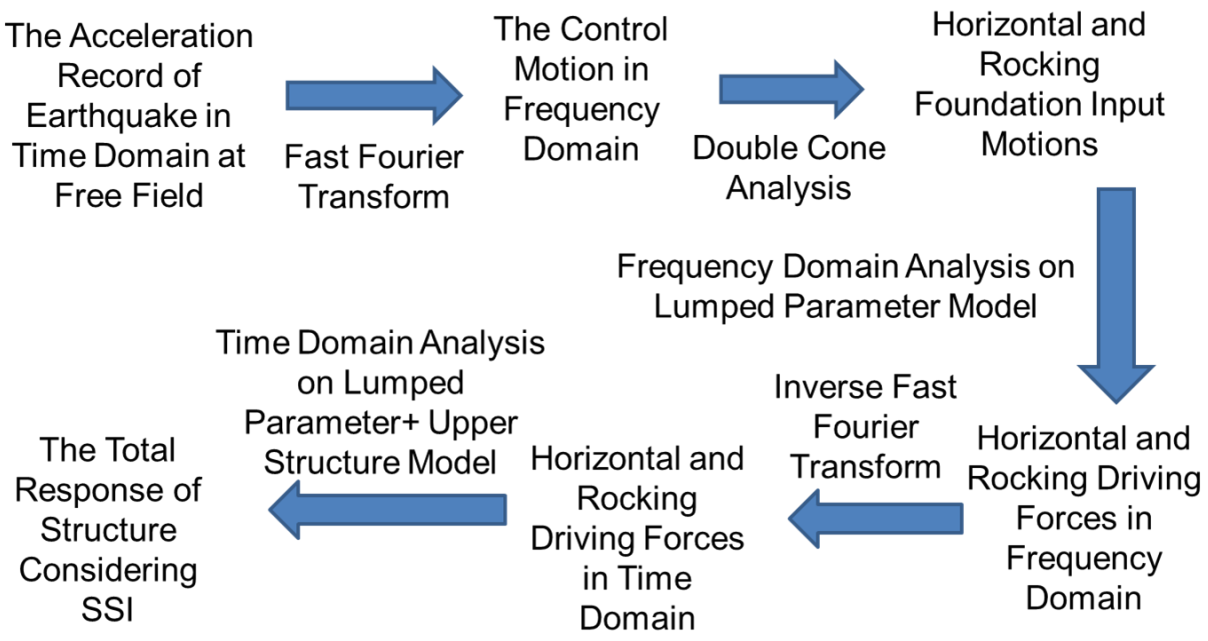

Figure 4-2: Flowchart of the analysis method

4.2.3 Outline of new LPM

A LPM is a very efficient tool for the time domain analysis of SSI, because its springs, dashpots, and masses are frequency independent, and it can be analyzed using well-known numerical methods. In the present study, a new LPM is developed by using the systematic procedure of Wolf (1994) for soil with Poisson ratio of 0.42. In this method, the exact values of dynamic stiffness, which are obtained by techniques such as the thin layer method (TLM), are divided into regular and singular parts (the value of the impedance calculated by using dimensionless spring and dashpot values for infinite frequency) as given by Equations (4-1), (4-2), and (4-3) according to the Wolf (1994). In these equations, S is the dynamic stiffness, S_s is the singular part of the dynamic stiffness, S_r is the remaining regular part of the dynamic stiffness, K is the static stiffness, p and q are real coefficients of the polynomials, N is the degree of polynomial placed on the denominator, $k(a_0)$ and $c(a_0)$ are spring and dashpot coefficients of the dynamic stiffness, k and c are values of spring and dashpot coefficients of the dynamic stiffness

at the infinite frequency, and a_0 is the dimensionless frequency given by Equation (4-4), where ω is the circular frequency, V_s is the shear wave velocity of the soil, and r is the radius of the foundation.

$$S(a_0) = K\left[k(a_0) + ia_0 c(a_0)\right] = S_s(a_0) + S_r(a_0) \tag{4-1}$$

$$\frac{S_s(a_0)}{K} = k + ia_0 c \tag{4-2}$$

$$\frac{S_r(a_0)}{K} \cong \frac{S_r(ia_0)}{K} = \frac{P(ia_0)}{KQ(ia_0)} = \frac{1 - k + p_1 ia_0 + p_2(ia_0)^2 + \ldots + p_{N-1}(ia_0)^{N-1}}{1 + q_1 ia_0 + q_2(ia_0)^2 + \ldots + q_N(ia_0)^N} \tag{4-3}$$

$$a_0 = \frac{\omega r}{V_s} \tag{4-4}$$

Next, 2N-1 real unknowns $p_1,\ldots,N$-1 and $q_1,\ldots,N$ are determined from a curve fitting technique on S_r by using the least squares method to obtain a minimum ε^2 value as given by Equation (4-5), where Q and P represent the polynomials placed on the numerator and denominator of Equation (4-3), respectively, and $w(a_0)$ is the weight function.

$$\varepsilon^2 = \sum_{j=1}^{J} w(a_{0j}) \left| S_r(a_{0j}) Q(ia_{0j}) - P(ia_{0j}) \right|^2 \tag{4-5}$$

Further, the regular part of the dynamic stiffness is written in the form of the partial fraction expansion in Equation (4-6), where s_ℓ are the roots of Q, and A_ℓ are the residues at the poles.

$$\frac{S_r(ia_0)}{K} = \sum_{\ell=1}^{N} \frac{A_\ell}{ia_0 - s_\ell} \tag{4-6}$$

As N = 1 is used in the present study, Equation (4-6) can be written in the form of Equation (4-7) for N = 1.

$$\frac{S_r(ia_0)}{K} = \frac{A_1}{ia_0 - s_1} \tag{4-7}$$

The dynamic stiffness of the foundation can be represented by a combination of the models in Figure 4-3(a) and (b). If we consider the dynamic stiffness of the model in Figure 4-3(a) and given in Eq. (4-8), we can easily determine the values of A_1 and s_1 to match the dynamic stiffness of the model to the regular part of the dynamic stiffness by using Equations (4-9) and (4-10). In addition, the singular part of the dynamic stiffness can be represented by the model in Figure 4-3(a). This systematic LPM rule is taken from Wolf (1994).

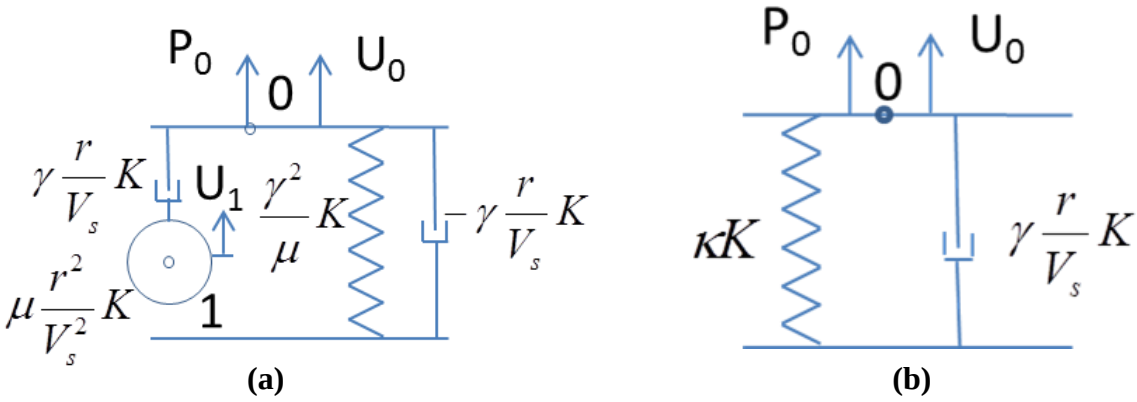

Figure 4-3: Models selected for the regular (a) and singular (b) parts of the dynamic stiffness

$$\left(\frac{\frac{\gamma^3}{\mu^2}}{ia_0 + \frac{\gamma}{\mu}} \right) U_0(a_0) = \frac{P_0(a_0)}{K} \tag{4-8}$$

$$\gamma = \frac{A}{s_1^2} \tag{4-9}$$

$$\mu = -\frac{A}{s_1^3} \tag{4-10}$$

The aforementioned technique is reliable when coupling is neglected. However, it is known that the horizontal and rocking degrees of freedom of an embedded foundation interact with each other. To manage this, discrete impedance values represented by the horizontal, rocking, and coupling parts of the model are calculated as given in Equations (4-11)-(4-13), where *e* is the embedment depth of the foundation, S_{hh}, S_{rr}, and S_{hr} are the horizontal, rocking, and coupling dynamic stiffness values of the rigid foundation, respectively, and S^m_{hh}, S^m_{rr}, and S^m_{hr} are the dynamic stiffness values of horizontal, rocking, and coupling part of this model, respectively. By using this discretization, a curve fitting technique can be applied to each part of the model separately.

The new model is shown in Figure 4-4. The main difference between this model and the one introduced by Wolf (1994) for embedded foundations is that the present model has a fictitious mass not only for the rocking part but also for the coupling part because of the high frequency dependence of the coupling impedance.

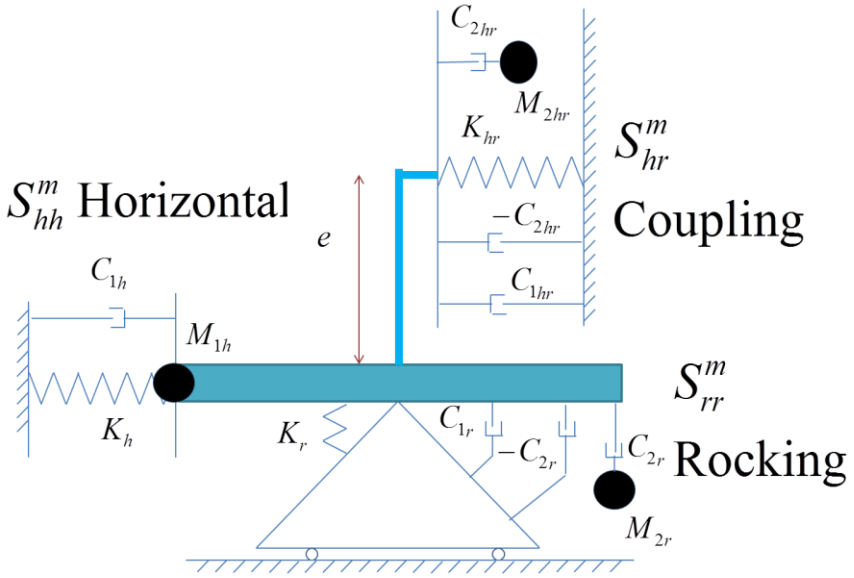

Figure 4-4: Schematic of the new lumped parameter model (LPM)

$$S^m_{hr}(\omega) = -\frac{S_{hr}(\omega)}{e} \tag{4-11}$$

$$S^m_{hh}(\omega) = S_{hh}(\omega) + \frac{S_{hr}(\omega)}{e} \tag{4-12}$$

$$S^m_{rr}(\omega) = S_{rr}(\omega) + eS_{hr}(\omega) \tag{4-13}$$

The dynamic stiffness of the horizontal, rocking, and coupling parts of the model shown in Figure 4-4 are given in Equations (4-14)-(4-16), respectively.

$$S^m_{hh}(\omega) = \left(-\omega^2 M_{1h} + K_h + i\omega C_{1h}\right) \tag{4-14}$$

$$S^m_{rr}(\omega) = -\omega^2 M_{1r} + K_r + i\omega C_{1r} - i\omega C_{2r}\frac{i\omega C_{2r}}{-\omega^2 M_{2r} + i\omega C_{2r}} \tag{4-15}$$

$$S_{hr}^{m}(\omega) = -\omega^2 M_{1hr} + K_{hr} + i\omega C_{1hr} - i\omega C_{2hr} \frac{i\omega C_{2hr}}{-\omega^2 M_{2hr} + i\omega C_{2hr}} \tag{4-16}$$

The equations of the parameters are given in Equations (4-17)-(4-22) where C_1, C_2, M_1, M_2 and K are lumped values for the damping (C), mass (M), and spring (K). The sub-indices indicate the different components of the model: h for horizontal, r for rocking, and hr for coupling. The correcting coefficient $K_{correct}$ is the used for obtaining a better fit to the exact impedances. Terms K^m_{hh}, K^m_{rr}, and K^m_{hr} represent the static stiffness of the horizontal, rocking, and coupling parts of the model, respectively. Terms γ_1, γ_2, μ_1, and μ_2 are dimensionless values, G is the shear modulus of the soil, r is the radius of the foundation, and e is the embedment depth of the foundation.

$$C_{1h} = \gamma_{1h} \frac{r}{V_s} K^m_{hh} \qquad C_{1r} = \gamma_{1r} \frac{r}{V_s} K^m_{rr} \qquad C_{1hr} = \gamma_{1hr} \frac{r}{V_s} K^m_{hr} \qquad C_{2r} = \gamma_{2r} \frac{r}{V_s} K^m_{rr} \qquad C_{2hr} = \gamma_{2hr} \frac{r}{V_s} K^m_{hr} \tag{4-17}$$

$$M_{1h} = \mu_{1h} \frac{r^2}{V_s^2} K^m_{hh} \qquad M_{2r} = \mu_{2r} \frac{r^2}{V_s^2} K^m_{rr} \qquad M_{2hr} = \mu_{2hr} \frac{r^2}{V_s^2} K^m_{hr} \tag{4-18}$$

$$K_h = Kh_{correct} K^m_{hh} \qquad K_r = Kr_{correct} K^m_{rr} \qquad K_{hr} = Khr_{correct} K^m_{hr} \tag{4-19}$$

$$K^m_{hh} = \frac{16Gr}{3(2-\nu)}\left(1 + \frac{e}{r}\right) \tag{4-20}$$

$$K^m_{rr} = \frac{8Gr^3}{3(1-\nu)}\left(1 + 2.3\frac{e}{r} + 0.58\left(\frac{e}{r}\right)^3\right) - \frac{8Gr^3}{3(2-\nu)}\left(\frac{e^2}{r^2} + \frac{e^3}{r^3}\right) \tag{4-21}$$

$$K^m_{hr} = \frac{8Gr}{3(2-\nu)}\left(1 + \frac{e}{r}\right) \tag{4-22}$$

Finally, the dimensionless coefficients of the model for different embedment ratios (e/r) are listed in Table 4-1. As can be seen from the table, there is no coupling part for a surface foundation (e/r = 0), and the coupling part for an embedment ratio of 0.25 has only one spring and dashpot. This means that the coupling impedance does not so depend on excitation frequency for low embedment ratios.

Table 4-1: Dimensionless parameters of lumped parameter model (LPM) for a Poisson ratio of 0.42

	e/r=0.00	e/r=0.25	e/r=0.50	e/r=1.00	e/r=1.50	e/r=2.00
$Kh_{correct}$	1.000	1.109	1.102	1.050	0.995	0.948
$Kr_{correct}$	1.000	0.886	0.858	0.895	0.898	0.878
$Khr_{correct}$	1.000	0.605	0.936	1.056	1.069	1.057
γ_{1h}	0.608	0.552	0.798	1.064	1.241	1.416
γ_{1r}	0.460	0.450	0.421	0.268	0.019	-0.355
γ_{1hr}	-	1.694	1.224	1.627	1.930	2.168
γ_{2r}	0.413	0.436	0.406	0.381	0.440	0.512
γ_{2hr}	-	-	0.082	0.416	0.514	0.575
μ_{1h}	-	-	0.029	0.050	0.082	0.103
μ_{2r}	0.178	0.190	0.165	0.145	0.194	0.263
μ_{2hr}	-	-	0.007	0.173	0.264	0.330

4.2.4 Determining the LPM parameters

(a) Comparing the impedances obtained by TLM and LPM

The TLM is a semi-analytical method by which the dynamic response of a foundation on layered soil can be computed by dividing the soil into thin layers horizontally, according to Park (2002). This method is first proposed by Tajimi (1980), Waas (1980) and Kausel (1981) in the same year. In the present study, the impedances obtained by TLM analyses are assumed to be exact, and a new LPM is built up by applying the curve fitting technique developed by Wolf (1994) to these impedances.

The soil and foundation model is shown in Figure 4-5. To calculate the homogeneous elastic half-space by the TLM, the soil is divided into thin layers that become progressively thinner from bottom to top. Moreover, to represent unbounded soil, a paraxial boundary is applied to the bottom of the model. The circular rigid foundation placed on this half-space is also divided into elements in order to use FEM to calculate the impedances, as shown in Figure 4-5 (Wen, 2006). According to Roesset (1980), the results for a circular foundation can be used in principle for a square foundation of same area, but only for superstructures with aspect ratios less than 4.

The comparison of the spring and dashpot coefficients calculated by LPM and TLM can be seen in Figures 4-6 to 4-11, for e/r = 0.5, 1.0, and 2.0. In these figures, the horizontal spring and dashpot coefficients fit reasonably well with the exact values over the entire dimensionless frequency range. However, the approximations for the rocking spring and dashpot coefficients are less good, within an error ratio of 20%. Moreover, the coupling spring coefficients fit the exact values better for dimensionless frequencies less than 1.5.

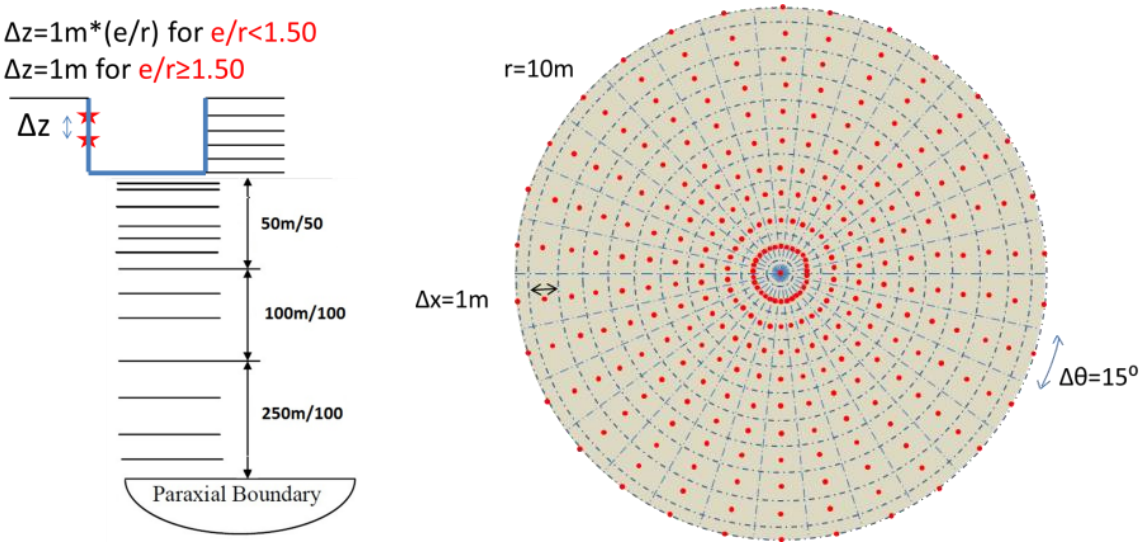

Figure 4-5: Soil model by the thin layer method (TLM) and model of the foundation by the finite element method (FEM)

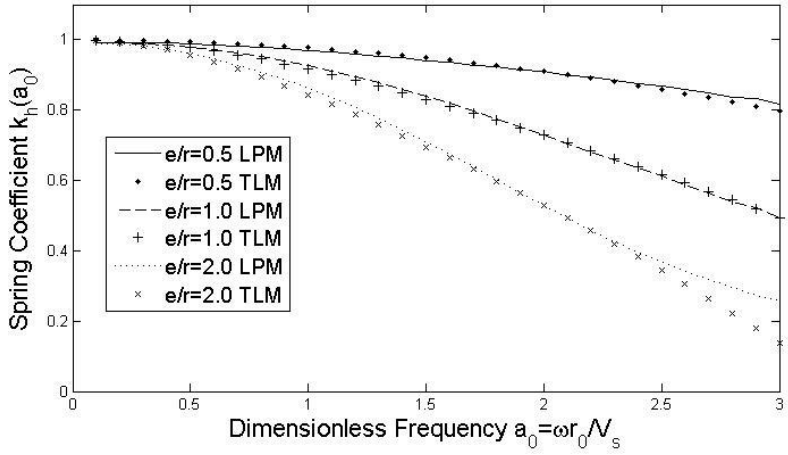

Figure 4-6: Spring coefficients for the horizontal component (k_h) of embedded foundations

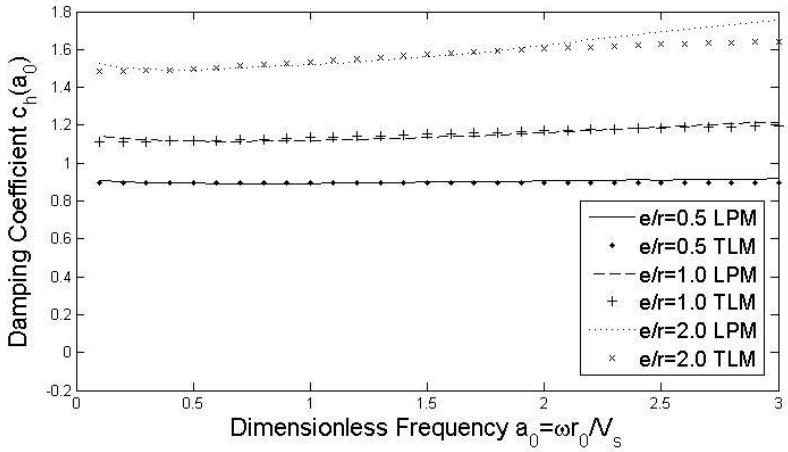

Figure 4-7: Damping coefficients for the horizontal component (c_h) of embedded foundations

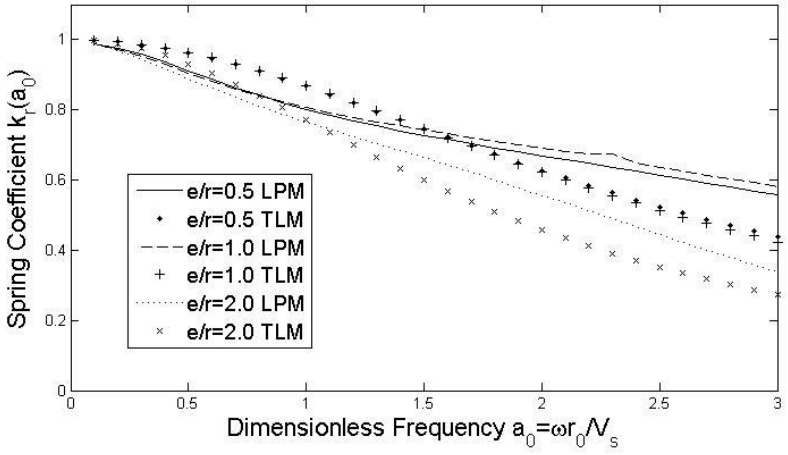

Figure 4-8: Spring coefficients for the rocking component (k_r) of embedded foundations

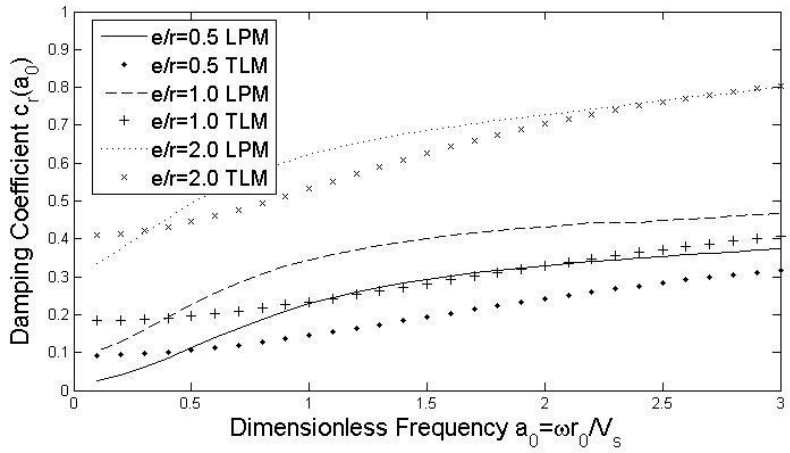

Figure 4-9: Damping coefficients for the rocking component (c_r) of embedded foundations

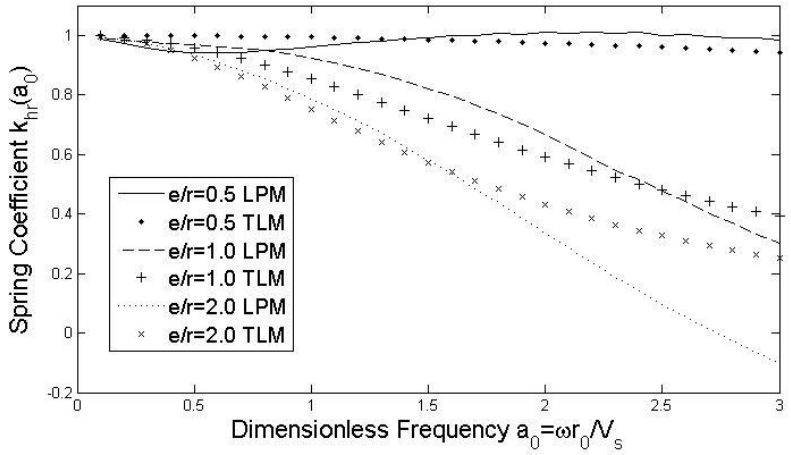

Figure 4-10: Spring coefficients for the coupling component (k_{hr}) of embedded foundations

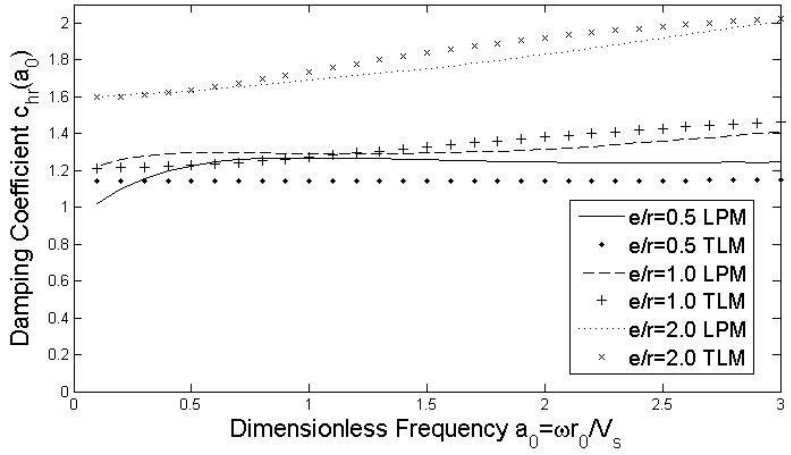

Figure 4-11: Damping coefficients for the coupling component (c_{hr}) of embedded foundations

(b) Verifying the LPM

To verify the improved LPM, the transfer functions obtained by classical frequency domain analysis (FDA) and LPM are compared in the Figure 4-12 where the shear wave velocity of the soil (V_s) is 100 m/s and natural periods of the superstructures (T_{fix}) are 1 and 0.5 sec. As can be seen in these figures, the transfer functions obtained by LPM are in good agreement with those obtained by FDA. From these results, it can be said that this approximation is almost adequate.

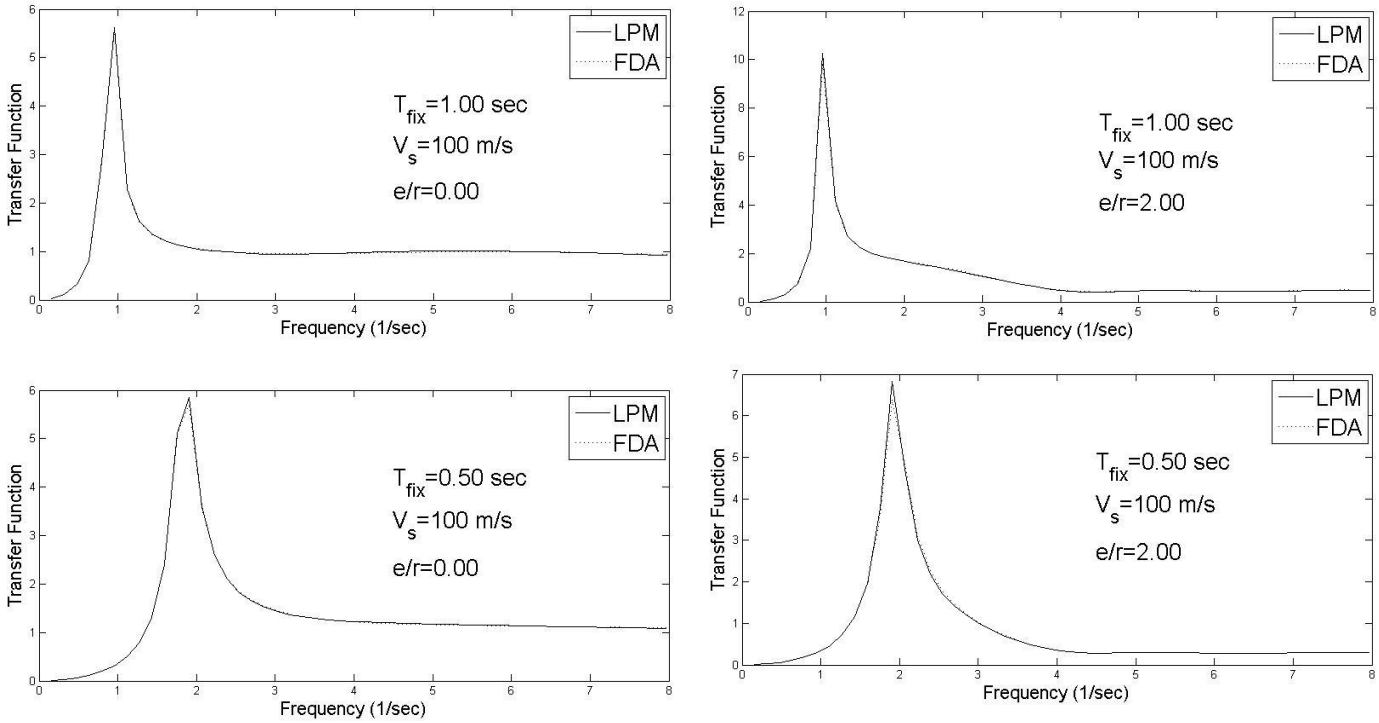

Figure 4-12: Transfer functions obtained by frequency domain analysis (FDA) and LPM

4.2.5 Determining the driving forces

The driving forces are those forces required to make a foundation motionless under FIM. To obtain these driving forces, the LPM should be analyzed in the frequency domain. The

driving forces are given in Equation (4-23), where P_g is the horizontal driving force, M_g is the rocking driving force, u_g is the HFIM and θ_g is the RFIM.

$$\begin{bmatrix} S_{hh}(\omega) & S_{hr}(\omega) \\ S_{hr}(\omega) & S_{rr}(\omega) \end{bmatrix} \begin{Bmatrix} u_g(\omega) \\ \theta_g(\omega) \end{Bmatrix} = \begin{Bmatrix} P_g(\omega) \\ M_g(\omega) \end{Bmatrix} \tag{4-23}$$

If u_g and θ_g are considered as given above, the situation corresponds to "with RFIM". If θ_g is taken as zero for the same u_g, the situation corresponds to "without RFIM". If u_g is taken as the free field motion (FFM) and θ_g is taken as zero, the situation corresponds to "without KI" in the present study. These situations are shown in Figure 4-13 where u_f is FFM graphically. The different effects of these situations on the nonlinear behavior of the superstructure are studied.

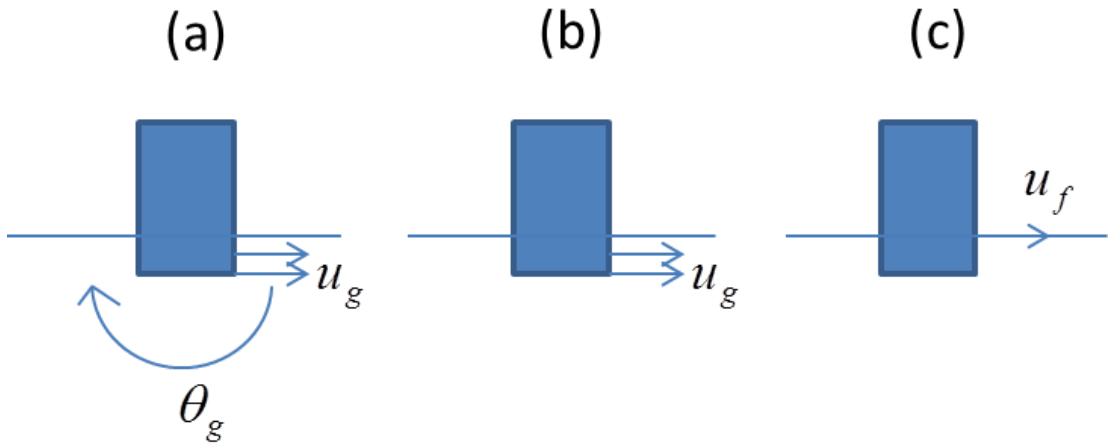

Figure 4-13: Analysis conditions (a) With RFIM (b) Without RFIM (c) Without KI

4.3 Analysis conditions

4.3.1 Model of SDOF structure

To cover existing residential buildings, a simple approximation is applied to determine the parameters of the structure as shown in Figure 4-14(a), where T_{fix} is the natural period of the

SDOF system under the fixed base situation, N is the number of stories, M_{floor} is the mass of each floor of the structure, b_{floor} is the thickness of the floor, b_{found} is the thickness of the foundation, ΔH is the story height, H is the total height of the structure and H_{eff} is the effective height of the structure. The mass ratio of the foundation to the structure is taken as 0.82, and analyses are done for foundation embedment ratios (e/r) of 0, 0.5, 1.0, and 2.0. The foundations are considered to be infinitely rigid, and the initial stiffness is taken to be proportional to the damping. The Newmark-Beta method (Newmark, 1959) is used with β = 0.25. Research is done on MDOF inelastic systems interacting with elastic soil by Ganjavi and Hao (2014), Ahmadi and Khoshnoudian (2015), Lu *et al*. (2016), and Ganjavi *et al*. (2016). However, according to Jennings and Bielak (1973), the main effect of SSI is on the first period of superstructures.

For simplicity, an inelastic structure is represented by an elasto-plastic model with zero hardening after yielding, as shown in Figure 4-14(b). The yield strength is set so that the maximum ductility factor equals to μ_{fix} as a given value under the fixed base model.

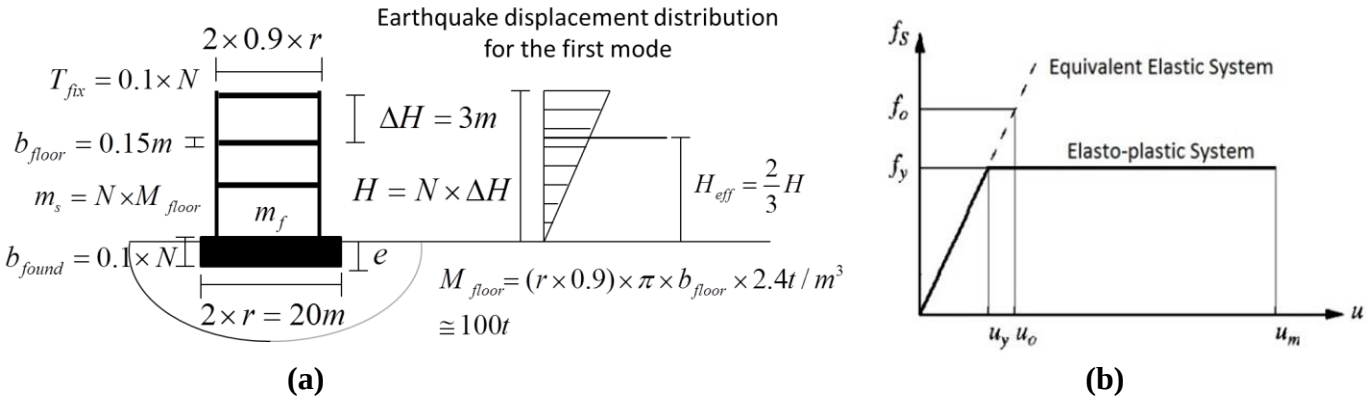

Fig. 4-14: (a) Analysis model for superstructures and (b) elasto-plastic model of superstructures used in the present study. f_0, f_y, u_0, u_y and u_m are the elastic demands of strength, yield strength, elastic displacement demand, yield displacement and ultimate displacement of the system, respectively

4.3.2 Soil parameters

The soil is idealized as a homogeneous elastic half-space with no material damping. The soil mass density (ρ) is 1.8×10^3 kg/m^3, and the shear wave velocity of soil (V_s) is selected either 100 or 200 m/s. To represent the soft soil condition, Poisson ratio (v) of the soil is taken as 0.42.

4.3.3 Selected earthquake records

The 1995 Hyogoken-Nanbu (Kobe Earthquake) TAK000 component of the Takatori Station Record is chosen as an input motion. According to Mylonakis *et al*. (2006), one of the main reasons for the collapse of 18 piers of the Hanshin Expressway (where it is placed on similar soil conditions with Takatori Station) during the 1995 Hyogoken-Nanbu Earthquake, is SSI, as noted in Section 1. Moreover, to assess the effect of a subduction zone earthquake record with similar amplitude, more peaks on acceleration spectra and longer duration of the record than Kobe Earthquake record, the 2011 off the Pacific Coast of Tohoku Earthquake (Tohoku Earthquake) EW component of MYG006 Station (K-NET Furukawa) is also used for analyses. The acceleration time histories and acceleration response spectra (h=5%) of the records are shown in Figures 4-15 to 4-17.

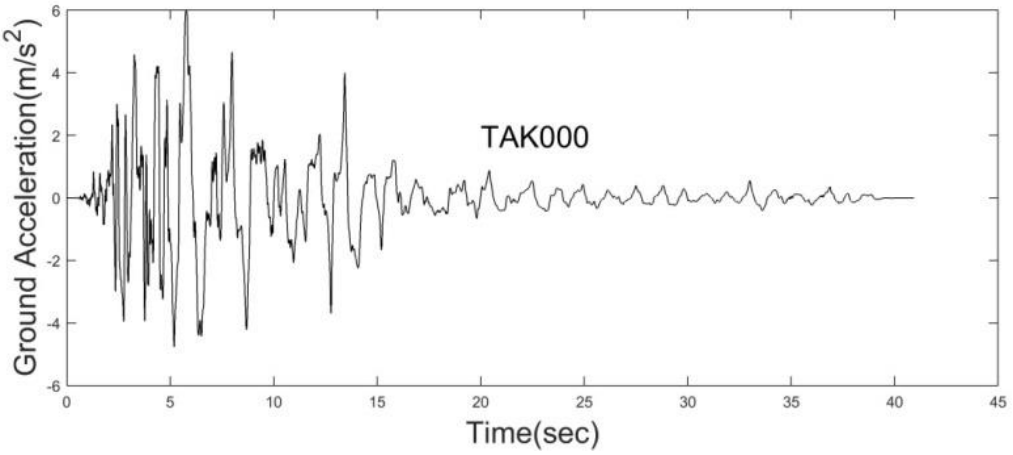

Figure 4-15: Acceleration time history of theKobe Earthquake TAK000 component at Takatori Station

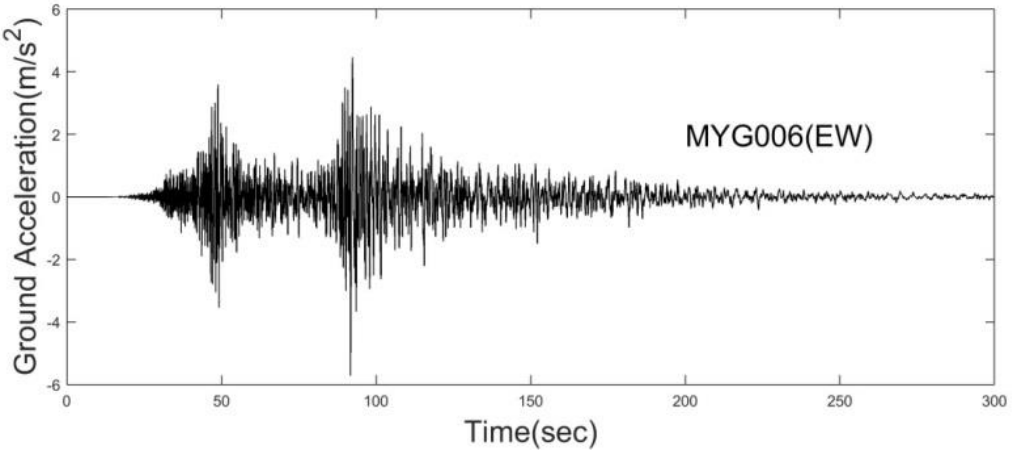

Figure 4-16: Acceleration time history of theTohoku Earthquake EW component at MYG006 Station

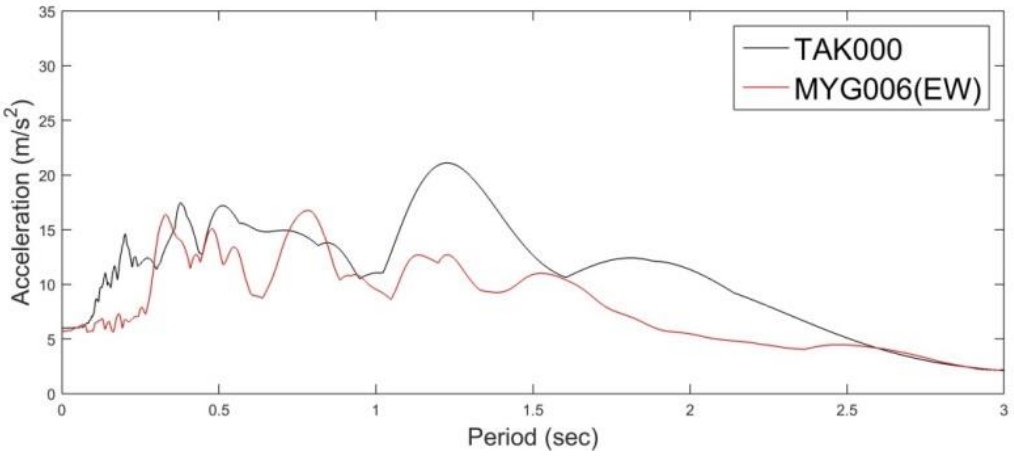

Figure 4-17: Acceleration response spectra of the TAK000, and MYG006 (EW) records (*h*=5%)

4.4 Effect of RFIM on the superstructure response

4.4.1 Analysis results for Kobe Earthquake record

In this section, nonlinear seismic response analyses are conducted using the proposed analytical model to analyze the effect of the rocking foundation input motion (RFIM) on the superstructure responses.

Specifically, time history nonlinear response analyses are carried out under some input motions considering the kinematic interaction by using the proposed analysis model. The effect of the RFIM on the nonlinear response of the superstructure is studied by comparing the maximum ductility factor μ_{max} with μ_{fix} in the case of different foundation embedment depth.

The results obtained by using the Kobe Earthquake record are shown in Figure 4-18 and 4-19 where the horizontal axis is the natural period of the superstructure, which represents the number of stories of the superstructure from 2 to 30 stories. All graphs show the ratio of the maximum response ductility factor μ_{max} to μ_{fix}. Figures 4-18 and 4-19 (a-c) show results for a shear wave velocity V_s = 100 m/s of surface ground and μ_{fix} = 2, 4, or 6. Figure 4-22 shows the results for a shear wave velocity V_s = 200 m/s of surface ground and μ_{fix} = 2. In each figure, (a, d) are with RFIM, (b, e) are without RFIM, (c, f) are without KI.

First, the differences in results that under the conditions (a) with RFIM and (c) without KI are considered. As shown in Figure 4-18 to Figure 4-19 (a, d) and (c, f), the responses with RFIM are almost the same as those without KI for every μ_{fix} of medium-rise buildings. However, the responses of low rise buildings with short natural periods (less than 0.5 sec) for (a, d) are smaller than those for (c, f) because of the low-pass filter effect of KI. Therefore, it can be concluded that a safer design is obtained for low rise buildings by neglecting KI.

Next, the differences in results between the conditions (a) with RFIM and (b) without RFIM are considered. It is clear that the responses of (b) are smaller than that those of (a). In particular, as μ_{fix} becomes larger and the embedment becomes deeper, the difference between μ_{fix} and μ_{max} becomes more pronounced. This means that earthquake responses considering only horizontal kinematic interaction are underestimated.

Next, the effect of RFIM on buildings with long natural periods is considered. When μ_{fix} is small, the responses of buildings with natural periods greater than 2 seconds, except for the e/r = 2 under considering RFIM, are smaller than those of the fixed-base model. It is estimated that the input ground motion is reduced because of the assumption of a slender building with a spread foundation on soft ground. In addition, the input ground motion is reduced because the rocking spring of the soil is relatively small and the natural period of the coupled system becomes long. However, if the embedment is deep (e/r = 2.0) considering RFIM, it is seen that the response increases because of the small rocking stiffness. In addition, when μ_{fix} is large, the building responses of (a) are larger than those of the fixed-base model for certain natural periods of buildings, even if the embedment is shallow.

Finally, the importance of RFIM on the nonlinear response of buildings is evaluated generally. It is notable that the maximum ductility factor for e/r = 2.0 in Figure 4-19 (a) is 1.5 times larger than those of both the fixed base model and (c) by means of the RFIM. Therefore, it can be concluded that an unreasonable design is obtained for such conditions by neglecting KI or SSI. This suggests the possibility that the rocking input motion has a major impact on the near to the ultimate state situation of the building. However, these results are valid only for mat foundations; a different approach is required for pile foundations.

A Fluctuation in ductility factors with natural frequency is seen in Figures 4-18 and 4-19. In the present study, there is a general tendency for the results to depend on the relationship between the spectral characteristics of the input ground motion and the equivalent natural period of the superstructure under plastic deformation. The aforementioned results are schematically summarized in Table 4-2.

However, if the shear wave velocity of the surface layers is as large as V_s = 200 m/s, as shown in Figure 4-19 (d-f), the variation due to the difference in embedment depth is less for any natural period, and it is found that the response is almost the same as that for the fixed base model in the cases of (d) and (f).

The maximum response ductility factor ratio of (a): with RFIM to (c): without KI is compared for each μ_{fix} in Figure 4-20 where the horizontal axis is the same as Figure 4-18 and 4-19. A ratio greater than one means that the response ductility factor increases if SSI is considered. From this figure, it is found that the response is underestimated in the case of deep embedment for 0.5 seconds or more of the building's natural period if RFIM is neglected.

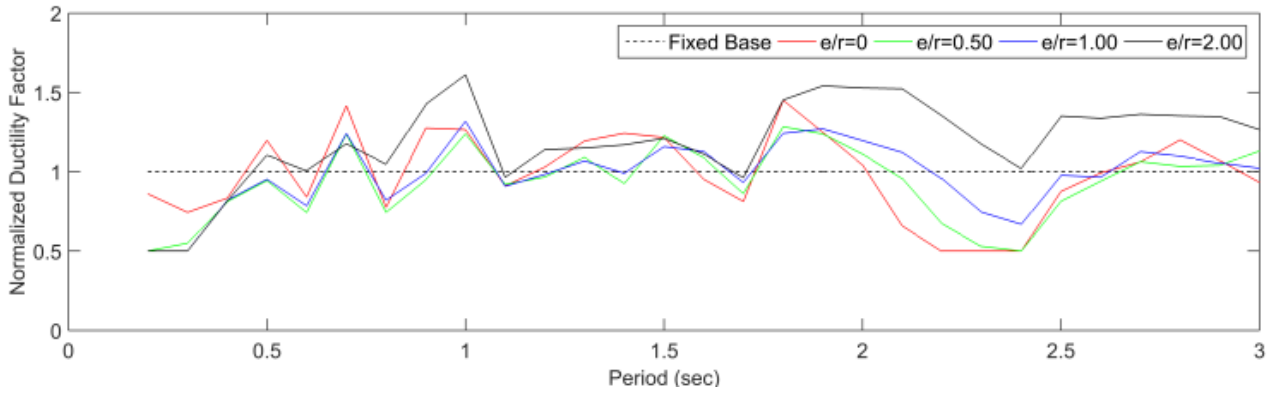

(a) With rocking foundation input motion (RFIM) (V_s = 100 m/s, μ_{fix} = 2)

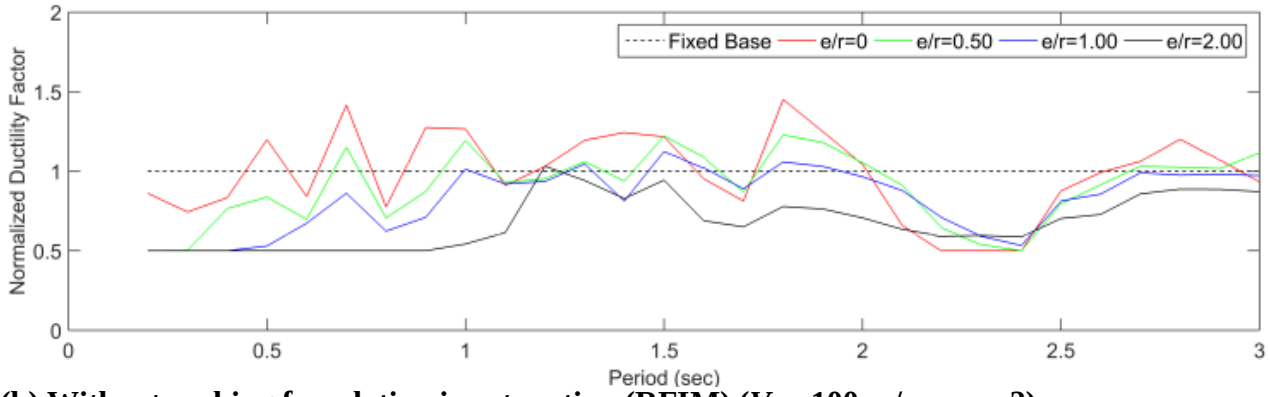

(b) Without rocking foundation input motion (RFIM) (V_s = 100 m/s, μ_{fix} = 2)

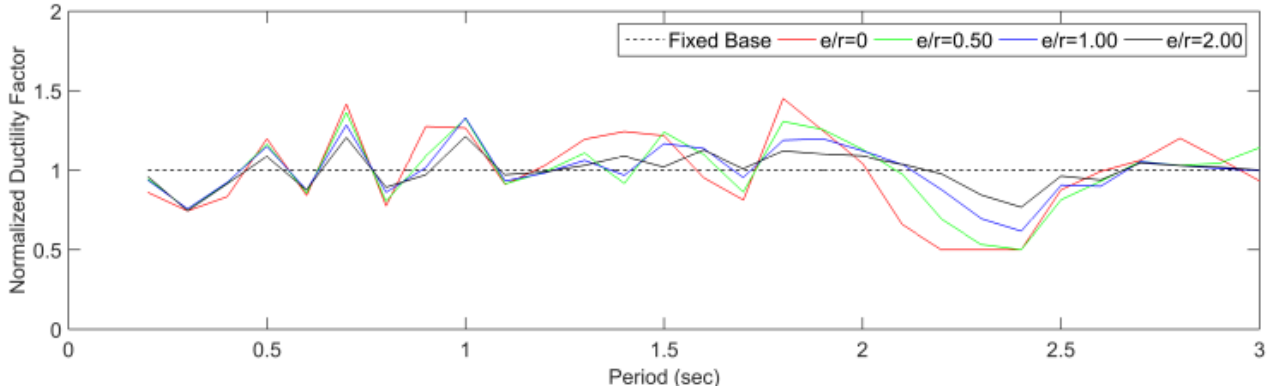

(c) Without kinematic interaction (KI) (V_s = 100 m/s, μ_{fix} = 2)

Fig. 4-18(1): Ductility factors for Kobe Earthquake TAK000 component at Takatori Station with and without RFIM, and without KI (h = 0.05, r = 10 m, ρ = 1.8x10^3 kg/m^3, ν = 0.42, m = N*100 t, m_f/m = 0.82)

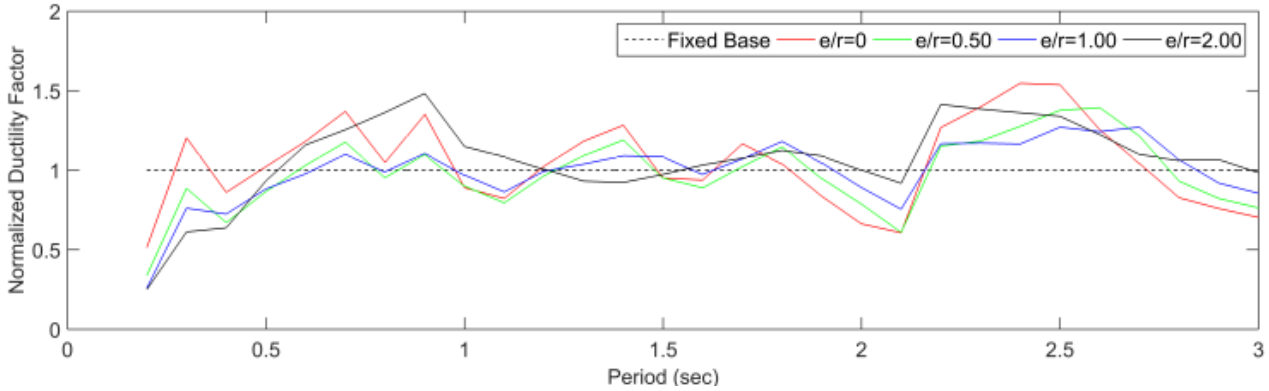

(d) With rocking foundation input motion (RFIM) (V_s = 100 m/s, μ_{fix} = 4)

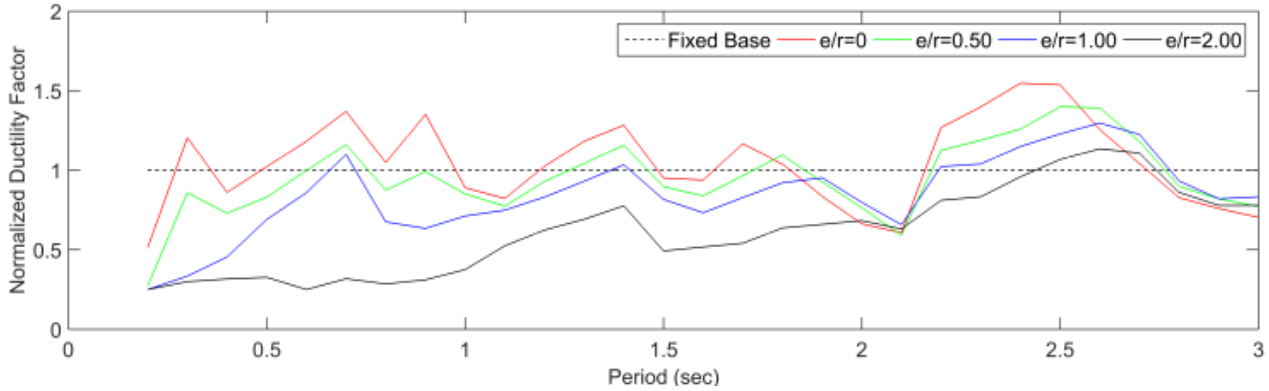

(e) Without rocking foundation input motion (RFIM) (V_s = 100 m/s, μ_{fix} = 4)

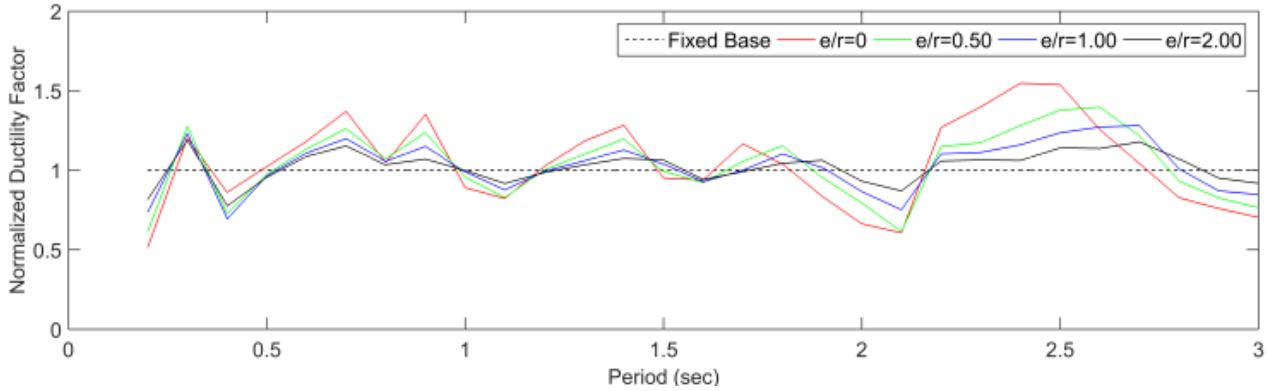

(f) Without kinematic interaction (KI) (V_s = 100 m/s, μ_{fix} = 4)

Fig. 4-18(2): Ductility factors for Kobe Earthquake TAK000 component at Takatori Station with and without RFIM, and without KI (h = 0.05, r = 10 m, ρ = 1.8x10^3 kg/m^3, ν = 0.42, m = N*100 t, m_f/m = 0.82)

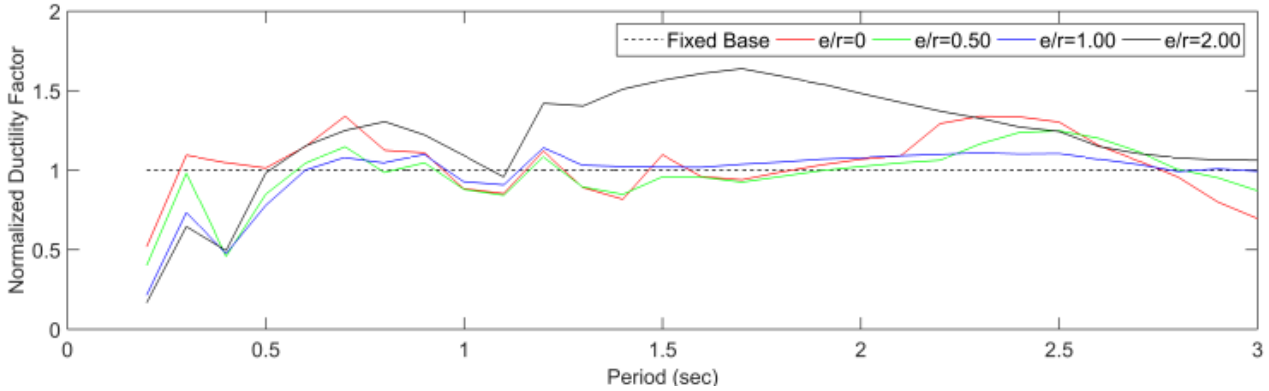

(a) With rocking foundation input motion (RFIM) (V_s = 100 m/s, μ_{fix} = 6)

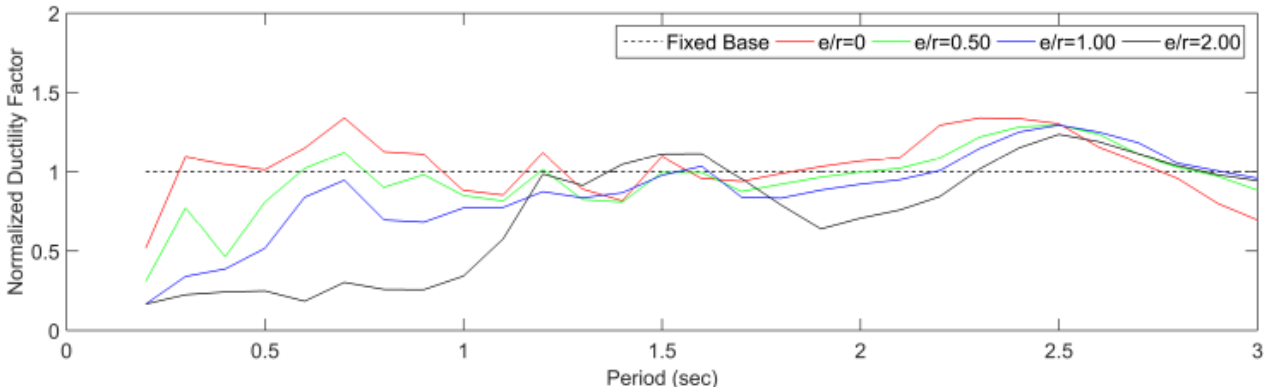

(b) Without rocking foundation input motion (RFIM) (V_s = 100 m/s, μ_{fix} = 6)

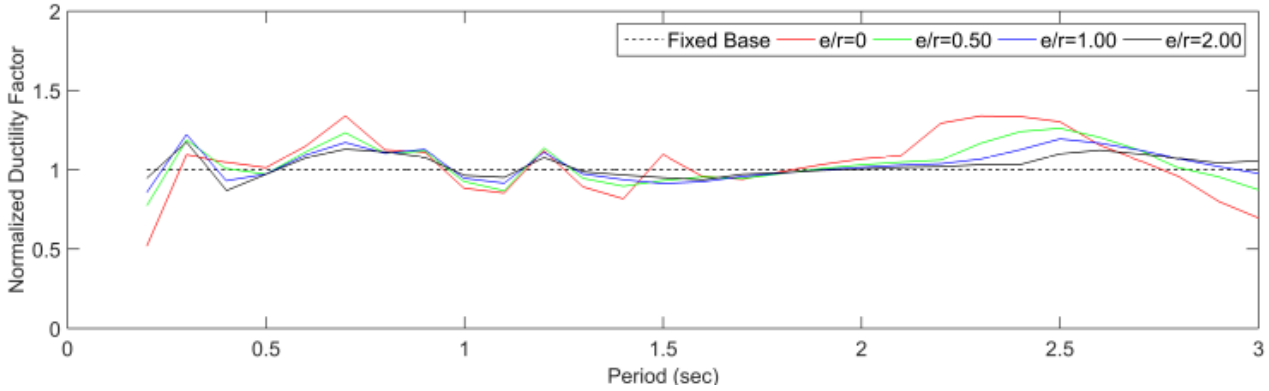

(c) Without kinematic interaction (KI) (V_s = 100 m/s, μ_{fix} = 6)

Fig. 4-19(1): Ductility factors for Kobe Earthquake TAK000 component at Takatori Station with and without RFIM, and without KI (h = 0.05, r = 10 m, ρ = 1.8x10^3 kg/m^3, v = 0.42, m = N*100 t, m_f/m = 0.82)

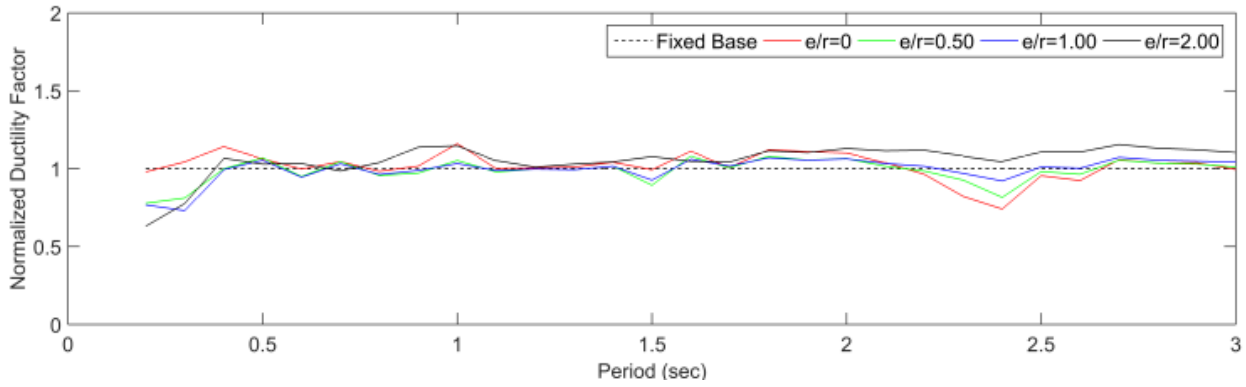

(d) With rocking foundation input motion (RFIM) (V_s = 200 m/s, μ_{fix} = 2)

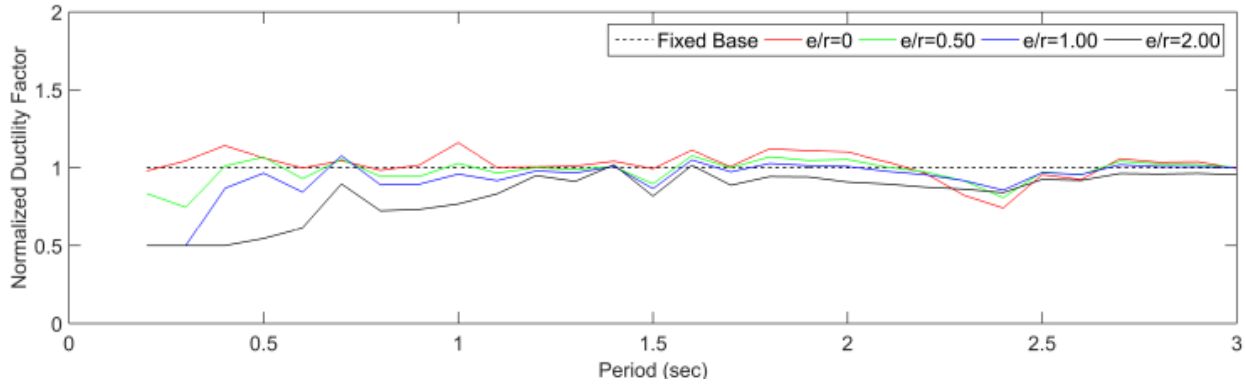

(e) Without rocking foundation input motion (RFIM) (V_s = 200 m/s, μ_{fix} = 2)

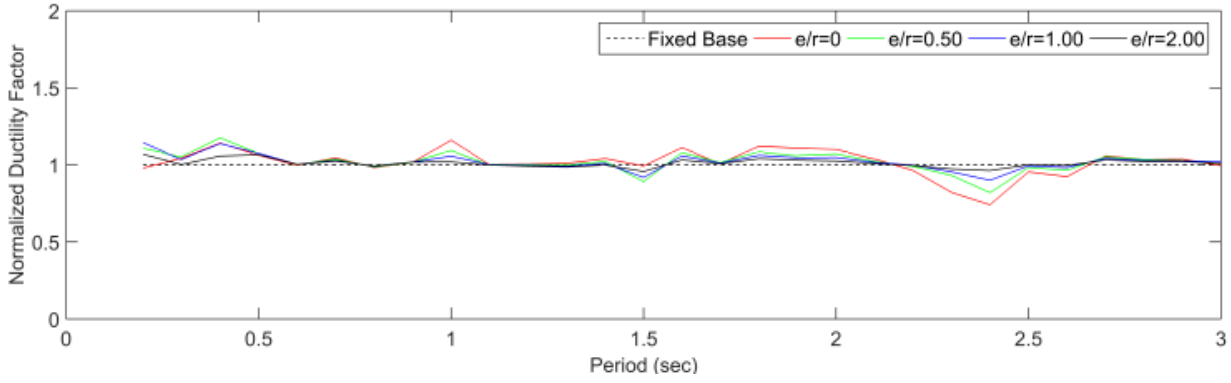

(f) Without kinematic interaction (KI) (V_s = 200 m/s, μ_{fix} = 2)

Fig. 4-19(2): Ductility factors for Kobe Earthquake TAK000 component at Takatori Station with and without RFIM, and without KI (h = 0.05, r = 10 m, ρ = 1.8x10^3 kg/m^3, v = 0.42, m = N*100 t, m_f/m = 0.82)

Table 4-2: Schematic of the discussion of the results of the analyses (for V_s = 100 m/s)

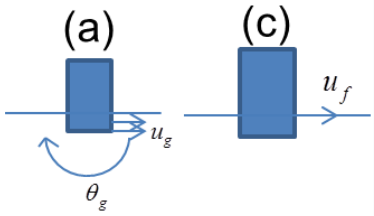	For middle rise buildings ⇒ Responses for (a) and (c) are almost equal For low rise buildings ⇒ Responses for (a) < (c)
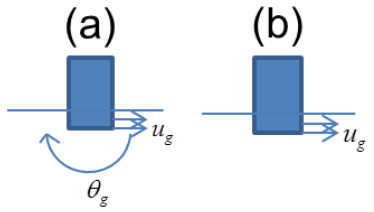	Responses for (b) smaller than (a) For ↑ μ_{fix} and ↑ e/r ⇒ Difference between μ_{fix} and μ_{max} ↑
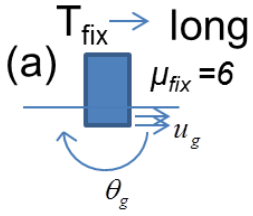	For e is shallow(in the case of the study e/r≤1) ⇒ Responses for (a)≈ Fixed based model For e is deep (in the case of the study e/r=2) ⇒ Responses for (a)> Fixed based model Due to small rocking stiffness

4.4.2 Analysis results for Tohoku Earthquake record

The results of V_s = 100 m/s and μ_{fix} = 6 are shown in Figure 4-21. In this case, the observation record at K-NET Furukawa (MYG006) of the main shock (EW component) in the 2011 Tohoku region Pacific Ocean Earthquake is used as input ground motion. It is found that μ_{max} fluctuates according to the spectral characteristic of the input ground motion in the long period domain. In Figure 4-22, the maximum ductility factor ratio of (a): with RFIM to (c): without KI is compared to the case of μ_{fix} =6. The same tendency as that of the Kobe Earthquake is found. From these results, it is concluded that inelastic building responses are not strongly dependent on the duration of input ground motions in the present study.

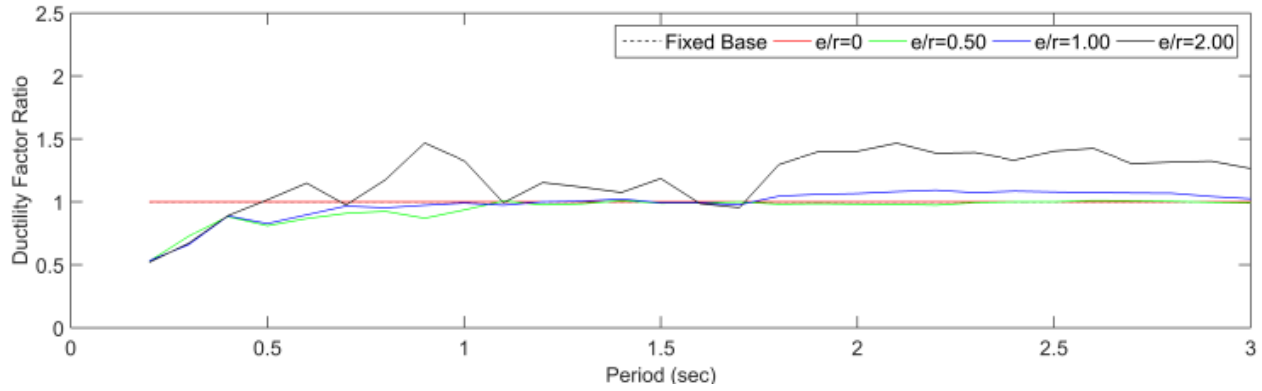

(a) With rocking foundation input motion (RFIM) (V_s = 100 m/s, μ_{fix} = 2)

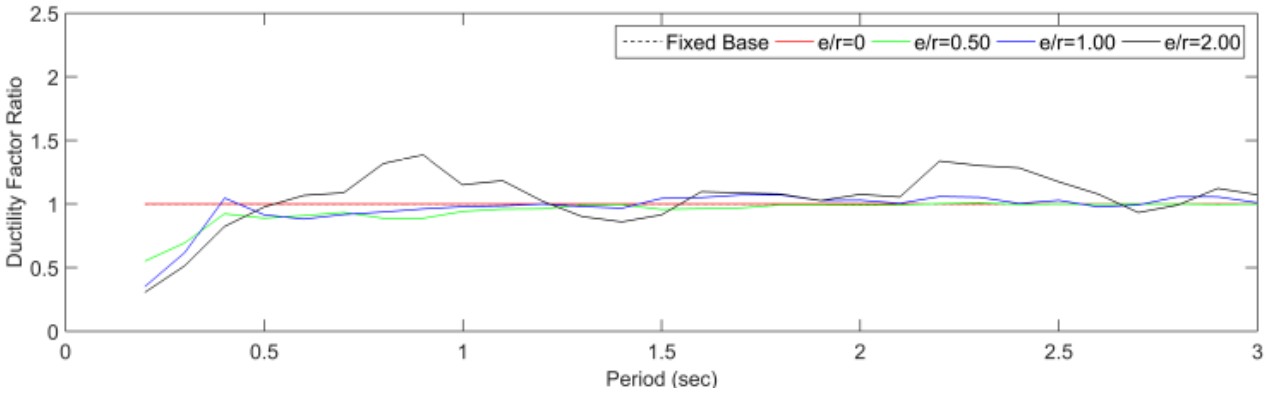

(b) Without rocking foundation input motion (RFIM) (V_s = 100 m/s, μ_{fix} = 4)

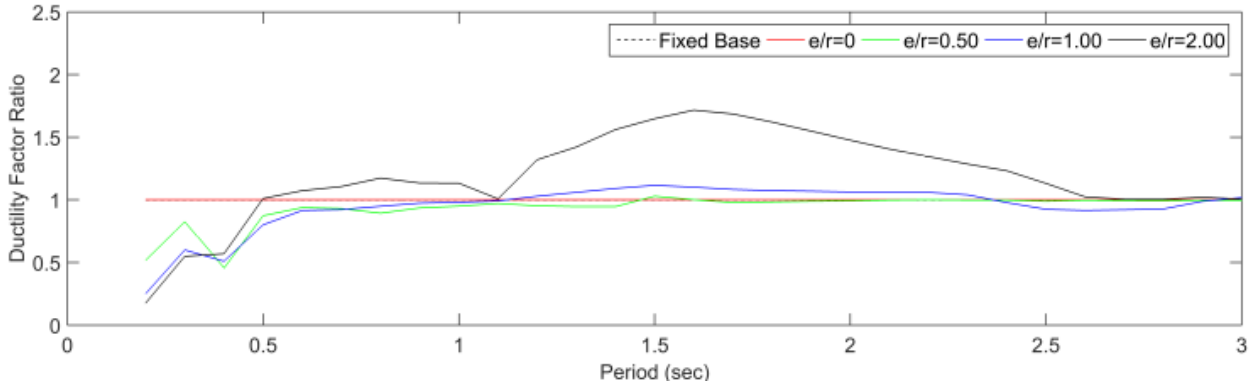

(c) Without kinematic interaction (KI) (V_s = 100 m/s, μ_{fix} = 6)

Fig. 4-20: Ductility factor Ratios for Kobe Earthquake TAK000 component at Takatori Station with RFIM to without KI (h = 0.05, r = 10 m, ρ = 1.8x10^3 kg/m^3, v = 0.42, m = N*100 t, m_f/m = 0.82)

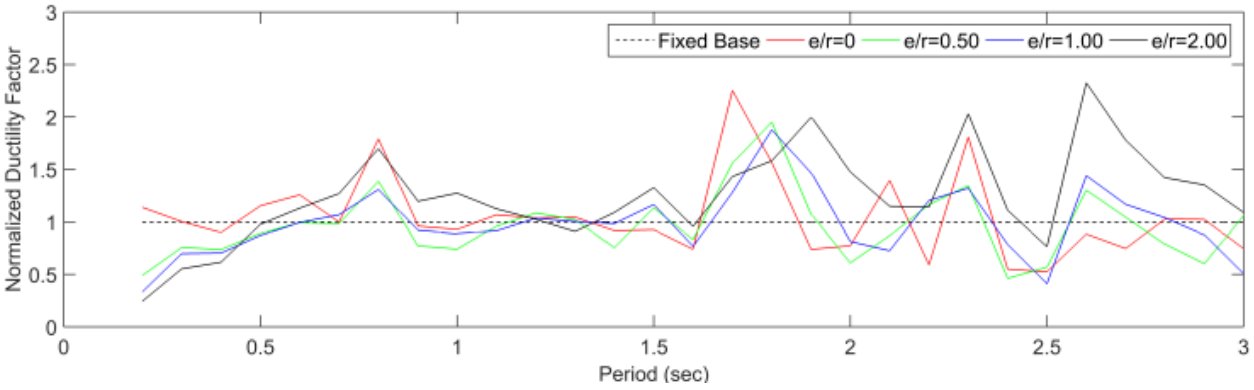

(a) With rocking foundation input motion (RFIM) (V_s = 100 m/s, μ_{fix} = 6)

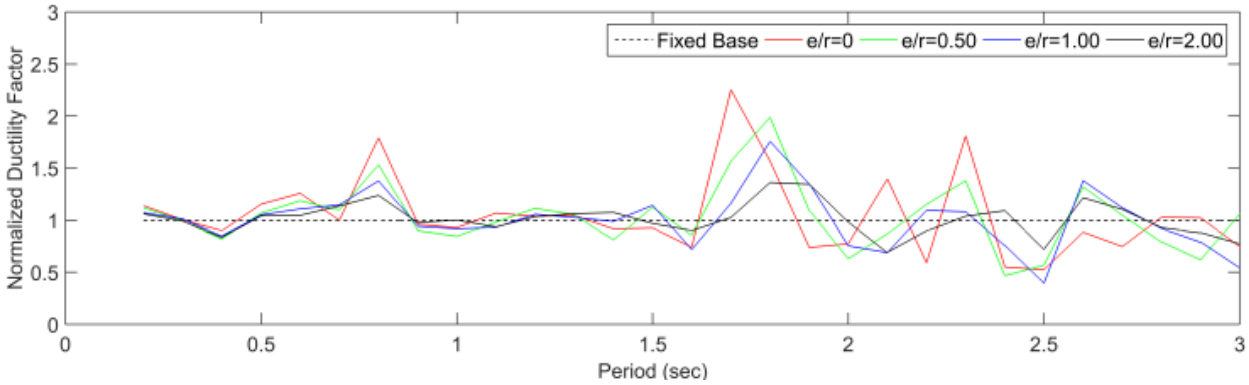

(b) Without kinematic interaction (KI) (V_s = 100 m/s, μ_{fix} = 6)

Fig. 4-21: Ductility factors for Tohoku Earthquake EW component at MYG006 with RFIM, and without KI (h = 0.05, r = 10 m, ρ = 1.8x10^3 kg/m^3, v = 0.42, m = N*100 t, m_f/m = 0.82)

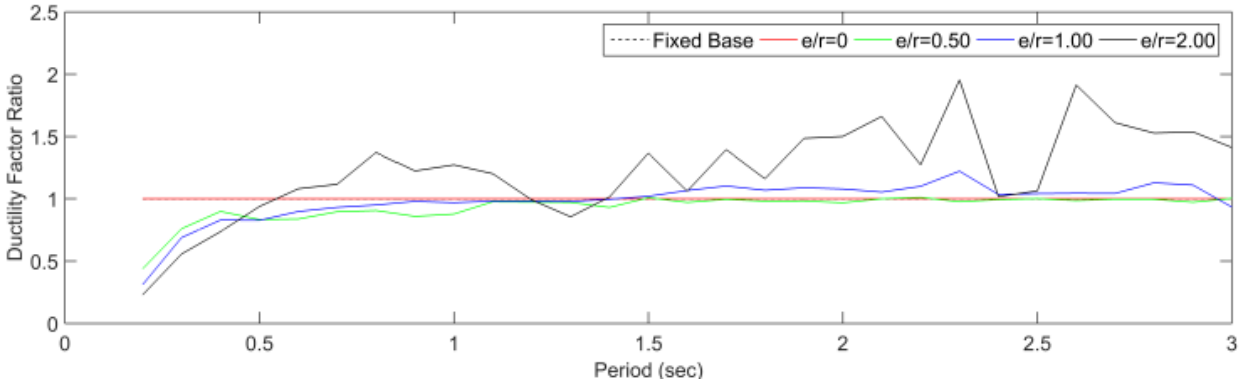

Fig. 4-22: Ductility factor Ratios for Tohoku Earthquake EW component at MYG006 with RFIM to without KI (h = 0.05, r = 10 m, ρ = 1.8x10^3 kg/m^3, V_s = 100 m/s, v = 0.42, m = N*100 t, m_f/m = 0.82, μ_{fix} = 6)

References for Chapter4

Ganjavi, B., & Hao, H. (2014). Strength reduction factor for MDOF soil–structure systems. The Structural Design of Tall and Special Buildings, 23(3), pp.161-180.

Ganjavi, B., Hao, H., & Hajirasouliha, I. (2016). Influence of Higher Modes on Strength and Ductility Demands of Soil–Structure Systems. Journal of Earthquake and Tsunami, 1650006.

Jennings, P. C., & Bielak, J. (1973). Dynamics of building-soil interaction. Bulletin of the Seismological Society of America, 63(1), pp.9-48.

Kausel, E. (1981). An explicit solution for the Green functions for dynamic loads in layered media. NASA STI/Recon Technical Report N, 82, 29505.

Khanmohammadi, L., Amiri, J. V., Davoodi, M. R., & Ghannad, M. A. (2014) Mathematical Analysis of Soil-Structure Interaction Including Kinematic and Inertial Interaction Effects. Jounal of mathematics and computer science, 12, pp.320-336.

Lu, Y., Hajirasouliha, I., & Marshall, A. M. (2016). Performance-based seismic design of flexible-base multi-storey buildings considering soil–structure interaction. Engineering Structures, 108, pp.90-103.

Mahsuli, M., & Ghannad, M. A. (2009). The effect of foundation embedment on inelastic response of structures. Earthquake Engineering & Structural Dynamics, 38(4), pp.423-437.

Meek, J. W., & Wolf, J. P. (1994). Cone models for embedded foundation. Journal of geotechnical engineering, 120(1), pp.60-80.

Mylonakis, G., Syngros, C., Gazetas, G., & Tazoh, T. (2006). The role of soil in the collapse of 18 piers of Hanshin Expressway in the Kobe earthquake. Earthquake engineering & structural dynamics, 35(5), pp.547-575.

Newmark, N. M. (1959). A method of computation for structural dynamics. Journal of the engineering mechanics division, 85(3), pp.67-94.

Park, J. (2002). Wave motion in finite and infinite media using the thin-layer method (Doctoral dissertation, Massachusetts Institute of Technology).

Roesset, J. M. (1980). A review of soil-structure interaction. Lawrence Livermore Laboratory.

Tajimi, H. (1980). A Contribution to Theoretical Prediction of Dynamic Stiffness Surface Foundations. In Proc. The 7th WCEE, Vol. 5, pp.105-112.

Waas, G. (1980). Dynamisch belastete Fundamente auf geschichtetem Baugrund. VDI-Berichte, (381), pp.185-189.

Wen, H. (2006). An Analytical Study on Effects of Foundation Type, Foundation Shape and Adjacent Building on Dynamic Soil Structure Interaction (Doctoral dissertation, Nagoya University).

Wolf, J. P. (1994). Foundation vibration analysis using simple physical models. Pearson Education.

Wolf, J. P., & Deeks, A. J. (2004). Foundation vibration analysis: A strength of materials approach. Butterworth-Heinemann.

Chapter 5

Dynamic Behavior of Adjacent Buildings with Different Foundation Embedment Depths

5.1 Introduction

In recent decades, structures have been built closer together due to the lack of space in large cities (Lou *et al.*, 2011). Therefore, research on this topic is necessary for reliable earthquake resistant designs in order to understand the key parameters of the effect of adjacency on the response of superstructures. In Section 3, a comprehensive history of research into DCI is given, which revealed that the soil and foundation types are fixed in many studies. A general comparison of DCI effects for different soil conditions, and foundation types (pile and mat foundations) has not been attempted. Moreover, the key DCI parameters during an earthquake cannot be specified definitely clearly for adjacent buildings that have different embedment conditions. Therefore, an analytical parametric study of rocking and horizontal responses of superstructures and their foundations is conducted. Different kinds of embedment situation and fixed base natural frequencies are considered for two and three closely spaced buildings placed on an elastic half-space and layered soil for different foundation types (mat or pile), shear wave velocities and soil material damping. Moreover, the effects of the mass and height of the superstructures on the DCI are also investigated.

In the present study, the mean power ratios (MRPs) and transfer function amplitudes of the superstructures and foundations are used to explain the effect of DCI on adjacent buildings

supported by mat and pile foundations placed on a half-space and layered soil. Firstly, the effect of DCI on identical buildings of different height but the same embedment depth is shown clearly for these two kinds of foundation by comparing MPRs, and transfer function amplitudes. Moreover, the wave-based DCI effect is determined by performing a parametric analysis to the clearance between the foundations. Next, the effect of DCI on different embedment depths is studied by using the same aforementioned physical indices. Moreover, a more detailed parametric analysis is applied for a mat foundation placed on a half-space for different heights and masses of adjacent buildings, shear wave velocities and material damping of soil by comparing the transfer function amplitudes. This research mainly considers the effect of DCI on the elastic conditions of soils and structures, but nonlinearity of soils is assumed by the soil profiles (shear velocities and material damping ratio) according to an equivalent nonlinear approach.

5.2 Analysis conditions

5.2.1 System of superstructures

The fixed base natural periods of the superstructures (T_{fix}) are taken as 0.5, 1.0, and 2.0 sec (fixed base natural frequencies of 2.0, 1.0 and 0.5 Hz). The masses of the superstructures (m_s) are taken as 2.5×10^6 kg, 5×10^6 kg, and 1×10^7 kg. The damping ratio of the superstructures h_{str} is taken as 3%.

5.2.2 Soil and foundation system

The soil is modeled as an elastic half-space and as layered elastic soil. For the elastic half-space, the soil mass density (ρ) is 1.7×10^3 kg/m^3, shear wave velocity of the soil (V_s) is either 100 or 200 m/s and the material damping of the soil h_s is 0%, 3% or 6%. V_s = 100 m/s and

h_s =6% is assumed for the situation that the soil is degraded under strong ground motions. For layered soil, the mass density, shear wave velocity, and material damping of the upper soil layer (ρ_1, V_{s1}, and h_s) are selected as 1.7x10^3 kg/m^3, 100 m/s and 3%, respectively; and the mass density, shear wave velocity, and material damping of the lower part of the soil (ρ_2, V_{s2}, and h_s) are selected as 1.8x10^3 kg/m^3, 300 m/s, and 3% respectively. The thickness of upper soil layer (H) is taken as 34 m of which the predominant frequency coincides with the soil-structure system of T_{fix} = 1.0 sec on a surface mat foundation. The Poisson ratio of soil (v) is taken as 0.45. The soil conditions are summarized in Figure 5-1.

The foundations are taken to be either mat or pile foundations. Slabs of foundations are selected as 20 x 20 m square mat foundations with embedment depths of 0, 2, 4, and 8 m and are considered as rigid. The foundation-to-superstructure mass ratio is selected as 0.2. It is assumed that there is no separation between the foundation and the soil. The properties of adjacent pile foundations can be seen in Figure 5-2, where S_{pile} is the pile interval, E_p is Young's modulus of the piles, v_p is the Poisson ratio of the piles, ρ_p is the mass density of the piles, and h_p is the material damping ratio of the piles. The pile diameters (d_{pile}) are selected as 0.75 m for T_{fix} = 0.5 sec buildings, 1.00 m for T_{fix} = 1.0 sec buildings and 1.50 m for T_{fix} = 2.0 sec buildings. The pile lengths (L_{pile}) are determined considering both 2 m anchors to the lower part of the soil and the embedment depths.

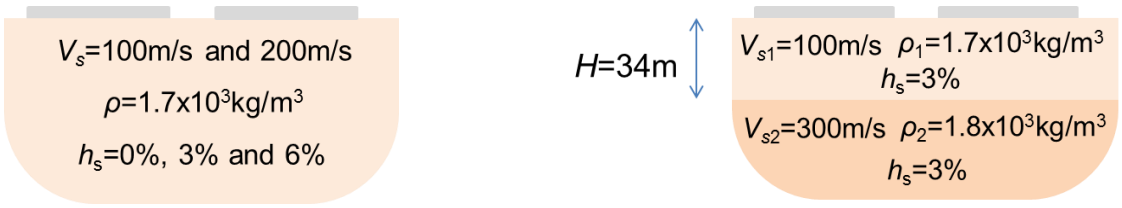

(a) Half-space soil **(b) Layered soil**

Figure 5-1: Selected soil conditions

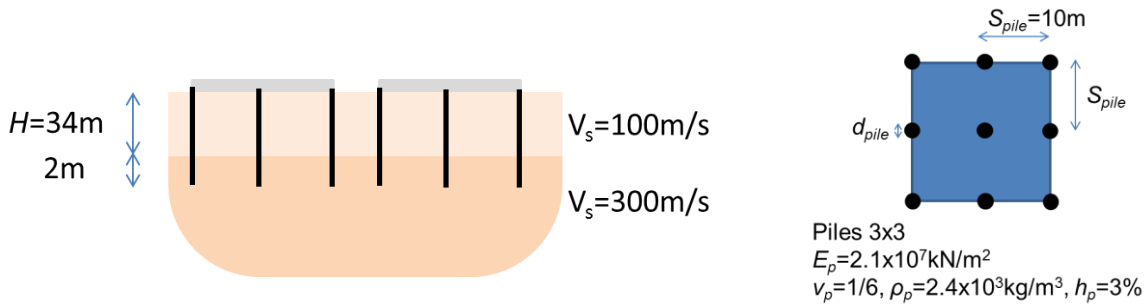

Figure 5-2: Properties of adjacent pile foundations

5.2.3 Layout of adjacent buildings

To see the effect of DCI for closely built structures, the clearance between foundations (D) is selected as 3 m or 6 m, because these values are seen in cities. Moreover, according to Alexander *et al.* (2013), the detrimental effect of DCI is only seen in closely spaced buildings. However, to determine the wave-based DCI effect, analyses for D = 3–72 m are also applied. The layout of the main and adjacent buildings can be seen in Figure 5-3, where D is the clearance between foundations, e_1 is the foundation embedment depth of the main building, e_2 and e_3 are the foundation embedment depths of the adjacent buildings, and U_{si} (i = 1–6) and U_{fi} (i = 1–6) are the directions of motion for the structure and its foundation, respectively. In the present study, T_{fix1} represents the fixed base natural period of the main superstructure, and T_{fix2} and T_{fix3} represent the fixed base natural periods of the adjacent superstructures.

5.2.4 Embedment cases of adjacent buildings

To determine the effect of foundation embedment depth on the DCI phenomenon, three different embedment situations are considered: 1) identical embedment depths (Figure 5-4), 2) shallower embedment depth for the main building (Figure 5-5), and 3) deeper embedment depth for the main building (Figure 5-6).

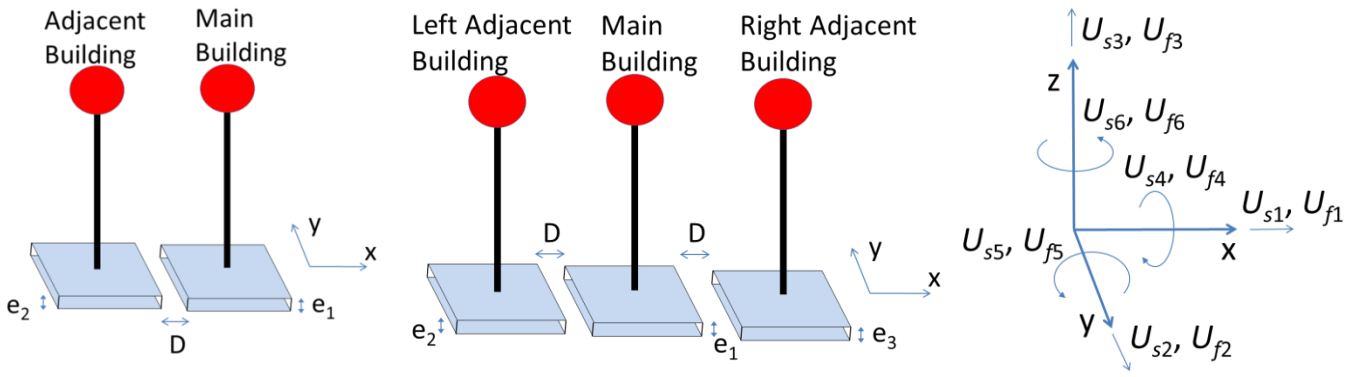

(a) 1 adjacent building case **(b) 2 adjacent buildings case** **(c) Motion directions**

Figure 5-3: Layout of adjacent buildings and motion directions

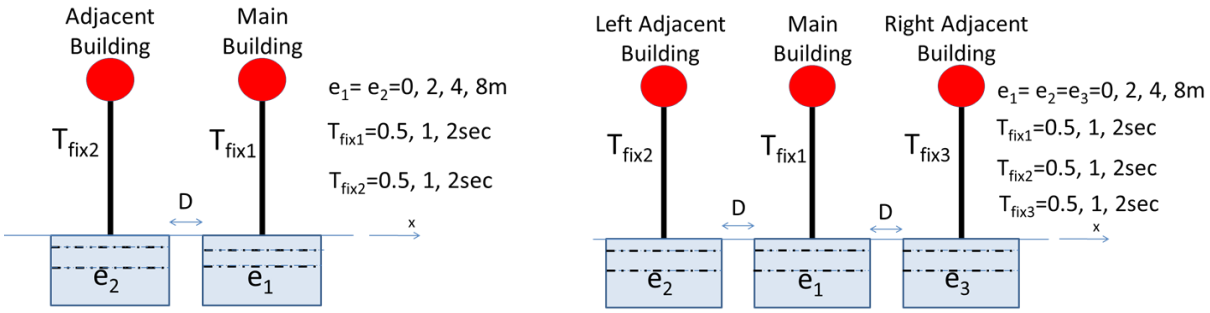

(a) 1 adjacent building case **(b) 2 adjacent buildings case**

Figure 5-4: Case of identical embedment depths

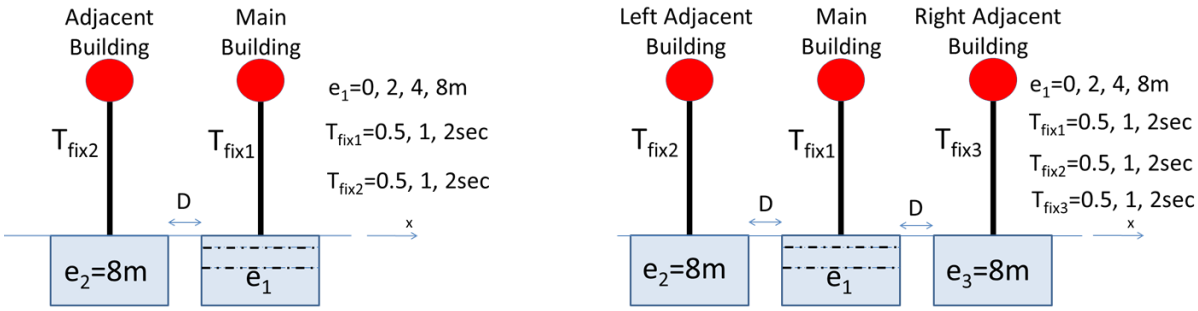

(a) 1 adjacent building case **(b) 2 adjacent buildings case**

Figure 5-5: Case of shallower embedment depth of the main building

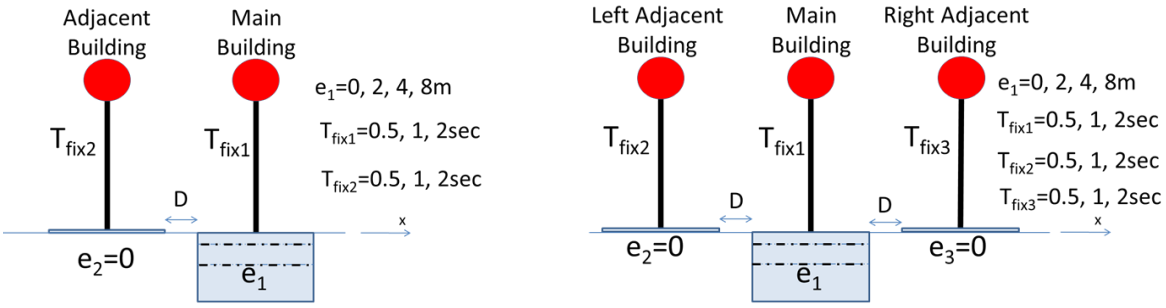

(a) 1 adjacent building case **(b) 2 adjacent buildings case**

Figure 5-6: Case of deeper embedment depth of the main building

5.3 Analysis method

To determine the key parameters affecting the DCI phenomenon through the responses of the superstructures, the responses of the adjacent buildings are analyzed by the substructure method of analysis using the flexible volume method constituted by the thin-layer method and the finite element method in three dimensions. During these analyses, the impedances, input motions, and transfer functions are calculated. The soil is modeled as thin layers with increasing thickness from top to bottom. Moreover, to represent unbounded soil, a paraxial boundary is applied to the bottom of the models. Moreover, a square massless rigid foundation placed on the soil is also divided into 3D finite elements, as shown in Figure 5-7 (Wen (2006)). The mass of the foundation is given as a point mass at the connection point of the foundation and the superstructure. Piles are modeled as 1 m long beam element.

To represent low, medium, and high story of buildings, 5, 10, and 20 story buildings are assumed. To prevent making the problem more complicated by considering superstructure modes other than the first natural mode, single degree of freedom (SDOF) systems are selected of

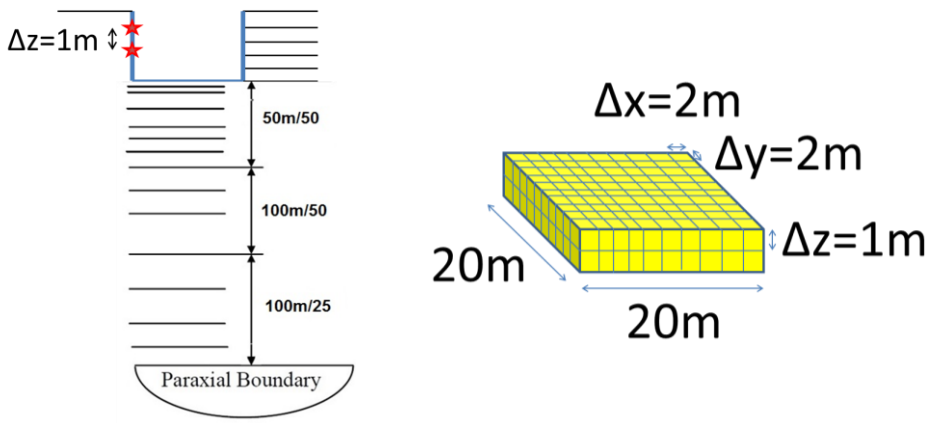

Figure 5-7: Analysis models of soil and foundation

effective height (H_{eff}) of 10, 20, and 40 m to represent 5, 10, and 20 story buildings, respectively. Buildings are modeled by beam elements with infinite bending stiffness.

To evaluate the effect of DCI, a similar method is applied as that used by Alexander *et al*. (2013). In this method, mean power values, which are the areas under the power spectra of the superstructure responses, are calculated. Then, the ratio of the adjacent building case (which is referred to Case-A in the present study) to the single building case (Case-S in the present study) is obtained and referred to as the mean power ratio (MPR) of the superstructures. The MPR shows the detrimental or beneficial effect of DCI on the responses of buildings. Since there is no effect of the phase and amplitude of the excitation on the MPR, the ratios of transfer functions are calculated directly. Frequency domain analysis is applied to the structure-soil-structure systems. Calculations are done for frequencies in the range of 0.1–10.0 Hz. Both the DCI effect along the placement of the buildings (*X* direction; in-plane DCI) and the DCI effect parallel to the placement of the buildings (*Y* direction; anti-plane DCI) are investigated.

5.4 Analysis results for half-space soil

In this section, all results are for h_s=3% unless specified otherwise.

5.4.1 Analysis results for *X* direction (in-plane DCI)

(a) Analysis results for 1 adjacent building, D = 3 m, V_s = 100 m/s

(1) Analysis results for identical embedment depths

The MPRs of superstructures (T_{fix1} = 0.5, 1.0 and 2.0 sec, mat foundations, half-space soil, D = 3 m, V_s = 100 m/s) for identical embedment depths ($e_1 = e_2$) on the X direction are given in Figure 5-8. Moreover, the MPRs of the foundation rocking motion of the superstructures for the same parameters are given in Figure 5-9.

When Figure 5-8 is examined for the effect of different heights of the adjacent building on the in-plane DCI, we find from the solid curve in Figure 5-8(a) that the highest MPRs are observed for short and light buildings (e.g. those with T_{fix1} = 0.5 sec), adjacent to tall and heavy buildings (e.g. those with T_{fix2} = 2.0 sec). In this figure, the mean powers of Case-A increase to about 20% compared with Case-S. This conclusion is similar to that of Alexander *et al*. (2013), where it is asserted that the power of an earthquake is transferred from tall and heavy structures to short and light structures.

For a heavy structure adjacent to a light structure, the MPRs are not higher than 1, as can be seen from the solid curve in Figure 5-8(c). This contradicts Alexander *et al*. (2013), where short and light structures act as passive dampers. A possible reason for this situation is that, a short and light adjacent structure (T_{fix2} = 0.5 sec) increases the mean power of the foundation rocking motion of the main structure (T_{fix1} = 2.0 sec), as can be seen from the solid curve in Figure 5-9(c).

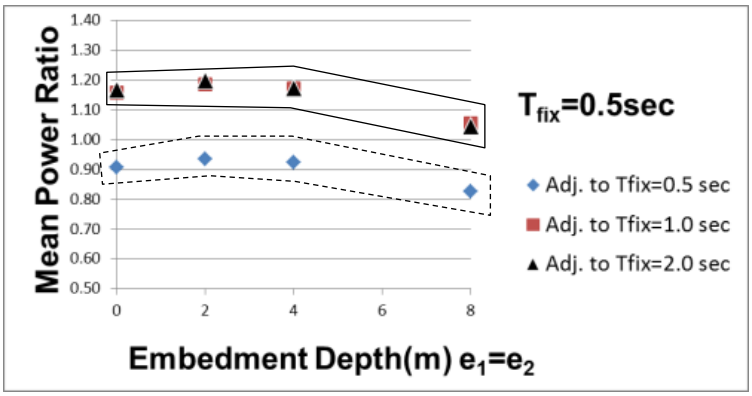

(a) For T_{fix1} = 0.5 sec

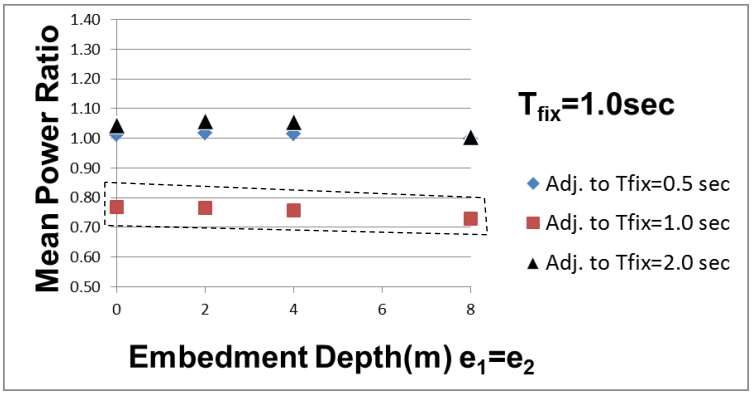

(b) For T_{fix1} = 1.0 sec

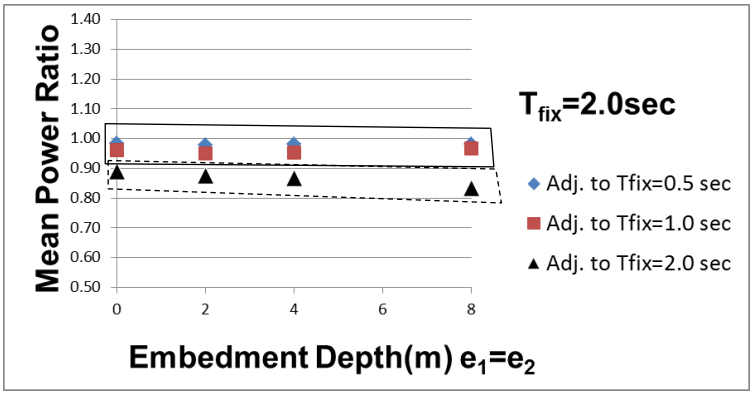

(c) For T_{fix1} = 2.0 sec

Figure 5-8: MPRs of horizontal superstructure motions for in-plane DCI ($e_1 = e_2$, D = 3 m, V_s = 100 m/s, 1 adj. building, U_{s1})

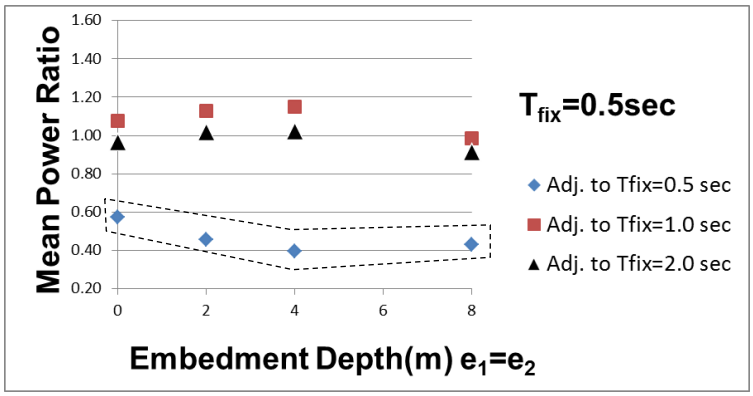

(a) For T_{fix1} = 0.5 sec

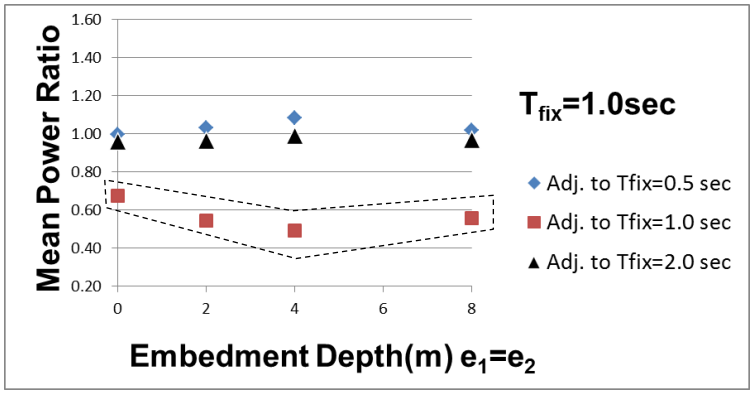

(b) For T_{fix1} = 1.0 sec

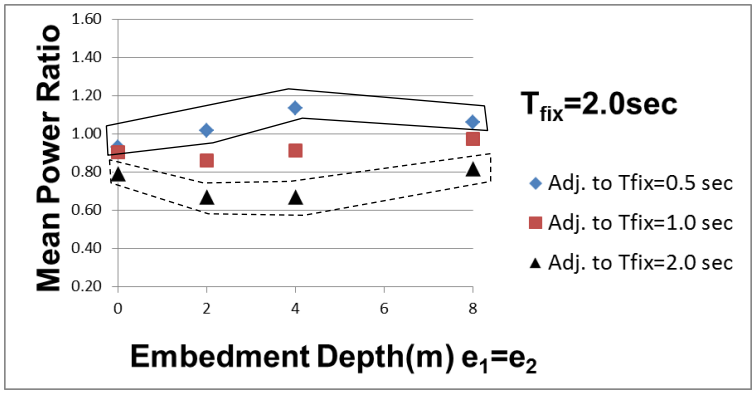

(c) For T_{fix1} = 2.0 sec

Figure 5-9: MPRs of foundation rocking motions for in-plane DCI ($e_1 = e_2$, D = 3 m, V_s = 100 m/s, 1 adj. building, U_{f5})

If Figures 5-8 and 5-9 are examined to determine the effect of foundation rocking motion on identical adjacent buildings of different heights, it can be claimed that there is a rocking restriction effect between identical adjacent buildings. This effect depends on the foundation embedment depths and the superstructure heights as can be seen from the dashed line in Figure 5-9. Moreover, it should be noted that the smallest MPR of the horizontal superstructure motion is obtained for identical adjacent buildings ($T_{fix1} = T_{fix2} = 1.0$ sec) for each embedment depth, as can be seen from the dashed curve in Figure 5-8(b). To explain this phenomenon, analyses are done for different clearance (D) values for twin adjacent buildings ($T_{fix1} = T_{fix2} = 0.5$, 1.0, and 2.0 sec) for only surface foundations ($e_1 = e_2 = 0$).

▪ Analyses for different *D* values

To understand wave transfer between adjacent buildings, (i.e. wave-based DCI), analyses for different D values become necessary. For the in-plane DCI case, there are two options for wave transfer between adjacent buildings as given in Figures 5-10(a) and 5-10(b), namely P and SV wave transfer, respectively. To understand which wave transfer is dominant, the MPRs of horizontal structural motions are calculated for Poisson ratio of soil (ν) of 0.25 and 0.45, twin adjacent buildings ($T_{fix1} = T_{fix2} = 0.5$ sec) on surface foundations ($e_1 = e_2 = 0$) over a wide range of D (3–72 m) as shown in Figure 5-11.

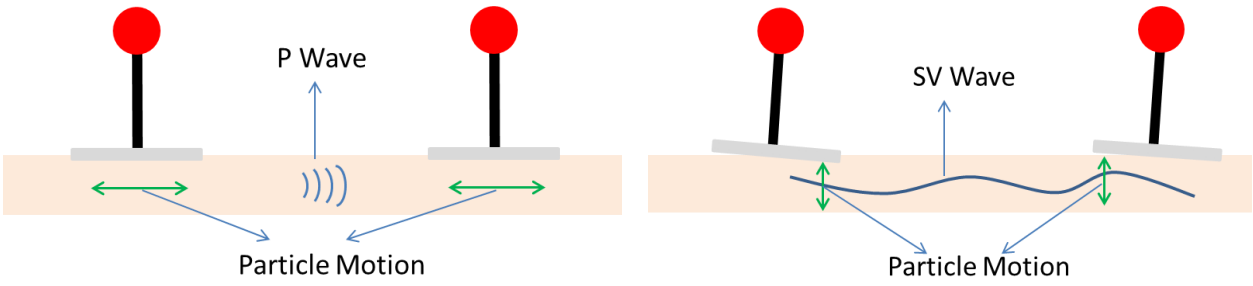

(a) P wave transfer **(b) SV wave transfer**

Figure 5-10: Possible wave transfers between adjacent buildings for in-plane DCI

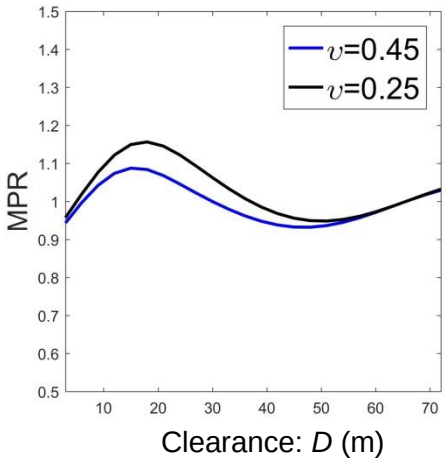

Figure 5-11: MPRs of horizontal superstructure motions for in-plane DCI ($e_1 = e_2 = 0$, D = 3 –72 m, V_s = 100 m/s, 1 adj. building, U_{s1}, v = 0.25 and 0.45)

As can be seen in Figure 5-11, the clearance at which the maximum effect of wave-based DCI is observed is not affected by the difference of Poisson ratio of soil (v). This means that a difference in P wave velocity (i.e., P wave effect), is not so important for wave transfer between buildings in the case of in-plane DCI. Therefore, it is concluded that in-plane wave-based DCI occurs by SV wave transfer between buildings. Such an interaction between buildings implies that the rocking motion of the foundations of adjacent buildings affects each other. To clarify this phenomenon, a rocking-fixed model (a constrained model that will be referred to as CM in brief) of the adjacent building is created to determine this SV wave transfer between buildings as shown in Figure 5-12. For comparison, the model shown in Figure 5-3(a) is referred to as the free model (FM). The MPRs of the horizontal structural motions for Poisson ratio of soil (v) of 0.45, twin adjacent buildings ($T_{fix1} = T_{fix2}$ = 0.5, 1.0, and 2.0 sec) on surface foundations ($e_1 = e_2 =$ 0) over a wide range of D (3 –72 m) are calculated as shown in Figure 5-13.

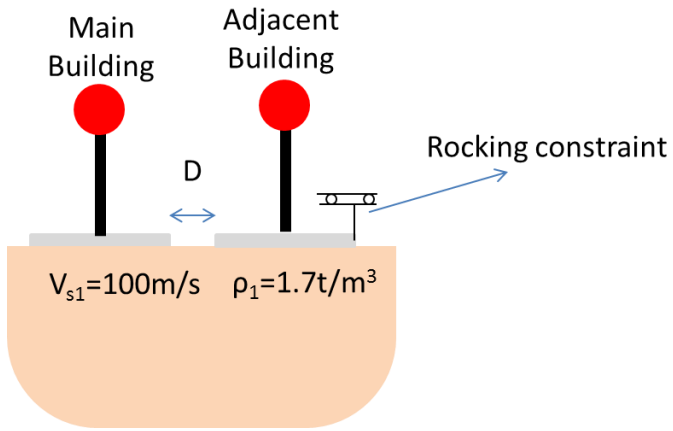

Figure 5-12: Constrained model (CM) for adjacent building

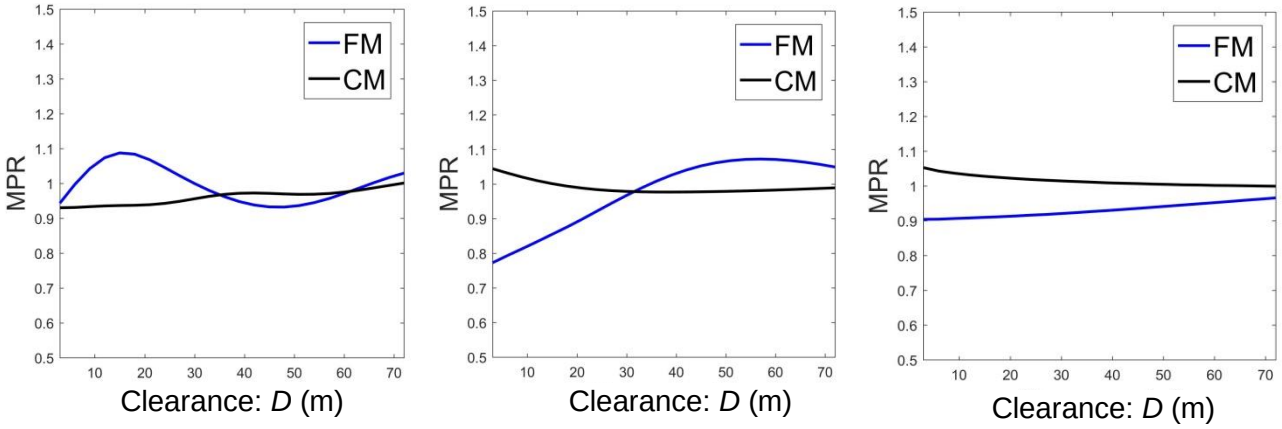

(a) $T_{fix1} = T_{fix2} = 0.5$ sec **(b) $T_{fix1} = T_{fix2} = 1.0$ sec** **(c) $T_{fix1} = T_{fix2} = 2.0$ sec**

Figure 5-13: MPRs of horizontal superstructure motion for free model (FM) and constrained model (CM) ($e_1 = e_2 = 0$, $D = 3$ –72 m, $V_s = 100$ m/s, 1 adj. building, U_{s1}, $\nu = 0.45$)

As shown in Figure 5-13, the wave-based DCI effect could not be observed for the CM because of the rocking constraint on the adjacent building, which prevents SV wave transfer between the buildings. Moreover, the wave-based DCI effect on the FM diminishes with increasing fixed based building period. This is because buildings with longer periods radiate waves with longer wavelengths and the effects of these waves are observed for wider clearances. If Figure 5-13(a) is comprehensively examined, it can be claimed that the detrimental effect of

wave-based DCI is also seen for narrow clearances. Therefore, the smallest MPRs of the horizontal superstructure motion are obtained for identical adjacent buildings ($T_{fix1} = T_{fix2} = 1.0$ sec) in Figure 5-8.

(2) Analysis results for shallower embedment depth of the main building

The MPRs of superstructures ($T_{fix1} = 0.5$, 1.0 and 2.0 sec, mat foundations, half-space soil, $D = 3$ m, $V_s = 100$ m/s) for different embedment depths of the main building (e_1) on the X direction are given in Figure 5-14 where the horizontal axis represents the foundation depth of the main building, and the foundation depth of the adjacent building (e_2) is selected as 8 m.

If Figure 5-14 is examined, it can be asserted that the beneficial effect of the in-plane DCI is more pronounced for a main building with a shallower foundation embedment depth, as can be seen inside the solid line in Figure 5-14. This is especially so for identical adjacent buildings with a natural period of 2.0 sec, as can be seen inside the solid line in Figure 5-14(c), because of power is transferred from the shallower foundation to the deeper foundation. To show this phenomenon, Case-A and Case-S transfer function amplitudes according to ground motion at the free surface (U_g) of the superstructures ($|U_{s1}/U_g|$) are given in Figure 5-15 for $T_{fix1} = T_{fix2} =$ 2.0 sec and $e_1 = 4$ m and $e_2 = 8$ m.

As can be seen in Figure 5-15, the MPR of the main building is clearly lower than that of the adjacent building. To explain this issue, in Figure 5-16, Case-S transfer function amplitudes of horizontal foundation motion ($|U_{f1}/U_g|$) are given for different embedment depths and superstructures.

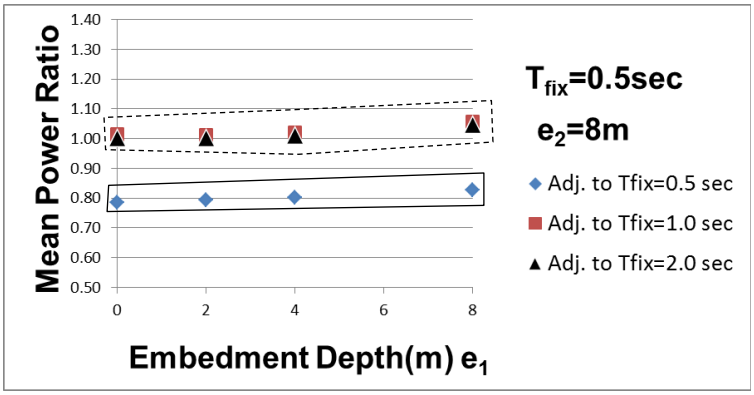

(a) For T_{fix1} = 0.5 sec

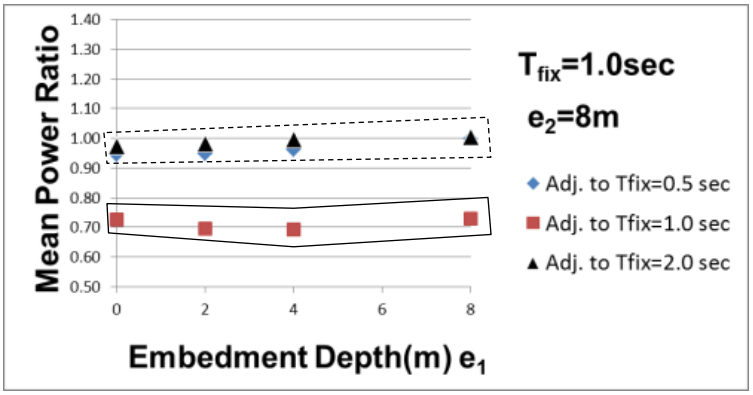

(b) For T_{fix1} = 1.0 sec

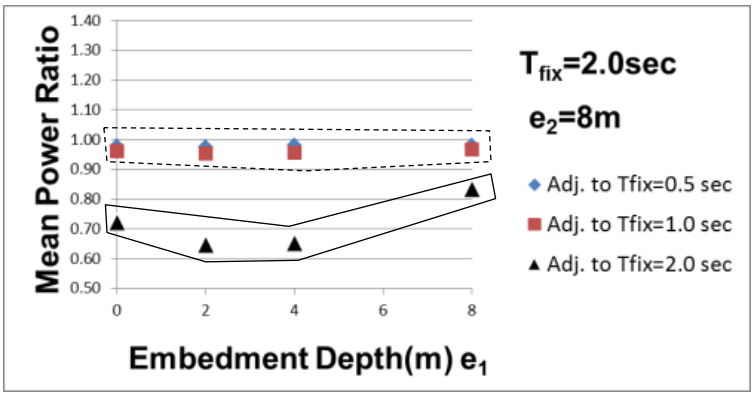

(c) For T_{fix1} = 2.0 sec

Figure 5-14: MPRs of horizontal superstructure motion for in-plane DCI (e_2 = 8 m, D = 3 m, V_s = 100 m/s, 1 adj. building, U_{s1})

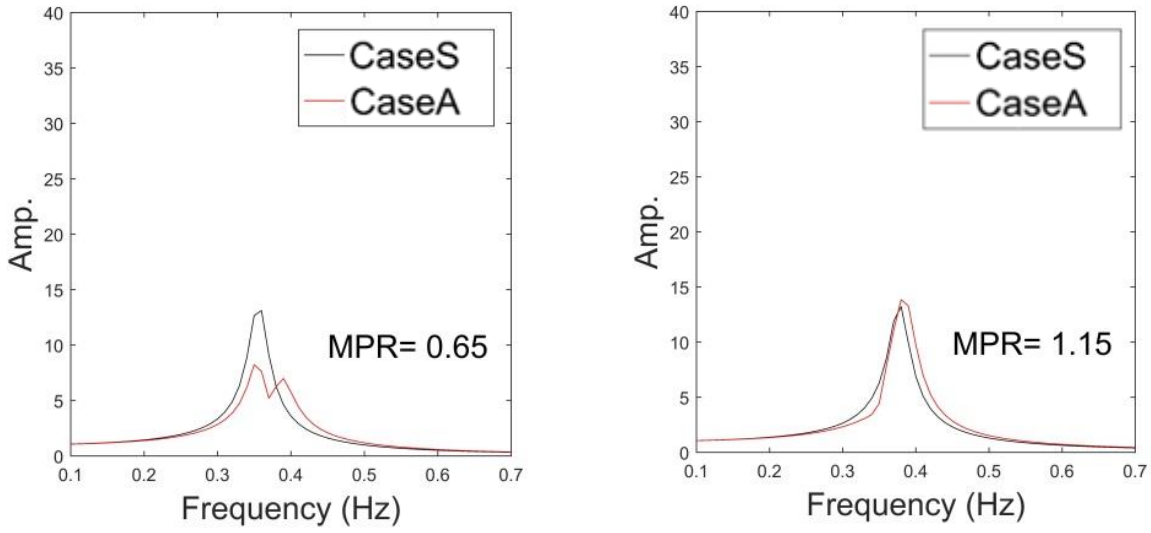

(a) Main building **(b) Adjacent building**

Figure 5-15: Case-A (Adjacent) and Case-S (Single) transfer function amplitudes ($|U_{s1}/U_g|$) and MPRs of superstructures ($T_{fix1} = T_{fix2}$ =2.0 sec, mat foundation, e_1 = 4 m, e_2 = 8 m, half-space soil, D = 3 m, V_s = 100 m/s)

If Figure 5-16 is examined, it can be seen that, high and low peaks only coincides in same frequencies for different embedment depths of foundations (especially for e_1 = 4 m and e_2 = 0) at Figure 5-16(c), where results for T_{fix} = 2.0 sec are given. Therefore, for identical adjacent buildings with different embedment ratios, it can be claimed that power transfer is higher for T_{fix} = 2.0 sec than T_{fix} = 0.5 sec and T_{fix} = 1.0 sec.

In contrast, as can be seen inside the dashed line in Figure 5-14, the in-plane DCI effect between tall and heavy buildings and short and light structures is negligible, similar to the identical embedment case.

.

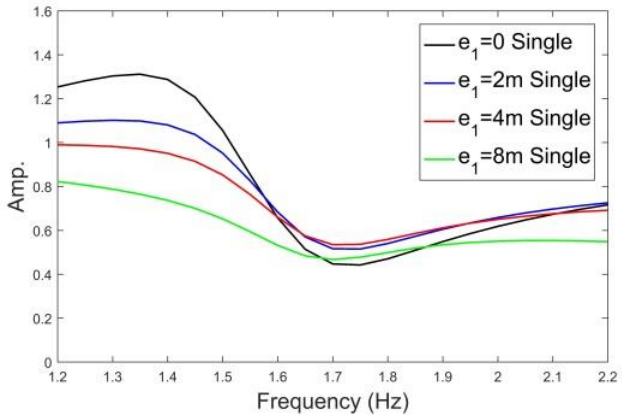

(a) For T_{fix} = 0.5 sec

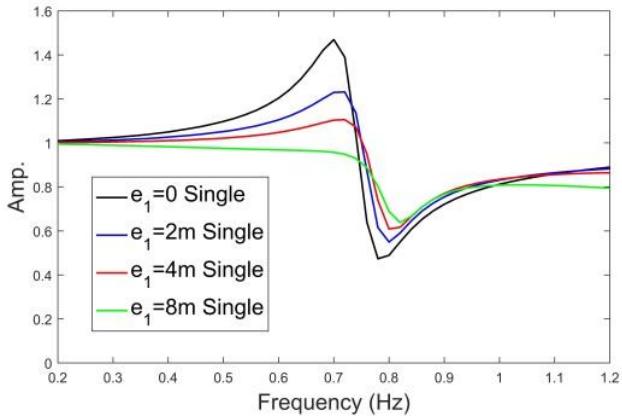

(b) For T_{fix} = 1.0 sec

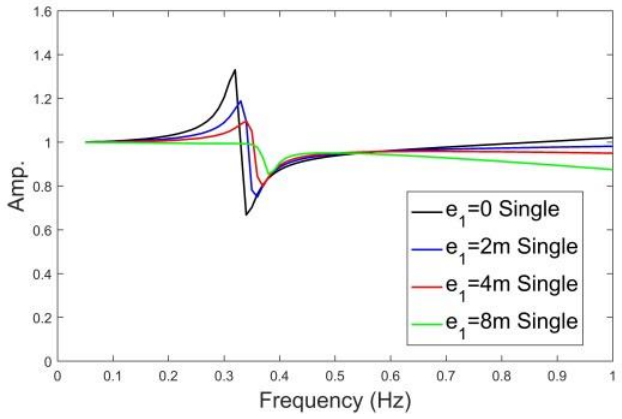

(c) For T_{fix} = 2.0 sec

Figure 5-16: Case-S transfer function amplitudes ($|U_{f1}/U_g|$) of horizontal foundation motion (h_s = 3%, V_s = 100 m/s)

(3) Analysis results for deeper embedment depth of the main building

The MPRs of superstructures (T_{fix1} = 0.5, 1.0 and 2.0 sec, mat foundations, half-space soil, D = 3 m, V_s = 100 m/s) for different embedment depths of the main building (e_1) on the X direction are given in Figure 5-17 where horizontal axis represents the foundation depth of the main building and the foundation depth of the adjacent building (e_2) is selected as 0.

If Figure 5-17 is examined, it can be said that the detrimental effect of in-plane DCI is more pronounced for the main building with a deeper foundation embedment depth, as can be seen inside the solid line in Figure 5-17. This is especially so for identical adjacent buildings with a natural period equals to 2.0 sec, as can be seen inside the solid line in Figure 5-17(c). This is because power is transferred from shallower foundation to deeper foundation, as noted previously. To show this phenomenon, Case-A and Case-S transfer function amplitudes ($|U_{s1}/U_g|$) of superstructures are given in Figure 5-18 for $T_{fix1} = T_{fix2}$ = 2.0 sec and e_1 = 4 m and e_2 = 0.

As can be seen in Figure 5-18, the MPR of the main building is clearly higher than that of the adjacent building. If Figure 5-17 is examined for the MPRs of identical adjacent buildings, it can be figure out that MPRs of greater than one are seen only for T_{fix} = 2.0 sec, as can be seen inside the solid line in Figure 5-17(c) for $e_1 > e_2$. The reason of this phenomenon is explained at Figure 5-16.

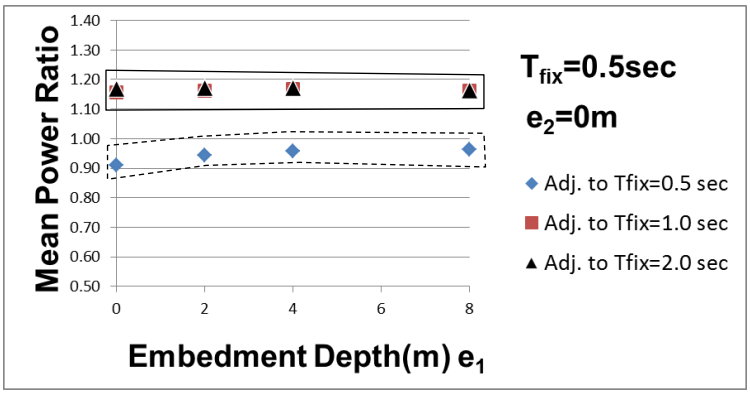

(a) For T_{fix1} = 0.5 sec

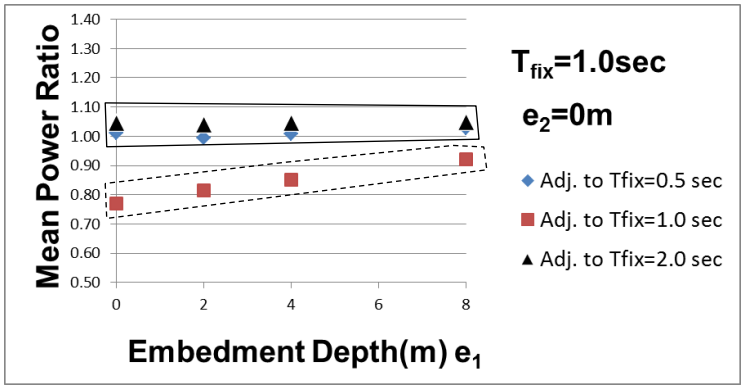

(b) For T_{fix1} = 1.0 sec

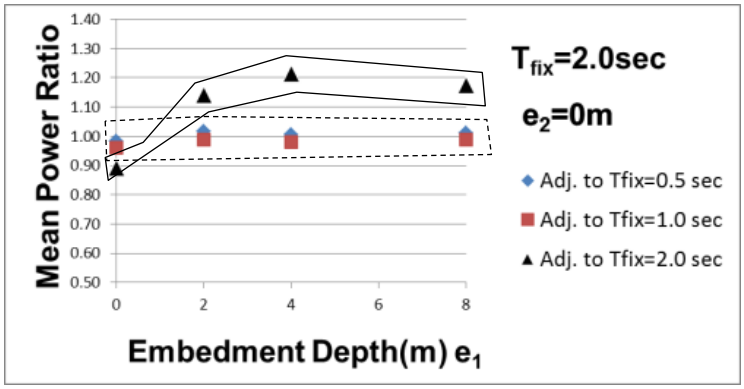

(c) For T_{fix1} = 2.0 sec

Figure 5-17: MPRs of horizontal superstructure motions for in-plane DCI (e_2 = 8 m, D = 3 m, V_s = 100 m/s, 1 adj. building, U_{s1})

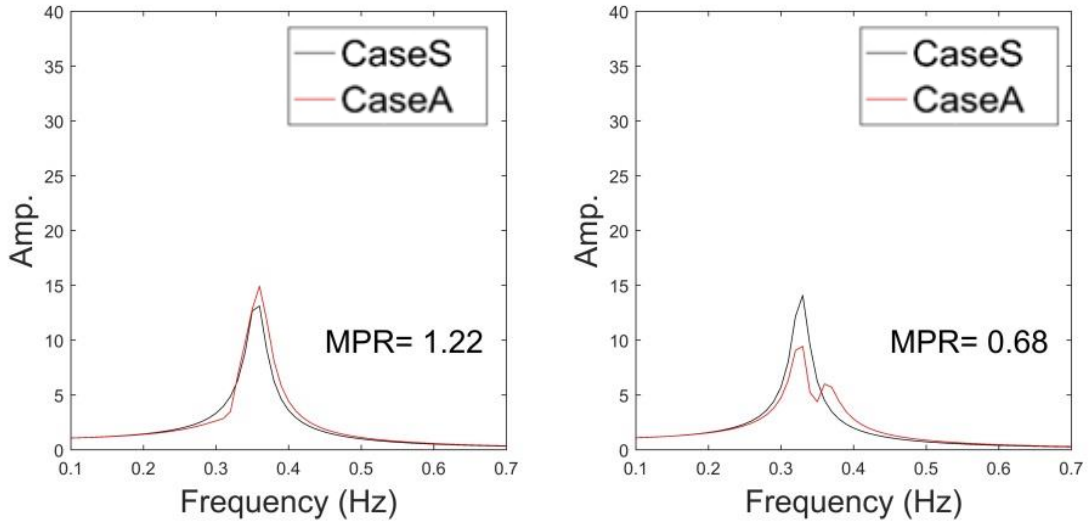

(a) Main building **(b) Adjacent building**

Figure 5-18: Case-A (Adjacent) and Case-S (Single) transfer function amplitudes ($|U_{s1}/U_g|$) and MPRs of superstructures ($T_{fix1} = T_{fix2} = 2.0$ sec, $e_1 = 4$ m, $e_2 = 0$, half-space soil, $D = 3$ m, $V_s = 100$ m/s)

The in-plane DCI effect on tall and heavy main buildings adjacent to short and light buildings is negligible, as can be seen inside the dashed line in Figure 5-17(b) and (c). However, the in-plane DCI effect on short and light main buildings adjacent to tall and heavy buildings is clearly distinguished, as can be seen inside the dashed line in Figure 5-17(a), for the reason stated at Section 5.4.1.

(b) Analysis results for 2 adjacent buildings, D= 3 m, V_s = 100 m/s

(1) Analysis results for identical embedment depths

The MPRs of superstructures (T_{fix1} = 0.5, 1.0 and 2.0 sec, mat foundations, half-space soil, D = 3 m, V_s = 100 m/s) for identical embedment depths ($e_1 = e_2 = e_3$) on the X direction are given in Figure 5-19.

If Figure 5-8 and 5-19 are compared to determine the effect of one more adjacent building, it can be asserted that the power effect of tall and heavy adjacent buildings on short and light main building is nearly doubled, as can be seen inside the solid line in Figure 5-8(a) and 5-19(a), which shows the increased detrimental effect of the in-plane DCI. Moreover, it can be said that the detrimental effect of the in-plane DCI is observed for identical adjacent tall and heavy buildings as can be seen inside the solid line in Figure 5-19(c). The reason of this phenomenon is that condition of main building is different than that of adjacent buildings because the main building is flanked by two buildings. Because of this difference, power is transferred to the main building. Moreover, the in-plane DCI effect on short and light main buildings adjacent to tall and heavy buildings and identical buildings, such as T_{fix1} = 0.5 sec, T_{fix2} = 0.5 sec and T_{fix3} = 2.0 sec, power transfer from tall and heavy building and restriction by the identical building balance each other and MPRs become close to 1 as can be seen inside the dashed line in Figures 5-19(a) and 5-19(b). The in-plane DCI effect on tall and heavy main buildings adjacent to short and light buildings is negligible, as can be seen inside the dashed line in Figure 5-19(c), for the reason stated at Section 5.4.1.

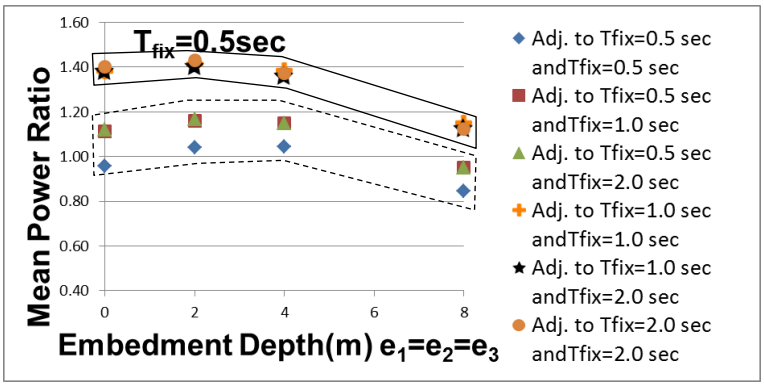

(a) For T_{fix1} = 0.5 sec

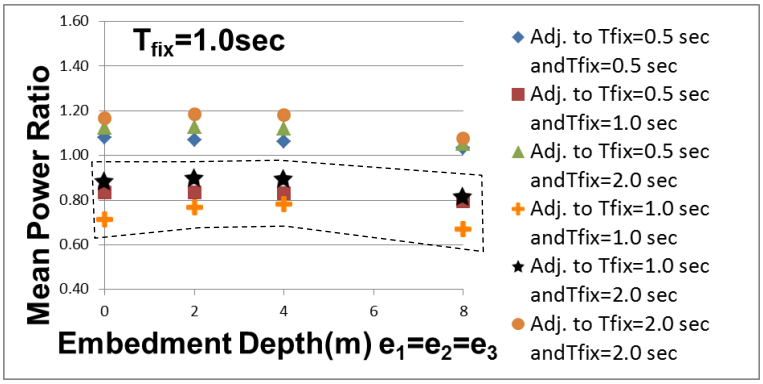

(b) For T_{fix1} = 1.0 sec

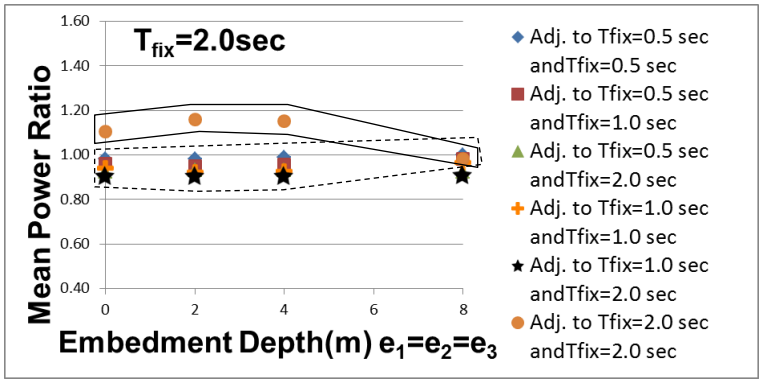

(c) For T_{fix1} = 2.0 sec

Figure 5-19: MPRs of horizontal superstructure motions for in-plane DCI ($e_1 = e_2 = e_3$, D = 3 m, V_s = 100 m/s, 2 adj. building, U_{s1})

(2) Analysis results for shallower embedment depth of the main building

The MPRs of superstructures (T_{fix1} = 0.5, 1.0 and 2.0 sec, mat foundations, half-space soil, D = 3 m, V_s = 100 m/s) for different embedment depths of the main building (e_1) on the X direction are given in Figure 5-20 where horizontal axis represents the foundation depth of the main building and the foundation depths of the adjacent buildings (e_2 and e_3) are selected as 8 m.

If Figure 5-14 and 5-20 are compared to determine the effect of one more adjacent building, it can be claimed that the effect of the in-plane DCI is on a similar level for 2 identical adjacent buildings with a deeper foundation embedment depth and 1 identical adjacent building case, as can be seen inside the solid line in Figures 5-14 and 5-20. Moreover, as can be seen inside the dashed line in Figures 5-14(a) and 5-20(a), a short and light main building is affected on similar extent when being adjacent to tall and heavy buildings for 1 and 2 adjacent building cases. The in-plane DCI effect on a tall and heavy main buildings adjacent to short and light buildings is negligible, as can be seen inside the dashed line in Figure 5-20(c).

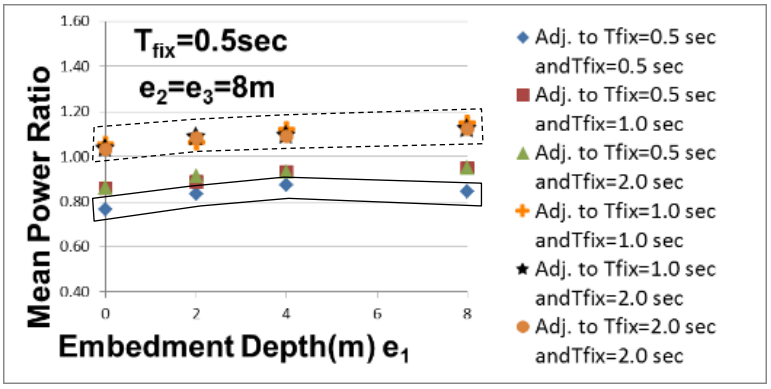

(a) For T_{fix1} = 0.5 sec

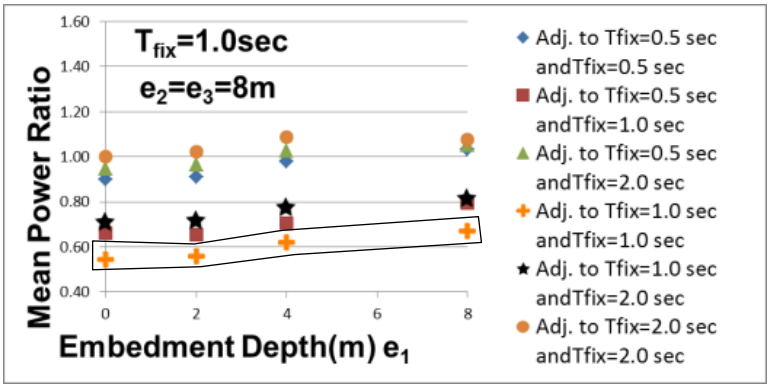

(b) For T_{fix1} = 1.0 sec

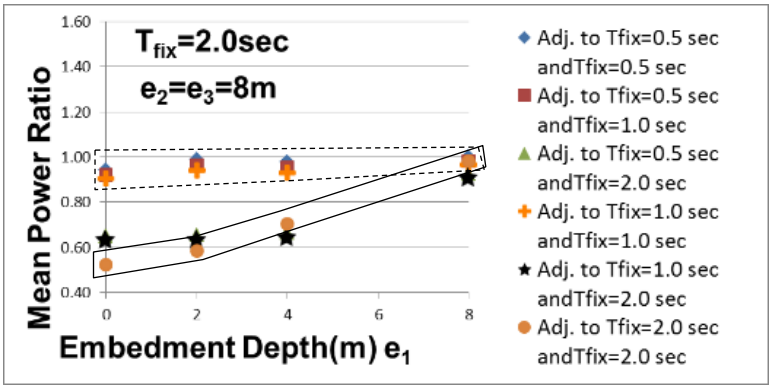

(c) For T_{fix1} = 2.0 sec

Figure 5-20: MPRs of horizontal superstructure motions for in-plane DCI ($e_2 = e_3$ = 8 m, D = 3 m, V_s = 100 m/s, 2 adj. building, U_{s1})

(3) Analysis results for deeper embedment depth of the main building

The MPRs of superstructures (T_{fix1} = 0.5, 1.0 and 2.0 sec, mat foundations, half-space soil, D = 3 m, V_s = 100 m/s) for different embedment depths of the main building (e_1) on the X direction are given in Figure 5-21 where horizontal axis represents the foundation depth of the main building and foundation depth of adjacent buildings (e_2 and e_3) are selected as 0.

If Figure 5-17 and 5-21 are compared to determine the effect of one more adjacent building, it can be asserted that detrimental effect of the in-plane DCI is doubled for 2 identical adjacent buildings with shallower foundation embedment depth than 1 identical adjacent building case , as can be seen inside the solid line in Figure 5-17 and Figure 5-21. This is especially so for identical adjacent buildings with fixed base natural period of 2.0 sec, as can be seen inside the solid line in Figure 5-17(c) and Figure 5-21(c), due to power is transferred from 1 more shallow foundation to deep foundation. Moreover, it should be noted that, as can be seen inside the dashed line in Figure 5-17(a) and Figure 5-21(a), short and light main building is affected nearly doubled when being adjacent to tall and heavy buildings than the 1 adjacent building case. The in-plane DCI effect on tall and heavy main buildings adjacent to short and light buildings is negligible, as can be seen inside the dashed line in Figure 5-21(c), for the reason stated at Section 5.4.1.

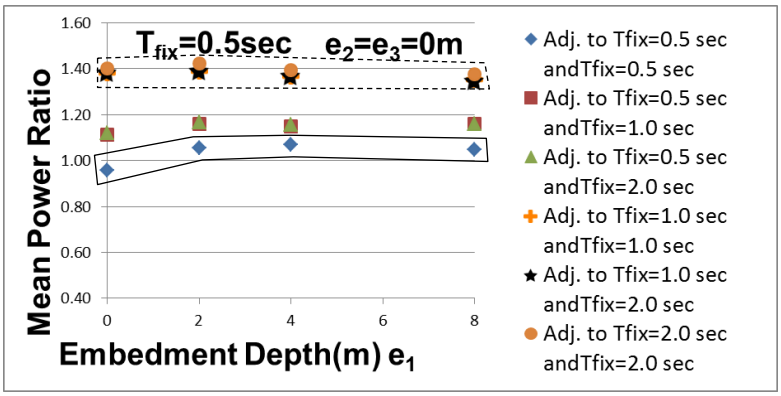

(a) For T_{fix1} = 0.5 sec

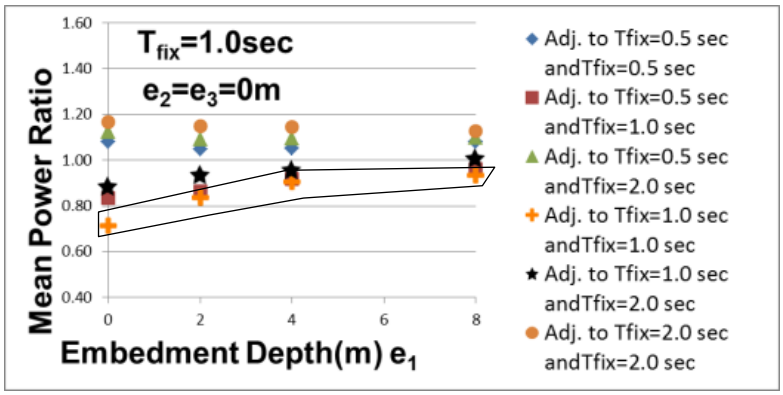

(b) For T_{fix1} = 1.0 sec

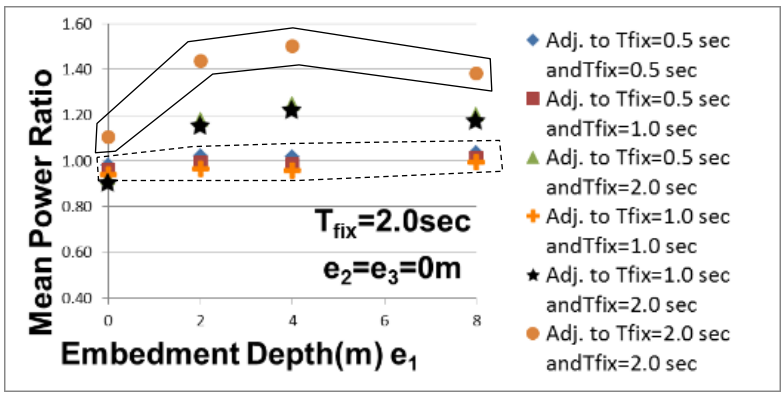

(c) For T_{fix1} = 2.0 sec

Figure 5-21: MPRs of horizontal superstructure motions for in-plane DCI ($e_2 = e_3 = 0$, D= 3 m, V_s = 100 m/s, 2 adj. building, U_{s1})

(c) Analysis results for 1 adjacent building, D = 3 m, V_s = 200 m/s

(1) Analysis results for identical embedment depths

The MPRs of superstructures (T_{fix1} = 0.5, 1.0 and 2.0 sec, mat foundations, half-space soil, D = 3 m, V_s = 200 m/s) for identical embedment depths ($e_1 = e_2$) on the X direction are given in Figure 5-22.

If the results of V_s = 100 and 200 m/s situations are compared, it can be said that the in-plane DCI effect on short and light buildings adjacent to tall and heavy buildings is strongly decreased by increasing values of V_s, as can be seen inside the solid line in Figure 5-22(a). Moreover, it should be added that the smallest MPRs are obtained for identical adjacent buildings for $T_{fix1} = T_{fix2}$ = 0.5sec as can be seen inside the dashed line in Figure 5-22(a). The reason of this result is considered to be that the wave-based DCI effect becomes negligible for V_s = 200 m/s.

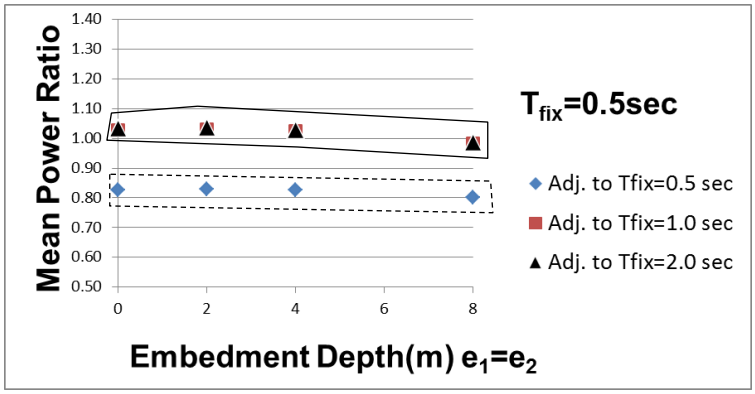

(a) For T_{fix1} = 0.5 sec

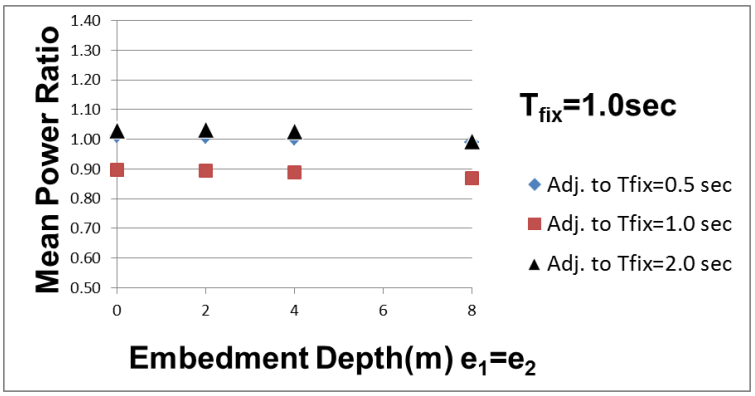

(b) For T_{fix1} = 1.0 sec

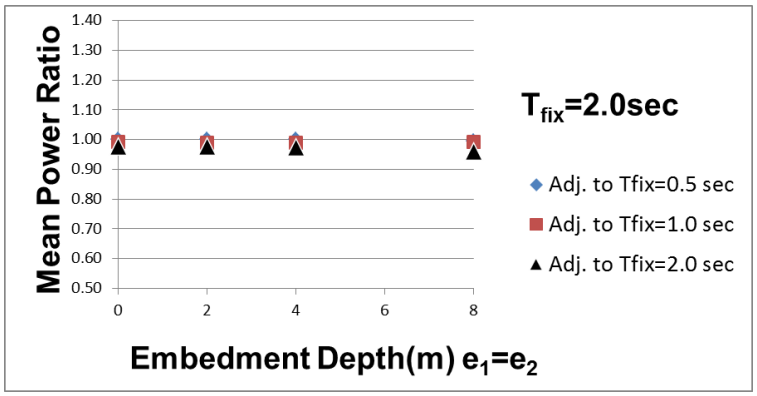

(c) For T_{fix1} = 2.0 sec

Figure 5-22: MPRs of horizontal superstructure motions for in-plane DCI ($e_1 = e_2$, D= 3 m, V_s = 200 m/s, 1 adj. building, U_{s1})

(2) Analysis results for shallower embedment depth of the main building

The MPRs of superstructures (T_{fix1} = 0.5, 1.0 and 2.0 sec, mat foundations, half-space soil, D = 3 m, V_s = 200 m/s) for different embedment depths of main building (e_1) on the X direction are given in Figure 5-23 where horizontal axis represents the foundation depth of the main building and the foundation depth of the adjacent building (e_2) is selected as 8 m. If the results of the V_s = 100 and 200 m/s situations are compared, it can be claimed that the beneficial effect of the in-plane DCI diminishes with increasing shear wave velocity of the soil, as can be seen inside the solid line in Figure 5-23(c). It is interesting that the beneficial effect of the in-plane DCI and the relationship with the foundation embedment depth of the main building change for V_s = 200 m/s. To explain this issue, in Figure 5-24, transfer function amplitudes of horizontal foundation motions of single buildings for different embedded depths and superstructures are given.

If Case-S transfer function amplitudes ($|U_{f1}/U_g|$) of horizontal foundation motion (T_{fix} = 2.0 sec) for V_s = 100 m/s (Figure 5-16(c)) and for V_s = 200 m/s (Figure 5-24(c)) are compared, it can be said that, high and low peaks coincide at the same frequencies at e_1 = 4 m and e_2 = 0 for V_s = 100 m/s, but because of the shift of the transfer functions for stiffer soil (V_s = 200 m/s), this effect could not be seen clearly. Therefore, for V_s = 200 m/s and T_{fix1} = T_{fix2} = 2.0sec, the highest effect of in-plane DCI is seen for e_1 = 8 m and e_2 = 0.

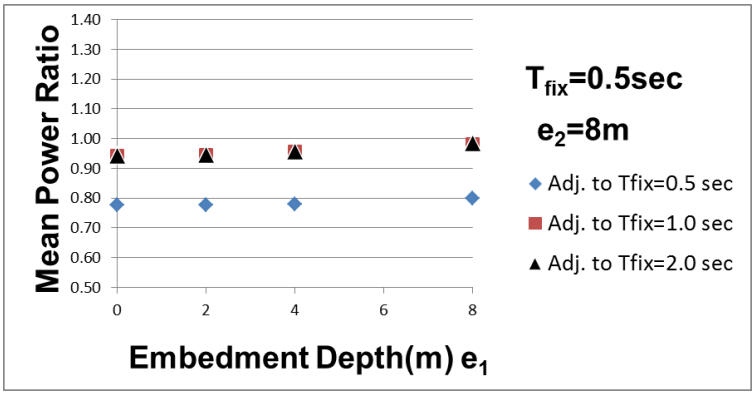

(a) For T_{fix1} = 0.5 sec

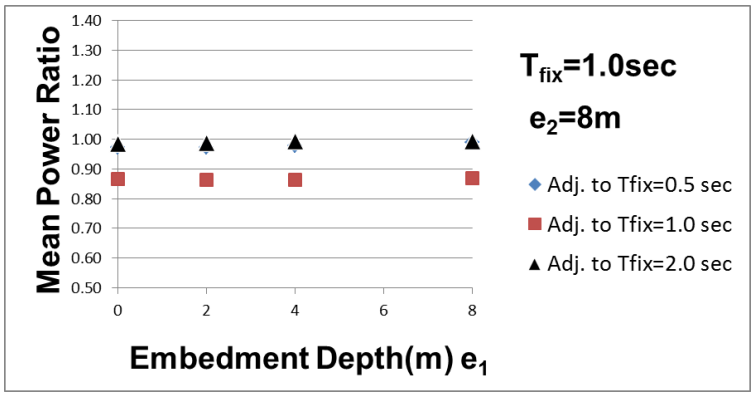

(b) For T_{fix1} = 1.0 sec

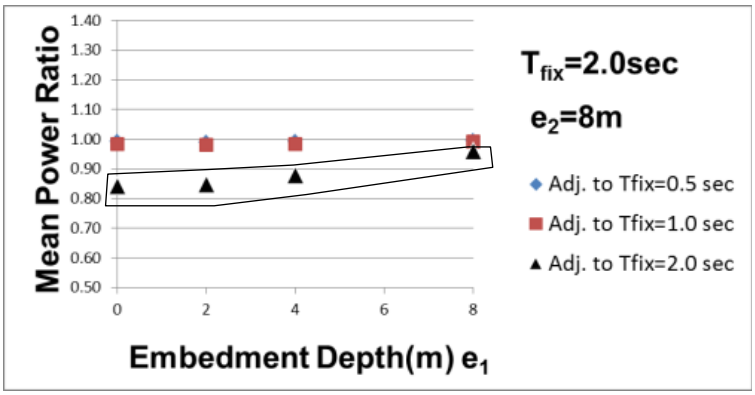

(c) For T_{fix1} = 2.0 sec

Figure 5-23: MPRs of horizontal superstructure motions for in-plane DCI (e_2 = 8 m, D = 3 m, V_s = 200 m/s, 1 adj. building, U_{s1})

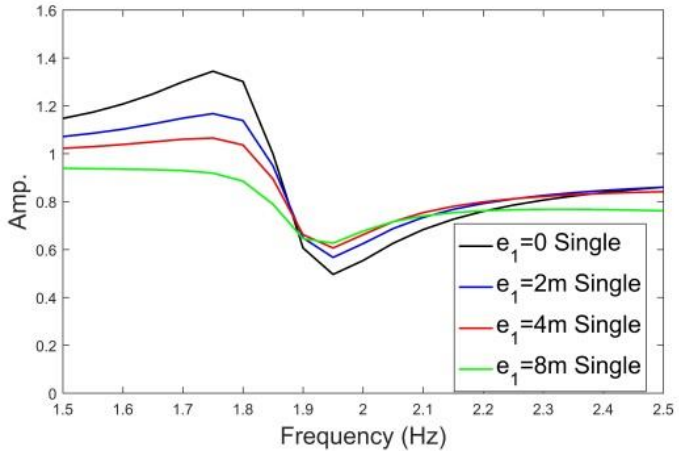

(a) For T_{fix} = 0.5 sec

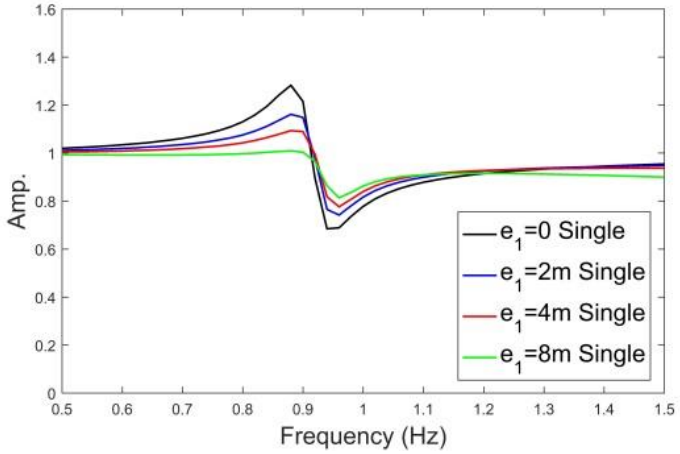

(b) For T_{fix} = 1.0 sec

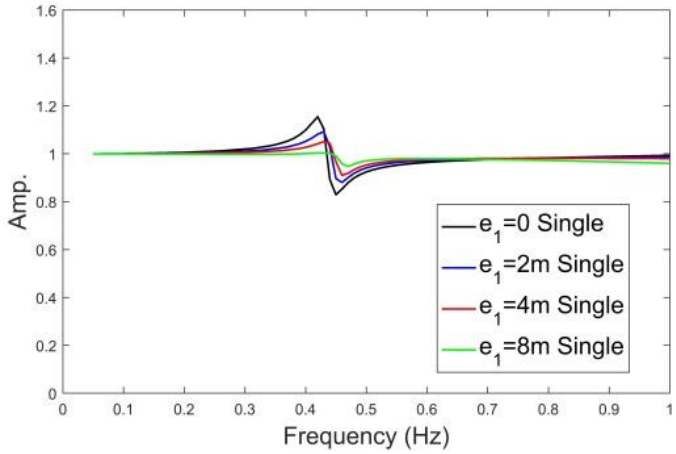

(c) For T_{fix} = 2.0 sec

Figure 5-24: Case-S transfer function amplitudes ($|U_{f1}/U_g|$) of horizontal foundation motion (h_s = 3%, V_s = 200 m/s)

(3) Analysis results for deeper embedment depth of the main building

The MPRs of superstructures (T_{fix1} = 0.5, 1.0 and 2.0 sec, mat foundations, half-space soil, D = 3 m, V_s = 200 m/s) for different embedment depths of the main building (e_1) on the X direction are given in Figure 5-25 where horizontal axis represents the foundation depth of the main building and the foundation depth of the adjacent building (e_2) is selected as 0.

If the results of V_s = 100 and 200 m/s situations are compared, it can be declared that the detrimental effect of the in-plane DCI diminishes with increasing shear wave velocity of the soil, as can be seen inside the solid line in Figure 5-25(c). Again, the effect of the in-plane DCI and the relationship of the foundation embedment depth of main building change for V_s = 200 m/s for the reason stated at the previous section.

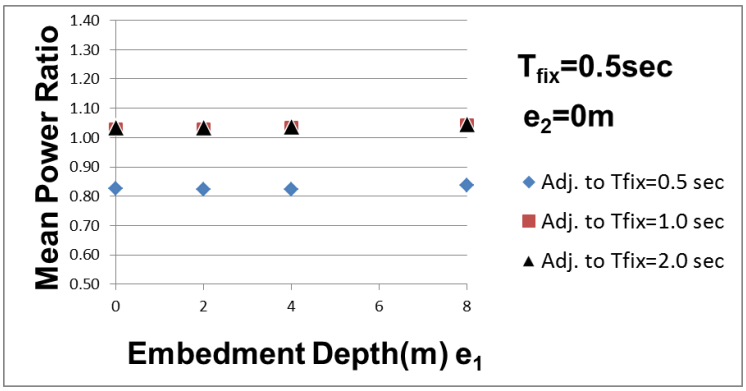

(a) For T_{fix1} = 0.5 sec

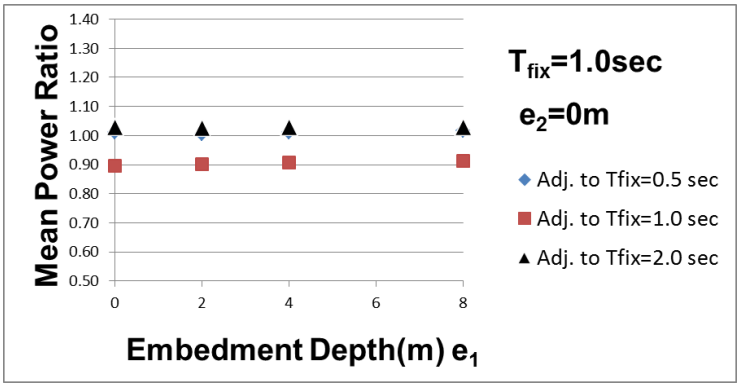

(b) For T_{fix1} = 1.0 sec

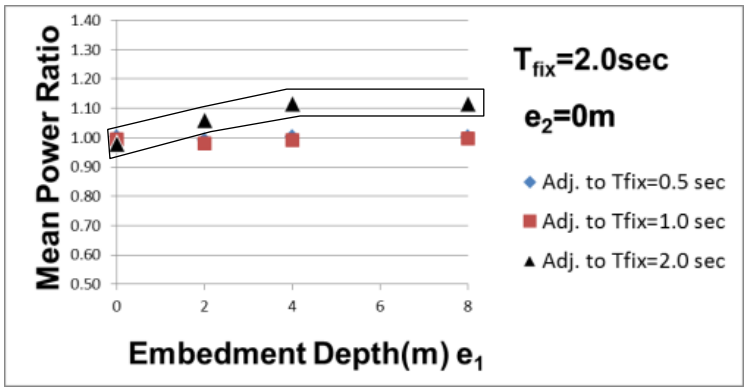

(c) For T_{fix1} = 2.0 sec

Figure 5-25: MPRs of horizontal superstructure motions for in-plane DCI (e_2= 0, D = 3 m, V_s = 200 m/s, 1 adj. building, U_{s1})

(d) Analysis results for 2 adjacent buildings, D = 3 m, V_s = 200 m/s

(1) Analysis results for identical embedment depths

The MPRs of superstructures (T_{fix1} = 0.5, 1.0 and 2.0 sec, mat foundations, half-space soil, D = 3 m, V_s = 200 m/s) for identical embedment depths ($e_1 = e_2 = e_3$) on the X direction are given in Figure 5-26.

If the results of V_s = 100 and 200 m/s situations are compared, it can be said that a similar relation is seen for 1 and 2 adjacent buildings cases. However, it is interesting to note that the detrimental effect of the in-plane DCI for identical adjacent tall and heavy buildings diminishes because of the stiffness of the soil, as can be seen inside the solid line in Figure 5-26(c).

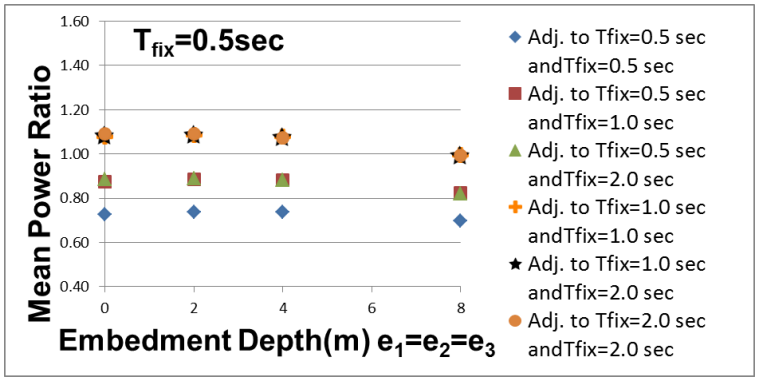

(a) For T_{fix1} = 0.5 sec

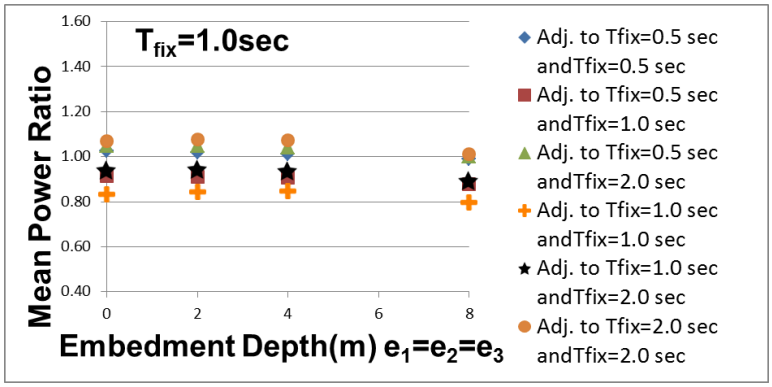

(b) For T_{fix1} = 1.0 sec

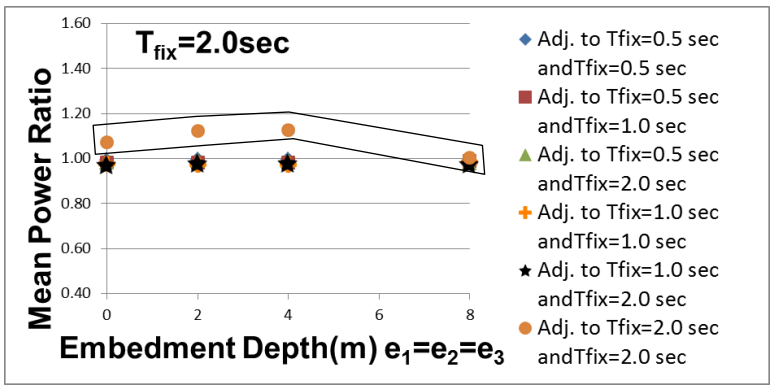

(c) For T_{fix1} = 2.0 sec

Figure 5-26: MPRs of horizontal superstructure motions for in-plane DCI ($e_1 = e_2 = e_3$, D = 3 m, V_s = 200 m/s, 2 adj. building, U_{s1})

(2) Analysis results for shallower embedment depth of the main building

The MPRs of superstructures (T_{fix1} = 0.5, 1.0 and 2.0 sec, mat foundations, half-space soil, D = 3 m, V_s = 200 m/s) for different embedment depths of the main building (e_1) on the X direction are given in Figure 5-27 where horizontal axis represents the foundation depth of the main building and the foundation depths of the adjacent buildings (e_2 and e_3) are selected as 8 m.

If the results of V_s = 100 and 200 m/s situations are compared, it can be said that a similar relation is seen for the cases of one and two adjacent buildings.

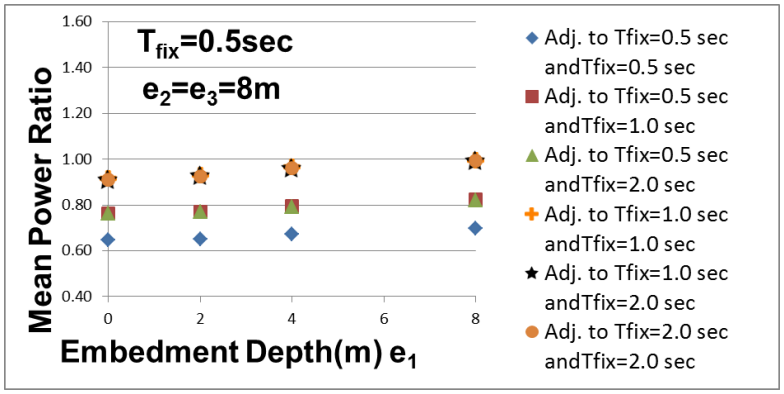

(a) For T_{fix1} = 0.5 sec

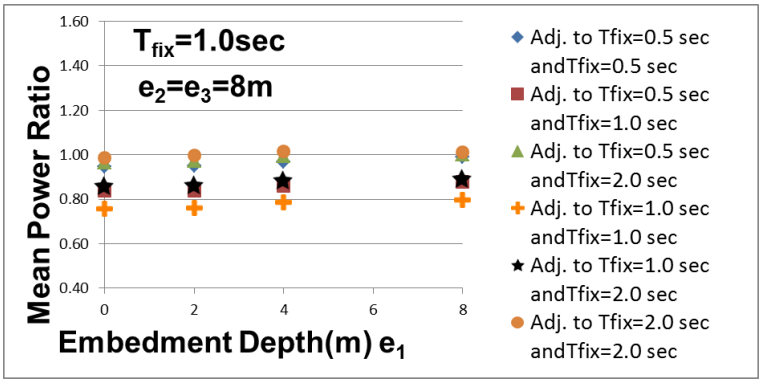

(b) For T_{fix1} = 1.0 sec

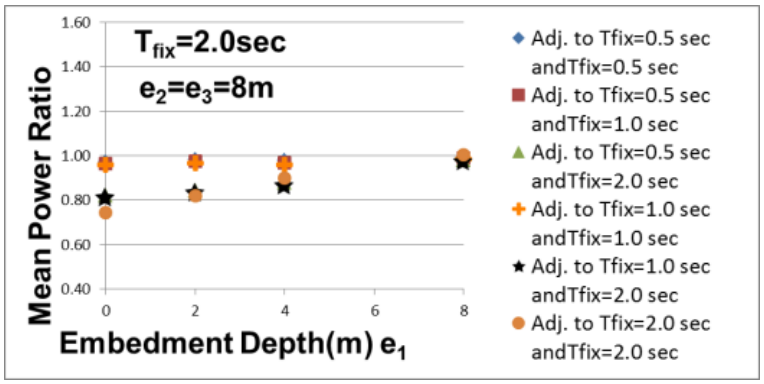

(c) For T_{fix1} = 2.0 sec

Figure 5-27: MPRs of horizontal superstructure motions for in-plane DCI ($e_2 = e_3$ = 8 m, D= 3 m, V_s = 200 m/s, 2 adj. building, U_{s1})

(3) Analysis results for deeper embedment depth of the main building

The MPRs of superstructures (T_{fix1} = 0.5, 1.0 and 2.0 sec, mat foundations, half-space soil, D = 3 m, V_s = 200 m/s) for different embedment depths of the main building (e_1) on the X direction are given in Figure 5-28 where horizontal axis represents the foundation depth of the main building and foundation depth of adjacent buildings (e_2 and e_3) are selected as 0.

If the results of V_s = 100 and 200 m/s situations are compared, it can be asserted that a similar relation is seen for the cases of 1 and 2 adjacent buildings, as can be seen inside the solid line in Figure 5-28(c).

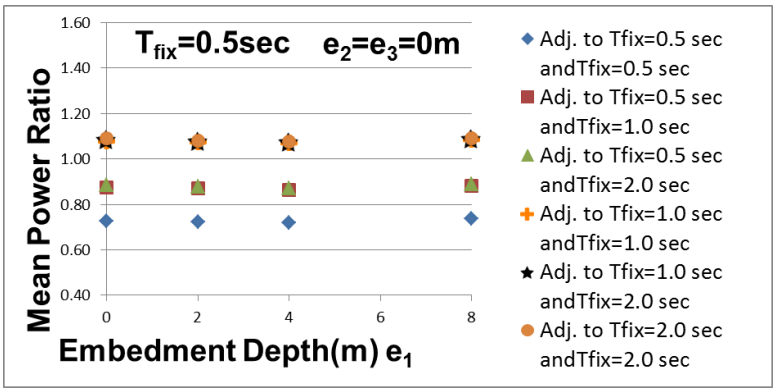

(a) For T_{fix1} = 0.5 sec

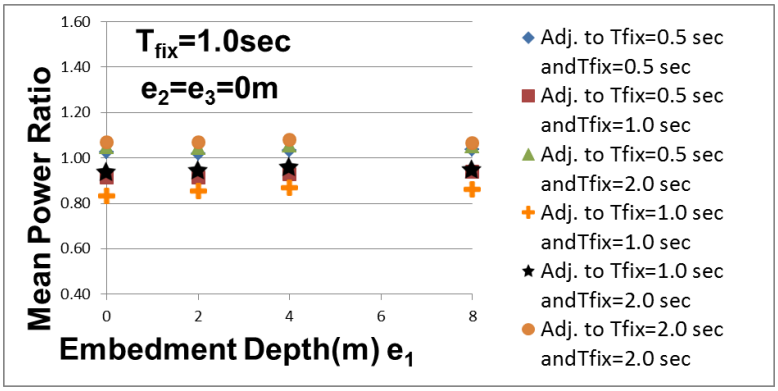

(b) For T_{fix1} = 1.0 sec

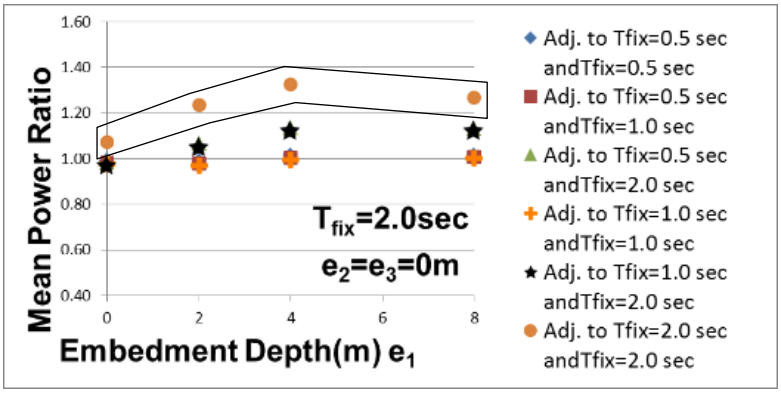

(c) For T_{fix1} = 2.0 sec

Figure 5-28: MPRs of horizontal superstructure motions for in-plane DCI (e_2 = e_3= 0, D = 3m, V_s = 200 m/s, 2 adj. building, U_{s1})

(e) Analysis results for 1 adjacent building, D = 6 m, V_s = 100 m/s

(1) Analysis results for identical embedment depths

The MPRs of superstructures (T_{fix1} = 0.5, 1.0 and 2.0 sec, mat foundations, half-space soil, D = 6m, V_s = 100 m/s) for identical embedment depths ($e_1 = e_2$) on the X direction are given in Figure 5-29.

If the results of D = 3 m and 6m situations are compared, it can be claimed that the in-plane DCI effect on short and light buildings adjacent to tall and heavy buildings not so dependent to the clearance, as can be seen inside the solid line in Figure 5-29(a). It can also be asserted that the in-plane DCI effect for adjacent buildings with identical embedment depths D= 6 m, and V_s = 100 m/s is more effective than D = 3 m, and V_s = 200 m/s.

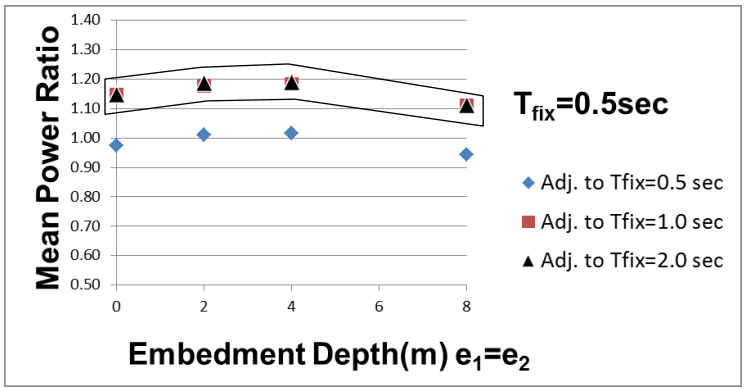

(a) For T_{fix1} = 0.5 sec

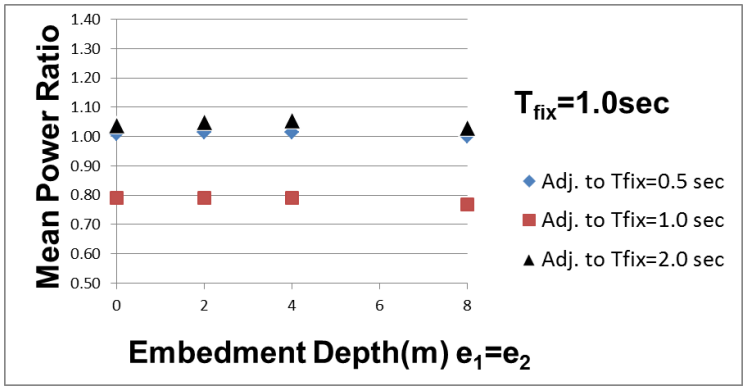

(b) For T_{fix1} = 1.0 sec

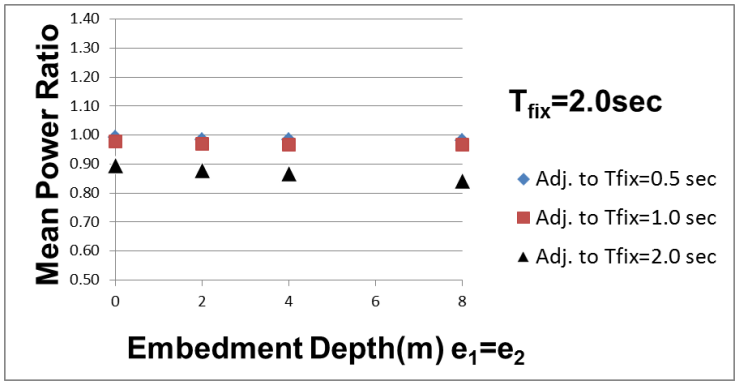

(c) For T_{fix1} = 2.0 sec

Figure 5-29: MPRs of horizontal superstructure motions for in-plane DCI ($e_1 = e_2$, D = 6 m, V_s = 100 m/s, 1 adj. building, U_{s1})

(2) Analysis results for shallower embedment depth of the main building

The MPRs of superstructures (T_{fix1} = 0.5, 1.0 and 2.0 sec, mat foundations, half-space soil, D = 6 m, V_s = 100 m/s) for different embedment depths of main building (e_1) on the X direction are given in Figure 5-30 where horizontal axis represents the foundation depth of the main building and the foundation depth of the adjacent building (e_2) is selected as 8 m.

If the results of the D = 3 m and 6m situations are compared, it can be said that there is a small effect due to the clearance on the power transfer induced from the in-plane DCI effect as it seen inside the solid line in Figure 5-30. It can be asserted that the in-plane DCI effect for such embedment depth situations for D = 6 m, and V_s = 100 m/s is more effective than D = 3 m, and V_s = 200 m/s.

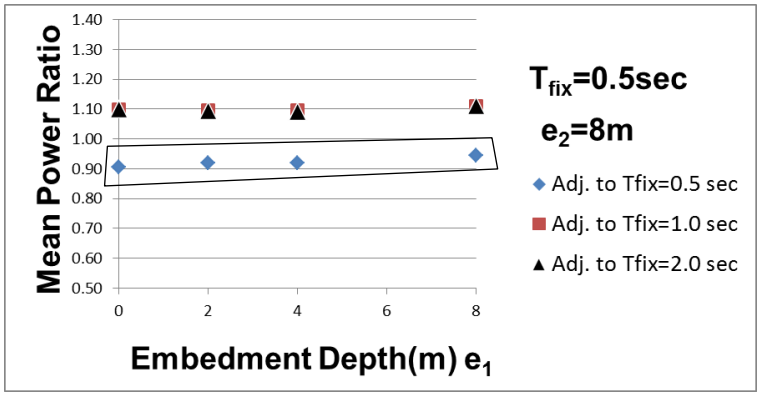

(a) For T_{fix1} = 0.5 sec

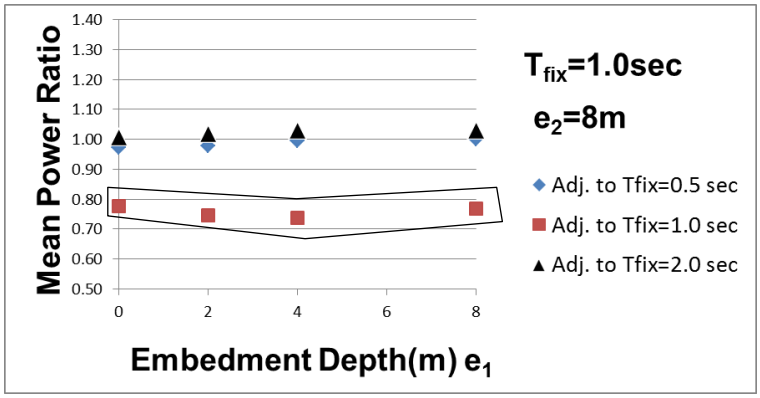

(b) For T_{fix1} = 1.0 sec

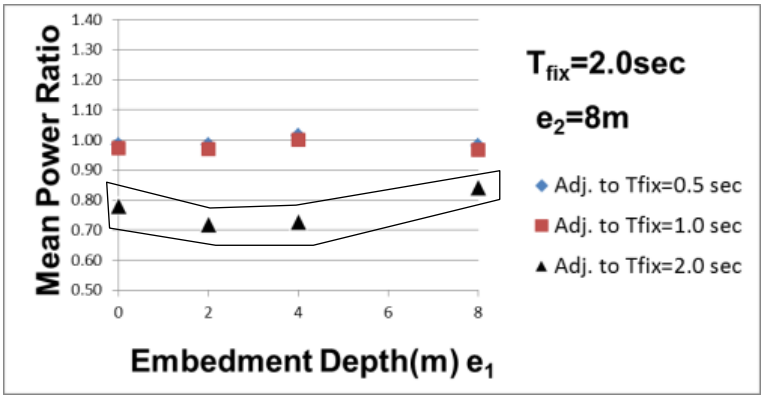

(c) For T_{fix1} = 2.0 sec

Figure 5-30: MPRs of horizontal superstructure motions for in-plane DCI (e_2 = 8 m, D= 6 m, V_s = 100 m/s, 1 adj. building, U_{s1})

(3) Analysis results for deeper embedment depth of the main building

The MPRs of superstructures (T_{fix1} = 0.5, 1.0 and 2.0 sec, mat foundations, half-space soil, D = 6 m, V_s = 100 m/s) for different embedment depths of the main building (e_1) on the X direction are given in Figure 5-31 where horizontal axis represents the foundation depth of the main building and the foundation depth of the adjacent building (e_2) is selected as 0.

If the results of D = 3 m and 6 m situations are compared, it can be said that there is a small effect due to the clearance on the power transfer induced from the in-plane DCI effect as it seen inside the solid line in Figure 5-31. It can be asserted that the in-plane DCI effect for such embedment depth situations for D = 6 m, and V_s = 100 m/s is more effective than D = 3 m, and V_s = 200 m/s.

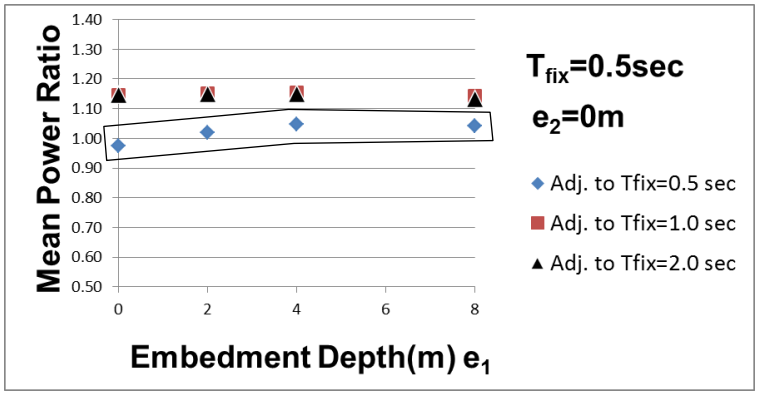

(a) For T_{fix1} = 0.5 sec

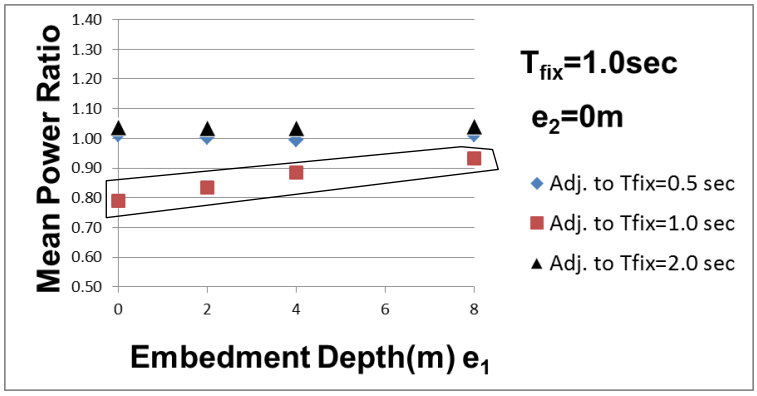

(b) For T_{fix1} = 1.0 sec

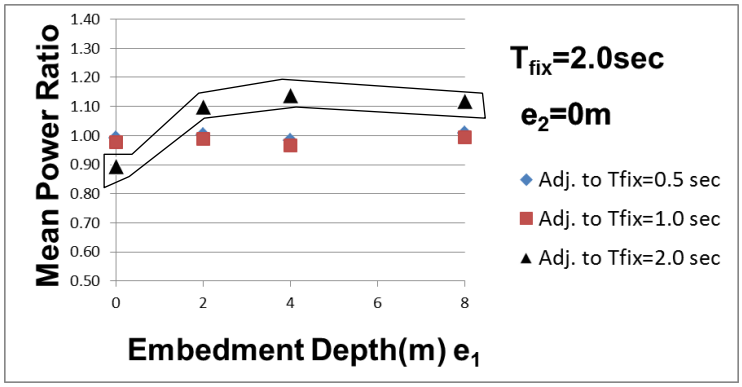

(c) For T_{fix1} = 2.0 sec

Figure 5-31: MPRs of horizontal superstructure motions for in-plane DCI (e_2 = 0, D = 6 m, V_s = 100 m/s, 1 adj. building, U_{s1})

(f) Analysis results for 2 adjacent buildings, D = 6 m, V_s = 100 m/s

(1) Analysis results for identical embedment depths

The MPRs of superstructures (T_{fix1} = 0.5, 1.0 and 2.0 sec, mat foundations, half-space soil, D = 6 m, V_s = 100 m/s) for identical embedment depths ($e_1 = e_2 = e_3$) on the X direction are given in Figure 5-32.

If the results of D = 3 m and 6m situations are compared, it can be said that the detrimental effect of in-plane DCI for identical adjacent tall and heavy buildings becomes negligible for D = 6 m for identical adjacent tall and heavy buildings, as can be seen inside the solid line in Figure 5-32(c). However, the effect of the in-plane DCI is not changed on short and light buildings adjacent to heavy and tall buildings, as can be seen inside the solid line in Figure 5-32(a).

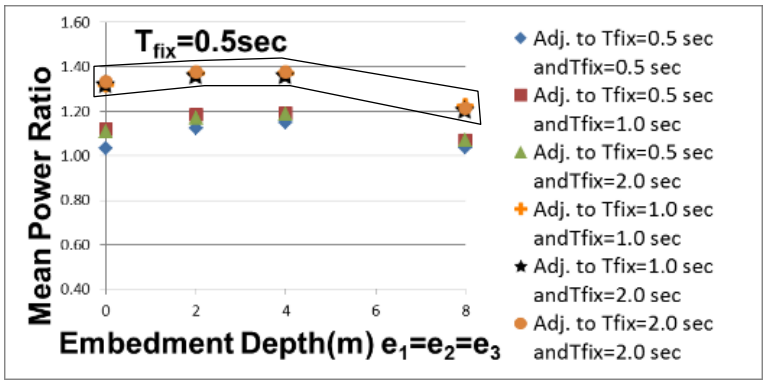

(a) For T_{fix1} = 0.5 sec

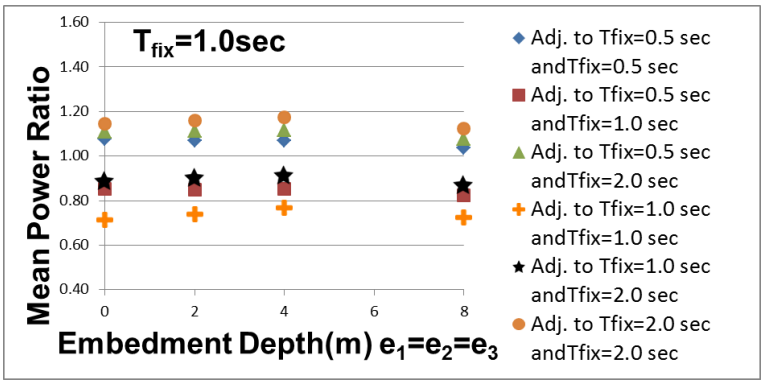

(b) For T_{fix1} = 1.0 sec

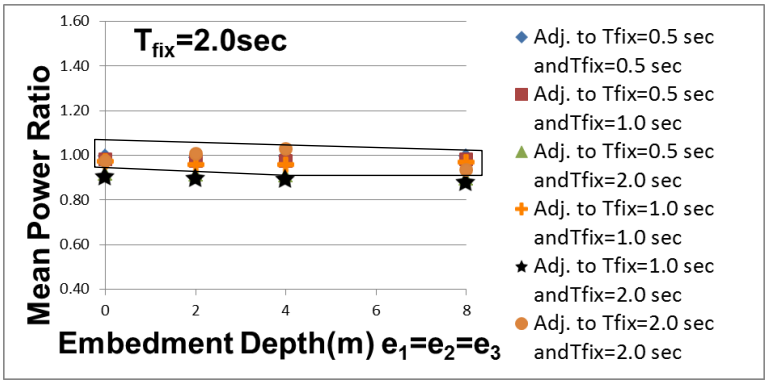

(c) For T_{fix1} = 2.0 sec

Figure 5-32: MPRs of horizontal superstructure motions for in-plane DCI ($e_1 = e_2 = e_3$, D = 6 m, V_s = 100 m/s, 2 adj. building, U_{s1})

(2) Analysis results for shallower embedment depth of the main building

The MPRs of superstructures (T_{fix1} = 0.5, 1.0 and 2.0 sec, mat foundations, half-space soil, D = 6 m, V_s = 100 m/s) for different embedment depths of the main building (e_1) on the X direction are given in Figure 5-33 where horizontal axis represents the foundation depth of the main building and the foundation depths of the adjacent buildings (e_2 and e_3) are selected as 8 m.

If the results of D = 3 m and 6 m situations are compared, it can be said that a similar relation is seen for the cases of one and two adjacent buildings.

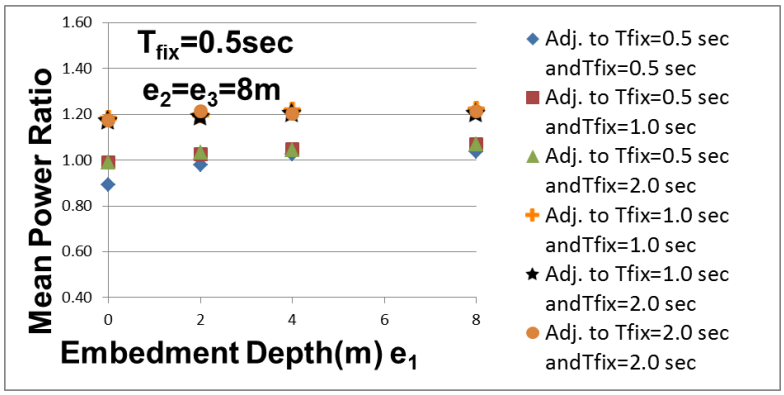

(a) For T_{fix1} = 0.5 sec

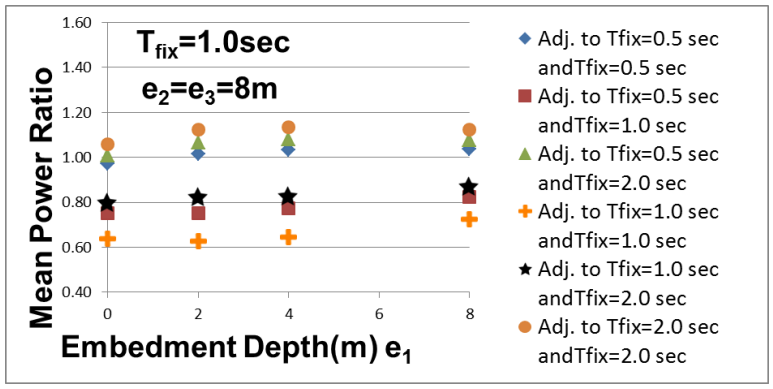

(b) For T_{fix1} = 1.0 sec

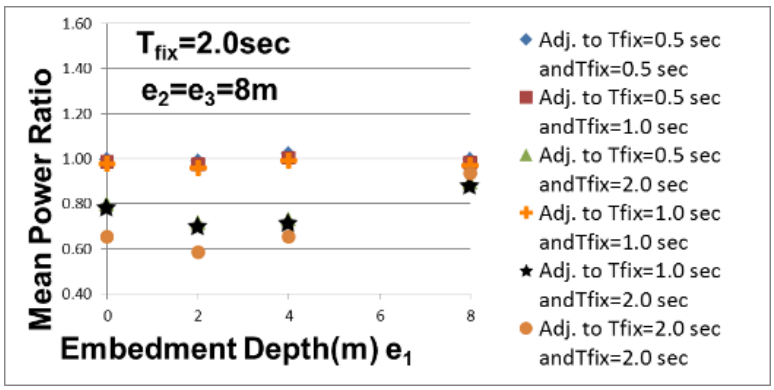

(c) For T_{fix1} = 2.0 sec

Figure 5-33: MPRs of horizontal superstructure motions for in-plane DCI ($e_2 = e_3 = 8$ m, $D = 6$ m, $V_s = 100$ m/s, 2 adj. building, U_{s1})

(3) Analysis results for deeper embedment depth of the main building

The MPRs of superstructures (T_{fix1} = 0.5, 1.0 and 2.0 sec, mat foundations, half-space soil, D = 6 m, V_s = 100 m/s) for different embedment depths of the main building (e_1) on the X direction are given in Figure 5-34 where horizontal axis represents the foundation depth of the main building and foundation depth of adjacent buildings (e_2 and e_3) are selected as 0.

If the results of D = 3 m and 6m situations are compared, it can be said that a similar relation is seen for the cases of one and two adjacent buildings.

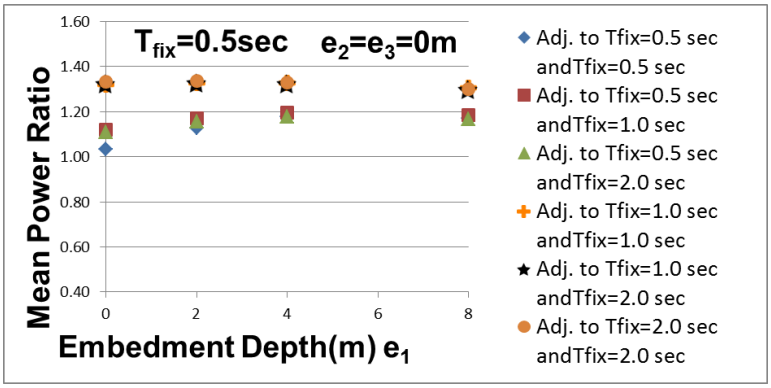

(a) For T_{fix1} = 0.5 sec

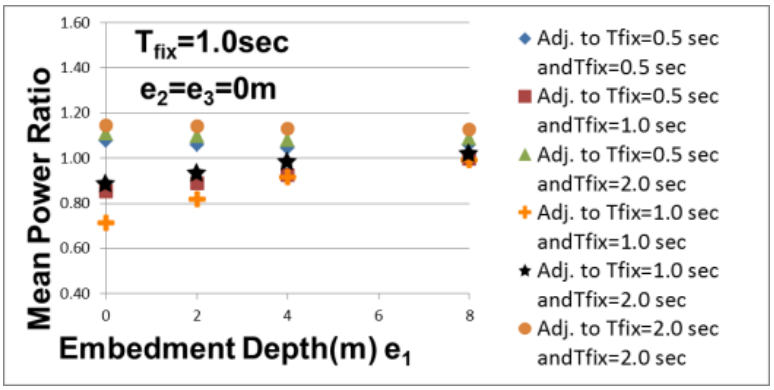

(b) For T_{fix1} = 1.0 sec

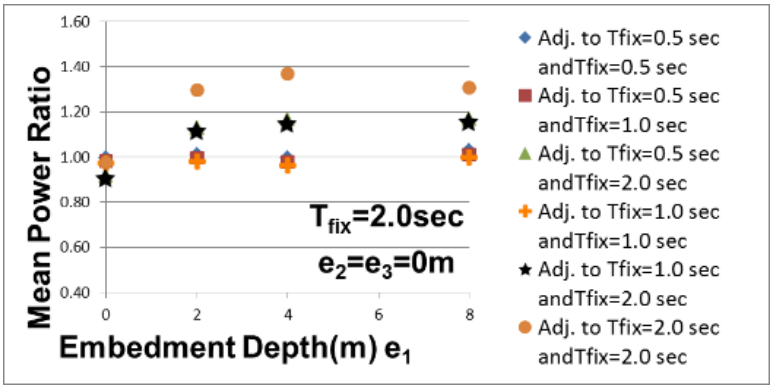

(c) For T_{fix1} = 2.0 sec

Figure 5-34: MPRs of horizontal superstructure motions for in-plane DCI ($e_2 = e_3 = 0$, D = 6 m, V_s = 100 m/s, 2 adj. building, U_{s1})

(g) Analysis results for 1 adjacent building, D = 6 m, V_s = 200 m/s

(1) Analysis results for identical embedment depths

The MPRs of superstructures (T_{fix1} = 0.5, 1.0 and 2.0 sec, mat foundations, half-space soil, D = 6 m, V_s = 100 m/s) for identical embedment depths ($e_1 = e_2$) on the X direction are given in Figure 5-35.

If the results of D = 3 m and 6m situations are compared, it can be claimed that similar results are obtained for these conditions.

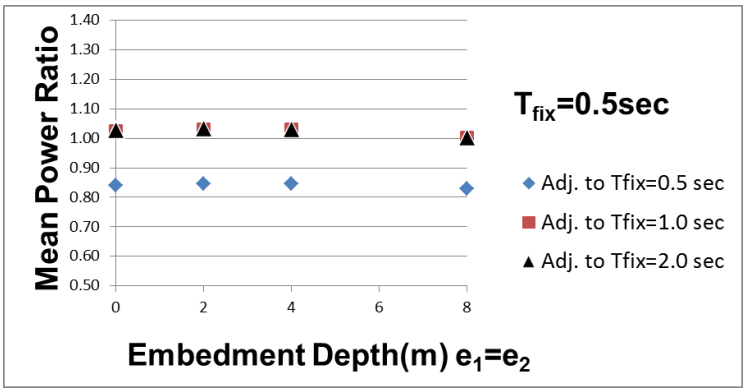

(a) For T_{fix1} = 0.5 sec

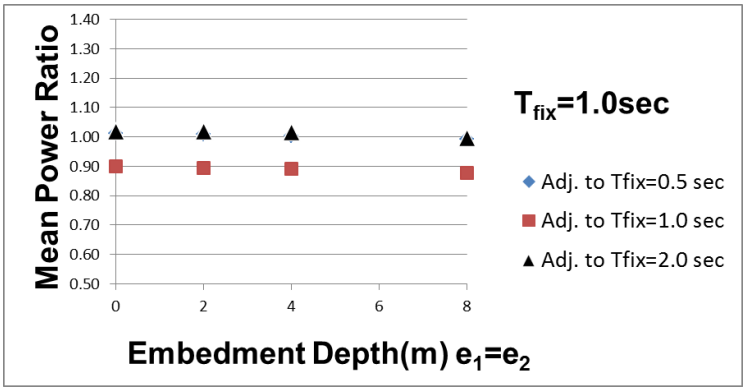

(b) For T_{fix1} = 1.0 sec

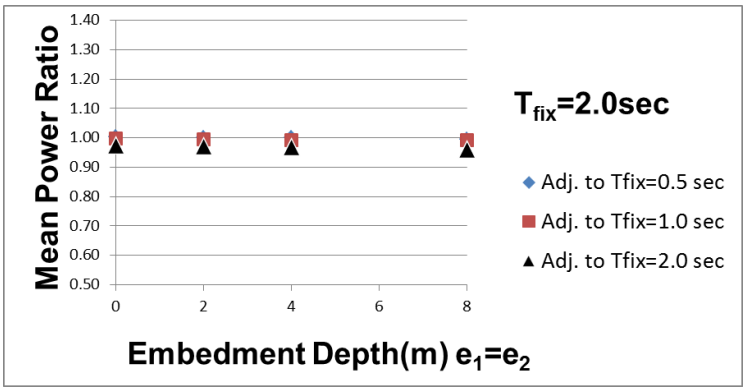

(c) For T_{fix1} = 2.0 sec

Figure 5-35: MPRs of horizontal superstructure motions for in-plane DCI ($e_1 = e_2$, D = 6 m, V_s = 200 m/s, 1 adj. building, U_{s1})

(2) Analysis results for shallower embedment depth of the main building

The MPRs of superstructures (T_{fix1} = 0.5, 1.0 and 2.0 sec, mat foundations, half-space soil, D = 6 m, V_s = 100 m/s) for different embedment depths of main building (e_1) on the X direction are given in Figure 5-36 where horizontal axis represents the foundation depth of the main building and the foundation depth of the adjacent building (e_2) is selected as 8 m.

If the results of D = 3 m and 6 m situations are compared, it can be claimed that similar results are obtained for these conditions.

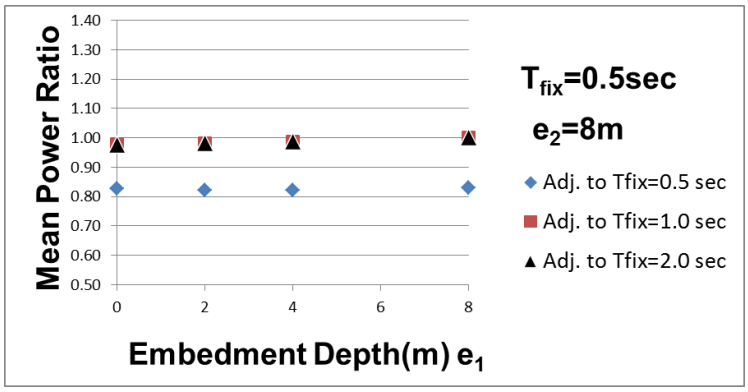

(a) For T_{fix1} = 0.5 sec

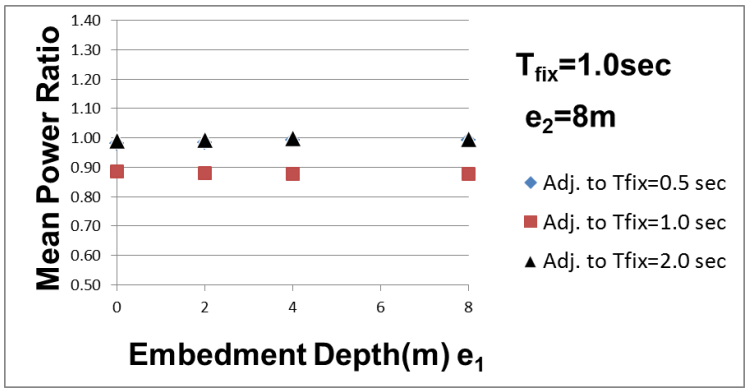

(b) For T_{fix1} = 1.0 sec

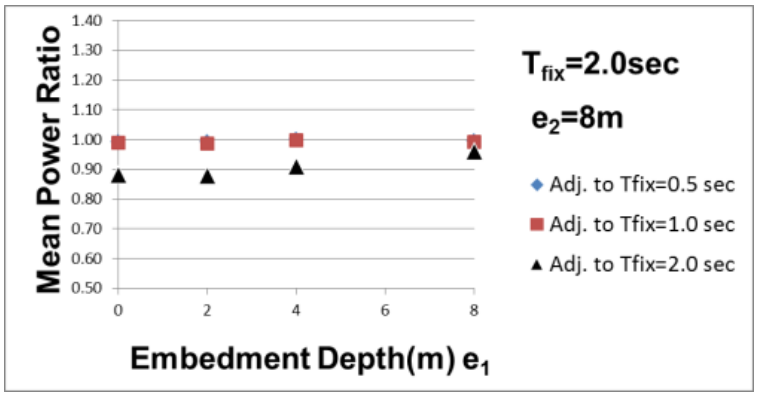

(c) For T_{fix1} = 2.0 sec

Figure 5-36: MPRs of horizontal superstructure motions for in-plane DCI (e_2 = 8 m, D = 6 m, V_s = 200 m/s, 1 adj. building, U_{s1})

(3) Analysis results for deeper embedment depth of the main building

The MPRs of superstructures (T_{fix1} = 0.5, 1.0 and 2.0 sec, mat foundations, half-space soil, D = 6 m, V_s = 100 m/s) for different embedment depths of the main building (e_1) on the X direction are given in Figure 5-37 where horizontal axis represents the foundation depth of the main building and the foundation depth of the adjacent building (e_2) is selected as 0.

If the results of D = 3 m and 6 m situations are compared, it can be claimed that similar results are obtained for these conditions.

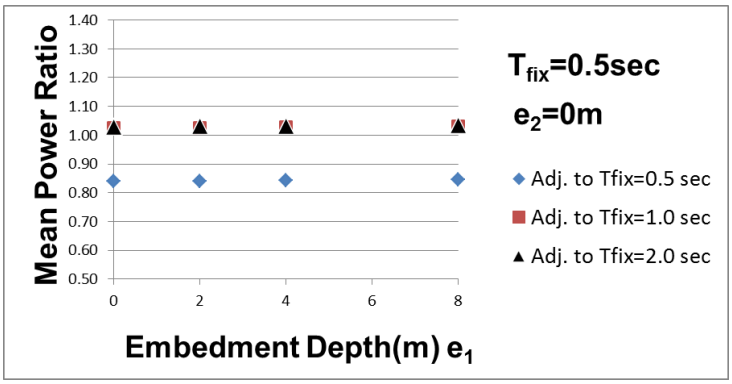

(a) For T_{fix1} = 0.5 sec

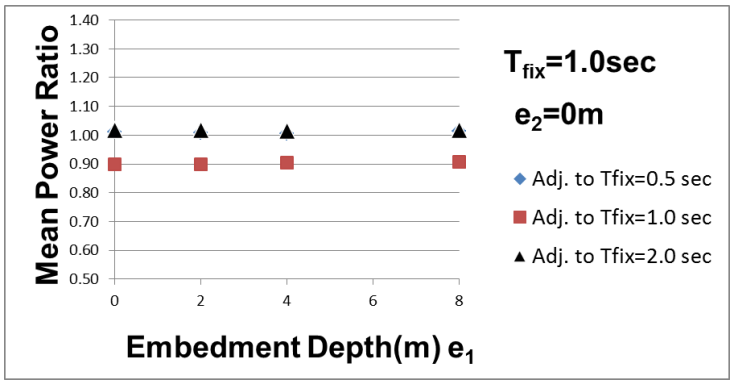

(b) For T_{fix1} = 1.0 sec

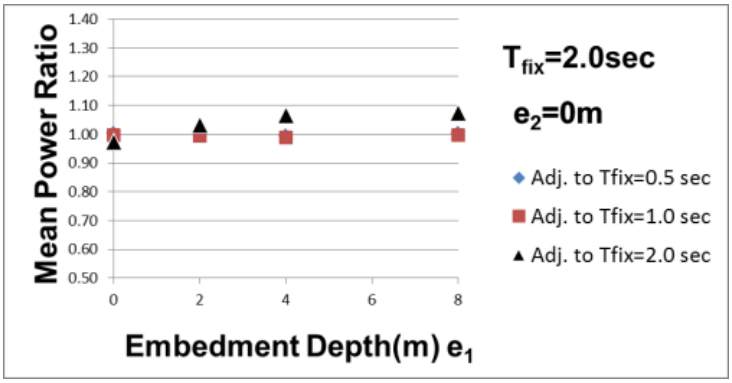

(c) For T_{fix1} = 2.0 sec

Figure 5-37: MPRs of horizontal superstructure motions for in-plane DCI (e_2 = 0, D = 6 m, V_s = 200 m/s, 1 adj. building, U_{s1})

(h) Analysis results for 2 adjacent buildings, D = 6 m, V_s = 200 m/s

(1) Analysis results for identical embedment depths

The MPRs of superstructures (T_{fix1} = 0.5, 1.0 and 2.0 sec, mat foundations, half-space soil, D = 6 m, V_s = 200 m/s) for identical embedment depths ($e_1 = e_2 = e_3$) on the X direction are given in Figure 5-38.

If the results of D = 3 m and 6 m situations are compared, it can be said that the detrimental effect of in-plane DCI for identical adjacent tall and heavy buildings becomes negligible for D = 6 m. This is the same as the relation between the situations D = 3 m, V_s = 100 m/s and D = 6 m, V_s = 100 m/s.

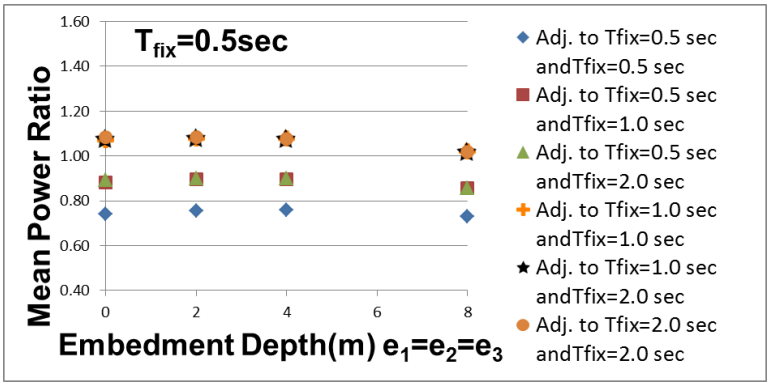

(a) For T_{fix1} = 0.5 sec

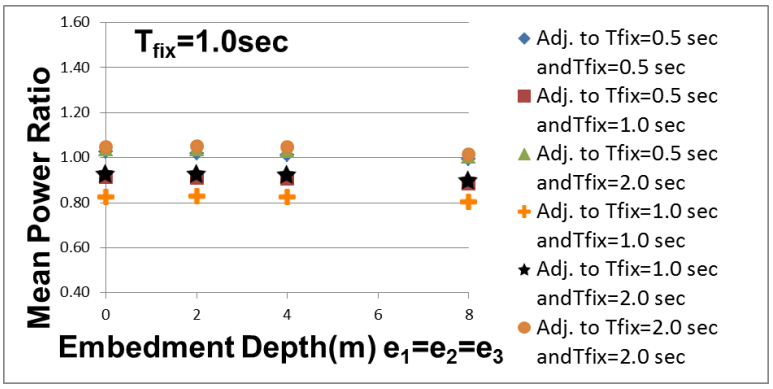

(b) For T_{fix1} = 1.0 sec

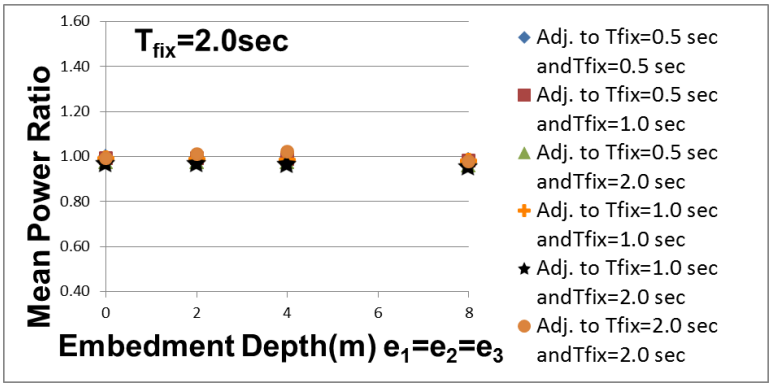

(c) For T_{fix1} = 2.0 sec

Figure 5-38: MPRs of horizontal superstructure motions for in-plane DCI ($e_1 = e_2 = e_3$, D = 6 m, V_s = 200 m/s, 2 adj. building, U_{s1})

(2) Analysis results for shallower embedment depth of the main building

The MPRs of superstructures (T_{fix1} = 0.5, 1.0 and 2.0 sec, mat foundations, half-space soil, D = 6 m, V_s = 200 m/s) for different embedment depths of the main building (e_1) on the X direction are given in Figure 5-39 where horizontal axis represents the foundation depth of the main building and the foundation depths of the adjacent buildings (e_2 and e_3) are selected as 8 m.

If the results of D = 3 m and 6m situations are compared, it can be said that similar relation is seen for the cases of one and two adjacent buildings.

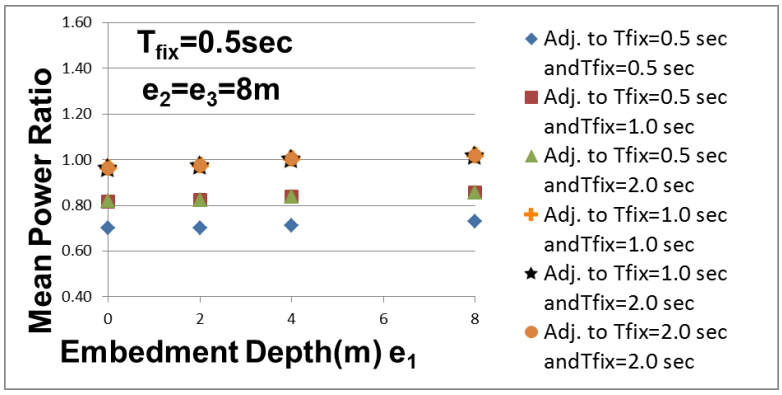

(a) For T_{fix1} = 0.5 sec

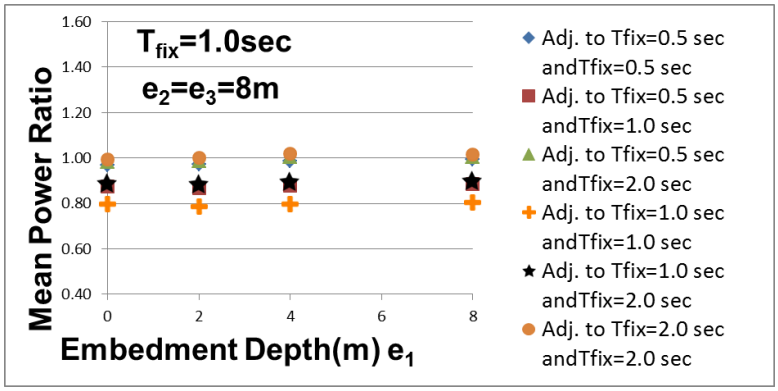

(b) For T_{fix1} = 1.0 sec

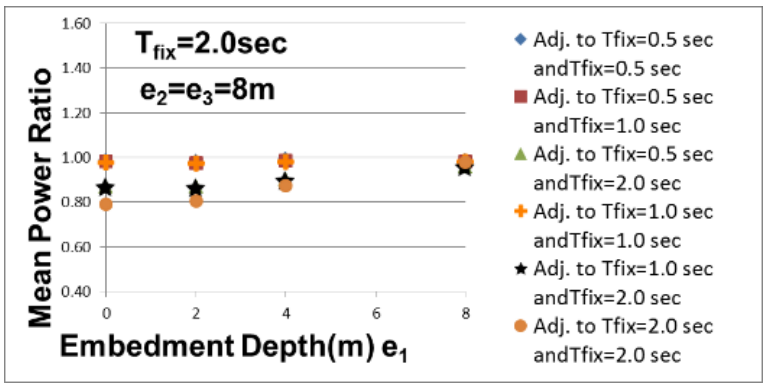

(c) For T_{fix1} = 2.0 sec

Figure 5-39: MPRs of horizontal superstructure motions for in-plane DCI ($e_2 = e_3 = 8$ m, $D = 6$ m, $V_s = 200$ m/s, 2 adj. building, U_{s1})

(3) Analysis results for deeper embedment depth of the main building

The MPRs of superstructures (T_{fix1} = 0.5, 1.0 and 2.0 sec, mat foundations, half-space soil, D = 3 m, V_s = 200 m/s) for different embedment depths of the main building (e_1) on the X direction are given in Figure 5-40 where horizontal axis represents the foundation depth of the main building and foundation depth of adjacent buildings (e_2 and e_3) are selected as 0.

If the results of D = 3 m and 6m situations are compared, it can be said that similar relation is seen for the cases of one and two adjacent buildings.

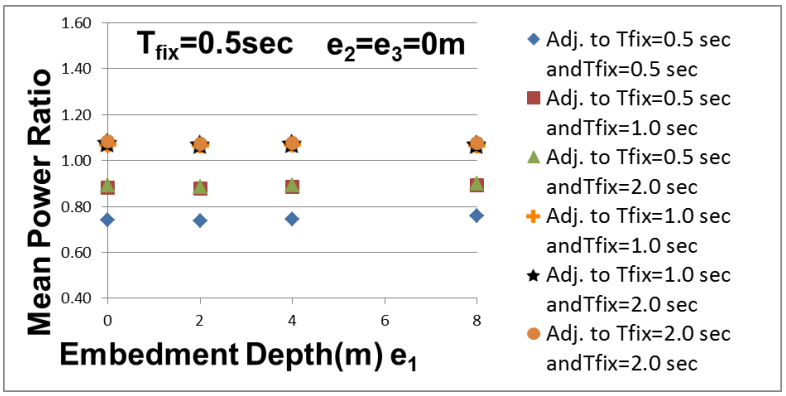

(a) For T_{fix1} = 0.5 sec

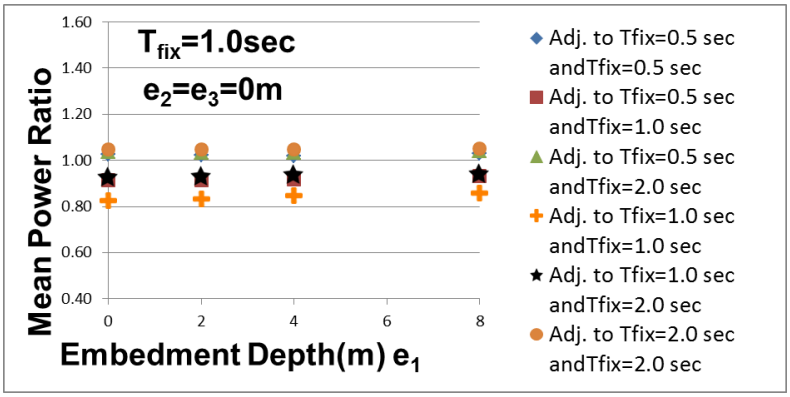

(b) For T_{fix1} = 1.0 sec

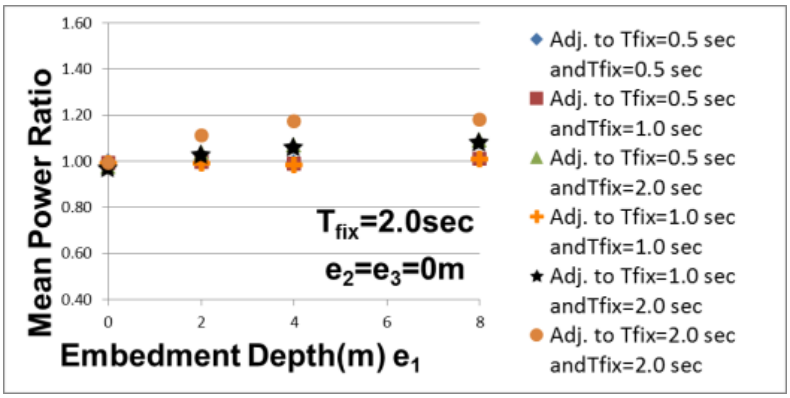

(c) For T_{fix1} = 2.0 sec

Figure 5-40: MPRs of horizontal superstructure motions for in-plane DCI (e_2 = e_3 = 0, D = 6 m, V_s = 200 m/s, 2 adj. building, U_{s1})

(i) Effect of m_s, H_{eff}, and h_s on transfer function amplitudes and MPR

In this section, to determine the effect of m_s, H_{eff}, and h_s on the in-plane DCI, transfer function amplitudes ($|U_{s1}/U_g|$) and MPRs of horizontal motions of identical superstructures (T_{fix1} = T_{fix2} = 1.0 and 2.0 sec, e_1 = 4 m and e_2 = 0, D = 3 m) on the X direction for half-space soil are calculated.

(1) Effect of m_s on in-plane DCI

Analyses for doubled mass of superstructures (m_s = 5x10^6 kg and 1x10^7 kg, T_{fix1} = T_{fix2} = 1.0 sec, H_{eff} = 20 m) are performed to clarify the effect of superstructure mass on the in-plane DCI. The transfer function amplitudes ($|U_{s1}/U_g|$) and MPRs of horizontal motions of identical superstructures are given in Figure 5-41. The other analysis parameters are the same as those given in Section 5.2. The rigidity of the m_s= 1x10^7 kg superstructure is calculated again to obtain a fixed natural period of 1.0 sec (T_{fix} = 1.0 sec).

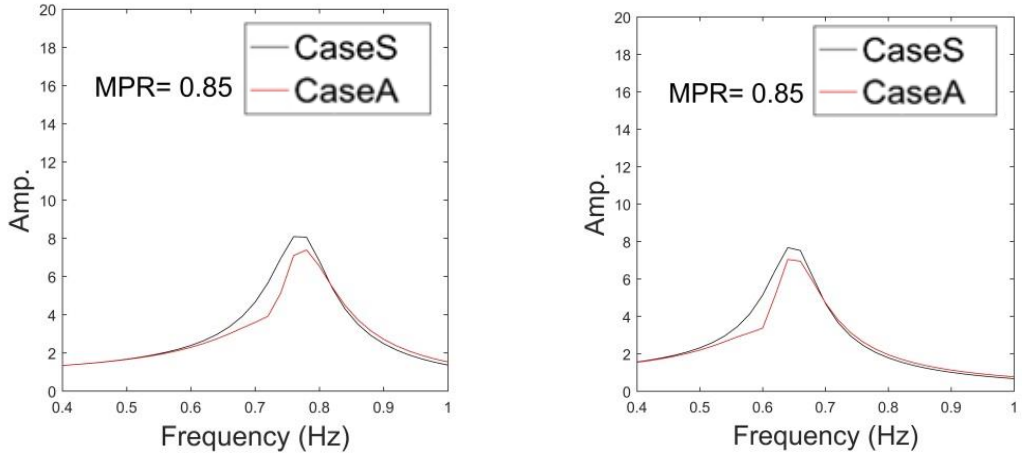

(a) m_s = 5x10^6 kg **(b) m_s = 1x10^7 kg**

Figure 5-41: Case-A (Adjacent) and Case-S (Single) transfer function amplitudes ($|U_{s1}/U_g|$) and MPRs of horizontal motions of identical superstructures (T_{fix1} = T_{fix2} = 1.0 sec, e_1 = 4 m, e_2 = 0, D = 3 m, H_{eff} = 20 m, V_s = 100 m/s, h_s = 3%)

If Figure 5-41(a) and 5-41(b) are compared, it can be asserted that the effect of superstructure mass on the DCI effect is negligible in this case.

(2) Effect of H_{eff} on in-plane DCI

Analyses for doubling the height of superstructures (H_{eff} = 20 m and 40 m, T_{fix1} = T_{fix2} = 1.0 sec) are performed to clarify the effect of superstructure height on the in-plane DCI phenomenon. Transfer function amplitudes ($|U_{s1}/U_g|$) and MPRs of the horizontal motions of identical superstructures (T_{fix1} = T_{fix2} = 1.0 sec, H_{eff} = 20 m and 40 m) are given in Figure 5-42. The other analysis parameters are the same as those given in Section 5.2.

If Figure 5-42(a) and 5-42(b) are compared, it can be claimed that the effect of superstructure height on the in-plane DCI is clearly greater than that of superstructure mass in the present study.

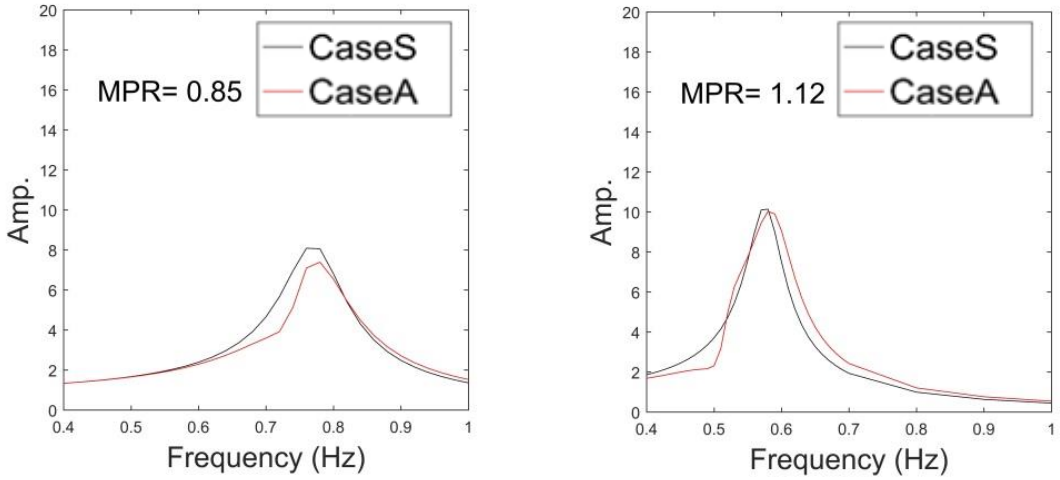

(a) H_{eff} = 20 m **(b) H_{eff} = 40 m**

Figure 5-42: Case-A (Adjacent) and Case-S (Single) transfer function amplitudes ($|U_{s1}/U_g|$) and MPRs of horizontal motions of identical superstructures (T_{fix1} = T_{fix2} = 1.0 sec, e_1 = 4 m, e_2 = 0, D = 3 m, m_s = 5x10^6 kg, V_s = 100 m/s, h_s = 3%)

(3) Effect of h_s on in-plane DCI

Analysis results of different h_s of the soil (h_s = 0 and 6%) for $T_{fix1} = T_{fix2}$ = 2.0 sec are also shown to clarify the effect of soil material damping on the in-plane DCI. Transfer function amplitudes ($|U_{s1}/U_g|$) and MPRs are given in Figure 5-43. The other analysis parameters are the same as those given in Section 5.2.

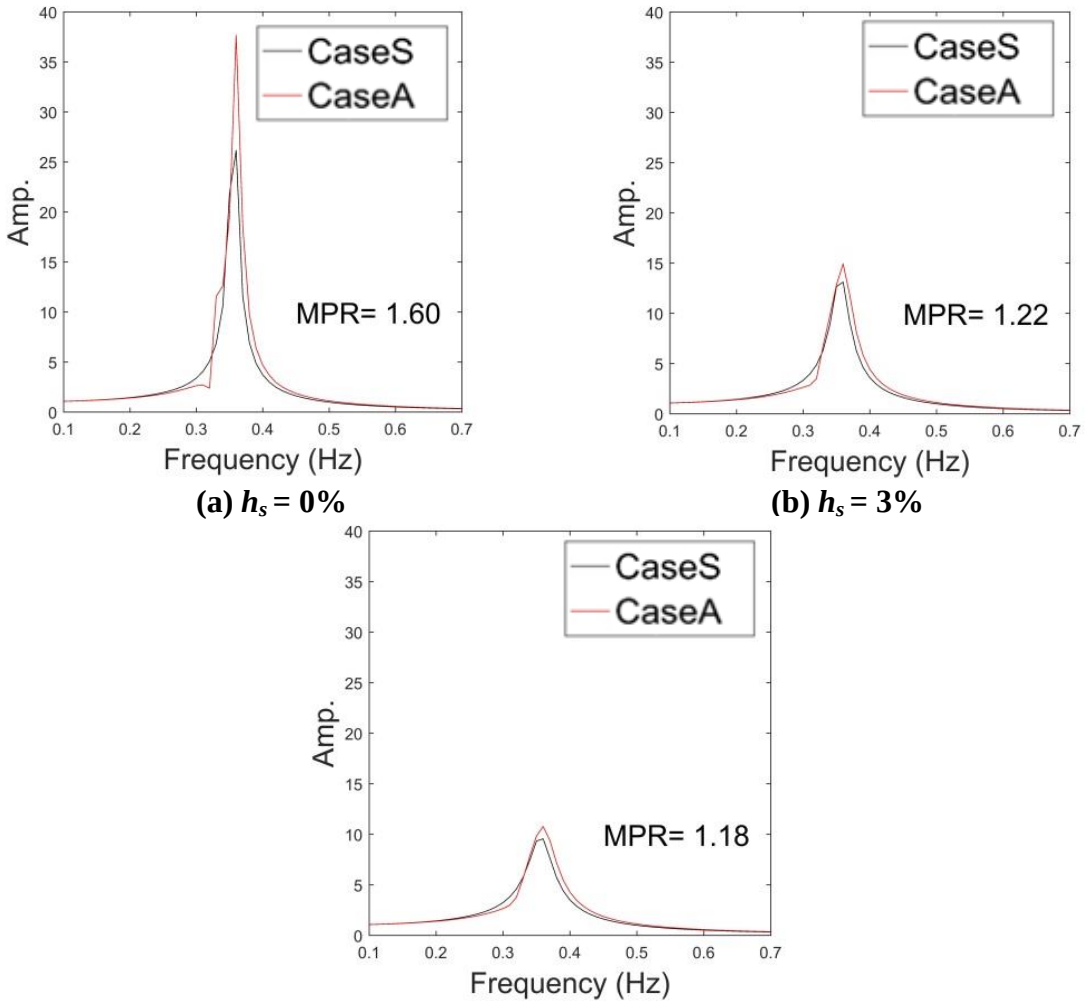

(a) h_s = 0% **(b) h_s = 3%**

(c) h_s = 6%

Figure 5-43: Case-A (Adjacent) and Case-S (Single) transfer function amplitudes ($|U_{s1}/U_g|$) and MPR of identical superstructures ($T_{fix1} = T_{fix2}$ = 2.0 sec, e_1 = 4 m, e_2 = 0, D = 3 m, V_s = 100 m/s)

If Figures 5-43(a), 5-43(b), and 5-43(c) are compared, it can be seen that peaks of the transfer function amplitudes ($|U_{s1}/U_g|$) are strongly affected by the soil material damping for $h_s <$ 3%. Moreover, the effect on MPR increases nearly three times for $h_s = 0\%$ compared to $h_s = 3\%$ (where the mean power for Case-A increases by 60% for $h_s = 0\%$, and by 22% for $h_s = 3\%$ compared to Case-S), but this parameter becomes insensitive for $h_s > 3\%$. The reason of this phenomenon is considered to be that, for zero damping, the restriction effect diminishes and the amplitudes of the rocking motion of the foundations increase. Therefore, it can be asserted that the effect of h_s becomes important on the in-plane DCI in small strain areas, but that the effect diminishes rapidly for larger strain areas.

5.4.2 Analysis results for *Y* direction (anti-plane DCI)

(a) Analysis results for 1 adjacent building, D = 3 m, V_s = 100 m/s

(1) Analysis results for identical embedment depths

The MPRs of superstructures (T_{fix1} = 0.5, 1.0 and 2.0 sec, mat foundations, half-space soil, D = 3 m, V_s = 100 m/s) for identical embedment depths ($e_1 = e_2$) on the *Y* direction are given in Figure 5-44. Moreover, the MPRs of the foundation rocking motion of the superstructures for the same parameters are given in Figure 5-45.

If Figure 5-44 is examined to determine the different types of adjacent building effects on the anti-plane DCI, it can be said that, as can be seen inside the solid line in Figure 5-44(a), a short and light building (e.g., one with a natural period of 0.5 sec) is not affected so much when adjacent to a tall and heavy building (e.g., one with a natural period of 2.0 sec) compared to the results of the *X* direction.

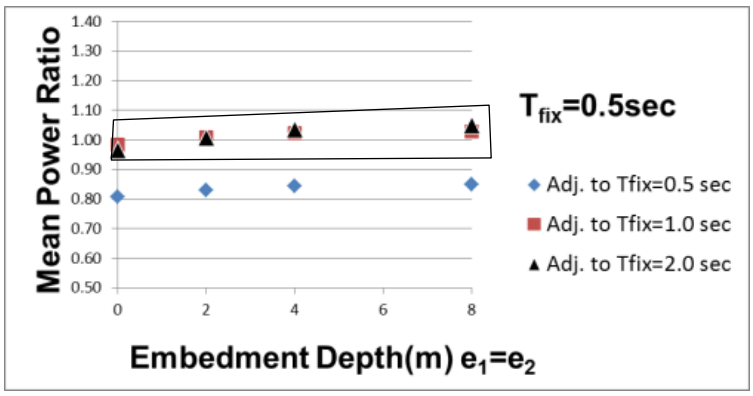

(a) For T_{fix1} = 0.5 sec

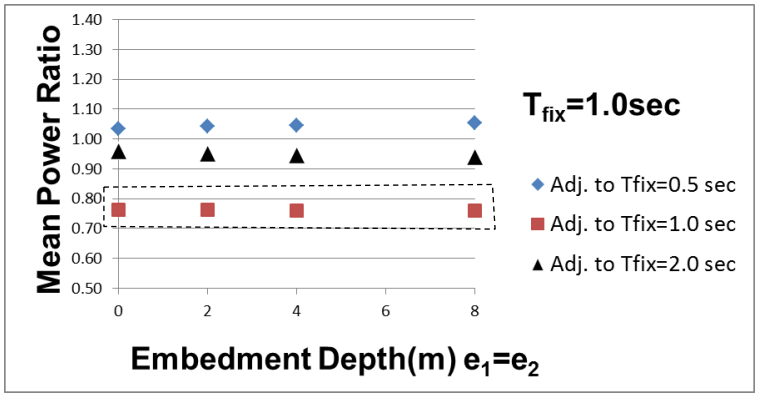

(b) For T_{fix1} = 1.0 sec

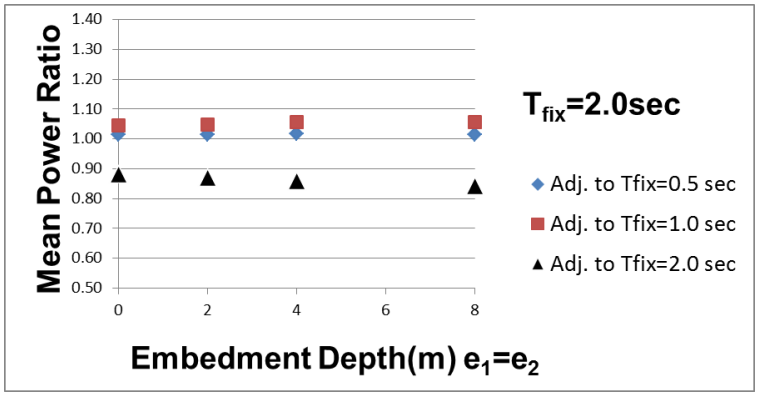

(c) For T_{fix1} = 2.0 sec

Figure 5-44: MPRs of horizontal superstructure motions for anti-plane DCI ($e_1 = e_2$, D = 3 m, V_s = 100 m/s, 1 adj. building, U_{s2})

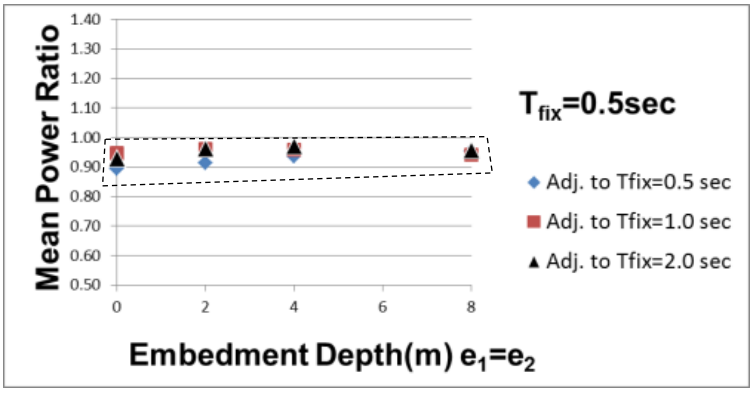

(a) For T_{fix1} = 0.5 sec

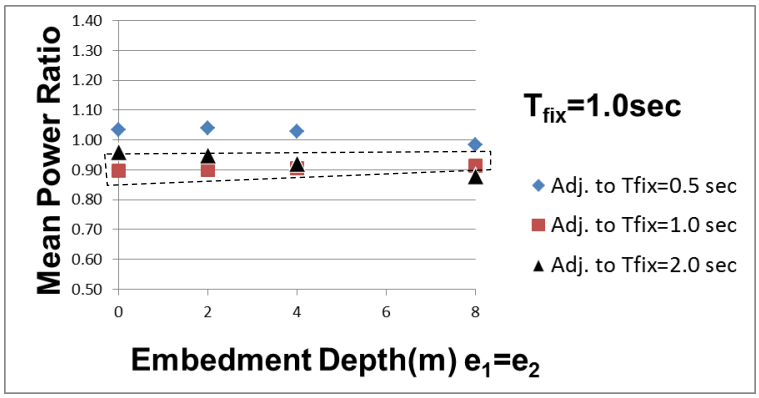

(b) For T_{fix1} = 1.0 sec

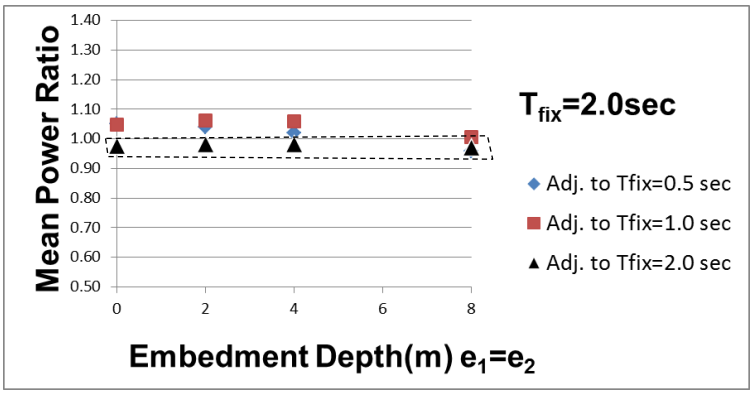

(c) For T_{fix1} = 2.0 sec

Figure 5-45: MPRs of foundation rocking motions for anti-plane DCI ($e_1 = e_2$, D= 3 m, V_s = 100 m/s, 1 adj. building, U_{f4})

If Figure 5-45 is examined to determine the different types of adjacent building effects on the MPRs of the foundation rocking motion, it can be claimed that there is a very low rocking restriction effect between identical adjacent buildings compared to the results of the *X* direction it is seen inside the dashed line in Figure 5-45. This is because the rocking restriction is seen on the *X* direction mainly because of the out of-phase rocking motion of the adjacent foundations. However, on the *Y* direction, the rocking motion of the adjacent foundation becomes in-phase. Moreover, it should be added that the smallest MPRs are obtained for identical adjacent buildings for $T_{fix1} = T_{fix2} = 1.0$ sec as can be seen inside the dashed line in Figure 5-44(b). To explain this phenomenon, analyses are done for different clearance (*D*) values for twin adjacent buildings ($T_{fix1} = T_{fix2} = 0.5$, 1.0 and 2.0 sec) for only surface foundations ($e_1 = e_2 = 0$).

▪ Analyses for different *D* values

To understand the wave transfer between adjacent buildings (i.e., wave-based DCI) analyses for different *D* values becomes necessary. For the anti-plane DCI case, there are two options for wave transfer between adjacent buildings: SH-wave transfer (Fig. 5-46(a)) or SV-wave transfer (Fig. 5-46(b)). To understand which wave transfer is dominant, MPRs of structural horizontal motions are calculated for FM and CM twin adjacent buildings ($T_{fix1} = T_{fix2} = 0.5$, 1.0, and 2.0 sec) on surface foundations ($e_1 = e_2 = 0$) over a wide range of *D* (3–72 m) as shown in Figure 5-46.

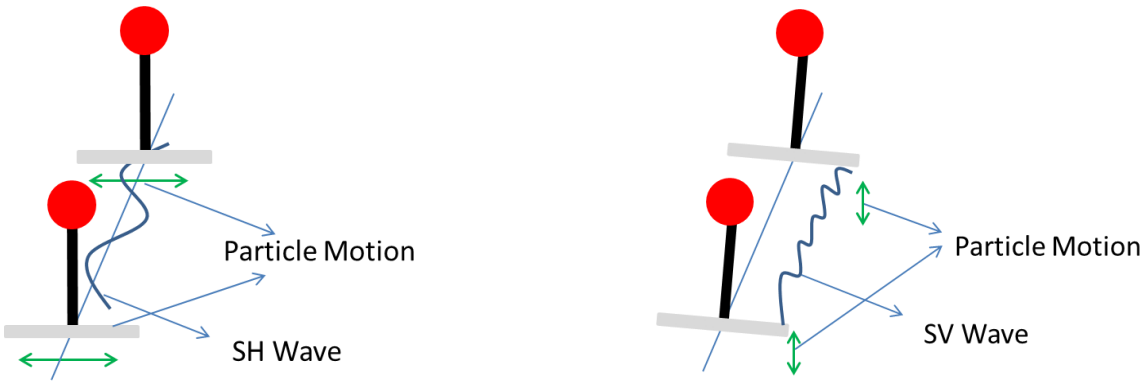

(a) SH wave transfer **(b) SV wave transfer**

Figure 5-46: Possible wave transfers between adjacent buildings for in-plane DCI

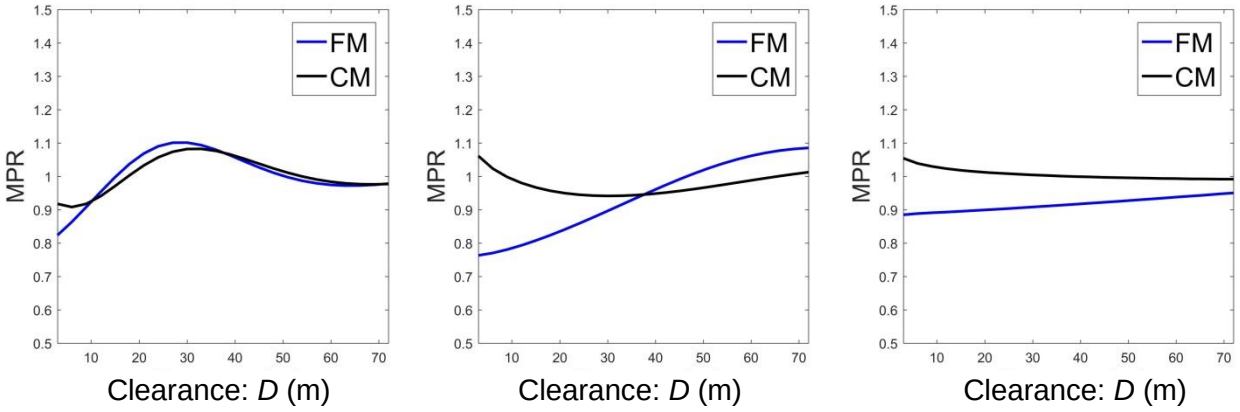

(a) $T_{fix1} = T_{fix2} = 0.5$ sec **(b) $T_{fix1} = T_{fix2} = 1.0$ sec** **(c) $T_{fix1} = T_{fix2} = 2.0$ sec**

Figure 5-47: MPRs of horizontal superstructure motion for FM and CM ($e_1 = e_2 = 0$, D = 3 m – 72 m, V_s = 100 m/s, 1 adj. building, U_{s1}, ν = 0.45)

If Figure 5-47(a) is examined, it can be asserted that the MPRs of the horizontal structure motion of FM and CM become high at nearly similar clearances. Therefore, it can be said that SH wave transfer is more dominant than SV wave transfer for the anti-plane DCI since the rocking of the foundation of the adjacent building has little effect on the wave-based DCI effect, except for short clearances (D < 10 m). However, if results for all buildings are investigated at

Figure 5-47, it can be said that FM gives smaller MPR values than those given by CM. To explain this issue, a new model is created connecting the foundations, as shown in Figure 5-48; this model is referred to the integrated model (IM). The MPRs of the horizontal structural motions for twin adjacent buildings ($T_{fix1} = T_{fix2} = 0.5$, 1.0, and 2.0 sec) on surface foundations ($e_1 = e_2 = 0$) according to D (1–10 m) are calculated as shown in Figure 5-49.

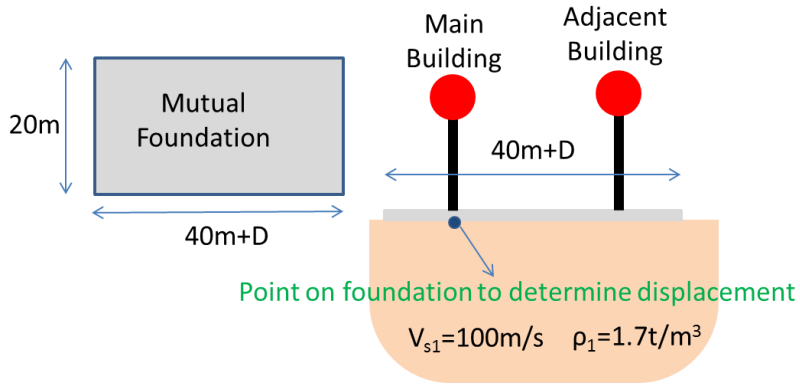

Figure 5-48: Integrated model (IM) for buildings

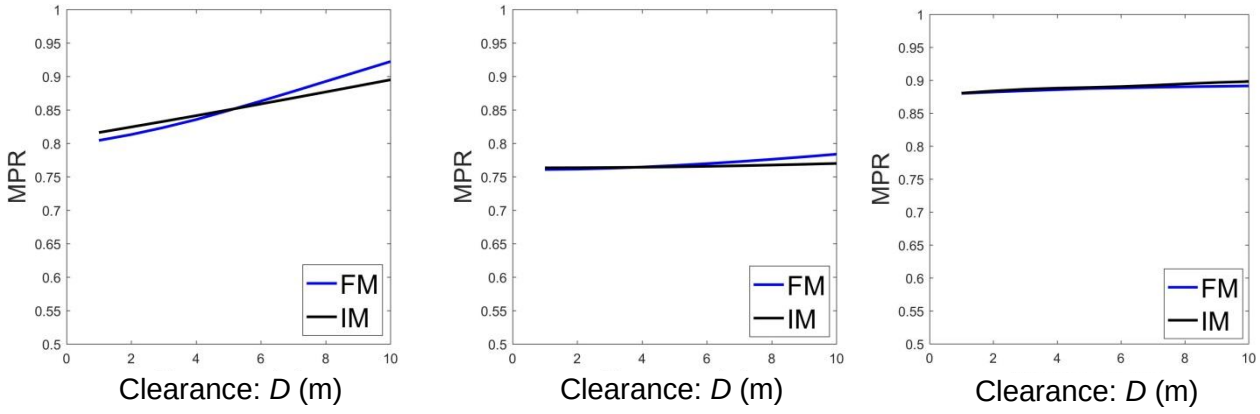

(a) $T_{fix1} = T_{fix2} = 0.5$ sec **(b) $T_{fix1} = T_{fix2} = 1.0$ sec** **(c) $T_{fix1} = T_{fix2} = 2.0$ sec**

Figure 5-49: MPRs of horizontal superstructure motions for FM and IM ($e_1 = e_2 = 0$, D= 1m-10 m, V_s = 100 m/s, 1 adj. building, U_{s1}, ν = 0.45)

As can be seen at Figure 5-49, the difference between the MPRs of the horizontal structure motions of FM and IM can be ignored, especially for short clearances. This shows that the soil between the buildings participates in the motions of the foundations by the out-of-plane DCI effect and increases the damping effect. Therefore, the MPRs of the FM model become smaller than those of the CM model at Figure 5-47 for short clearances. Moreover, similar to the in-plane DCI effect, the smallest MPRs of the horizontal structure motions are obtained for identical adjacent buildings for $T_{fix1} = T_{fix2} = 1.0$ sec because of the detrimental effect of wave-based DCI that is also seen for $D = 3$ m and $T_{fix1} = T_{fix2} = 0.5$ sec. However, it should be noted that, the MPRs of the horizontal structure motions of twin buildings depend lesser to the fixed based natural periods of buildings than those at the in-plane DCI.

(2) Analysis results for shallower embedment depth of the main building

The MPRs of superstructures ($T_{fix1} = 0.5$, 1.0 and 2.0 sec, mat foundations, half-space soil, $D = 3$ m, $V_s = 100$ m/s) for different embedment depths of main building (e_1) on the Y direction are given in Figure 5-50 where horizontal axis represents the foundation depth of the main building and the foundation depth of the adjacent building (e_2) is selected as 8 m.

If Figure 5-50 is examined, it can be asserted that the detrimental effect of the anti-plane DCI is more pronounced for a main building with a shallower foundation embedment depth for identical adjacent buildings with a natural period of 2.0 sec, as can be seen inside the solid line in Figure 5-50(c). This is because power is transferred from the deeper foundation to the shallower foundation by the anti-plane DCI effect. It is interesting to note that direction of the power transfer effect at the anti-plane DCI is opposite compared to those at the in-plane DCI. Moreover, it should be noted that, this horizontal vibration power transfer effect is slightly higher for anti-

plane DCI than for in-plane DCI. To show this phenomenon, Case-A and Case-S transfer function amplitudes ($|U_{s2}/U_g|$) of superstructures for $T_{fix1} = T_{fix2} = 2.0$ sec and $e_1 = 0$ and $e_2 = 8$ m are given in Figure 5-51 for $D = 3$ m and $V_s = 100$ m/s. If Figure 5-50 is examined for MPRs of identical adjacent buildings, it can be seen that MPRs of greater than one are seen only for $T_{fix} = 2.0$ sec, as can be seen inside the solid line in Figure 5-50(c) for $e_1 < e_2$.

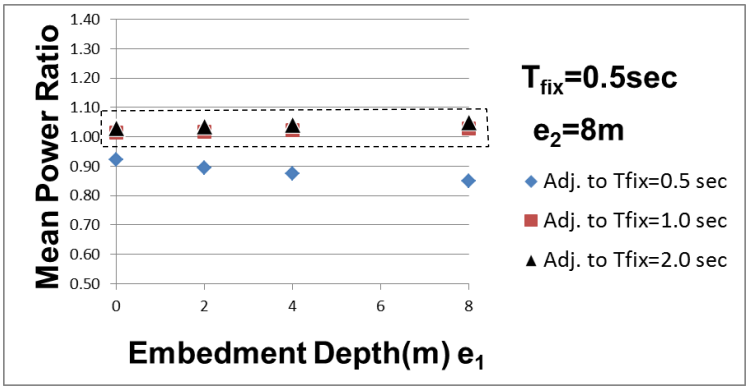

(a) For T_{fix1} = 0.5 sec

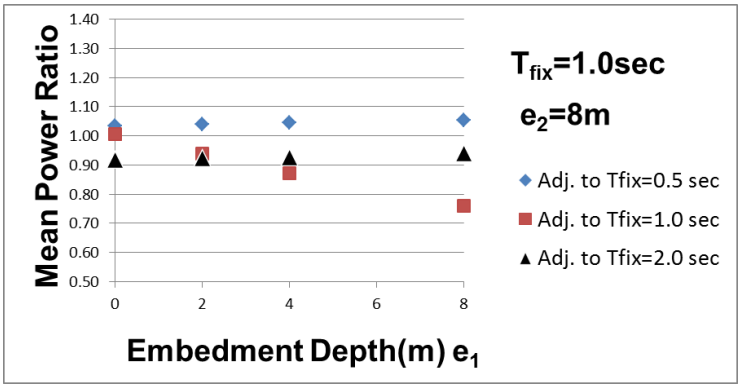

(b) For T_{fix1} = 1.0 sec

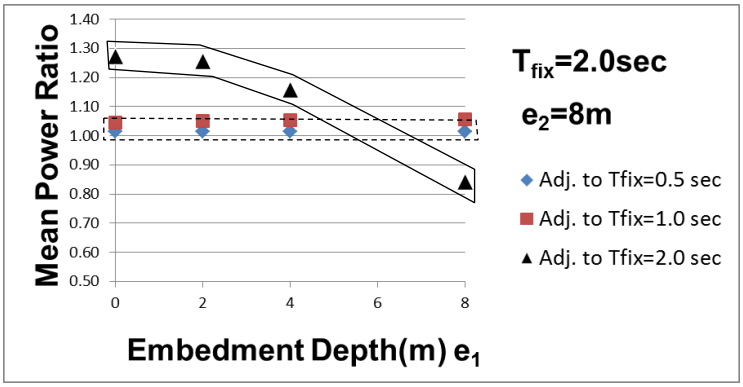

(c) For T_{fix1} = 2.0 sec

Figure 5-50: MPRs of horizontal superstructure motions for anti-plane DCI (e_2 = 8 m, D = 3 m, V_s = 100 m/s, 1 adj. building, U_{s2})

As can be seen on Figure 5-51, the MPR of the main building is clearly higher than that of the adjacent building. However, the anti-plane DCI effects between tall and heavy buildings and short and light structures are negligible, as can be seen inside the dashed line in Figure 5-50.

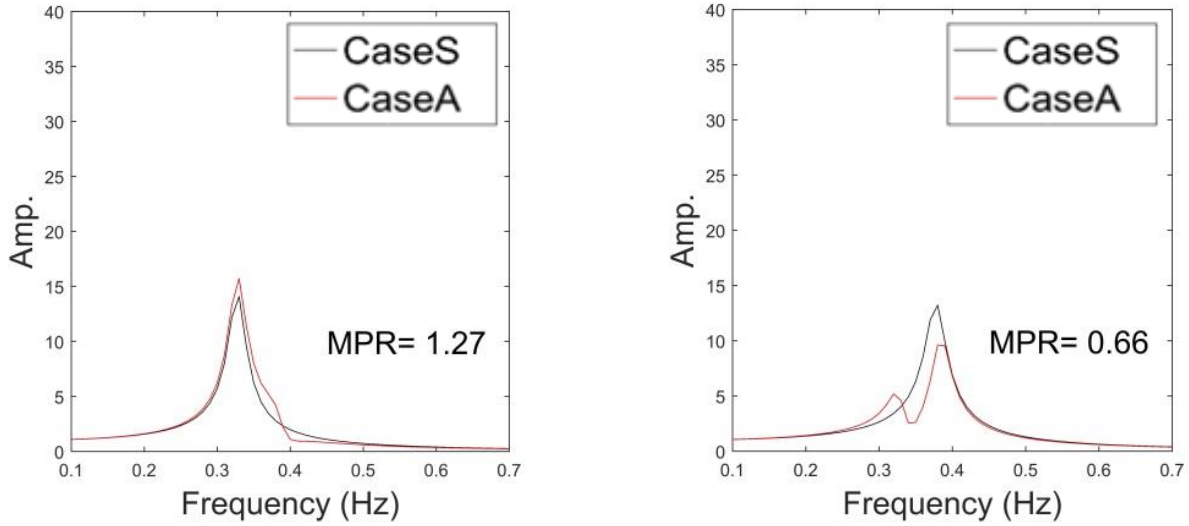

(a) Main building **(b) Adjacent building**

Figure 5-51: Case-A (Adjacent) and Case-S (Single) transfer function amplitudes ($|U_{s2}/U_g|$) and MPR of superstructures ($T_{fix1} = T_{fix2} = 2.0$ sec, $e_1 = 0$, $e_2 = 8$ m, half-space soil, $D = 3$ m, $V_s = 100$ m/s)

(3) Analysis results for deeper embedment depth of the main building

The MPRs of superstructures (T_{fix1} = 0.5, 1.0 and 2.0 sec, mat foundations, half-space soil, D = 3 m, V_s = 100 m/s) for different embedment depths of the main building (e_1) on the Y direction are given in Figure 5-52 where horizontal axis represents the foundation depth of the main building and the foundation depth of the adjacent building (e_2) is selected as 0.

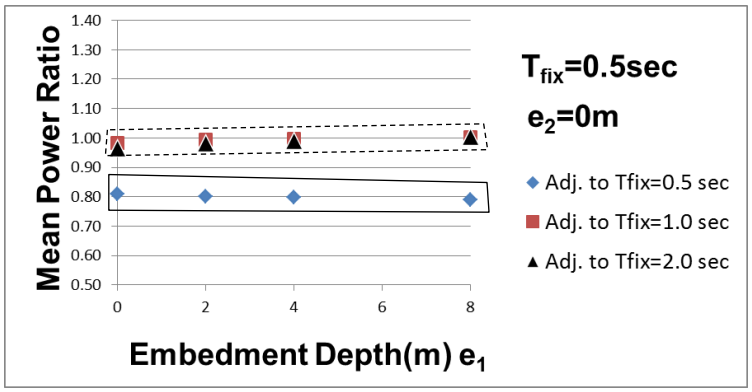

(a) For T_{fix1} = 0.5 sec

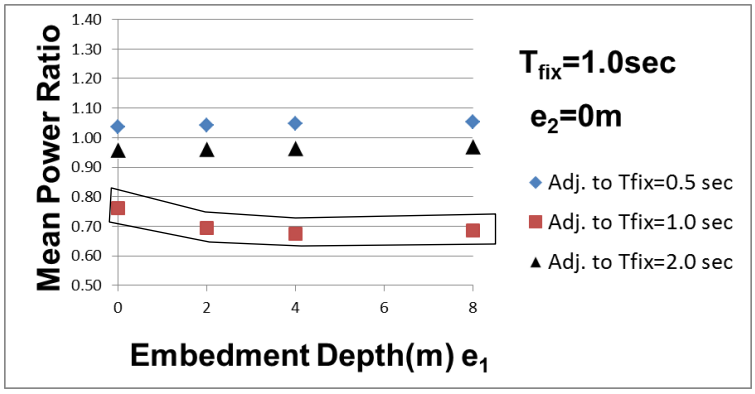

(b) For T_{fix1} = 1.0 sec

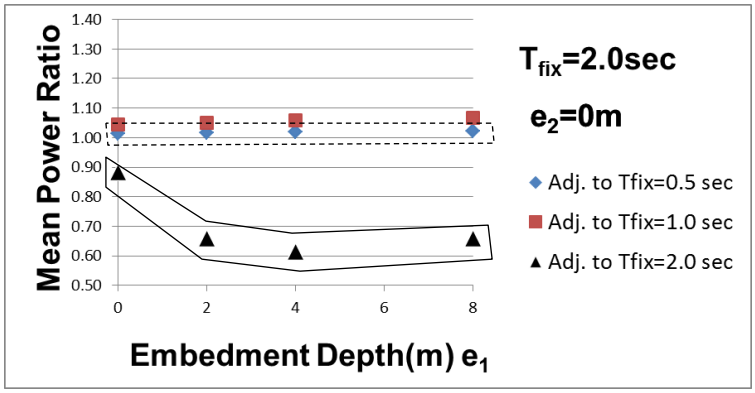

(c) For T_{fix1} = 2.0 sec

Figure 5-52: MPRs of horizontal superstructure motions for anti-plane DCI (e_2 = 8 m, D = 3 m, V_s = 100 m/s, 1 adj. building, U_{s2})

If Figure 5-52 is examined, it can be said that the beneficial effect of the anti-plane DCI is more pronounced for the main building with deeper foundation embedment depth, as can be seen inside the solid line in Figure 5-52. This is especially so for identical adjacent buildings with natural period of 2.0 sec, as can be seen inside the solid line in Figure 5-52(c), because power is transferred from deeper foundations to shallower foundations by the anti-plane DCI effect, as noted previously. To show this phenomenon, Case-A and Case-S transfer function amplitudes ($|U_{s2}/U_g|$) of superstructures for $T_{fix1} = T_{fix2} = 2.0$ sec and $e_1 = 4$ m and $e_2 = 0$ are given in Figure 5-53 for $D = 3$ m and $V_s = 100$ m/s. As can be seen in Figure 5-53, the MPR of the main building is clearly lower than that of the adjacent building as expected. The anti-plane DCI effects between tall and heavy buildings and short and light structures are negligible, as can be seen inside the dashed line in Figure 5-52.

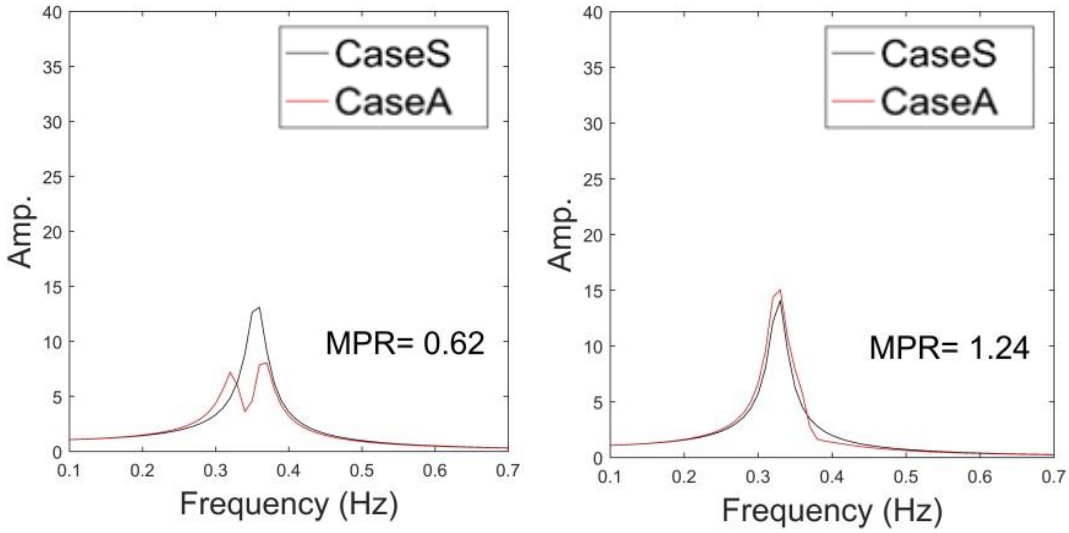

(a) Main building **(b) Adjacent building**

Figure 5-53: Case-A (Adjacent) and Case-S (Single) transfer function amplitudes ($|U_{s2}/U_g|$) and MPR of superstructures ($T_{fix1} = T_{fix2} = 2.0$ sec, $e_1 = 4$ m, $e_2 = 0$, half-space soil, $D = 3$ m, $V_s = 100$ m/s)

(b) Analysis results for 2 adjacent buildings, D = 3 m, V_s = 100 m/s

(1) Analysis results for identical embedment depths

The MPRs of superstructures (T_{fix1} = 0.5, 1.0 and 2.0 sec, mat foundations, half-space soil, D = 3 m, V_s = 100 m/s) for identical embedment depths ($e_1 = e_2 = e_3$) on the Y direction are given in Figure 5-54.

If Figures 5-44 and 5-54 are compared to determine the effect of one more adjacent building, it can be asserted that the power effect of tall and heavy adjacent buildings on short and light main building is nearly doubled, as can be seen inside the solid line in Figure 5-44(a) and Figure 5-54(a). This shows the increased detrimental effect of the anti-plane DCI, as also seen for the in-plane DCI. Moreover, it can be said that the beneficial effect of the anti-plane DCI is observed for identical adjacent tall and heavy buildings as can be seen inside the solid line in Figure 5-54(c), whereas the reverse effect is seen for the in-plane DCI. The reason of this phenomenon is that condition of the main building is different than that of the adjacent buildings because the main building is flanked by two buildings. Because of this difference, power is transferred from the main building. The anti-plane DCI effect on tall and heavy main buildings adjacent to short and light buildings is negligible, as can be seen inside the dashed line in Figure 5-54(c).

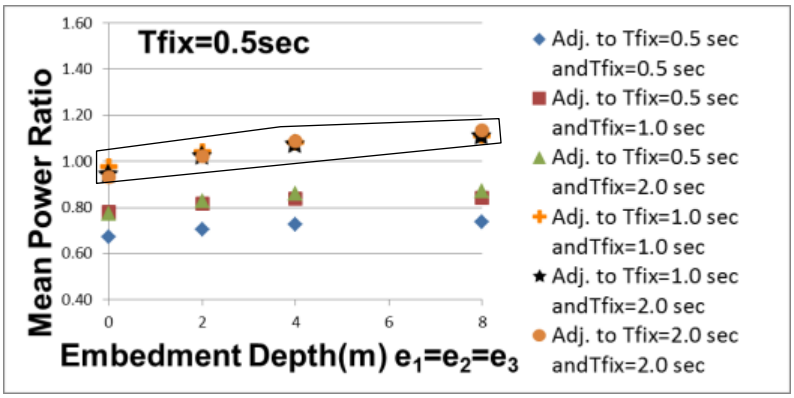

(a) For T_{fix1} = 0.5 sec

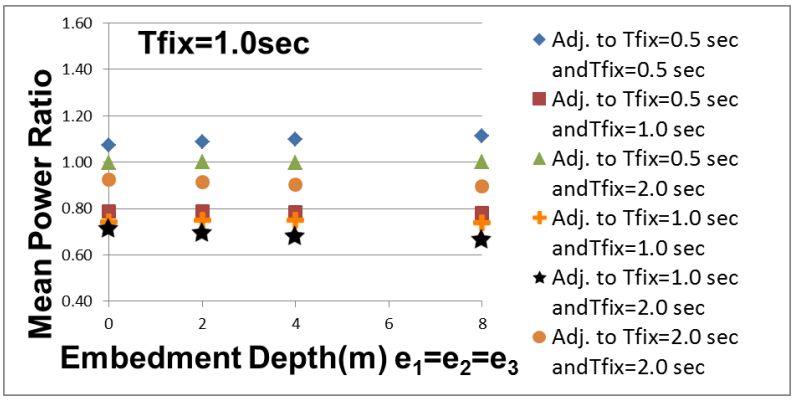

(b) For T_{fix1} = 1.0 sec

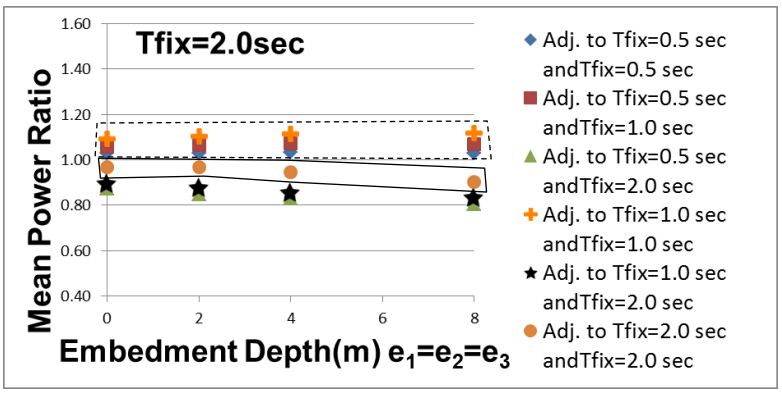

(c) For T_{fix1} = 2.0 sec

Figure 5-54: MPRs of horizontal superstructure motions for anti-plane DCI ($e_1 = e_2 = e_3$, D = 3 m, V_s = 100 m/s, 2 adj. building, U_{s2})

(2) Analysis results for shallower embedment depth of the main building

The MPRs of (T_{fix1} = 0.5, 1.0 and 2.0 sec, mat foundations, half-space soil, D = 3 m, V_s = 100 m/s) for different embedment depths of the main building (e_1) on the Y direction are given in Figure 5-55 where horizontal axis represents the foundation depth of the main building and the foundation depths of the adjacent buildings (e_2 and e_3) are selected as 8 m.

If Figures 5-50 and 5-55 are compared to determine the effect of one more adjacent building, it can be asserted that the detrimental effect of anti-plane DCI is doubled for 2 identical adjacent buildings with shallower foundation embedment depth compared to the case of 1 identical adjacent building. This is especially so for identical adjacent buildings with fixed base natural period of 2.0 sec, as can be seen inside the solid line in Figures 5-50(c) and 5-55(c), because power is transferred from 1 more deeper foundation to shallower foundation. It should also be noted that the horizontal vibration power transfer effect for 2 adjacent buildings is clearly higher for anti-plane DCI than for in-plane DCI. Moreover, it should be noted that, as can be seen inside the dashed line in Figures 5-50(a) and 5-55(a), a short and light main building is affected nearly twice as much when adjacent to tall and heavy buildings than in the case of 1 adjacent building. The anti-plane DCI effect on tall and heavy main buildings adjacent to short and light buildings is negligible, as can be seen inside the dashed line in Figure 5-55(c).

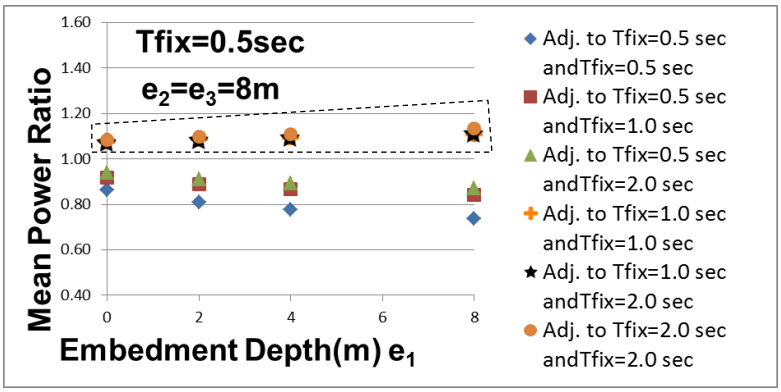

(a) For T_{fix1} = 0.5 sec

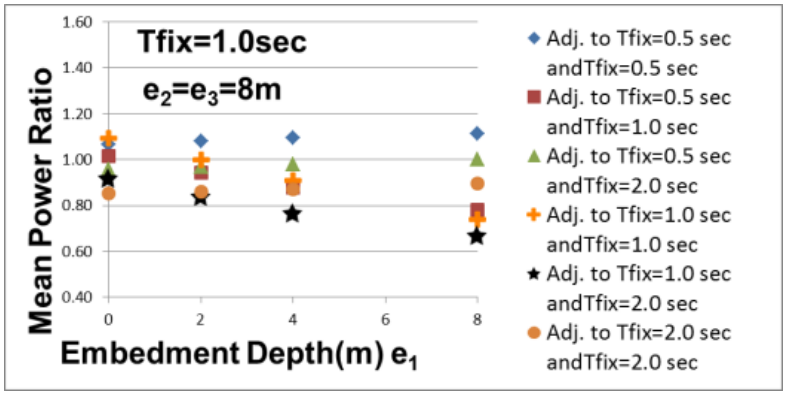

(b) For T_{fix1} = 1.0 sec

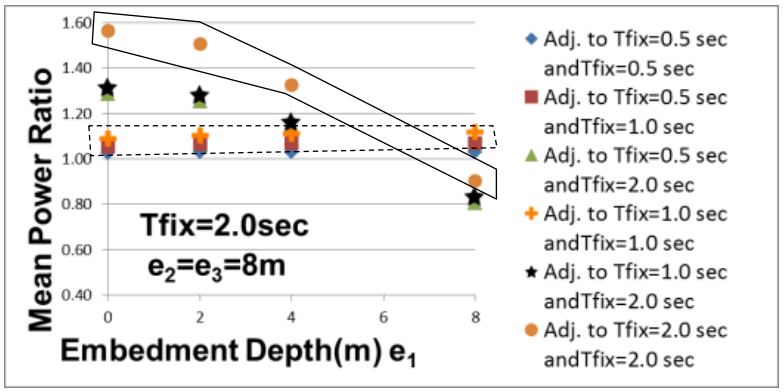

(c) For T_{fix1} = 2.0 sec

Figure 5-55: MPRs of horizontal superstructure motions for anti-plane DCI ($e_2 = e_3 = 8$ m, $D = 3$ m, $V_s = 100$ m/s, 2 adj. building, U_{s2})

(3) Analysis results for deeper embedment depth of the main building

The MPRs of superstructures (T_{fix1} = 0.5, 1.0 and 2.0 sec, mat foundations, half-space soil, D = 3 m, V_s = 100 m/s) for different embedment depths of the main building (e_1) on the Y direction are given in Figure 5-56 where horizontal axis represents the foundation depth of the main building and foundation depth of adjacent buildings (e_2 and e_3) are selected as 0.

If Figure 5-52 and 5-56 are compared to determine the effect of one more adjacent building, it can be claimed that the effect of the anti-plane DCI is on a similar level for 2 identical adjacent buildings with a deeper foundation embedment depth and the case of 1 identical adjacent building, as can be seen inside the solid line in Figures 5-52(c) and 5-56(c).

Moreover, as can be seen inside the dashed line in Figures 5-52(a) and 5-56(a), a short and light main building is affected to a similar extent when adjacent to tall and heavy buildings for the cases of 1 and 2 adjacent buildings. The anti-plane DCI effect on tall and heavy main buildings adjacent to short and light buildings is negligible, as can be seen inside the dashed line in Figure 5-56(c).

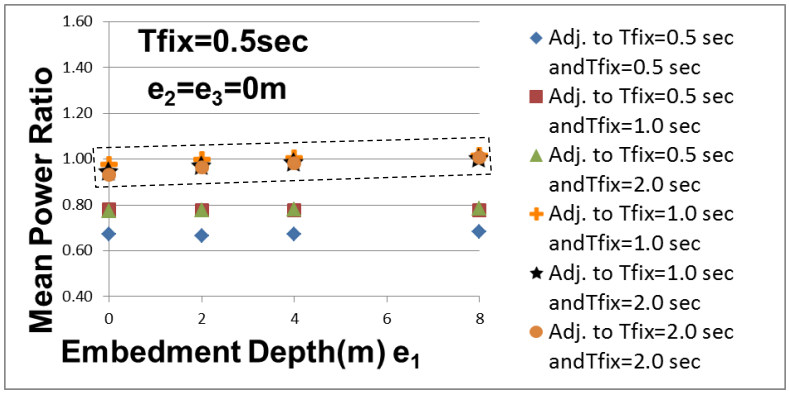

(a) For T_{fix1} = 0.5 sec

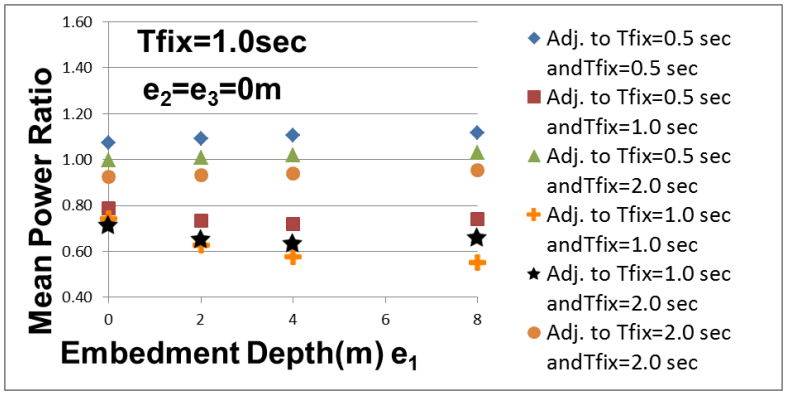

(b) For T_{fix1} = 1.0 sec

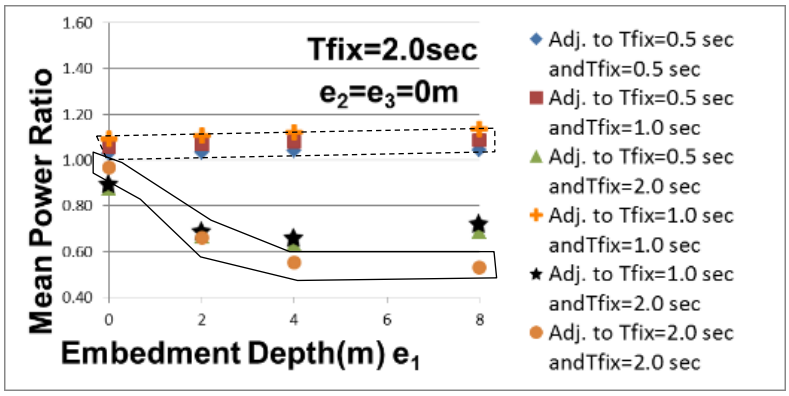

(c) For T_{fix1} = 2.0 sec

Figure 5-56: MPRs of horizontal superstructure motions for anti-plane DCI ($e_2 = e_3 = 0$, D = 3 m, V_s = 100 m/s, 2 adj. building, U_{s2})

(c) Analysis results for 1 adjacent building, D = 3 m, V_s = 200 m/s

(1) Analysis results for identical embedment depths

The MPRs of superstructures (T_{fix1} = 0.5, 1.0 and 2.0 sec, mat foundations, half-space soil, D = 3 m, V_s = 200 m/s) for identical embedment depths ($e_1 = e_2$) on the Y direction are given in Figure 5-57.

If the results of V_s = 100 and 200 m/s situations are compared, it can be said that the smallest MPRs are obtained for identical adjacent buildings for T_{fix} = 0.5sec as can be seen inside the dashed line in Figure 5-57(a). The reason of this result is considered to be that the wave-based DCI effect becomes negligible for V_s = 200 m/s.

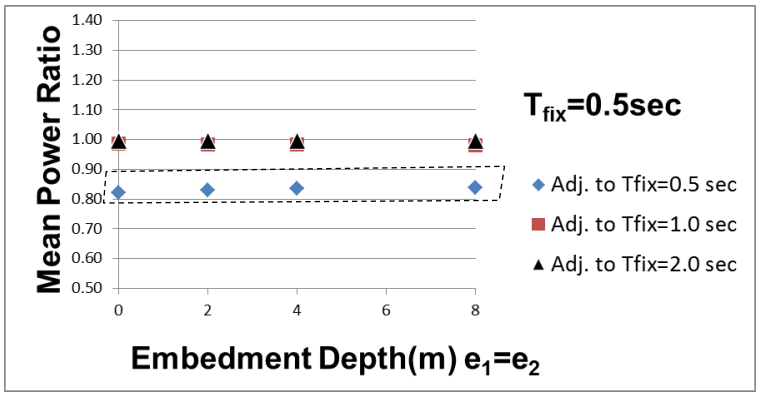

(a) For T_{fix1} = 0.5 sec

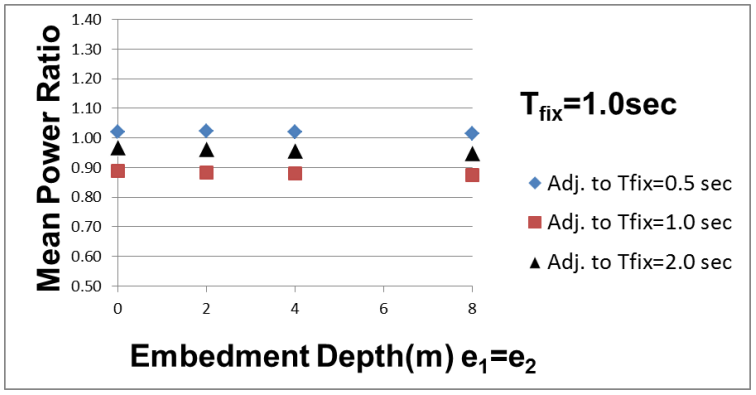

(b) For T_{fix1} = 1.0 sec

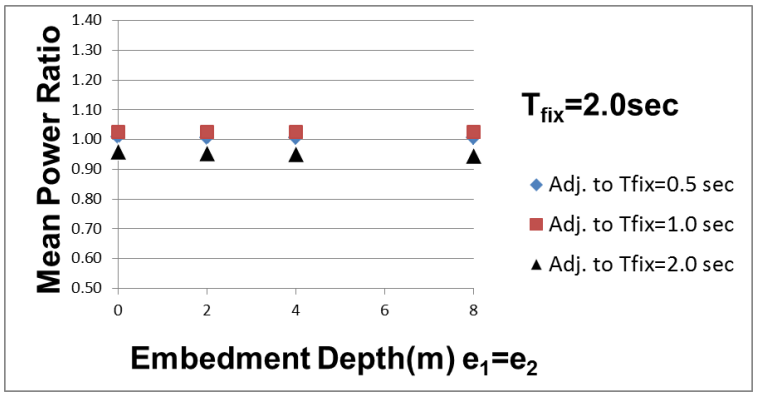

(c) For T_{fix1} = 2.0 sec

Figure 5-57: MPRs of horizontal superstructure motions for anti-plane DCI ($e_1 = e_2$, D = 3 m, V_s = 200 m/s, 1 adj. building, U_{s2})

(2) Analysis results for shallower embedment depth of the main building

The MPRs of superstructures (T_{fix1} = 0.5, 1.0 and 2.0 sec, mat foundations, half-space soil, D = 3 m, V_s = 200 m/s) for different embedment depths of main building (e_1) on the Y direction are given in Figure 5-58 where horizontal axis represents the foundation depth of the main building and the foundation depth of the adjacent building (e_2) is selected as 8 m.

If the results of V_s = 100 and 200 m/s situations are compared, it can be claimed that the detrimental effect of the anti-plane DCI diminishes with increasing shear wave velocity of the soil, as can be seen inside the solid line in Figure 5-58(c).

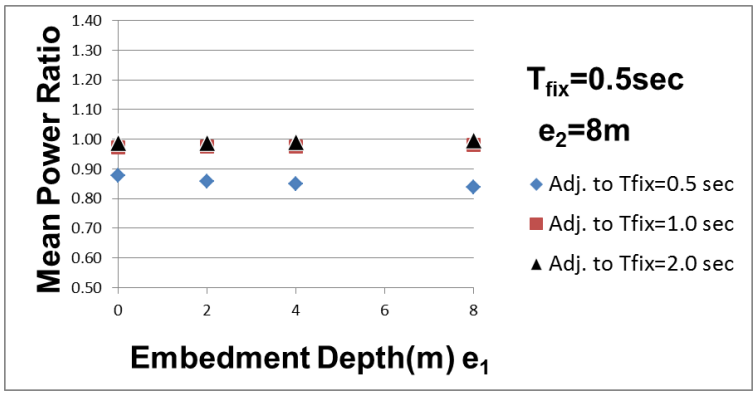

(a) For T_{fix1} = 0.5 sec

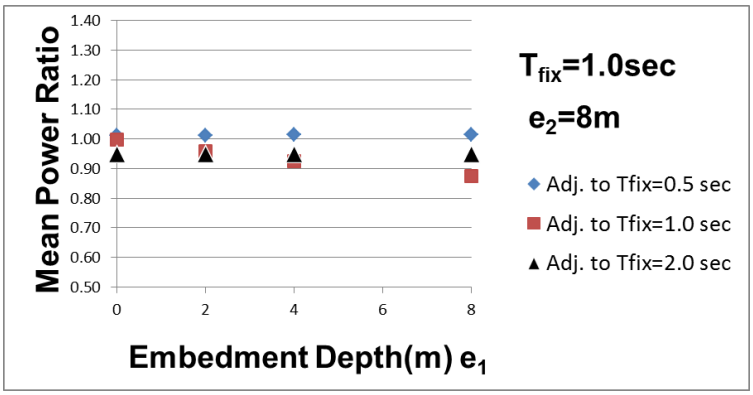

(b) For T_{fix1} = 1.0 sec

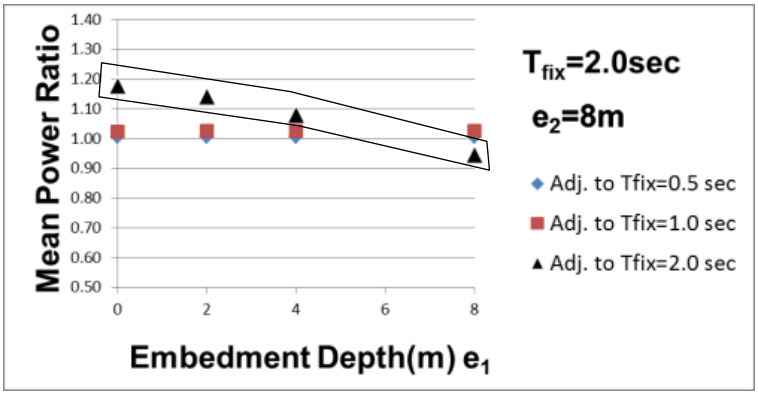

(c) For T_{fix1} = 2.0 sec

Figure 5-58: MPRs of horizontal superstructure motions for anti-plane DCI (e_2 = 8 m, D= 3 m, V_s = 200 m/s, 1 adj. building, U_{s2})

(3) Analysis results for deeper embedment depth of the main building

The MPRs of superstructures (T_{fix1} = 0.5, 1.0 and 2.0 sec, mat foundations, half-space soil, D = 3 m, V_s = 200 m/s) for different embedment depths of the main building (e_1) on the Y direction are given in Figure 5-59 where horizontal axis represents the foundation depth of the main building and the foundation depth of the adjacent building (e_2) is selected as 0.

If the results of V_s = 100 and 200 m/s situations are compared, it can be declared that the beneficial effect of the anti-plane DCI diminishes with increasing shear wave velocity of the soil, as can be seen inside the solid line in Figure 5-59(c). Also, the effect of the anti-plane DCI and the relationship of the foundation embedment depth of the main building change for V_s = 200 m/s for the same reason given for the in-plane DCI effect.

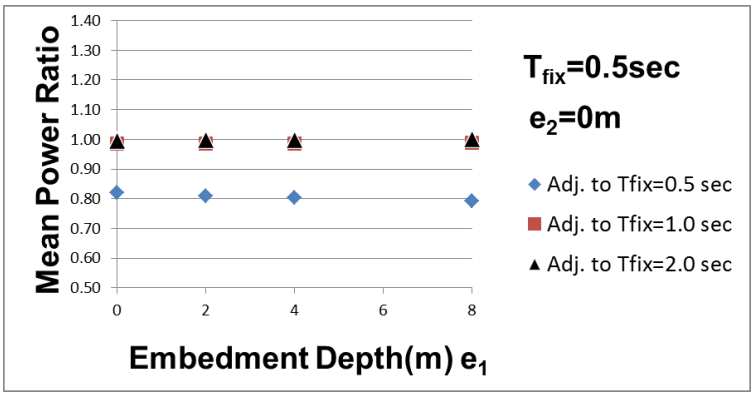

(a) For T_{fix1} = 0.5 sec

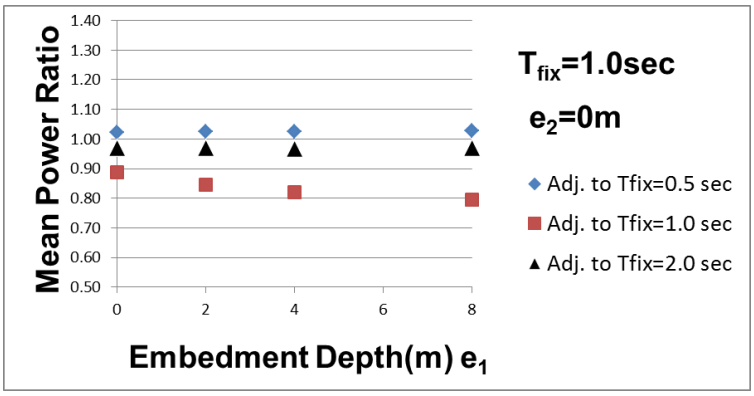

(b) For T_{fix1} = 1.0 sec

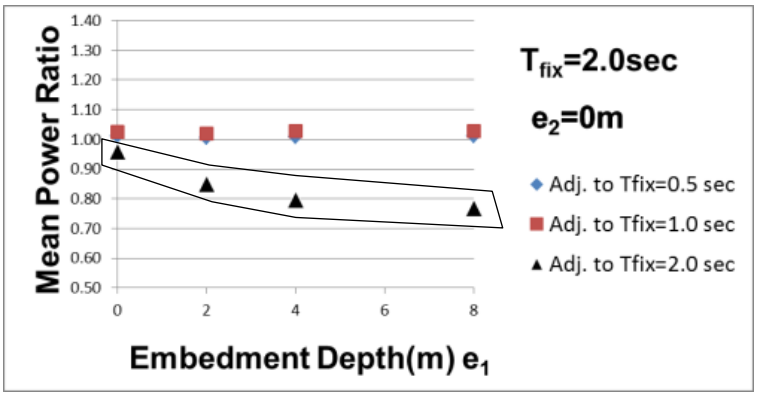

(c) For T_{fix1} = 2.0 sec

Figure 5-59: MPRs of horizontal superstructure motions for anti-plane DCI (e_2 = 0, D = 3 m, V_s = 200 m/s, 1 adj. building, U_{s2})

(d) Analysis results for 2 adjacent buildings, D = 3 m, V_s = 200 m/s

(1) Analysis results for identical embedment depths

The MPRs of superstructures (T_{fix1} = 0.5, 1.0 and 2.0 sec, mat foundations, half-space soil, D = 3 m, V_s = 200 m/s) for identical embedment depths ($e_1 = e_2 = e_3$) on the Y direction are given in Figure 5-60.

If the results of V_s = 100 and 200 m/s situations are compared, it can be said that a similar relation is seen for the cases of 1 and 2 adjacent buildings.

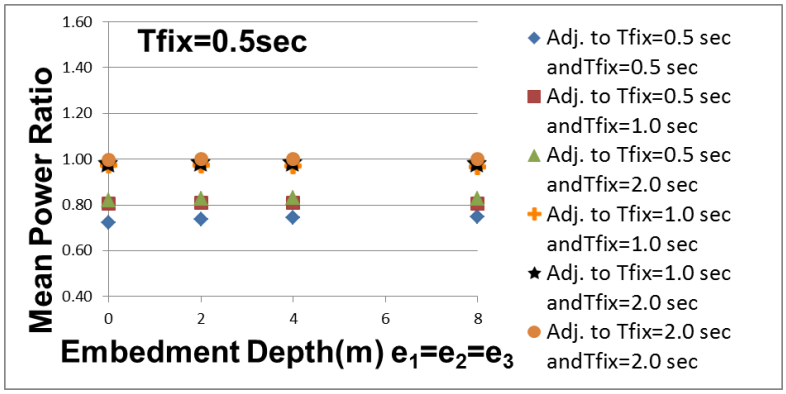

(a) For T_{fix1} = 0.5 sec

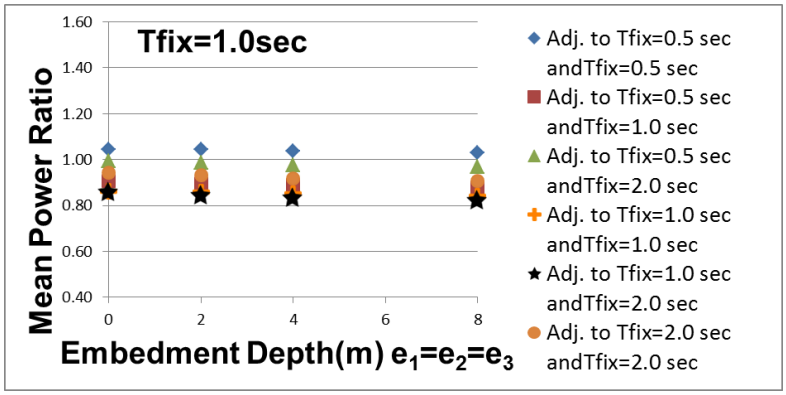

(b) For T_{fix1} = 1.0 sec

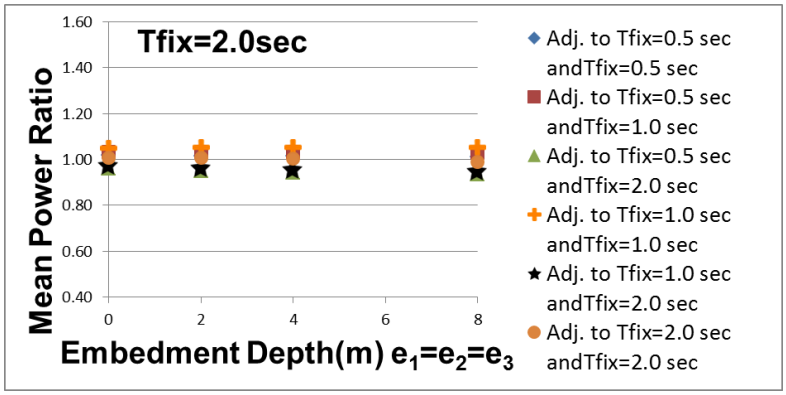

(c) For T_{fix1} = 2.0 sec

Figure 5-60: MPRs of horizontal superstructure motions for anti-plane DCI ($e_1 = e_2 = e_3$, D = 3 m, V_s = 200 m/s, 2 adj. building, U_{s2})

(2) Analysis results for shallower embedment depth of the main building

The MPRs of superstructures (T_{fix1} = 0.5, 1.0 and 2.0 sec, mat foundations, half-space soil, D = 3 m, V_s = 200 m/s) for different embedment depths of the main building (e_1) on the Y direction are given in Figure 5-61 where horizontal axis represents the foundation depth of the main building and the foundation depths of the adjacent buildings (e_2 and e_3) are selected as 8 m.

If the results of V_s = 100 and 200 m/s situations are compared, it can be said that a similar relation is seen for the cases of 1 and 2 adjacent buildings.

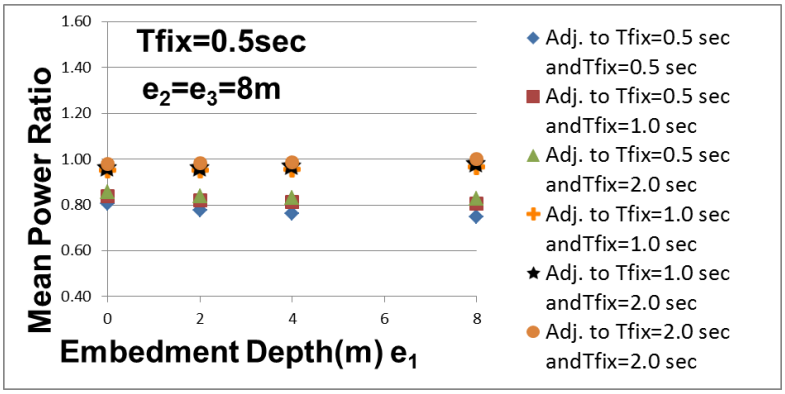

(a) For T_{fix1} = 0.5 sec

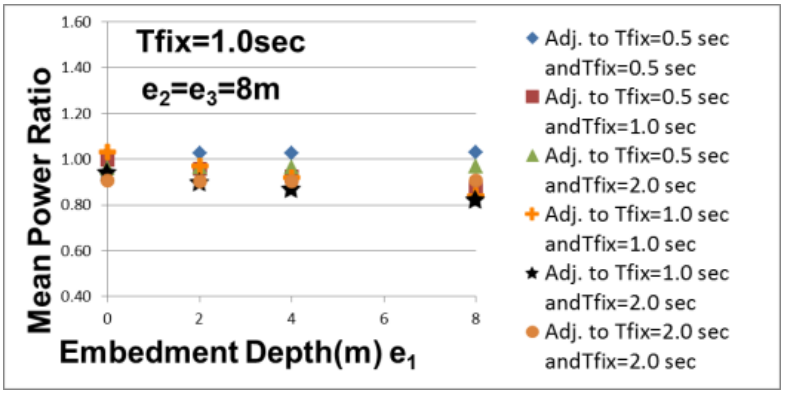

(b) For T_{fix1} = 1.0 sec

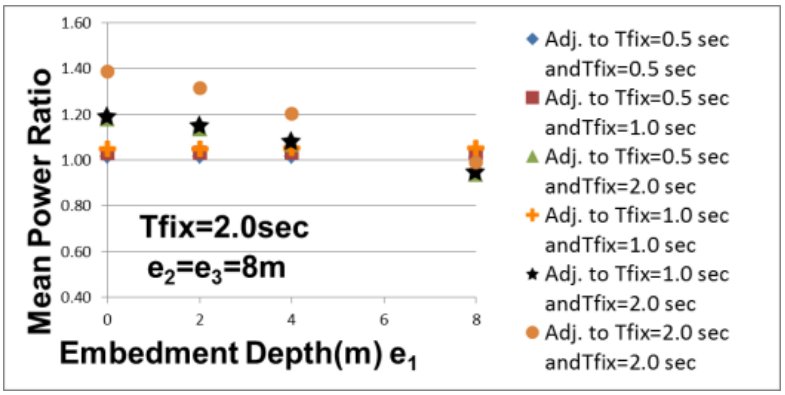

(c) For T_{fix1} = 2.0 sec

Figure 5-61: MPRs of horizontal superstructure motions for anti-plane DCI ($e_2 = e_3 = 8$ m, $D = 3$ m, $V_s = 200$ m/s, 2 adj. building, U_{s2})

(3) Analysis results for deeper embedment depth of the main building

The MPRs of superstructures (T_{fix1} = 0.5, 1.0 and 2.0 sec, mat foundations, half-space soil, D = 3 m, V_s = 200 m/s) for different embedment depths of the main building (e_1) on the Y direction are given in Figure 5-62 where horizontal axis represents the foundation depth of the main building and foundation depth of adjacent buildings (e_2 and e_3) are selected as 0.

If the results of V_s = 100 and 200 m/s situations are compared, it can be said that a similar relation is seen for the cases of 1 and 2 adjacent buildings.

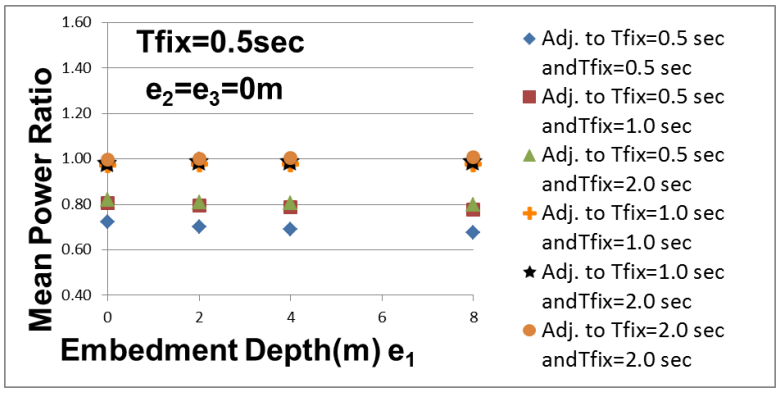

(a) For T_{fix1} = 0.5 sec

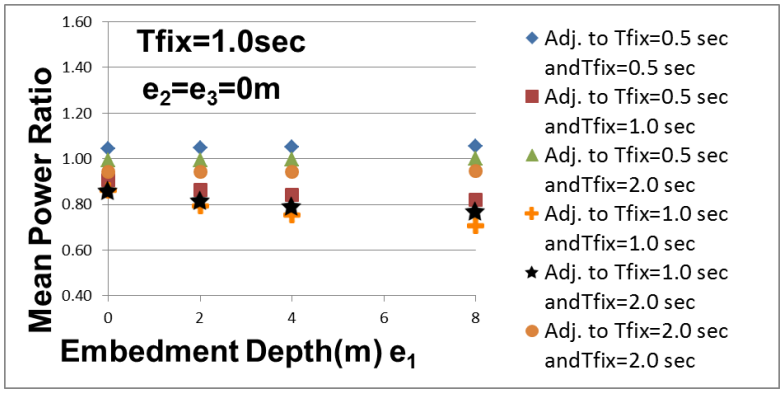

(b) For T_{fix1} = 1.0 sec

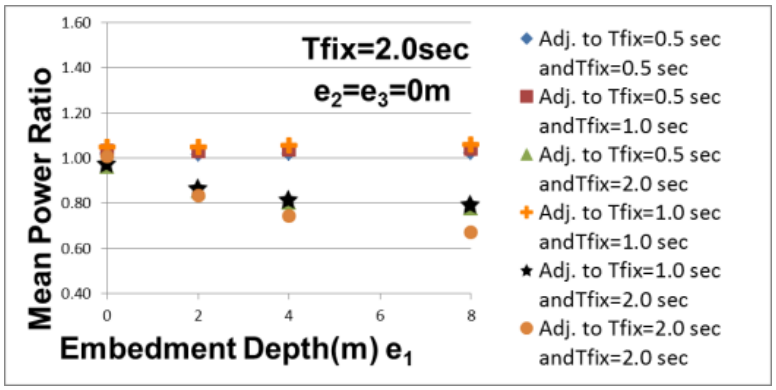

(c) For T_{fix1} = 2.0 sec

Figure 5-62: MPRs of horizontal superstructure motions for anti-plane DCI ($e_2 = e_3 = 0$, D = 3 m, V_s = 200 m/s, 2 adj. building, U_{s2})

(e) Analysis results for 1 adjacent building, D = 6 m, V_s = 100 m/s

(1) Analysis results for identical embedment depths

The MPRs of superstructures (T_{fix1} = 0.5, 1.0 and 2.0 sec, mat foundations, half-space soil, D = 6 m, V_s = 100 m/s) for identical embedment depths ($e_1 = e_2$) on the Y direction are given in Figure 5-63.

If the results of the D = 3 m and 6 m situations are compared, it can be asserted that the effect of the anti-plane DCI does not depend so much to the clearance for such building types.

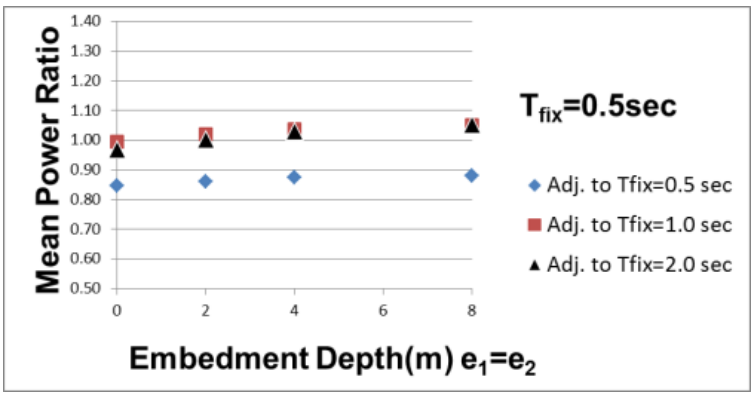

(a) For T_{fix1} = 0.5 sec

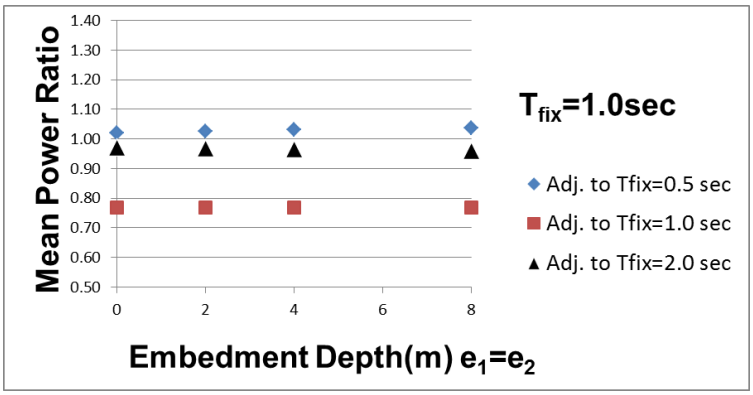

(b) For T_{fix1} = 1.0 sec

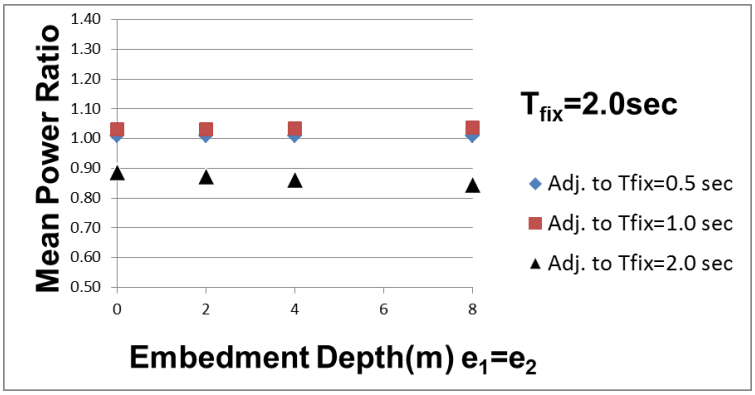

(c) For T_{fix1} = 2.0 sec

Figure 5-63: MPRs of horizontal superstructure motions for anti-plane DCI ($e_1 = e_2$, D = 6 m, V_s = 100 m/s, 1 adj. building, U_{s2})

(2) Analysis results for shallower embedment depth of the main building

The MPRs of superstructures (T_{fix1} = 0.5, 1.0 and 2.0 sec, mat foundations, half-space soil, D = 6 m, V_s = 100 m/s) for different embedment depths of main building (e_1) on the Y direction are given in Figure 5-64 where horizontal axis represents the foundation depth of the main building and the foundation depth of the adjacent building (e_2) is selected as 8 m.

If the results of the D = 3 m and 6m situations are compared, it can be said that there is a small effect of the clearance on the power transfer induced from the anti-plane DCI effect, as it seen inside the solid line in Figure 5-64. It can also be asserted that the anti-plane DCI effect for such embedment depths situations for D = 6 m and V_s = 100 m/s is more effective than D = 3 m and V_s = 200 m/s.

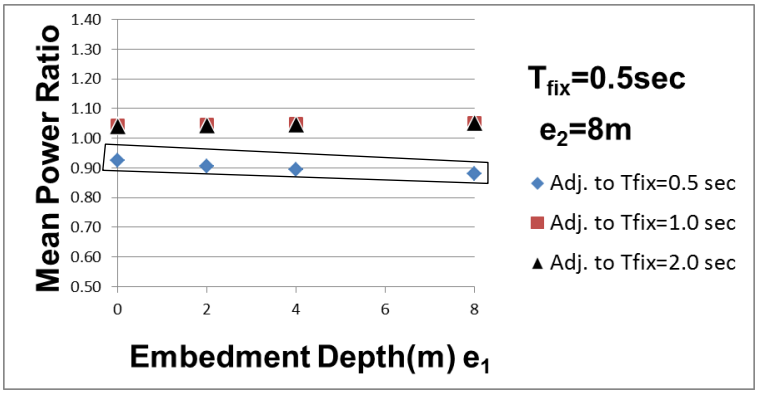

(a) For T_{fix1} = 0.5 sec

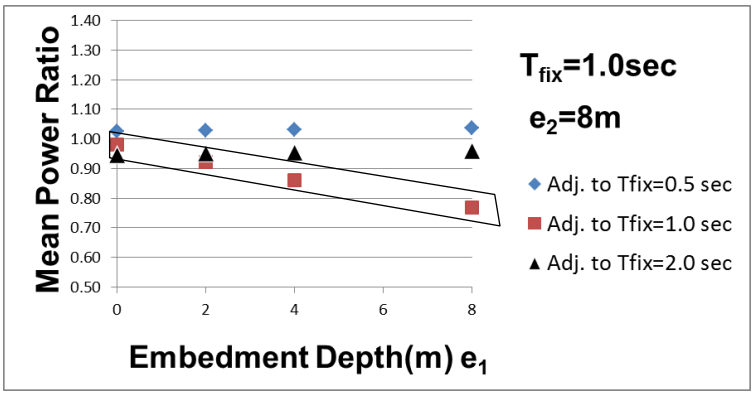

(b) For T_{fix1} = 1.0 sec

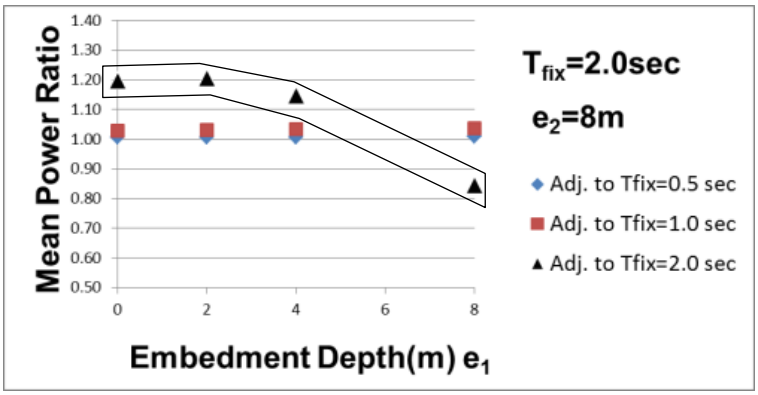

(c) For T_{fix1} = 2.0 sec

Figure 5-64: MPRs of horizontal superstructure motions for anti-plane DCI (e_2 = 8 m, D = 6 m, V_s = 100 m/s, 1 adj. building, U_{s2})

(3) Analysis results for deeper embedment depth of the main building

The MPRs of superstructures (T_{fix1} = 0.5, 1.0 and 2.0 sec, mat foundations, half-space soil, D = 6 m, V_s = 100 m/s) for different embedment depths of the main building (e_1) on the Y direction are given in Figure 5-65 where horizontal axis represents the foundation depth of the main building and the foundation depth of the adjacent building (e_2) is selected as 0.

If the results of the D = 3 m and 6m situations are compared, it can be said that there is a small effect of the clearance on the power transfer induced from the anti-plane DCI effect as it seen inside the solid line in Figure 5-65. It can also be asserted that the anti-plane DCI effect for such embedment depth situations for D = 6 m and V_s = 100 m/s is more effective than for D = 3 m and V_s = 200 m/s.

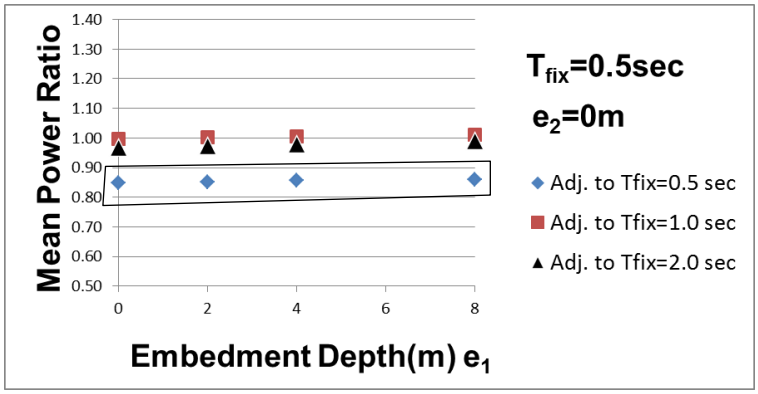

(a) For T_{fix1} = 0.5 sec

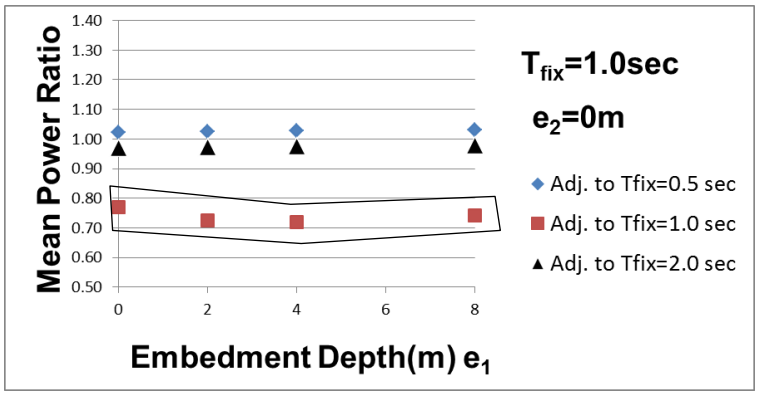

(b) For T_{fix1} = 1.0 sec

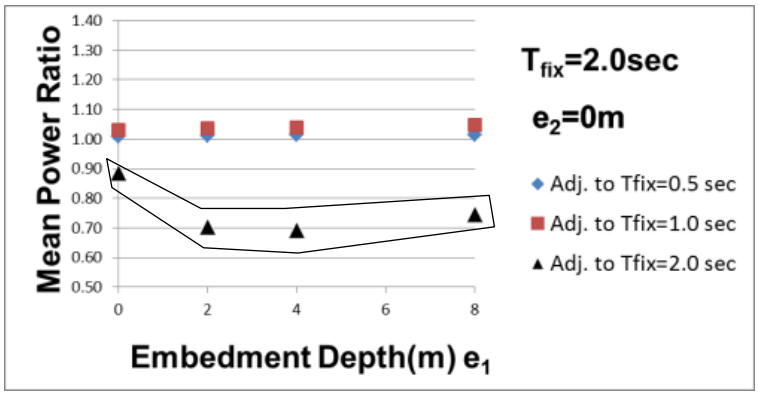

(c) For T_{fix1} = 2.0 sec

Figure 5-65: MPRs of horizontal superstructure motions for anti-plane DCI (e_2 = 0, D = 6 m, V_s = 100 m/s, 1 adj. building, U_{s2})

(f) Analysis results for 2 adjacent buildings, D = 6 m, V_s = 100 m/s

(1) Analysis results for identical embedment depths

The MPRs of superstructures (T_{fix1} = 0.5, 1.0 and 2.0 sec, mat foundations, half-space soil, D = 6 m, V_s = 100 m/s) for identical embedment depths ($e_1 = e_2 = e_3$) on the Y direction are given in Figure 5-66.

If the results of the D = 3 m and 6 m situations are compared, it can be asserted that the effect of the anti-plane DCI does not depend so much to the clearance for such building types.

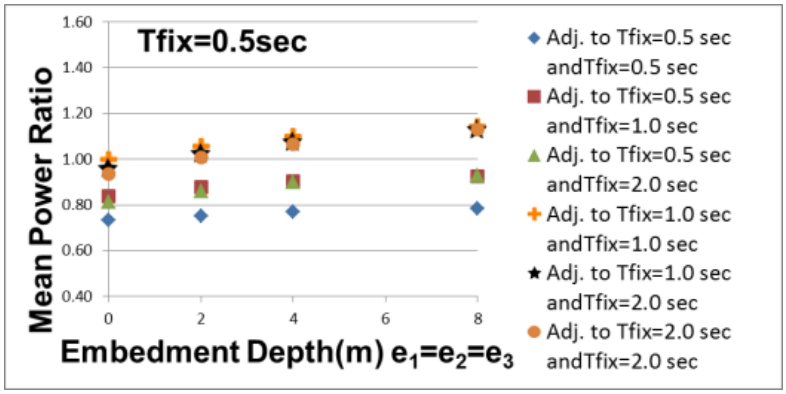

(a) For T_{fix1} = 0.5 sec

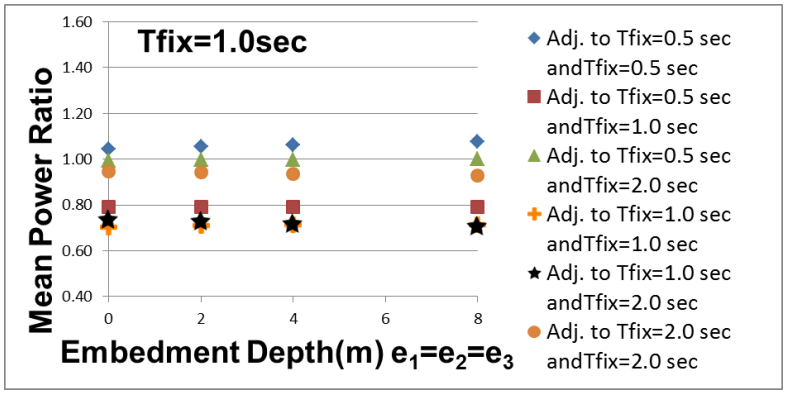

(b) For T_{fix1} = 1.0 sec

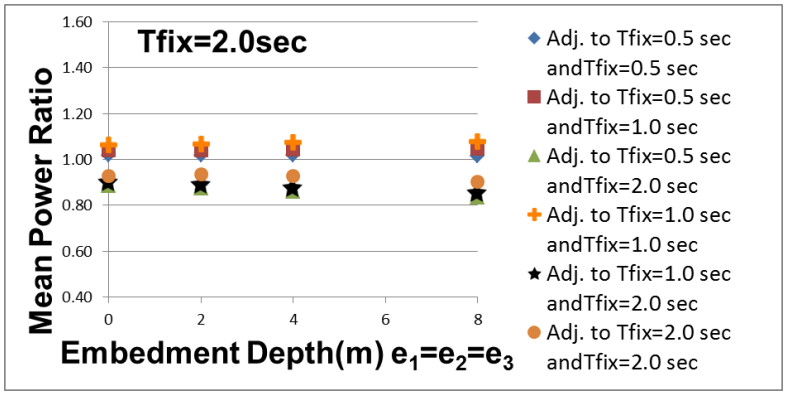

(c) For T_{fix1} = 2.0 sec

Figure 5-66: MPRs of horizontal superstructure motions for anti-plane DCI ($e_1 = e_2 = e_3$, D = 6m, V_s = 100 m/s, 2 adj. building, U_{s2})

(2) Analysis results for shallower embedment depth of the main building

The MPRs of superstructures (T_{fix1} = 0.5, 1.0 and 2.0 sec, mat foundations, half-space soil, D = 6 m, V_s = 100 m/s) for different embedment depths of the main building (e_1) on the Y direction are given in Figure 5-67 where horizontal axis represents the foundation depth of the main building and the foundation depths of the adjacent buildings (e_2 and e_3) are selected as 8 m.

If the results of the D = 3 m and 6 m situations are compared, it can be said that a similar relation is seen for the cases of 1 and 2 adjacent buildings.

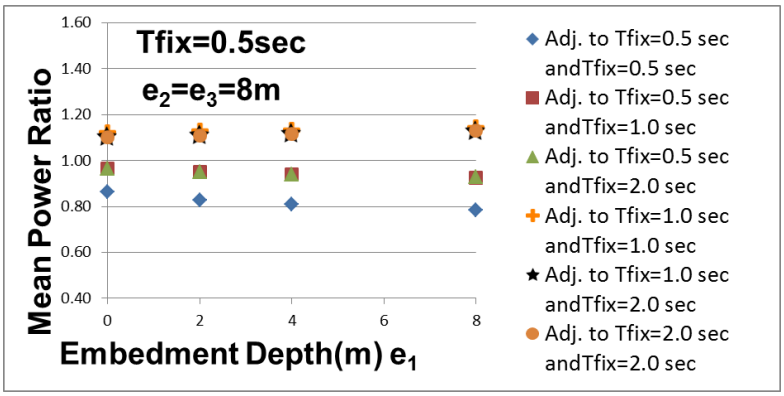

(a) For T_{fix1} = 0.5 sec

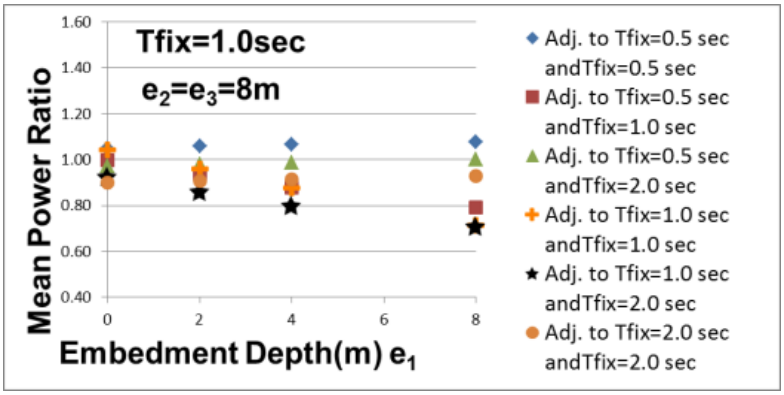

(b) For T_{fix1} = 1.0 sec

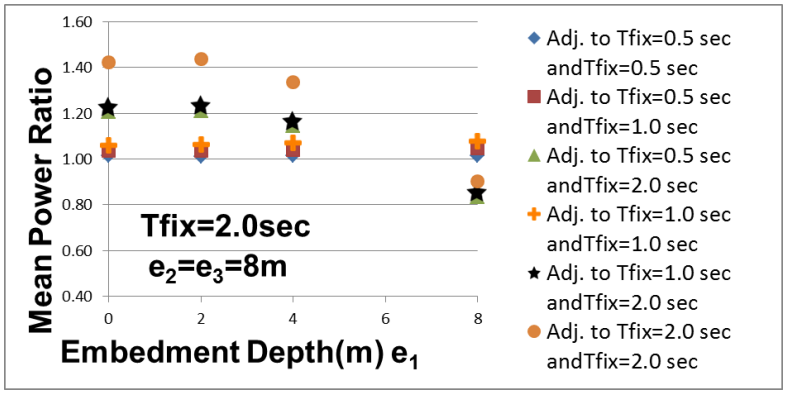

(c) For T_{fix1} = 2.0 sec

Figure 5-67: MPRs of horizontal superstructure motions for anti-plane DCI (e_2 = e_3 = 8 m, D = 6 m, V_s = 100 m/s, 2 adj. building, U_{s2})

(3) Analysis results for deeper embedment depth of the main building

The MPRs of superstructures (T_{fix1} = 0.5, 1.0 and 2.0 sec, mat foundations, half-space soil, D = 6 m, V_s = 100 m/s) for different embedment depths of the main building (e_1) on the Y direction are given in Figure 5-68 where horizontal axis represents the foundation depth of the main building and foundation depth of adjacent buildings (e_2 and e_3) are selected as 0.

If the results of the D = 3 m and 6 m situations are compared, it can be said that a similar relation is seen for the cases of 1 and 2 adjacent buildings.

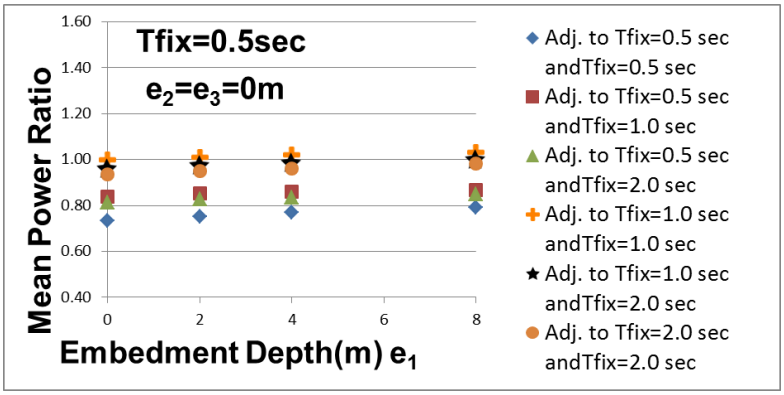

(a) For T_{fix1} = 0.5 sec

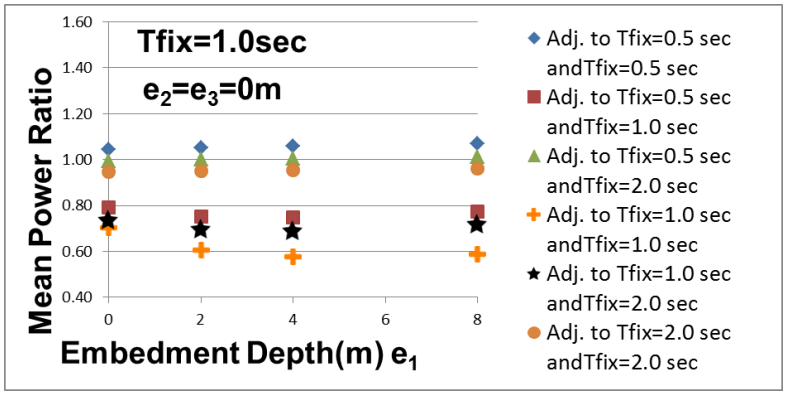

(b) For T_{fix1} = 1.0 sec

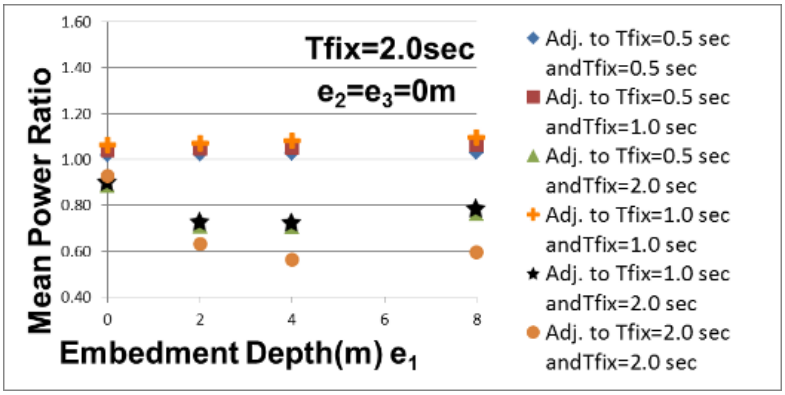

(c) For T_{fix1} = 2.0 sec

Figure 5-68: MPRs of horizontal superstructure motions for anti-plane DCI ($e_2 = e_3 = 0$, D = 6 m, V_s = 100 m/s, 2 adj. building, U_{s2})

(g) Analysis results for 1 adjacent building, D = 6 m, V_s = 200 m/s

(1) Analysis results for identical embedment depths

The MPRs of superstructures (T_{fix1} = 0.5, 1.0 and 2.0 sec, mat foundations, half-space soil, D = 6 m, V_s = 200 m/s) for identical embedment depths ($e_1 = e_2$) on the Y direction are given in Figure 5-69.

If the results of the D = 3 m and 6m situations are compared, it can be claimed that similar results are obtained for these conditions.

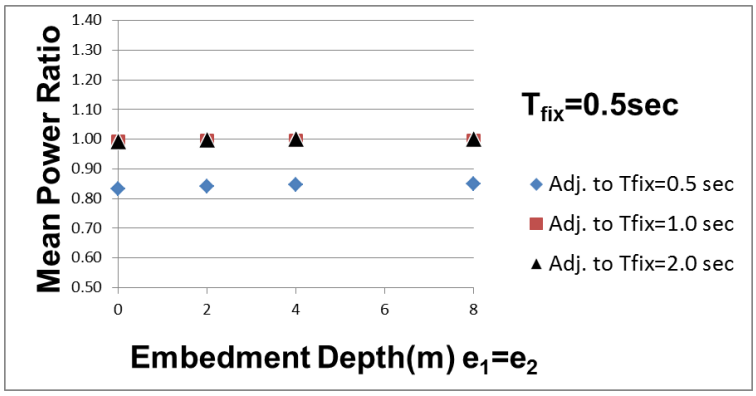

(a) For T_{fix1} = 0.5 sec

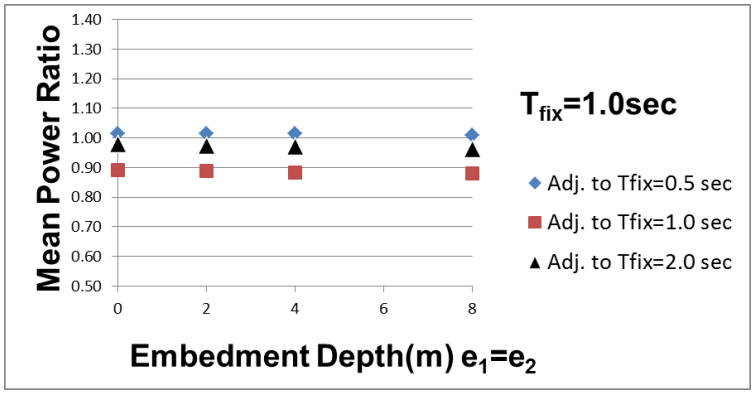

(b) For T_{fix1} = 1.0 sec

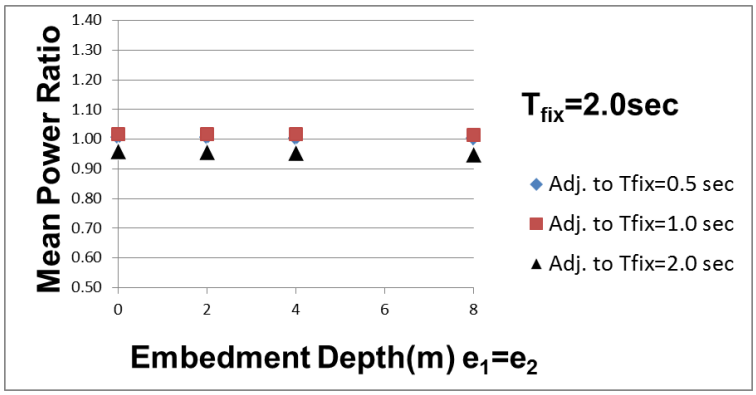

(c) For T_{fix1} = 2.0 sec

Figure 5-69: MPRs of horizontal superstructure motions for anti-plane DCI ($e_1 = e_2$, D = 6 m, V_s = 200 m/s, 1 adj. building, U_{s2})

(2) Analysis results for shallower embedment depth of the main building

The MPRs of superstructures (T_{fix1} = 0.5, 1.0 and 2.0 sec, mat foundations, half-space soil, D = 6 m, V_s = 200 m/s) for different embedment depths of main building (e_1) on the Y direction are given in Figure 5-70 where horizontal axis represents the foundation depth of the main building and the foundation depth of the adjacent building (e_2) is selected as 8 m.

If the results of the D = 3 m and 6m situations are compared, it can be claimed that similar results are obtained for these conditions.

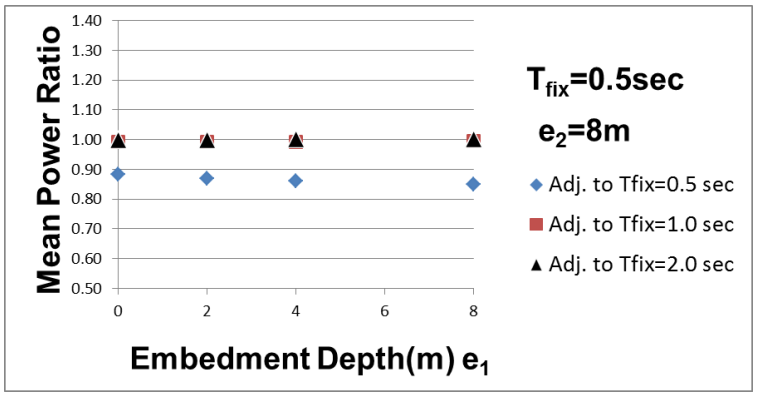

(a) For T_{fix1} = 0.5 sec

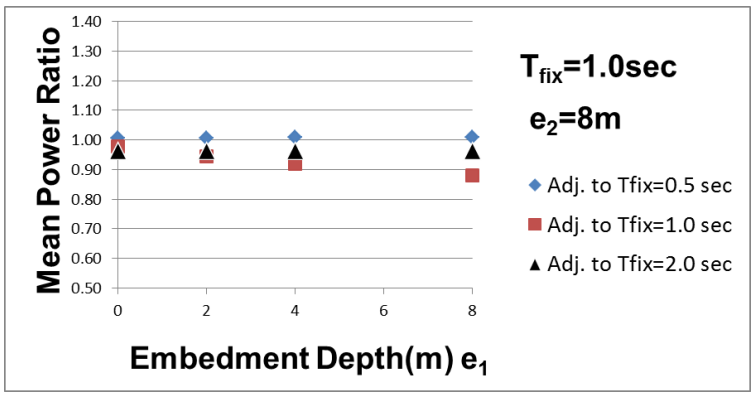

(b) For T_{fix1} = 1.0 sec

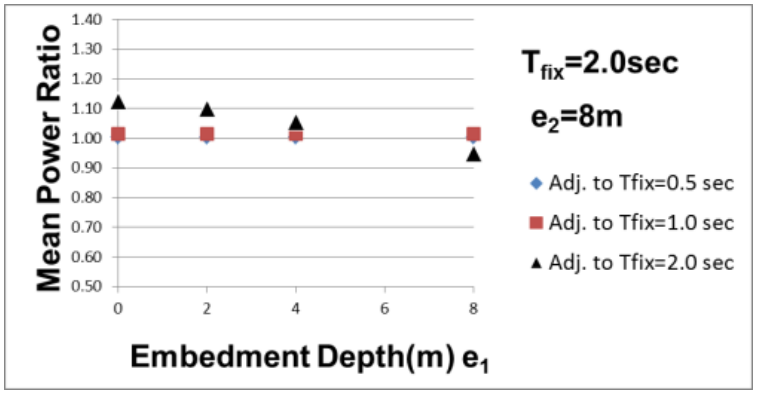

(c) For T_{fix1} = 2.0 sec

Figure 5-70: MPRs of horizontal superstructure motions for anti-plane DCI (e_2 = 8 m, D = 6 m, V_s = 200 m/s, 1 adj. building, U_{s2})

(3) Analysis results for deeper embedment depth of the main building

The MPRs of superstructures (T_{fix1} = 0.5, 1.0 and 2.0 sec, mat foundations, half-space soil, D = 6 m, V_s = 200 m/s) for different embedment depths of the main building (e_1) on the Y direction are given in Figure 5-71 where horizontal axis represents the foundation depth of the main building and the foundation depth of the adjacent building (e_2) is selected as 0.

If the results of the D= 3 m and 6 m situations are compared, it can be claimed that similar results are obtained for these conditions.

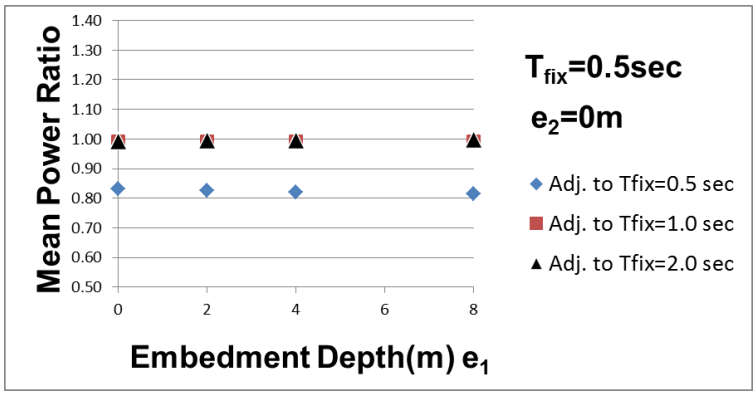

(a) For T_{fix1} = 0.5 sec

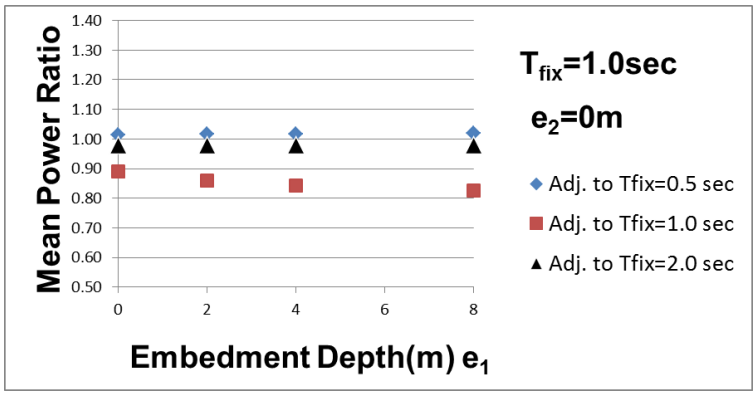

(b) For T_{fix1} = 1.0 sec

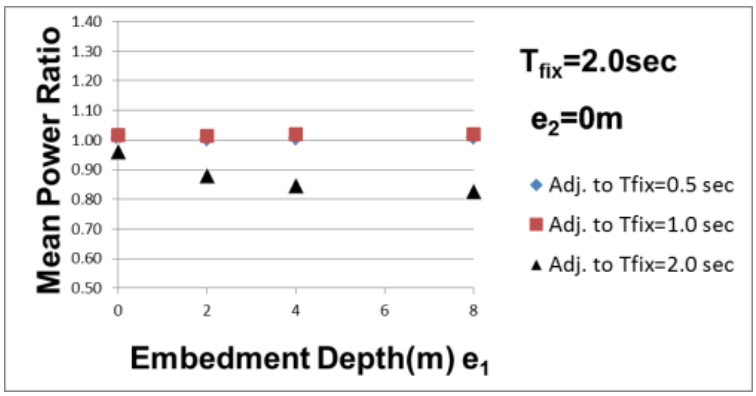

(c) For T_{fix1} = 2.0 sec

Figure 5-71: MPRs of horizontal superstructure motions for anti-plane DCI (e_2 = 0, D = 6 m, V_s = 200 m/s, 1 adj. building, U_{s2})

(h) Analysis results for 2 adjacent buildings, D = 6 m, V_s = 200 m/s

(1) Analysis results for identical embedment depths

The MPRs of superstructures (T_{fix1} = 0.5, 1.0 and 2.0 sec, mat foundations, half-space soil, D = 6 m, V_s = 200 m/s) for identical embedment depths ($e_1 = e_2 = e_3$) on the Y direction are given in Figure 5-72.

If the results of D = 3 m and 6m situations are compared, it can be asserted that the effect of the anti-plane DCI does not depend so much to the clearance for such building types.

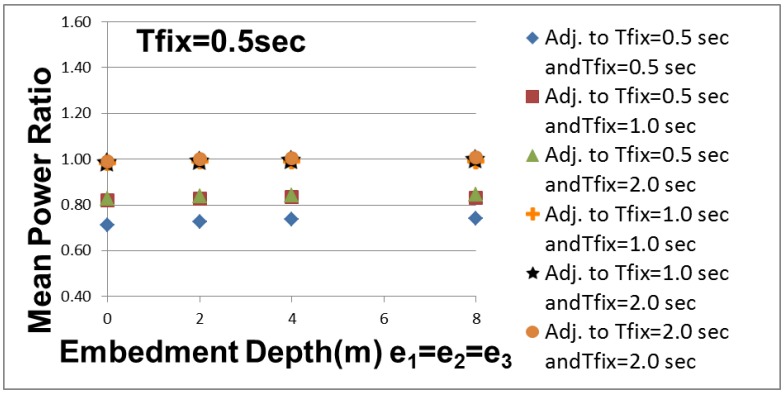

(a) For T_{fix1} = 0.5 sec

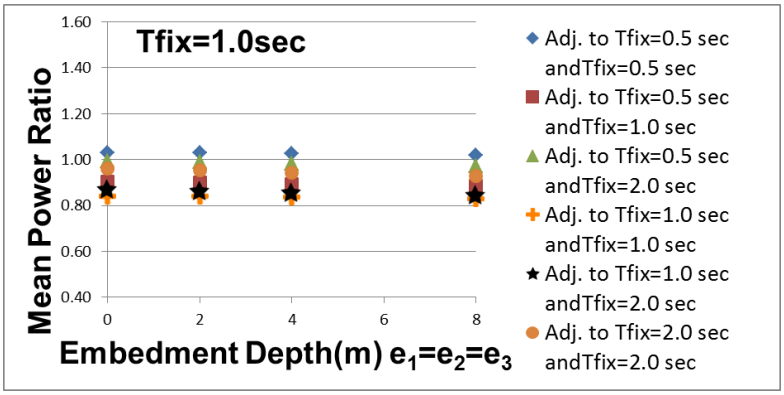

(b) For T_{fix1} = 1.0 sec

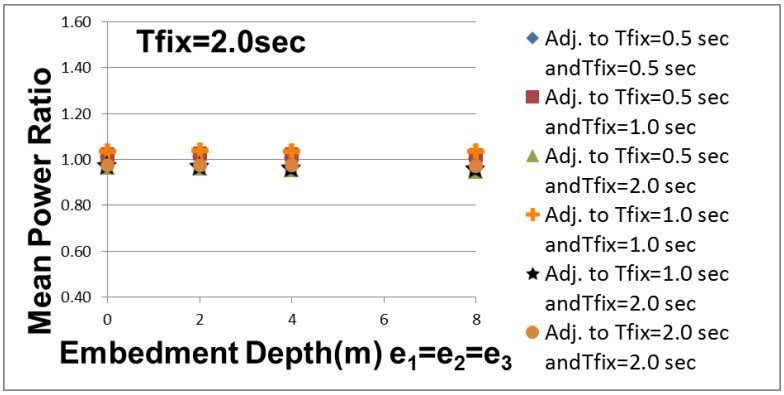

(c) For T_{fix1} = 2.0 sec

Figure 5-72: MPRs of horizontal superstructure motions for anti-plane DCI ($e_1 = e_2 = e_3$, D = 6 m, V_s = 200 m/s, 2 adj. building, U_{s2})

(2) Analysis results for shallower embedment depth of the main building

The MPRs of superstructures (T_{fix1} = 0.5, 1.0 and 2.0 sec, mat foundations, half-space soil, D = 6 m, V_s = 200 m/s) for different embedment depths of the main building (e_1) on the Y direction are given in Figure 5-73 where horizontal axis represents the foundation depth of the main building and the foundation depths of the adjacent buildings (e_2 and e_3) are selected as 8 m.

If the results of the D = 3 m and 6m situations are compared, it can be said that similar relation is seen for 1 and 2 adjacent buildings cases.

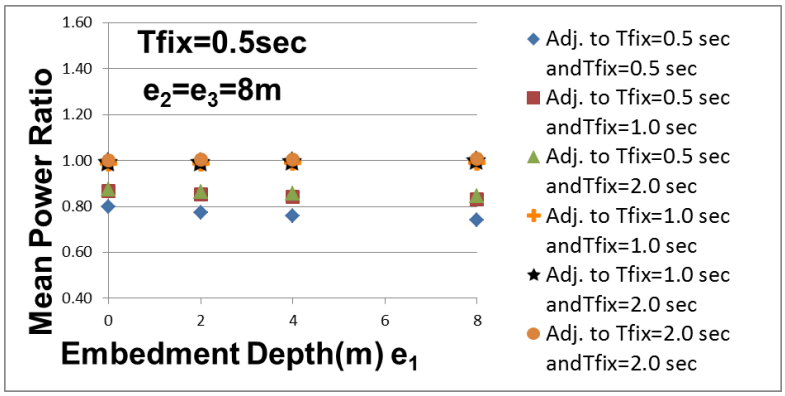

(a) For T_{fix1} = 0.5 sec

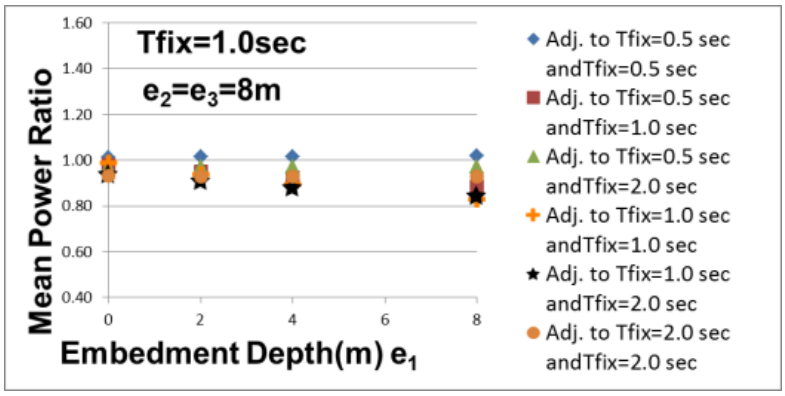

(b) For T_{fix1} = 1.0 sec

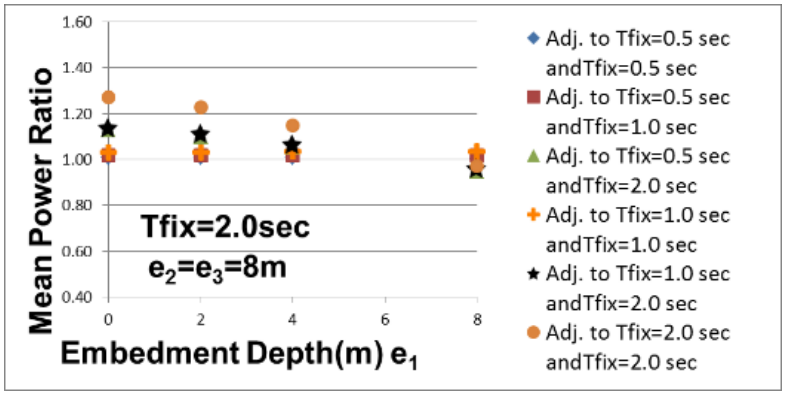

(c) For T_{fix1} = 2.0 sec

Figure 5-73: MPRs of horizontal superstructure motions for anti-plane DCI ($e_2 = e_3 = 8$ m, $D = 6$ m, $V_s = 200$ m/s, 2 adj. building, U_{s2})

(3) Analysis results for deeper embedment depth of the main building

The MPRs of superstructures (T_{fix1} = 0.5, 1.0 and 2.0 sec, mat foundations, half-space soil, D = 6 m, V_s = 200 m/s) for different embedment depths of the main building (e_1) on the Y direction are given in Figure 5-74 where horizontal axis represents the foundation depth of the main building and foundation depth of adjacent buildings (e_2 and e_3) are selected as 0.

If the results of the D = 3 m and 6m situations are compared, it can be said that similar relation is seen for 1 and 2 adjacent buildings cases.

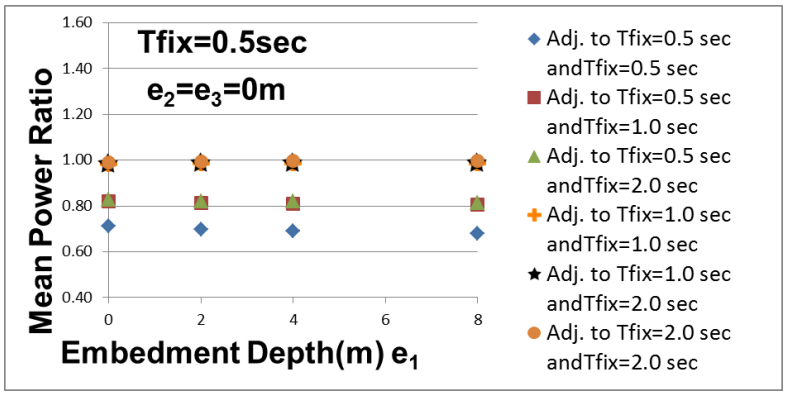

(a) For T_{fix1} = 0.5 sec

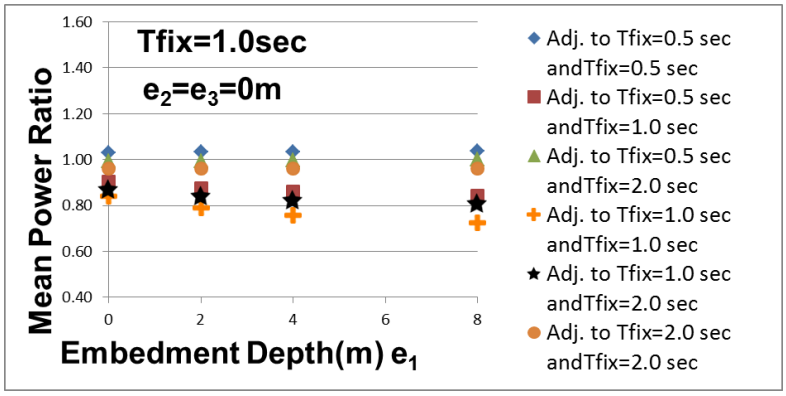

(b) For T_{fix1} = 1.0 sec

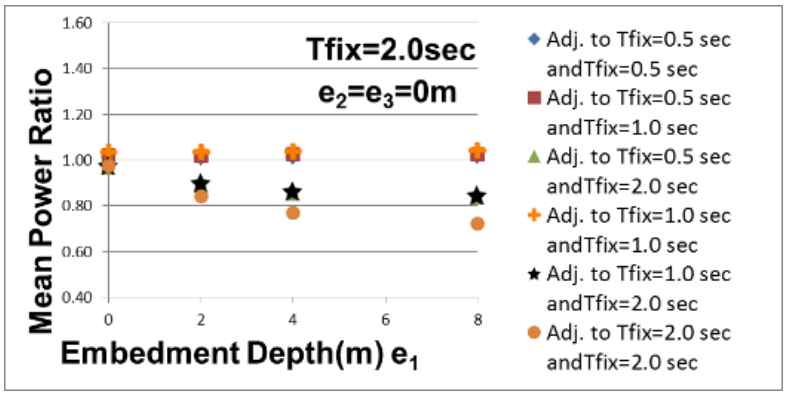

(c) For T_{fix1} = 2.0 sec

Figure 5-74: MPRs of horizontal superstructure motions for anti-plane DCI ($e_2 = e_3 = 0$, D = 6 m, V_s = 200 m/s, 2 adj. building, U_{s2})

(i) Effect of m_s, H_{eff}, and h_s on transfer function amplitudes and MPR

In this section, to determine the effects of m_s, H_{eff}, and h_s on the anti-plane DCI, transfer function amplitudes ($|U_{s2}/U_g|$) and MPRs of horizontal motions of identical superstructures (T_{fix1} = T_{fix2} = 1.0 and 2.0 sec, e_1 = 0 and e_2 = 4 m, D = 3 m) on the Y direction for half-space soil are calculated.

(1) Effect of m_s on anti-plane DCI

Analyses of doubling the mass of the superstructures (m_s = 5x10^6 kg and 1x10^7 kg, T_{fix1} = T_{fix2} = 1.0 sec, H_{eff} = 20 m) are performed to clarify the effect of superstructure mass on the anti-plane DCI. The transfer function amplitudes ($|U_{s2}/U_g|$) and MPRs of horizontal motions of identical superstructures are given in Figure 5-75. The other analysis parameters are the same as those given in Section 5.2. The rigidity of the m_s = 1x10^7 kg superstructure is calculated again to obtain a fixed natural period of 1.0 sec (T_{fix} = 1.0 sec).

If Figures 5-75(a) and 5-75(b) are compared, it can be asserted that the effect of superstructure mass is low on anti-plane DCI but higher than in-plane DCI for this limited case.

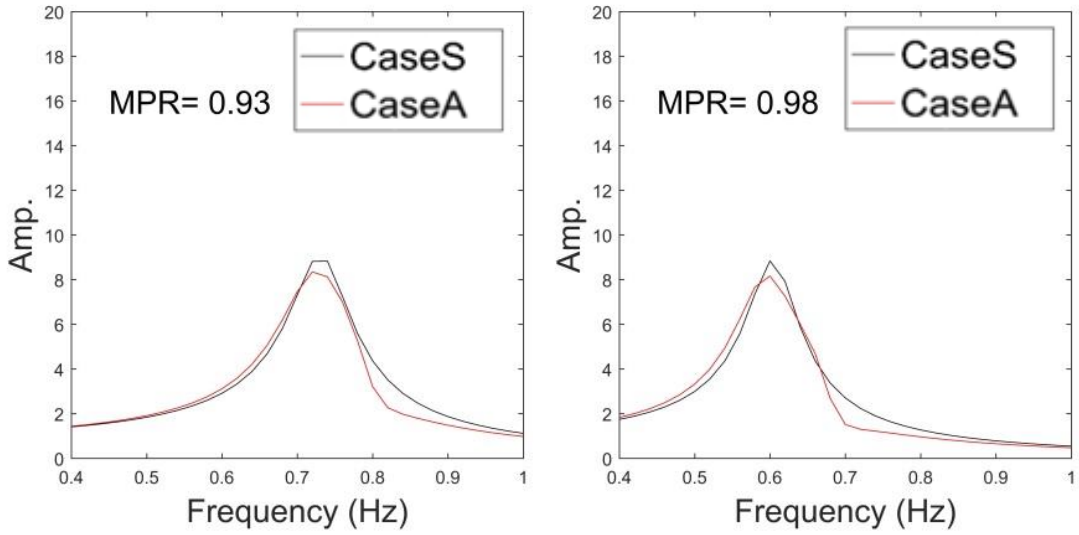

(a) m_s = 5x10^6 kg **(b) m_s = 1x10^7 kg**

Figure 5-75: Case-A (Adjacent) and Case-S (Single) transfer function amplitudes ($|U_{s2}/U_g|$) and MPRs of horizontal motions of identical superstructures (T_{fix1} = T_{fix2} = 1.0 sec, e_1 = 0, e_2 = 4 m, D = 3 m, H_{eff} = 20 m, V_s = 100 m/s, h_s = 3%)

(2) Effect of H_{eff} on anti-plane DCI

Analyses of doubling the height of the superstructures (H_{eff} = 20 m and 40 m, T_{fix1} = T_{fix2} = 1.0 sec) are performed to clarify the effect of superstructure height on the anti-plane DCI phenomenon. Transfer function amplitudes ($|U_{s2}/U_g|$) and MPRs of the horizontal motions of identical superstructures (T_{fix1} = T_{fix2} = 1.0 sec, H_{eff} = 20 m and 40 m) are given in Figure 5-76. The other analysis parameters are the same as those given in Section 5-2.

If Figures 5-76(a) and 5-76(b) are compared, it can be claimed that the effect of superstructure height is clearly higher than that of superstructure mass on anti-plane DCI, as similar to the in-plane DCI, for this limited case.

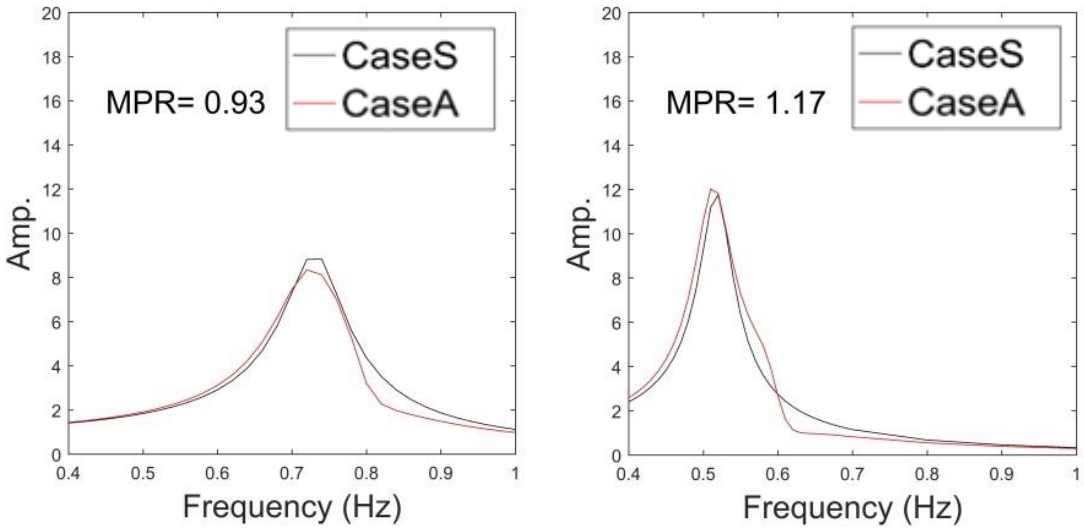

(a) H_{eff} = 20 m **(b) H_{eff} = 40 m**

Figure 5-76: Case-A (Adjacent) and Case-S (Single) transfer function amplitudes ($|U_{s2}/U_g|$) and MPRs of horizontal motions of identical superstructures (T_{fix1} = T_{fix2} = 1.0 sec, e_1 = 0, e_2 = 4 m, D = 3 m, m_s = 5x10^6 kg, V_s = 100 m/s, h_s = 3%)

(3) Effect of h_s on anti-plane DCI

Analysis results of different h_s of the soil (h_s = 0 and 6%) for $T_{fix1} = T_{fix2}$ = 2.0 sec are also shown to clarify the effect of soil material damping on the anti-plane DCI. Transfer function amplitudes ($|U_{s1}/U_g|$) and MPRs are given in Figure 5-77. The other analysis parameters are the same as those given in Section 5.2.

If Figures 5-77(a), 5-77(b), and 5-77(c) are compared, it can be asserted that the differences in the transfer function amplitude peaks are slightly less affected by soil material damping compared to the case of in-plane DCI. The reason of this difference between in-plane and anti-plane DCI is considered to be that there is lower rocking restriction in anti-plane DCI compared to in-plane DCI. Therefore, the effect of soil material damping becomes less for anti-plane DCI than in-plane DCI.

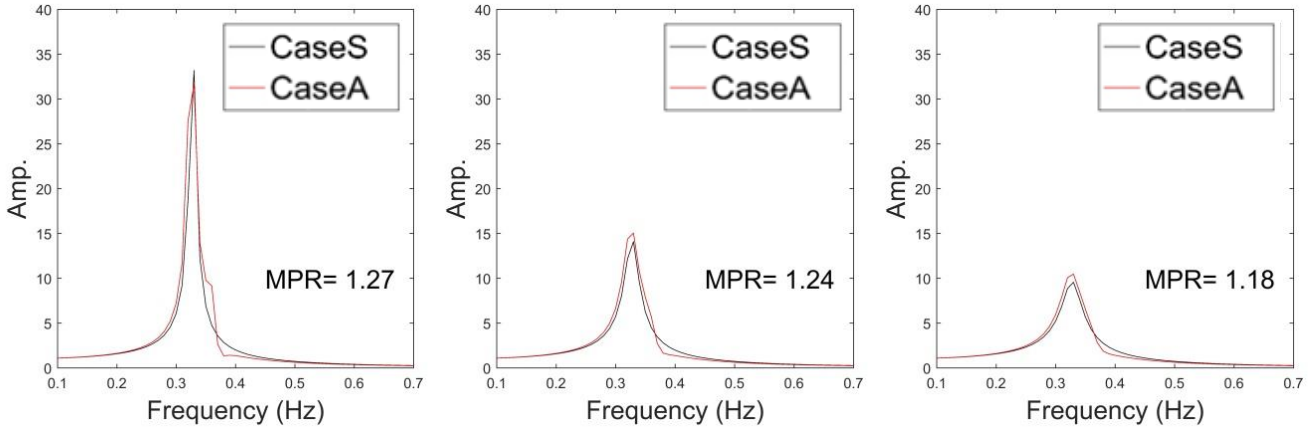

(a) h_s = 0% **(b) h_s = 3%** **(c) h_s = 6%**

Figure 5-77: Case-A (Adjacent) and Case-S (Single) transfer function amplitudes ($|U_{s2}/U_g|$) and MPR of identical superstructures ($T_{fix1} = T_{fix2}$ = 2.0 sec, e_1 = 0, e_2 = 4 m, D = 3 m, V_s = 100 m/s)

5.5 Analysis results for layered soil

5.5.1 Analysis results for *X* direction (in-plane DCI)

(a) Analysis results for identical embedment depths

(1) Analysis results for mat foundation, 1 adjacent building

The MPRs of superstructures (T_{fix1} = 0.5, 1.0 and 2.0 sec, mat foundations, layered soil, D = 3 m) for identical embedment depths ($e_1 = e_2$) on the X direction are given in Figure 5-78.

If Figures 5-78 and 5-8 are compared, to determine the effect of layered soil on the in-plane DCI phenomenon for mat foundations, it can be said that the MPRs between the two soil conditions do not change appreciably. Only a small lowering of the MPRs compared to the half-space is observed for $T_{fix1} = T_{fix2}$ = 0.5 sec due to the diminished wave-based DCI effect for layered soil and a small increment of MPRs comparing the half-space is observed for $T_{fix1} = T_{fix2}$ = 2.0 sec due to the diminished rocking restriction effect for layered soil as can be seen inside the solid line in Figures 5-8(a and c) and 5-78(a and c). Moreover, no special effect of the predominant frequency of the soil on the in-plane DCI can be seen in the present study.

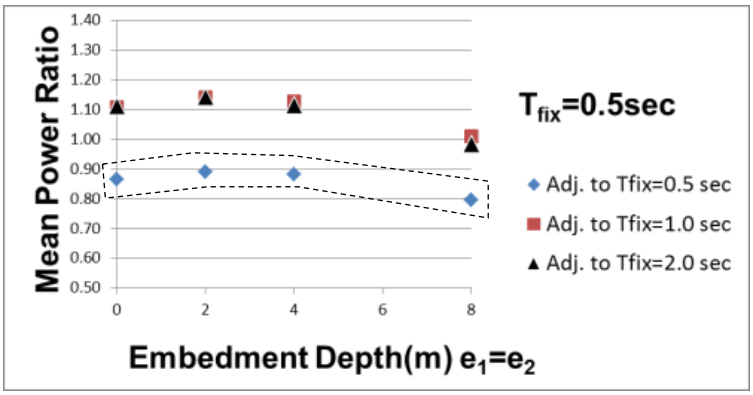

(a) For T_{fix1} = 0.5 sec

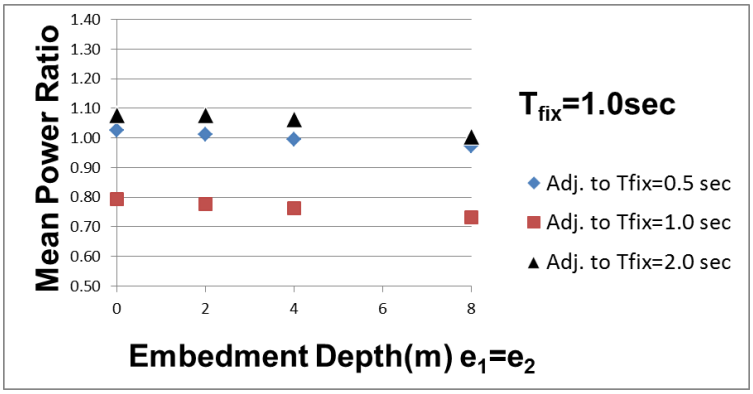

(b) For T_{fix1} = 1.0 sec

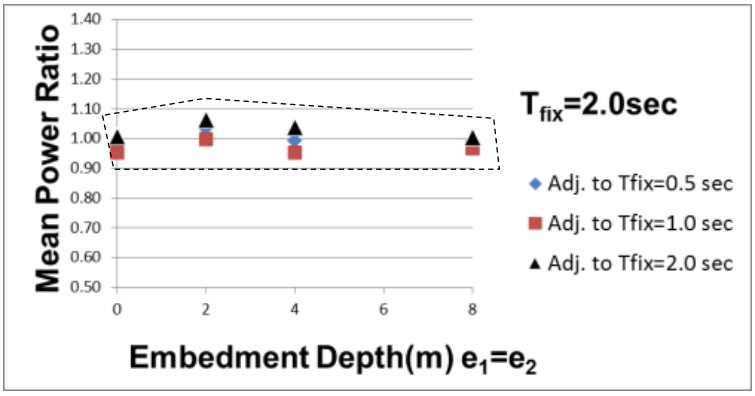

(c) For T_{fix1} = 2.0 sec

Figure 5-78: MPRs of horizontal superstructure motions for in-plane DCI ($e_1 = e_2$, D = 3 m, 1 adj. building, U_{s1}, mat foundation, layered soil)

To show the effect of DCI on rocking foundation input motions for a mat foundation placed on layered soil, a massless mat foundation model is created for T_{fix2} = 0.5, 1.0 and 2.0 sec as can be seen in Figure 5-79. In Figure 5-80, the transfer function amplitudes of U_{s1} according to ground motion at the free surface (U_g) ($|U_{s1}/U_g|$) of Case-S for an embedment depth of 4 m are given. The predominant period of the soil layer (T_s) is also depicted in this figure. The amplitudes and phases of the rocking foundation input motion of these models (U_{f5}/U_g) and the real part of the rocking impedances are given in Figure 5-81.

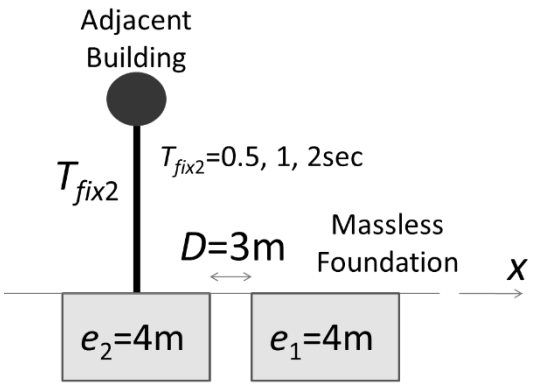

Figure 5-79 Analysis model for calculating impedances and input motions of massless foundation

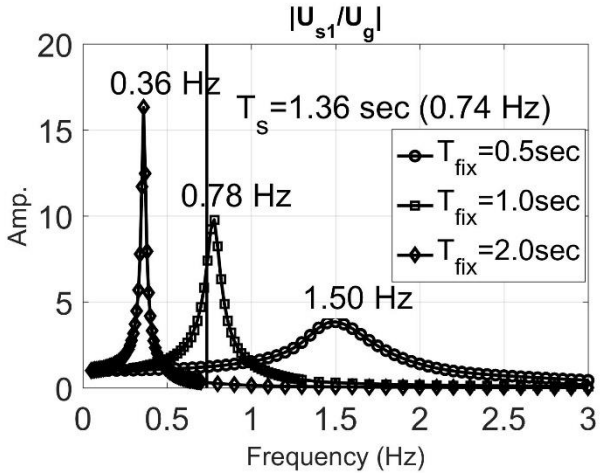

Figure 5-80 Transfer function amplitudes ($|U_{s1}/U_g|$) of Case-S (mat foundation, e_1 = 4 m, layered soil)

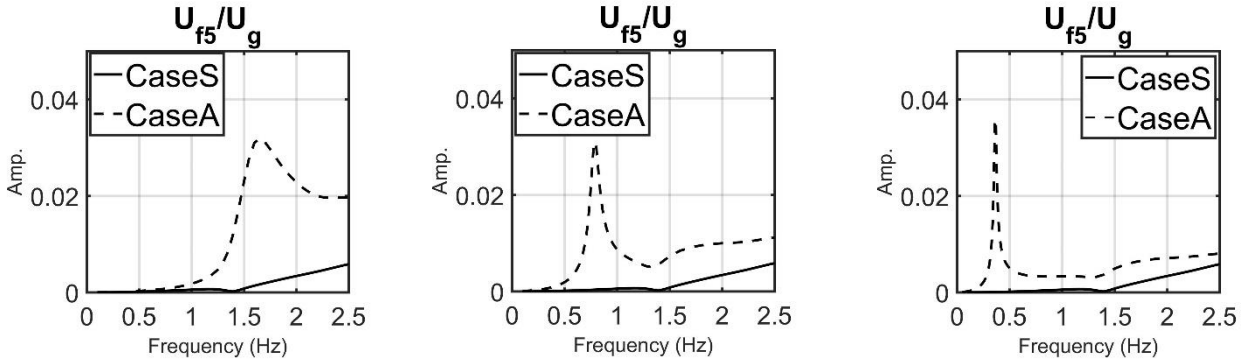

(1) T_{fix2} = 0.5 sec **(2) T_{fix2} = 1.0 sec** **(3) T_{fix2} = 2.0 sec**

(a) Amplitudes of rocking foundation input motion

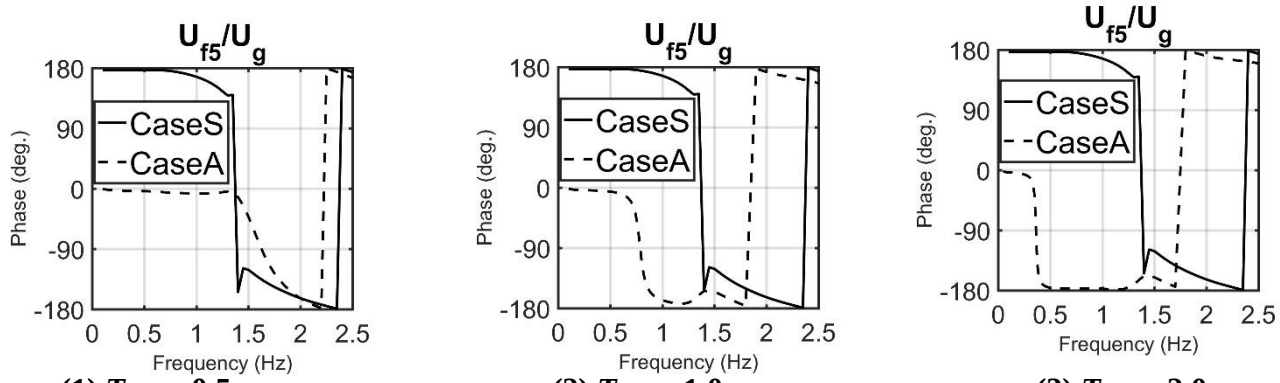

(1) T_{fix2} = 0.5 sec **(2) T_{fix2} = 1.0 sec** **(3) T_{fix2} = 2.0 sec**

(b) Phases of rocking foundation input motion

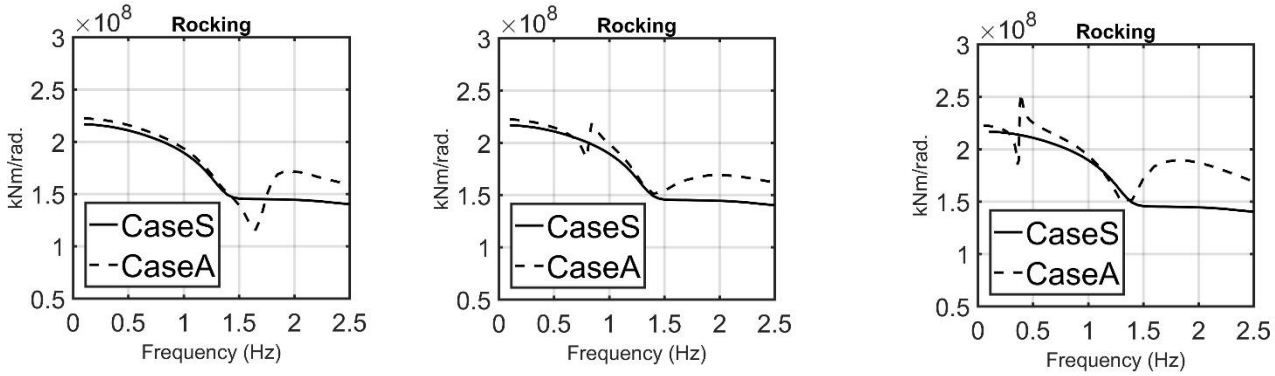

(1) T_{fix2} = 0.5 sec **(2) T_{fix2} = 1.0 sec** **(3) T_{fix2} = 2.0 sec**

(c) Real part of rocking impedances

Fig. 81 Amplitudes and phases of rocking foundation input motion (U_{f5}/U_g), as well as real part of rocking impedances of massless foundation for Case-S and Case-A

When Figures 5-81(b) and (c) are examined, it can be said that the relationships of the phases and rocking impedances between Case-A and Case-S show differences with the vicinity of the predominant frequency of each adjacent soil-structure system as a boundary. It is found that the massless foundation rocks in the opposite direction to the adjacent foundation before this frequency as shown in Figure 5-82(a), where T_{input} represents the period of the peak input motion ($T_{input} \geq T_{fix2}$). However, when a main building is also represented in the model, both foundations vibrate with the same phase. Therefore, the effect of this reverse phase rocking input motion contributes to the rocking restriction effect between adjacent buildings. This rocking restriction effect is defined as input rocking restriction in the present study. In contrast, for frequencies that are higher than the vicinity of the predominant frequency of each of the adjacent soil-structure systems ($T_{input} < T_{fix2}$), the same phase rocking motion of foundation of the adjacent building is observed as shown in Figure 5-82(b). However, as can be seen at the Figure 5-81(c), the real parts of the impedances for Case-A are higher than those for Case-S. This rocking restriction effect is defined as an impedance rocking restriction in the present study.

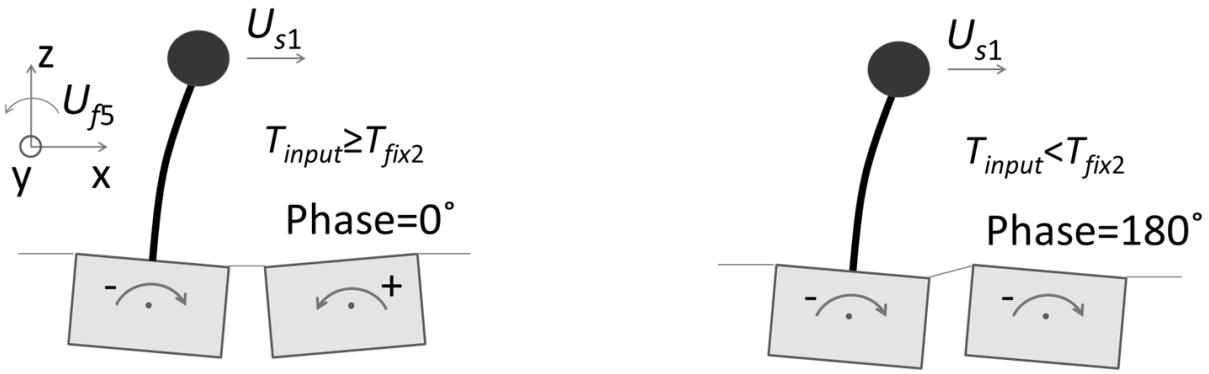

(a) Reverse phase rocking (input rocking restriction)

(b) Same phase rocking (impedance rocking restriction)

Figure 5.82 Rocking modes of massless foundation and adjacent soil-structure system

(2) Analysis results for pile foundation, 1 adjacent building

Next, results for pile foundations are given. The MPRs of superstructures (T_{fix1} = 0.5, 1.0 and 2.0 sec, pile foundations, layered soil, D = 3 m) for identical embedment depths ($e_1 = e_2$) on the X direction are shown in Figure 5-83.

If Figures 5-83 and 5-78 are compared to determine the pile foundation effects on the DCI, it can be said that almost all MPRs are smaller than those of mat foundations. However, for some cases (T_{fix1} = 0.5 sec – T_{fix2} = 1.0 and 2.0 sec) as shown in the solid line in Figure 5-83(a), the MPRs are higher than those of mat foundations; the MPRs can increase by as much as 30% compared to Case-S. To understand this phenomenon, transfer function amplitudes of the foundation rocking motion ($|U_{f5}/U_g|$) of Case-S and Case-A (T_{fix1} = 0.5 sec – T_{fix2} = 1.0 sec pile and mat foundations) are shown in Figure 5-84.

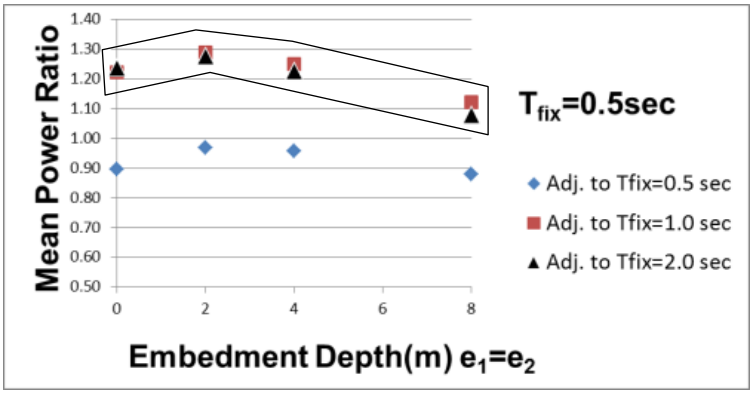

(a) For T_{fix1} = 0.5 sec

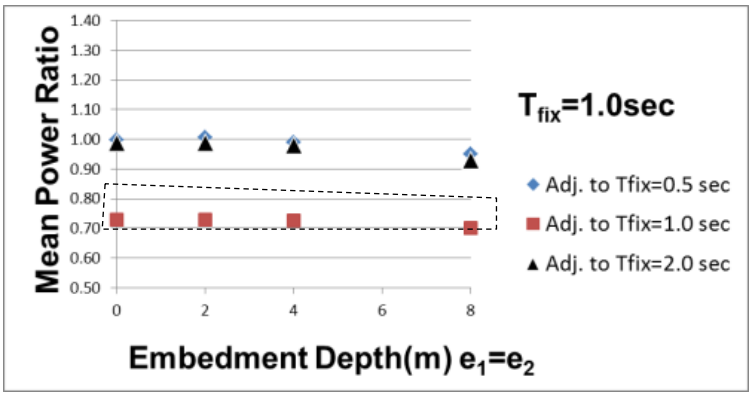

(b) For T_{fix1} = 1.0 sec

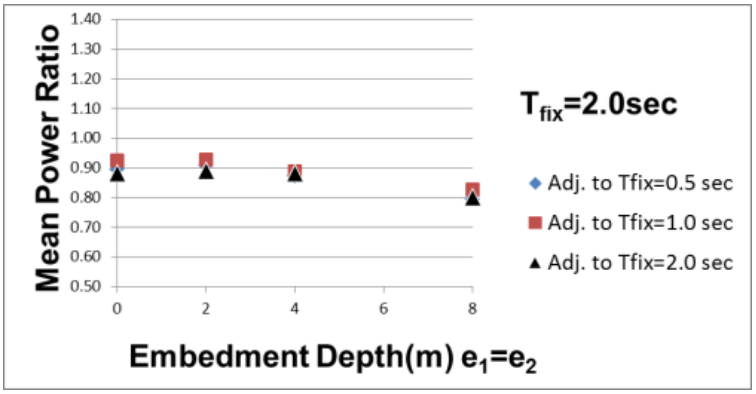

(c) For T_{fix1} = 2.0 sec

Figure 5-83: MPRs of horizontal superstructure motions for in-plane DCI ($e_1 = e_2$, D = 3 m, 1 adj. building, U_{s1}, pile foundation, layered soil)

As can be seen in Figure 5-84(a), the rocking motion amplitude of the foundation for Case-A is lower than for Case-S because of the aforementioned rocking restriction phenomenon. However, if Figure 5-84(b) is examined, it is found that that the rocking motion amplitude of the foundation for Case-A is higher than that for Case-S. It can be said that, because of the lack of a rocking restriction effect on the building (T_{fix1} = 0.5 sec and pile foundation), the MPR of the main building on the pile foundation becomes higher than that on the mat foundation.

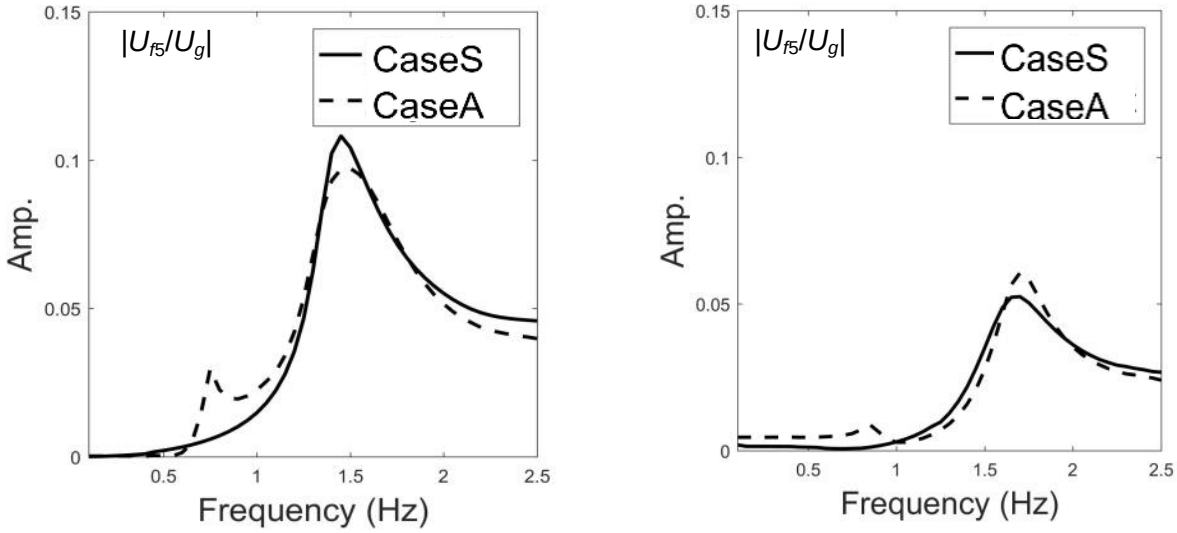

(a) Mat foundations **(b) Pile foundations**

Figure 5-84: Case-A (Adjacent) and Case-S (Single) transfer function amplitudes of foundation rocking motion ($|U_{f5}/U_g|$) for *X* direction (T_{fix1} = 0.5 sec – T_{fix2} = 1.0sec, $e_1 = e_2 = 0$, layered soil)

Another important point about the effect of pile foundation on the DCI, for identical adjacent buildings $T_{fix1} = T_{fix2}$ = 1.0 sec, is that the beneficial effect of DCI is observed as shown at the dashed line in Figure 5-83(b) compared to Figure 5-78(b). Transfer function amplitudes of foundation rocking motion ($|U_{f5}/U_g|$) for Case-S and Case-A are shown in Figure 5-85. In this figure, the rocking motion diminishes nearly 70% comparing with that of the main building on

the mat foundation, but the ratio of Case-A to Case-S does not change so much. It can be considered that the rocking restriction is also effective for the pile foundation like the mat foundation for building with T_{fix} = 1.0 sec and that phenomenon infuses the beneficial DCI effect on the structures with pile foundations.

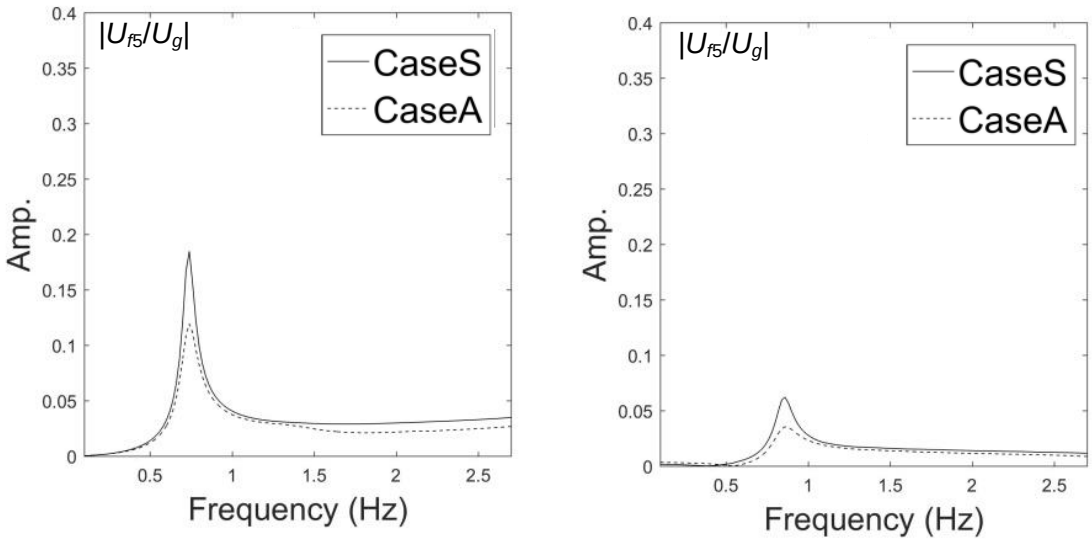

(a) Mat foundations **(b) Pile foundations**

Figure 5-85: Transfer function amplitudes of foundation rocking motion ($|U_{f5}/U_g|$) of the main superstructures both Case-A (Adjacent) and Case-S (Single) for *x* direction (T_{fix1} = T_{fix2} = 1.0 sec, e_1 = e_2 = 0, layered soil)

(b) Analysis results for shallower embedment depth of the main building

(1) Analysis results for mat foundation, 1 adjacent building

The MPRs of superstructures (T_{fix1} = 0.5, 1.0 and 2.0 sec, mat foundations, layered soil, D = 3 m) for different embedment depths of main building (e_1) on the X direction are given in Figure 5-86 where horizontal axis represents the foundation depth of the main building and the foundation depth of the adjacent building (e_2) is selected as 8 m.

If Figure 5-86 is examined, it can be asserted that the beneficial effect of the in-plane DCI is more pronounced for a main building with a shallower foundation embedment depth, as can be seen inside the solid line in Figure 5-86. This is especially so for identical adjacent buildings with a natural period of 2.0 sec, as can be seen inside the solid line in Figure 5-86(c), because power is transferred from the shallower foundation to the deeper foundation in the same way as for half-space soil. If Figures 5-86 and 5-14 are compared to determine the horizontal vibration power transfer difference between the two types of soils, it can be said that there is a slightly more beneficial effect on layered soil compared to half-space soil.

On the other hand, the in-plane DCI effect between tall and heavy buildings and short and light structures is negligible, as can be seen inside the dashed line in Figure 5-86. This is similar to the identical embedment case.

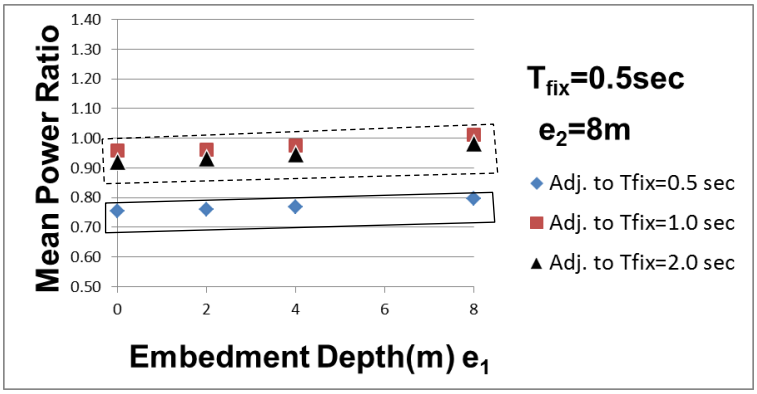

(a) For T_{fix1} = 0.5 sec

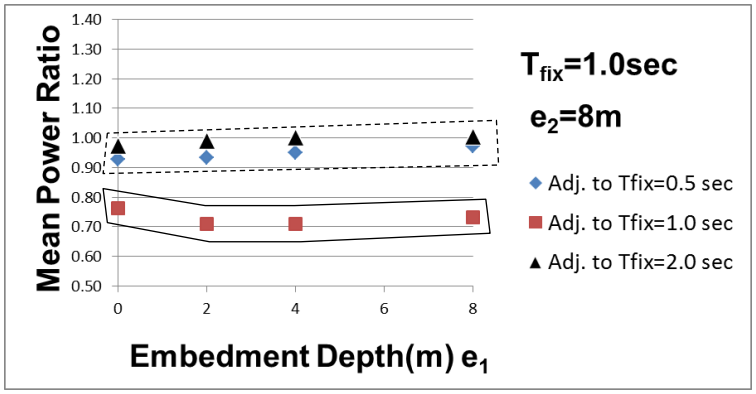

(b) For T_{fix1} = 1.0 sec

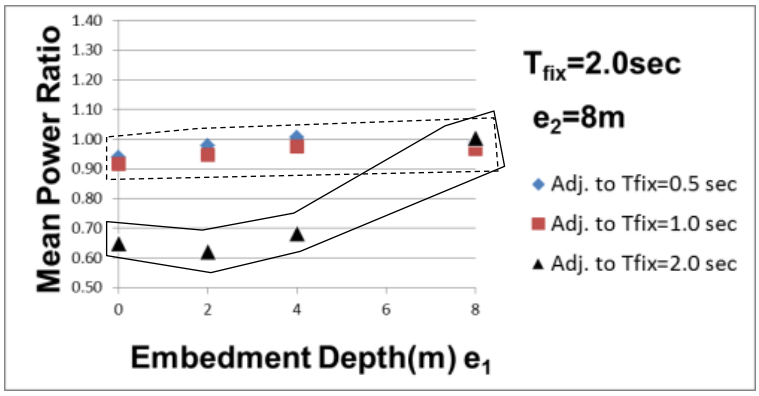

(c) For T_{fix1} = 2.0 sec

Figure 5-86: MPRs of horizontal superstructure motions for in-plane DCI (e_2 = 8 m, D = 3 m, 1 adj. building, U_{s1}, mat foundation, layered soil)

(2) Analysis results for pile foundation, 1 adjacent building

The MPRs of superstructures (T_{fix1} = 0.5, 1.0 and 2.0 sec, pile foundations, layered soil, D = 3 m) for different embedment depths of main building (e_1) on the X direction are given in Figure 5-87 where horizontal axis represents the foundation depth of the main building and the foundation depth of the adjacent building (e_2) is selected as 8 m.

If Figure 5-87(c) is examined, a horizontal power transfer similar to that in Figure 5-86(c) cannot be determined. To explain this issue, in Figure 5-88, Case-S transfer function amplitudes of horizontal foundation motions ($|U_{f1}/U_g|$) for different embedment depths and superstructures are given. As can be seen from this figure, low and high peak transfer function amplitudes of the horizontal foundation motion do not coincide as they do in Figure 5-16, because effect of embedment on transfer function amplitudes diminishes for pile foundations. Therefore, power transfer could not be seen for pile foundations.

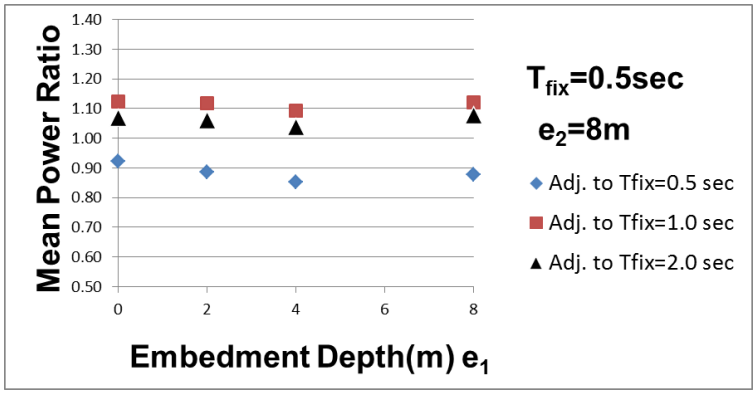

(a) For T_{fix1} = 0.5 sec

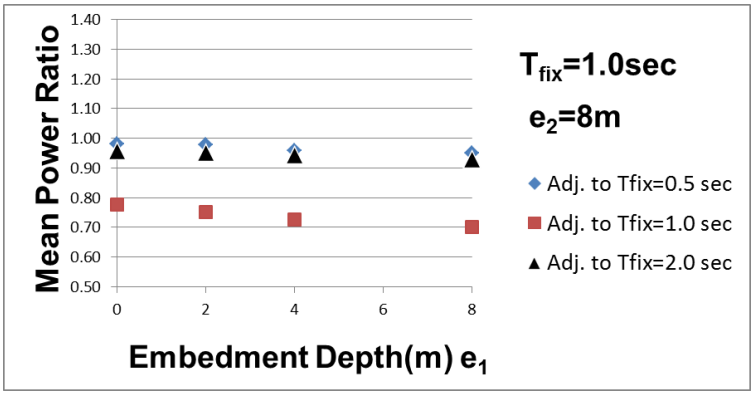

(b) For T_{fix1} = 1.0 sec

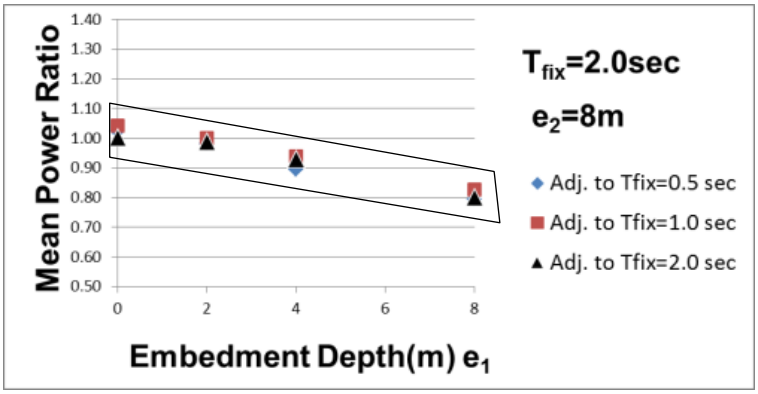

(c) For T_{fix1} = 2.0 sec

Figure 5-87: MPRs of horizontal superstructure motions for in-plane DCI (e_2 = 8 m, D = 3 m, 1 adj. building, U_{s1}, pile foundation, layered soil)

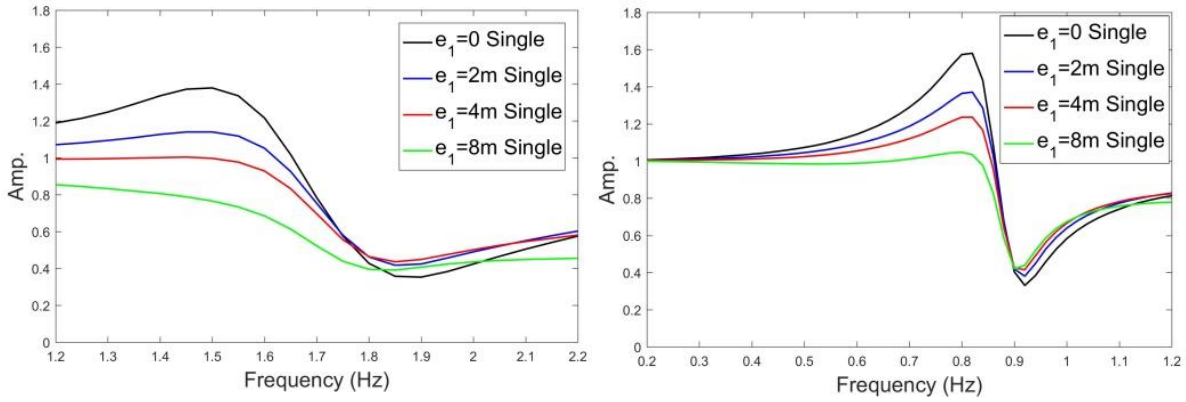

(a) For T_{fix} = 0.5 sec **(b) For T_{fix} = 1.0 sec**

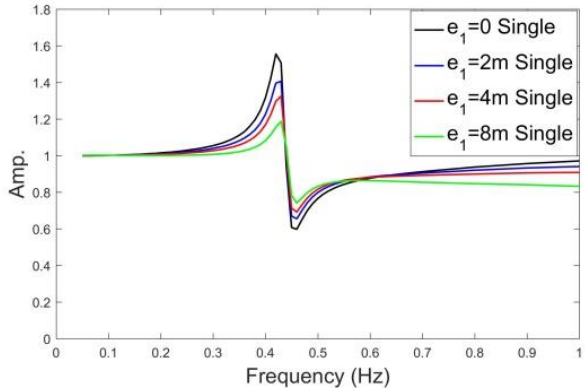

(c) For T_{fix} = 2.0 sec

Figure 5-88: Case-S transfer function amplitudes ($|U_{f1}/U_g|$) of horizontal foundation motion for (h_s = 3%, layered soil, pile foundation)

(c) Analysis results for deeper embedment depth of the main building

(1) Analysis results for mat foundation, 1 adjacent building

The MPRs of superstructures (T_{fix1} = 0.5, 1.0 and 2.0 sec, mat foundations, layered soil, D = 3 m) for different embedment depths of the main building (e_1) on the X direction are given in Figure 5-89 where horizontal axis represents the foundation depth of the main building and the foundation depth of the adjacent building (e_2) is selected as 0.

If Figure 5-89 is examined, it can be said that the detrimental effect of in-plane DCI is more pronounced for a main building with deeper foundation, especially for identical adjacent

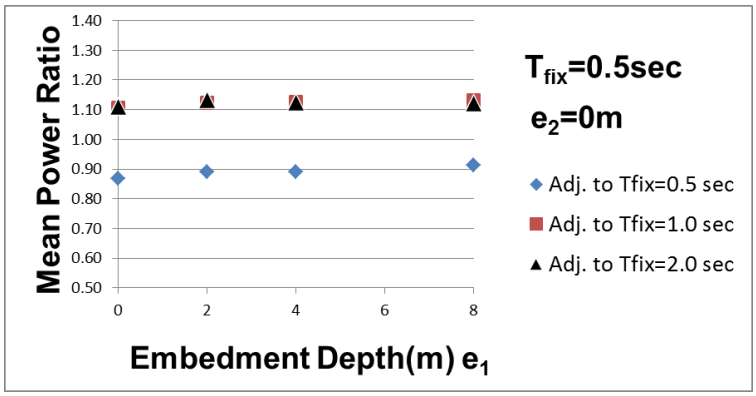

(a) For T_{fix1} = 0.5 sec

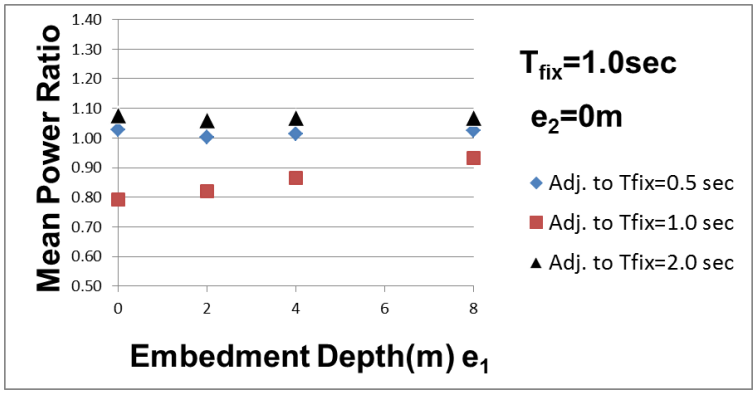

(b) For T_{fix1} = 1.0 sec

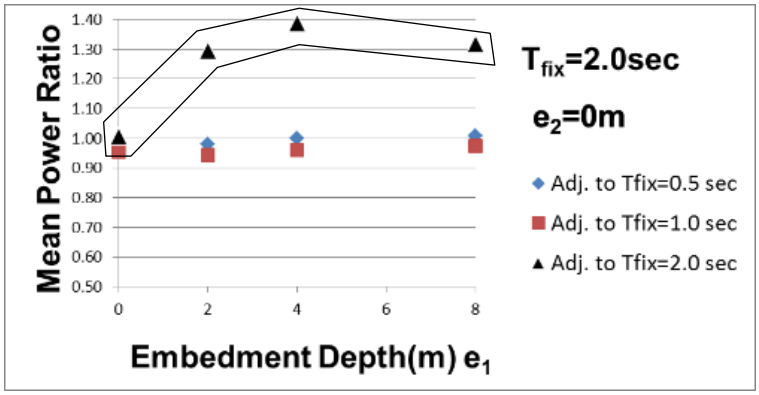

(c) For T_{fix1} = 2.0 sec

Figure 5-89: MPRs of horizontal superstructure motions for in-plane DCI (e_2 = 8 m, D = 3 m, 1 adj. building, U_{s1}, mat foundation, layered soil)

buildings with natural period of 2.0 sec, as can be seen inside the solid line in Figure 5-89(c). This is because power is transferred from shallower foundation to deeper foundation, similar to half-space soil. However, it should be noted that the detrimental effect of in-plane DCI for tall adjacent buildings with deeper embedment is higher for layered soil than for half-space soil. The reason of this phenomenon is considered to be that amount of horizontal vibration power transfer increases for tall buildings on layered soil because of the lowered radiation damping compared to half-space soil.

(2) Analysis results for pile foundation, 1 adjacent building

The MPRs of superstructures (T_{fix1} = 0.5, 1.0 and 2.0 sec, pile foundations, layered soil, D = 3 m) for different embedment depths of the main building (e_1) on the X direction are given in Figure 5-90 where horizontal axis represents the foundation depth of the main building and the foundation depth of the adjacent building (e_2) is selected as 0.

As can be seen at Figure 5-90, a similar tendency on the MPRs is seen because of the lacking of horizontal vibration power transfer.

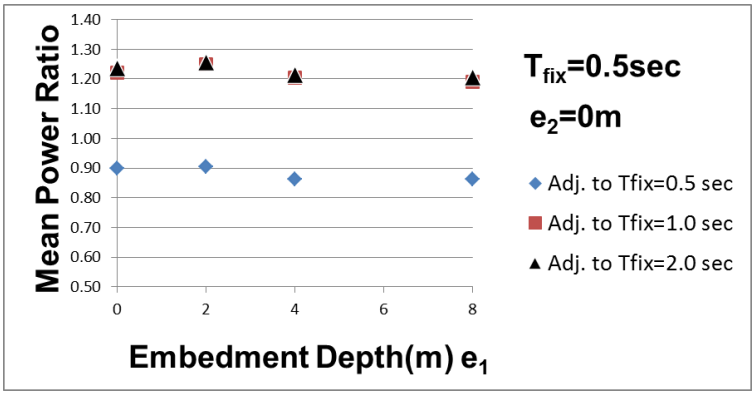

(a) For T_{fix1} = 0.5 sec

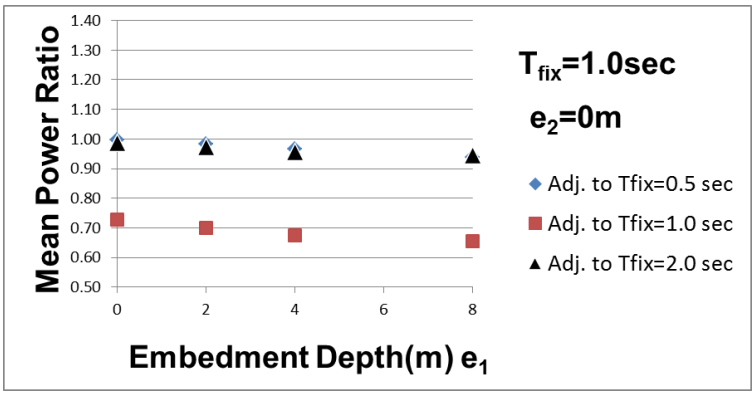

(b) For T_{fix1} = 1.0 sec

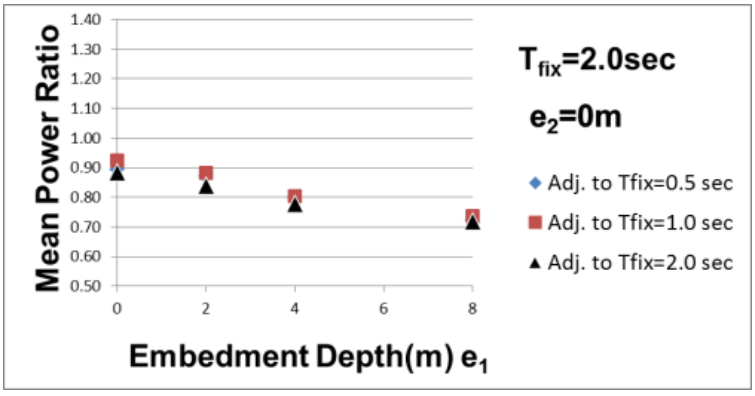

(c) For T_{fix1} = 2.0 sec

Figure 5-90: MPRs of horizontal superstructure motions for in-plane DCI (e_2 = 8 m, D = 3 m, 1 adj. building, U_{s1}, pile foundation, layered soil)

5.5.2 Analysis results for *Y* direction (anti-plane DCI)

(a) Analysis results for identical embedment depths

(1) Analysis results for mat foundation, 1 adjacent building

The MPRs of superstructures (T_{fix1} = 0.5, 1.0 and 2.0 sec, mat foundations, layered soil, D = 3 m) for identical embedment depths ($e_1 = e_2$) on the *Y* direction are given in Figure 5-91.

If Figures 5-91 and 5-44 are compared to determine the effect of layered soil on the anti-plane DCI phenomenon for mat foundations, it can be said that the MPRs do not change appreciably between the two soil conditions. Moreover, no special effect of the predominant frequency of the soil on the anti-plane DCI can be seen in the present study.

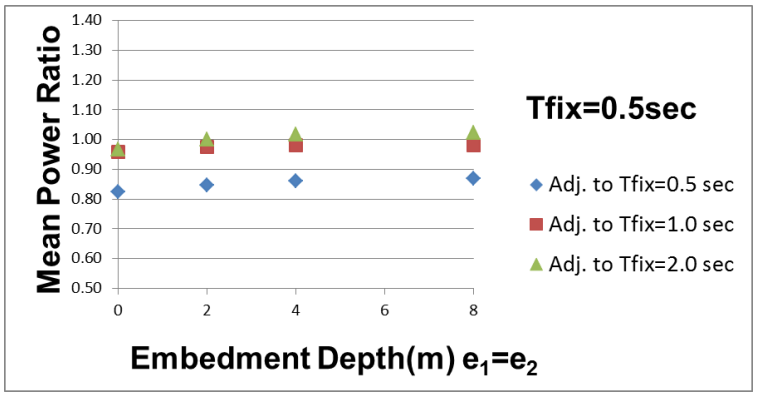

(a) For T_{fix1} = 0.5 sec

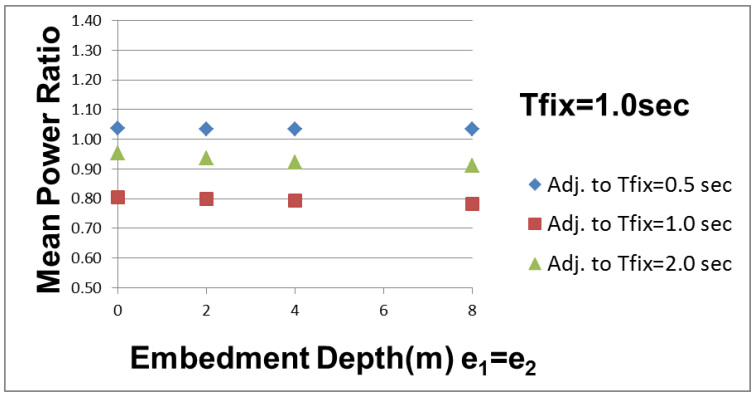

(b) For T_{fix1} = 1.0 sec

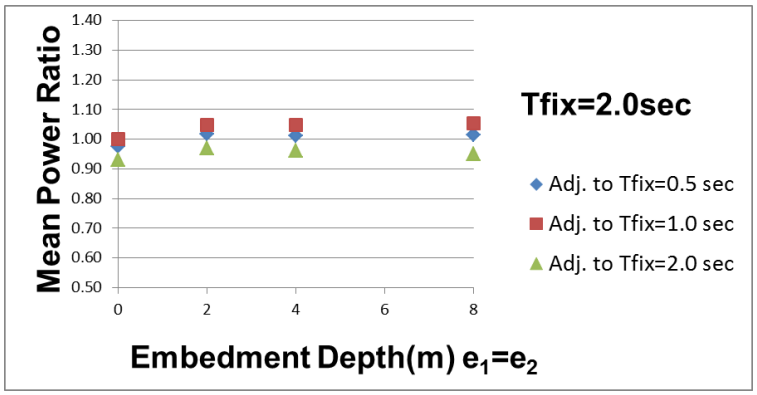

(c) For T_{fix1} = 2.0 sec

Figure 5-91: MPRs of horizontal superstructure motions for anti-plane DCI ($e_1 = e_2$, D = 3 m, 1 adj. building, U_{s2}, mat foundation, layered soil)

(2) Analysis results for pile foundation, 1 adjacent building

Next, results for pile foundations are given. The MPRs of superstructures (T_{fix1} = 0.5, 1.0 and 2.0 sec, pile foundations, layered soil, D = 3 m) for identical embedment depths ($e_1 = e_2$) on the Y direction are shown in Figure 5-92. The effect of the anti-plane DCI is not so different for pile and mat foundation, as can be seen at Figures 5-91 and 5-92.

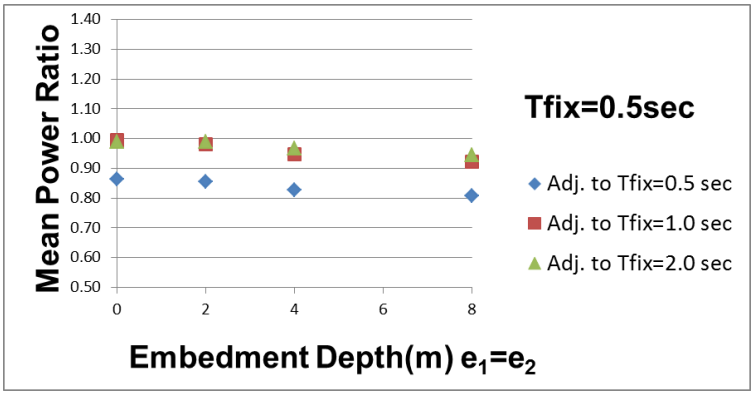

(a) For T_{fix1} = 0.5 sec

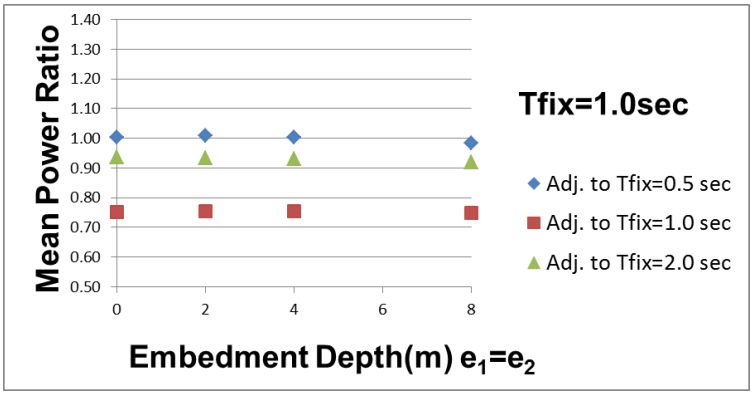

(b) For T_{fix1} = 1.0 sec

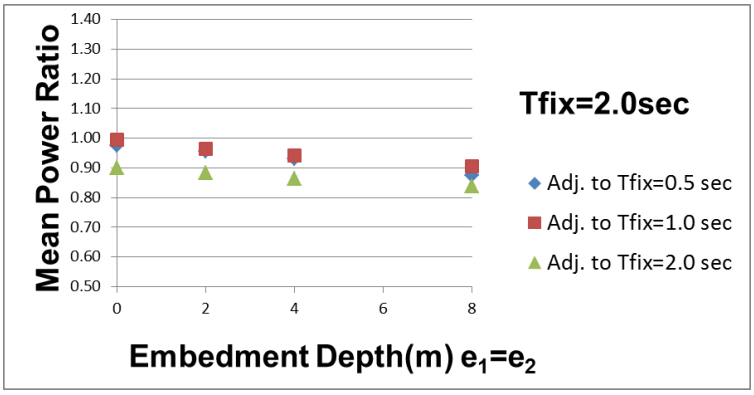

(c) For T_{fix1} = 2.0 sec

Figure 5-92: MPRs of horizontal superstructure motions for anti-plane DCI ($e_1 = e_2$, D = 3 m, 1 adj. building, U_{s2}, pile foundation, layered soil)

(b) Analysis results for shallower embedment depth of the main building

(1) Analysis results for mat foundation, 1 adjacent building

The MPRs of superstructures (T_{fix1} = 0.5, 1.0 and 2.0 sec, mat foundations, layered soil, D = 3 m) for different embedment depths of main building (e_1) on the Y direction are given in Figure 5-93 where horizontal axis represents the foundation depth of the main building and the foundation depth of the adjacent building (e_2) is selected as 8 m.

If Figures 5-93 and 5-50 are compared to determine the effect of layered soil on the horizontal vibrational wave transfer on the Y direction for mat foundations, it can be said that the detrimental effect of anti-plane DCI is higher for tall adjacent buildings with shallower embedment for layered soil than for half-space soil, as shown inside the solid line in Figure 5-93(c). The reason of this phenomenon is considered to be that amount of horizontal vibration power transfer increases for tall buildings on layered soil because of the lowered radiation damping compared to half-space soil, similar to in-plane DCI.

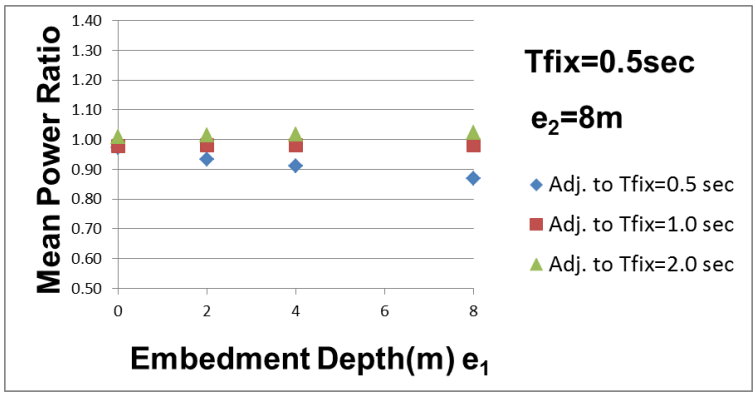

(a) For T_{fix1} = 0.5 sec

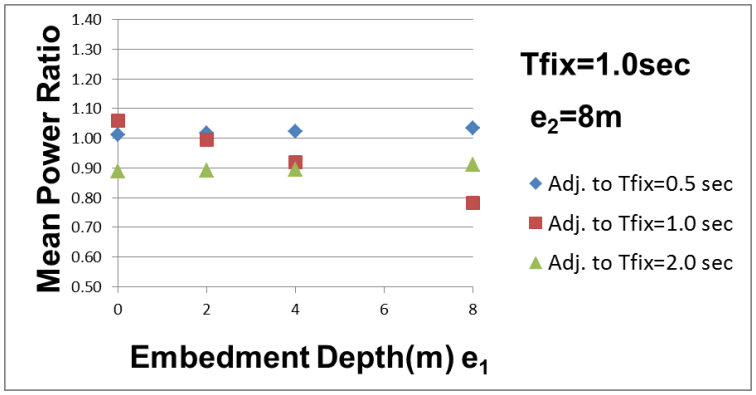

(b) For T_{fix1} = 1.0 sec

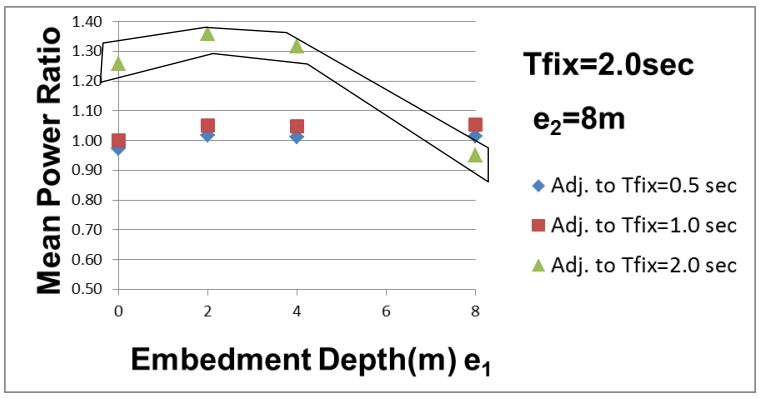

(c) For T_{fix1} = 2.0 sec

Figure 5-93: MPRs of horizontal superstructure motions for anti-plane DCI (e_2 = 8 m, D = 3 m, 1 adj. building, U_{s2}, mat foundation, layered soil)

(2) Analysis results for pile foundation, 1 adjacent building

The MPRs of superstructures (T_{fix1} = 0.5, 1.0 and 2.0 sec, pile foundations, layered soil, D = 3 m) for different embedment depths of main building (e_1) on the Y direction are given in Figure 5-94 where horizontal axis represents the foundation depth of the main building and the foundation depth of the adjacent building (e_2) is selected as 8 m.

Horizontal vibration power transfer cannot be observed for pile foundation even on the Y direction, as can be seen inside the solid line in Figure 5-94(c) for the reason given in Section 5.5.1.

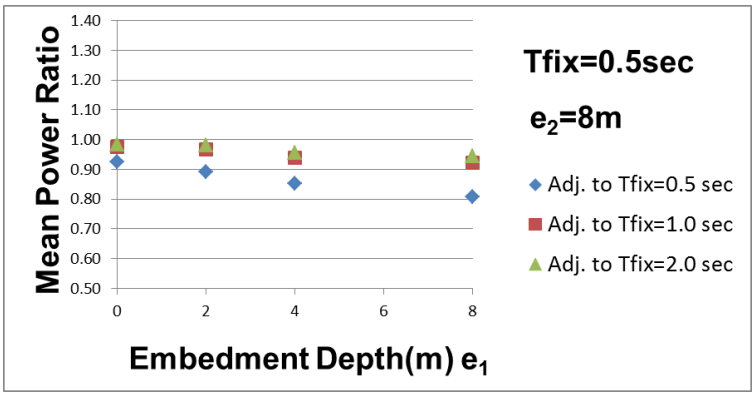

(a) For T_{fix1} = 0.5 sec

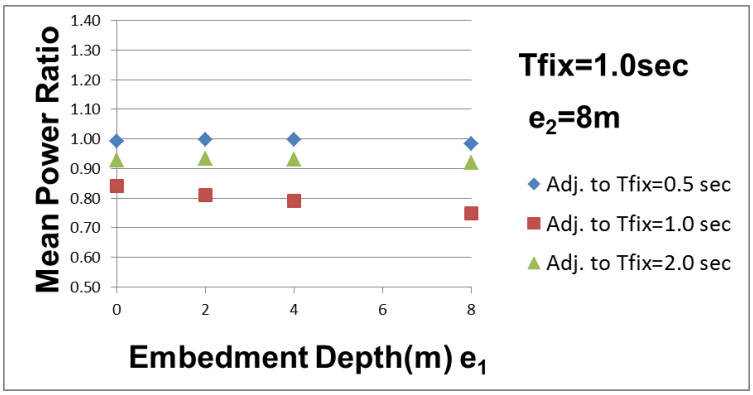

(b) For T_{fix1} = 1.0 sec

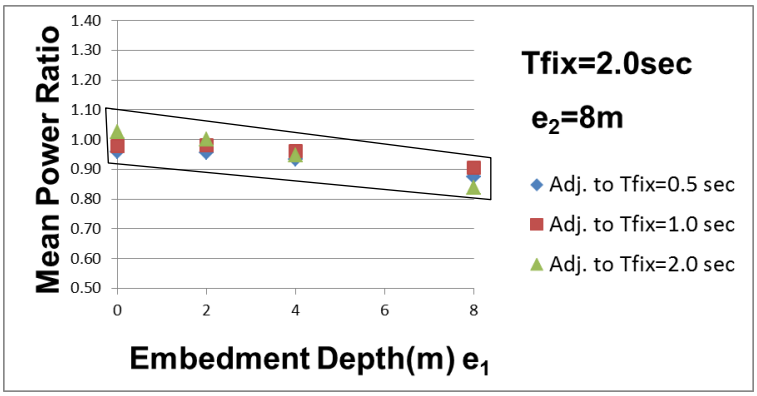

(c) For T_{fix1} = 2.0 sec

Figure 5-94: MPRs of horizontal superstructure motions for anti-plane DCI (e_2 = 8 m, D = 3 m, 1 adj. building, U_{s2}, pile foundation, layered soil)

(c) Analysis results for deeper embedment depth of the main building

(1) Analysis results for mat foundation, 1 adjacent building

The MPRs of superstructures (T_{fix1} = 0.5, 1.0 and 2.0 sec, mat foundations, layered soil, D = 3 m) for different embedment depths of the main building (e_1) on the Y direction are given in Figure 5-95 where horizontal axis represents the foundation depth of the main building and the foundation depth of the adjacent building (e_2) is selected as 0.

If Figures 5-95 and 5-14 are compared to determine the difference in horizontal vibration power transfer between the two soil types, it can be said that there is a slightly more beneficial effect on layered soil compared to half-space soil on the Y direction.

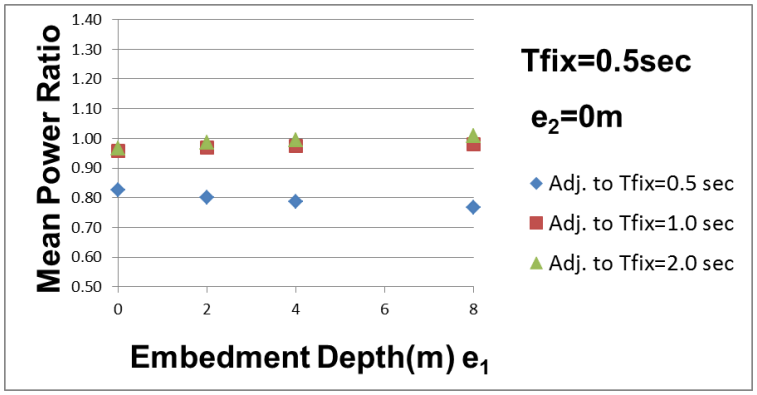

(a) For T_{fix1} = 0.5 sec

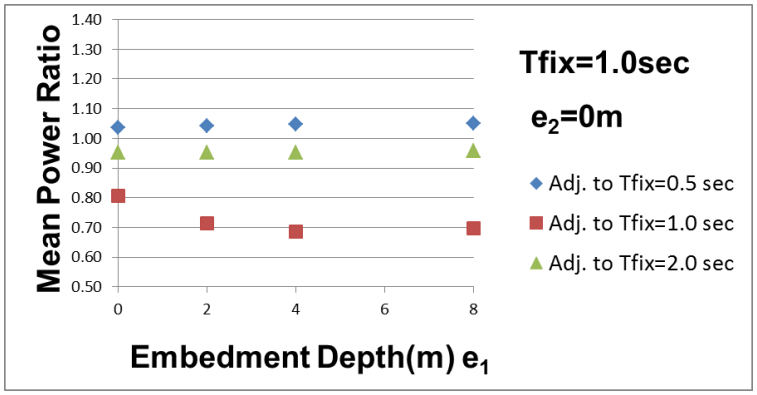

(b) For T_{fix1} = 1.0 sec

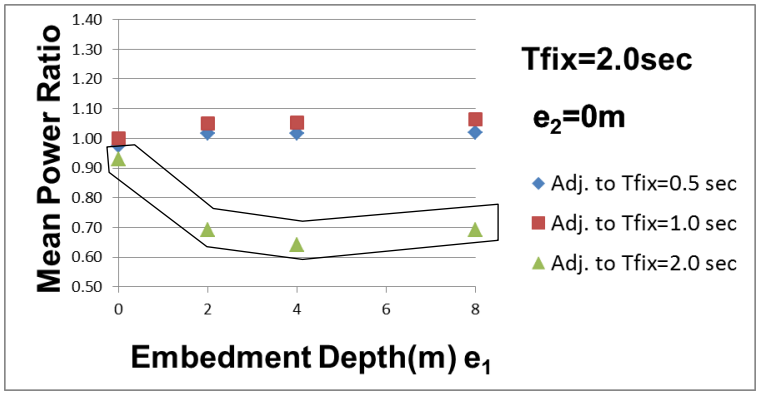

(c) For T_{fix1} = 2.0 sec

Figure 5-95: MPRs of horizontal superstructure motions for anti-plane DCI (e_2 = 0, D = 3 m, 1 adj. building, U_{s2}, mat foundation, layered soil)

(2) Analysis results for pile foundation, 1 adjacent building

The MPRs of superstructures (T_{fix1} = 0.5, 1.0 and 2.0 sec, pile foundations, layered soil, D = 3 m) for different embedment depths of the main building (e_1) on the Y direction are given in Figure 5-96 where horizontal axis represents the foundation depth of the main building and the foundation depth of the adjacent building (e_2) is selected as 0.

Horizontal vibration power transfer cannot be observed for pile foundation even on the Y direction, as can be seen inside the solid line in Figure 5-96(c) for the reason given in Section 5.5.1.

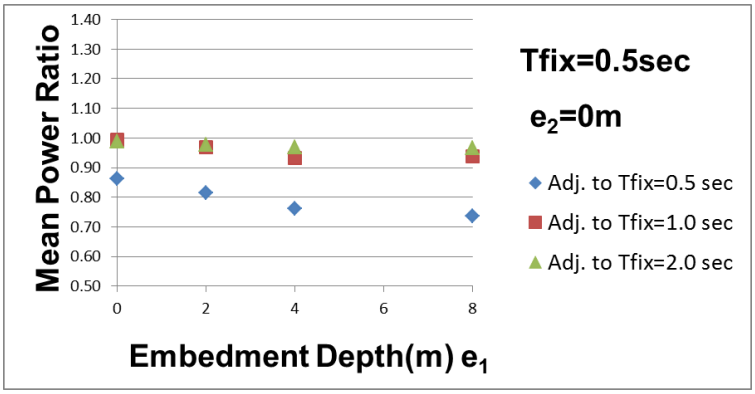

(a) For T_{fix1} = 0.5 sec

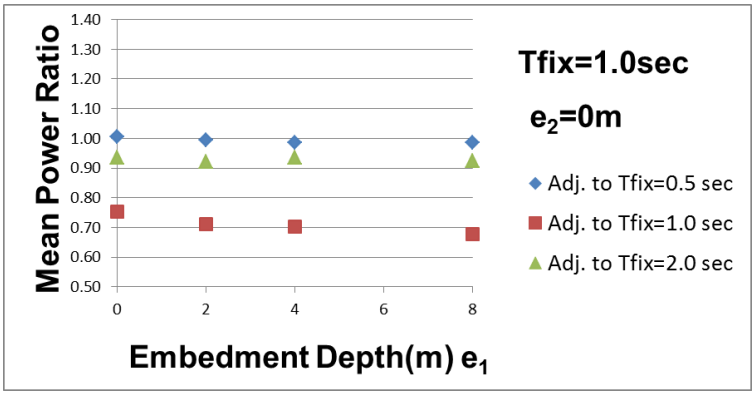

(b) For T_{fix1} = 1.0 sec

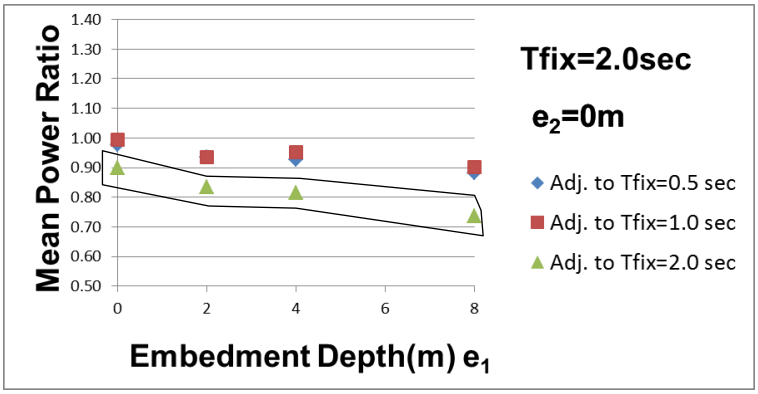

(c) For T_{fix1} = 2.0 sec

Figure 5-96: MPRs of horizontal superstructure motions for anti-plane DCI (e_2 = 0, D = 3 m, 1 adj. building, U_{s2}, pile foundation, layered soil)

References for Chapter5

Alexander, N. A., Ibraim, E., & Aldaikh, H. (2013). A simple discrete model for interaction of adjacent buildings during earthquakes. Computers & Structures, 124, pp.1-10.

Lou, M., Wang, H., Chen, X., & Zhai, Y. (2011). Structure–soil–structure interaction: literature review. Soil Dynamics and Earthquake Engineering, 31(12), pp.1724-1731.

Wen H. (2006) An Analytical Study on Effects of Foundation Type, Foundation Shape and Adjacent Building on Dynamic Soil Structure Interaction. Diss. Nagoya University. (In Japanese)

Chapter 6

Conclusions and Future Research

6.1 Conclusions

The present study aims at determining the effects of SSI and DCI on the responses of superstructures by conducting various parametric analyses. For the SSI branch of the study, a new lumped parameter model (LPM) that depends on the impedances of foundations with different embedment depths is constructed. Nonlinear earthquake response analyses using the proposed LPM are then carried out using active-fault and subduction-zone earthquake records. This is done both with and without RFIM to assess the effects of RFIM on the ductility demands of structures. For the DCI branch of the study, a wide analytical parametric study is conducted for different foundation types, embedment situations and fixed based natural frequencies of two or three closely spaced buildings. As soil model, elastic half-space and layered soil for different kinds of shear wave velocity and soil material damping are selected. The reasoning is that if the key parameters of the DCI phenomenon are understood, the importance of DCI effects on the design of structures can be determined more easily.

In Chapter 2, a wide literature review is given related to soil-structure interaction.

In Chapter 3, a wide literature review is given related to structure-soil-structure interaction.

In Chapter 4, a new LPM is constructed that depends on the impedances of embedded foundations with different embedment depths placed on an elastic half-space for the Poisson

ratio of 0.42 and shear wave velocity value of either 100 or 200 m/s to represent soft soil conditions. Verification is done by using the horizontal, rocking, and coupling impedances of the model and the response of the superstructure. According to the comparison, it can be said that the LPM approximation is almost adequate to represent the SSI effect.

Nonlinear response analyses are then carried out for an SDOF elasto-plastic structure with fixed ductility capacity values of 2, 4, or 6, and predominant periods of 0.2 to 3 seconds. Analyses are carried out for the proposed LPM model under active fault and subduction zone earthquake records both with and without RFIM to assess the effects of RFIM on the ductility demands of superstructures. Earthquake records from both the Takatori Station record of the 1995 Hyogoken-Nanbu Earthquake (Kobe Earthquake) and the 2011 off the Pacific Coast of Tohoku Earthquake (Tohoku Earthquake) EW component of MYG006 Station are used for these analyses. The results of the analyses are as follows:

a) By increasing the ductility factor value, the effect of RFIM becomes more important, especially for high-rise buildings with embedment ratios greater than 1. The reason of this phenomenon is considered to be that the equivalent elastic stiffness of the superstructure becomes softer for increasing values of ductility capacity. Hence, the inertial interaction becomes less important and the additional force coming from the rocking motion becomes more important in the superstructure response.
b) For V_s = 200 m/s, the effect of RFIM is more limited than for V_s = 100 m/s, because the RFIM amplitude decreases.
c) As a design suggestion, RFIM should be considered for collapse limiting designs, especially for high rise buildings with embedment ratios greater than 1 in this case. Even

those designs that neglect the kinematic interaction underestimate the effect of an earthquake in some critical situations.

However, it should be noted that these results are obtained for restricted parameters. For more reliable results, the range of parameters considered in the analyses should be increased.

In Chapter 5, a wide parametric study is conducted to determine the in-plane and anti-plane DCIs of closely spaced adjacent buildings (D = 3 m and 6 m) on the MPRs of superstructures from the adjacent building case to single building case. The soil and the superstructures are considered to be elastic. The soil is modeled as thin layers for different foundation embedment ratios taking place on a homogeneous elastic half-space and layered soil by also considering rocking and horizontal responses of foundations for fixed base natural periods and foundation embedment depth, material damping and shear wave velocity of soil. Moreover, the effects of superstructure mass and height on the DCI phenomenon are also investigated.

Consequently, for mat foundations, it is claimed that for 2 identical adjacent buildings with different foundation embedment depths, the in-plane DCI effect increases the mean power of more-deeply embedded superstructures and decreases the mean power of less-deeply embedded ones because of the power transfer between them. However, for anti-plane DCI, power is transferred in opposite direction compared to the in-plane DCI, and this horizontal vibration power transfer effect is slightly higher for anti-plane DCI than for in-plane DCI. Anti-plane DCI decreases the mean power of more-deeply embedded superstructures and increases the mean power of less-deeply embedded ones. The amount of transferred power depends strongly on the shear wave velocity of the soil but less so on the clearance between the foundations. For

the case of 3 identical adjacent buildings, the power transfer increases compared to the case of 2 identical adjacent buildings. This effect is found mainly in the case of tall adjacent buildings. However, for identical adjacent buildings with different embedment depths of pile foundations, the power cannot be transferred because the predominant frequencies of soil-structure systems change very slightly according to the embedment depth.

No power transfer is observed for 2 identical adjacent buildings with the same embedment depth. The mean power of both buildings diminishes because of the rocking restriction effect of the in-plane DCI and the increased damping effect of the anti-plane DCI. However for the case of 3 identical adjacent buildings with mat foundations, power is transferred to the center building for the in-plane DCI and from the center building for the anti-plane DCI. This is because the center building is flanked by two other buildings so a condition difference arises between adjacent buildings. This effect depends strongly on the clearance between the foundations but less so on the shear wave velocity of the soil. Moreover, the DCI effect on a tall and heavy main buildings adjacent to short and light buildings is on negligible for both DCI effects, However, the DCI effect on a short and light main buildings adjacent to tall and heavy buildings increases the mean power of the main building up to 20% for 2 adjacent buildings and 40% for 3 adjacent buildings for the in-plane DCI; nevertheless, this effect is negligible for the anti-plane DCI.

For buildings with identically embedded mat foundations, MPRs between the elastic and layered soil conditions do not change appreciably both for in-plane and anti-plane DCI. However, it should be noted that the detrimental effect of in-plane DCI for tall adjacent buildings with deeper embedment is slightly higher for layered soil than for half-space soil. The reason of this phenomenon is considered to be that amount of horizontal vibration power transfer increases for

tall buildings on layered soil because of the lowered radiation damping compared to half-space soil.

The material damping of the soil is effective on the in-plane DCI for small damping ratios, which means small strain areas. However, h_s is not an effective parameter for the anti-plane DCI effect. Moreover, for power transfer between identical adjacent buildings, the building height is more effective than the superstructure mass for both DCI effects, according to the limited analyses carried out.

As a result, the DCI effects on buildings with mat and pile foundations can be summarized by the five key points below:

a) Mass ratio of adjacent buildings: This has detrimental consequences for a lighter adjacent building for in-plane DCI only.
b) Rocking restriction: This is a beneficial effect that is seen only for in-plane DCI. In addition, this effect is greater for mat foundations. Special attention should be paid to short and light buildings placed on pile foundations because of the absence of this effect.
c) Wave-based DCI effect: This can be either beneficial or detrimental according to the clearance; it becomes more effective (even for small clearances for soft soil conditions) for shorter and lighter structures. Its mechanism depends strongly on the direction of excitation.
d) Participation of soil in the motion of foundations: This is a beneficial effect because it increases the radiation damping effect and is seen only for anti-plane DCI. In addition, this effect is greater for mat foundations.

e) Horizontal vibration power transfer between different embedment depths: A high detrimental effect of DCI is observed for identical tall adjacent buildings with mat foundations; this effect is greater for anti-plane DCI than for in-plane DCI and for layered soil than for half-space soil. However, this effect cannot be observed for pile foundations. Therefore, if the foundations of adjacent tall buildings are designed by piles, the detrimental consequences of the DCI can be prevented.

As a general result of the present study, importance of considering RFIM for deeply embedded mat foundations (e/r > 1), especially for tall buildings, is now understood. Also, for pile supported buildings, the detrimental effect of DCI could not be seen for tall buildings. Both results imply the advantages of pile foundations over mat foundations for safer earthquake resistant structural design of tall structures.

6.2 Future Research

As future research, the effect of RFIM should also be determined for layered soil conditions and including geometric and material soil nonlinearity to obtain more general results. For future DCI research, the DCI effect on more than 3 adjacent buildings for different layouts should also be examined. The effect of DCI between buildings with pile and mat foundations should also be addressed. Additionally, DCI effects that diminish the superstructure response could be exploited for the passive control of structures. It is also better to verify the results of the present study by some experimental research.

Publication List

1. Articles

- Ogut OC, Mori M. and Fukuwa N. (2016.3): Effect of rocking foundation input motion on the inelastic behavior of structures. J. Struct. Constr. Eng. AIJ, Vol. 81, No. 721, .447-457.

- Ogut OC, Mori M. and Fukuwa N. (2017.4): In-plane dynamic behavior of two adjacent buildings focused on different embedment depths and foundation types. J. Struct. Constr. Eng. AIJ, Vol. 82, No. 734, (In Press).

2. International Conferences

- Ogut OC, Mori M. and Fukuwa N.: "EFFECT OF ROCKING FOUNDATION INPUT MOTION ON THE NONLINEAR RESPONSE CHARACTERISTICS OF SUPERSTRUCTURE." 16th World Conference of Earthquake Engineering. Chile. (2017.1).

3. National Conferences

- Ogut O.C., "21024 DETERMINING THE DUCTILITY DEMAND OF SDOF SYSTEMS INTERACTING WITH ELASTIC SOIL." Summaries of Technical Papers of Annual Meeting Architectural Institute of Japan. Sapporo-Japan. (2013): 47-48.

- Ogut O.C. and Mori M., "21025 THE EFFECT OF ROCKING FOUNDATION INPUT MOTION ON THE RESPONSE OF SDOF STRUCTURES." Summaries of Technical Papers of Annual Meeting Architectural Institute of Japan. Kobe-Japan. (2014): 49-50.

- Ogut OC, Mori M. and Fukuwa N.: "Dynamic behavior of tall adjacent buildings having different foundation embedment depths." Summaries of Technical Papers of Annual Meeting Architectural Institute of Japan. Fukuoka-Japan (2016).

Acknowledgments

I would like to express the special thanks to my supervisor Prof. Masafumi Mori of Nagoya University, for patient encouragements in distressed days and invaluable guidance for this study. I am also indebted to Prof. Nobuo Fukuwa of Nagoya University for invaluable guidance on my research process, Prof. Masaomi Teshigawara of Nagoya University for beneficial talk during the 16th World Conference of Earthquake Engineering, and Prof. Jun Tobita of Nagoya University for good comments and ideas that were very useful to improve my academic skills.

I would like to express my sincere appreciation to Assoc. Prof. Takuya Nagae of Nagoya University for him friendship. Moreover, I would also like to thank Asst. Prof. Hirai Takashi of Nagoya University for his kind supports whenever I need to help and Miho Shimizu for her friendly guidance on the problems that I faced in the lab. Additionally, I am very indebted to Dr. Cem Yenidogan of Nagoya University for him beneficial advices for my future carrier. It also should be added that the program coded by Prof. Xuezhang Wen of Hunan University is used in the present study and I gratefully acknowledge contribution of him.

It was a nice experience to learn Japanese language at Faculty of Language and Culture of Nagoya University, so I am indebted to my all Japanese teachers who teach me this wonderful language. I would also like to express my special thanks to Ministry of Education, Culture, Sports, Science and Technology of Japan (MEXT) for financial support during my research.

Finally, I would like to say thanks to my family and my friend Mehmet Cagri Ilter for their supports.